



National Library
of Canada

Bibliothèque nationale
du Canada

Canadian Theses Service

Service des thèses canadiennes

Ottawa, Canada
K1A 0N4

NOTICE

The quality of this microform is heavily dependent upon the quality of the original thesis submitted for microfilming. Every effort has been made to ensure the highest quality of reproduction possible.

If pages are missing, contact the university which granted the degree.

Some pages may have indistinct print especially if the original pages were typed with a poor typewriter ribbon or if the university sent us an inferior photocopy.

Previously copyrighted materials (journal articles, published tests, etc.) are not filmed.

Reproduction in full or in part of this microform is governed by the Canadian Copyright Act, R.S.C. 1970, c. C-30.

AVIS

La qualité de cette microforme dépend grandement de la qualité de la thèse soumise au microfilmage. Nous avons tout fait pour assurer une qualité supérieure de reproduction.

S'il manque des pages, veuillez communiquer avec l'université qui a conféré le grade.

La qualité d'impression de certaines pages peut laisser à désirer, surtout si les pages originales ont été dactylographiées à l'aide d'un ruban usé ou si l'université nous a fait parvenir une photocopie de qualité inférieure.

Les documents qui font déjà l'objet d'un droit d'auteur (articles de revue, tests publiés, etc.) ne sont pas microfilmés.

La reproduction, même partielle, de cette microforme est soumise à la Loi canadienne sur le droit d'auteur, SRC 1970, c. C-30.

THE UNIVERSITY OF ALBERTA

LARGE STRAIN CONSOLIDATION OF OIL SAND TAILINGS SLUDGE

by

GORDON WAYNE POLLOCK

A THESIS

SUBMITTED TO THE FACULTY OF GRADUATE STUDIES AND RESEARCH

IN PARTIAL FULFILMENT OF THE REQUIREMENTS FOR THE DEGREE

OF MASTER OF SCIENCE

DEPARTMENT OF CIVIL ENGINEERING

EDMONTON, ALBERTA

FALL 1988

Permission has been granted to the National Library of Canada to microfilm this thesis and to lend or sell copies of the film.

The author (copyright owner) has reserved other publication rights, and neither the thesis nor extensive extracts from it may be printed or otherwise reproduced without his/her written permission.

L'autorisation a été accordée à la Bibliothèque nationale du Canada de microfilmer cette thèse et de prêter ou de vendre des exemplaires du film.

L'auteur (titulaire du droit d'auteur) se réserve les autres droits de publication; ni la thèse ni de longs extraits de celle-ci ne doivent être imprimés ou autrement reproduits sans son autorisation écrite.

ISBN 0-315-45647-7

THE UNIVERSITY OF ALBERTA

RELEASE FORM

NAME OF AUTHOR GORDON WAYNE POLLOCK
TITLE OF THESIS LARGE STRAIN CONSOLIDATION OF OIL
SAND TAILINGS SLUDGE
DEGREE FOR WHICH THESIS WAS PRESENTED . MASTER OF SCIENCE
YEAR THIS DEGREE GRANTED FALL 1988

Permission is hereby granted to THE UNIVERSITY OF ALBERTA LIBRARY to reproduce single copies of this thesis and to lend or sell such copies for private, scholarly or scientific research purposes only.

The author reserves other publication rights, and neither the thesis nor extensive extracts from it may be printed or otherwise reproduced without the author's written permission.

(SIGNED) *Gordon Pollock*

PERMANENT ADDRESS:

1903-15th AVE. SOUTH.
LETHBRIDGE, ALBERTA
CANADA T1K 0X1

DATED *May 27* 1988

THE UNIVERSITY OF ALBERTA
FACULTY OF GRADUATE STUDIES AND RESEARCH

The undersigned certify that they have read, and recommend to the Faculty of Graduate Studies and Research, for acceptance, a thesis entitled LARGE STRAIN CONSOLIDATION OF OIL SAND TAILINGS SLUDGE submitted by GORDON WAYNE POLLOCK in partial fulfilment of the requirements for the degree of MASTER OF SCIENCE.

J. O. Scott
.....
Supervisor
Edward
.....
Lon Hepler
.....
.....

Date *May 27, 1988*

ABSTRACT

A resulting waste material from the mining of oil sands in Northern Alberta is a slow consolidating, high water content, clay-water-bitumen material termed sludge.

To assess the effectiveness and feasibility of long range disposal plans for the sludge, an understanding of the consolidation rates and behaviour of the material is necessary. To achieve this, the following research was performed. Laboratory testing was conducted to determine the sludge's (and sludge-sand mixes') consolidation parameters. Consolidation theories were examined to determine the appropriate model. Then the resulting laboratory data was combined with the theory to model the consolidation of sludge slurries occurring in 10 m tall standpipes.

The testing of the material to determine its compressibility was conducted with a step loading large strain slurry consolidometer. This apparatus also allowed constant head permeability tests to be performed on the samples without inducing consolidation from seepage forces. Along with the sludge, tests were also performed on sludge-sand mixes and a sludge-sand mix with flocculent in order to determine the effects of the sand and the flocculent on the consolidation parameters.

The compressibility and permeability of the above materials were found to be highly nonlinear. The experimental results showed that the effect of the sand was to enhance consolidation and compressibility by diluting the

consolidation resisting effects of the sludge. A compressibility, sludge-sand "family of curves" was established for the tested oil sand tailings. The permeability tests revealed a time dependent flow discharge under a constant gradient. A valuable result from the permeability tests was that the relationship between hydraulic conductivity and the fines void ratio was the same for all slurries. The effect of the flocculent was solely to keep the sand in suspension in a high water content slurry, and it did not affect the compressibility and permeability.

A consolidation theory developed by Gibson, England, and Hussey (1967), incorporating large strains, self weight, and nonlinear soil properties, was used along with the laboratory data to model the consolidation in the standpipes. The measured standpipe data was adequately modelled, even though the predicted results were very sensitive to permeability input.

Acknowledgements

The author would like to thank Dr. J. D. Scott for his interest, expertise, and continual guidance throughout the work of this thesis.

Special thanks to Steve Gamble whose hard work and patience resulted in a friendship as well as a successful testing programme. Appreciation is also extended to Christine Hereygers and Jay Khajuria for their work in the laboratory.

The author also wishes to recognize the financial and equipment support which Syncrude Canada Ltd. donated to this project. As well, W.H. Shaw, B.A. Isaac, E. Lau, and H. Barnes are to be thanked for their assistance.

Table of Contents

Chapter	Page
1. INTRODUCTION	1
1.1 Statement of Problem	1
1.2 Objectives of Research Program	2
1.3 Scope of Thesis	3
1.4 Organization of Thesis	4
2. LITERATURE REVIEW	6
2.1 Oil Sand Tailings	6
2.1.1 Introduction	6
2.1.2 Oil Sand Operations	8
2.1.3 Tailings Sludge Description	10
2.1.4 Pond Dynamics	15
2.1.5 Sedimentation and Consolidation	17
2.2 Permeability and Consolidation Testing on Slurries and Soft Clays	21
2.2.1 Introduction	21
2.2.2 Permeability Testing	21
2.2.2.1 <u>Indirect Methods of Determining Hydraulic Conductivity</u>	21
2.2.2.2 <u>Direct Methods of Determining Hydraulic Conductivity</u>	23
2.2.2.3 <u>Deviations from Darcy's Law</u>	24
2.2.2.4 <u>Steady State Flow</u>	26
2.2.2.5 <u>Summary</u>	26
2.2.3 Consolidation Testing	27
2.2.3.1 <u>Traditional Consolidation Test</u>	27
2.2.3.2 <u>Improved Consolidation Tests</u>	28
2.2.3.3 <u>Slurry Consolidation Testing</u>	30

2.2.3.4	<u>Initial State of Slurried Material</u>	31
2.2.3.5	<u>Summary</u>	32
3.	LARGE STRAIN CONSOLIDATION ANALYSES	34
3.1	Consolidation Theory Developments	34
3.1.1	Terzaghi's Theory	34
3.1.2	Nonlinearity and Varying Permeability Theoretical Developments	35
3.1.3	Finite Strain Developments	36
3.1.4	Self Weight Consolidation	38
3.2	Gibson, England, and Hussey (1967) Finite Strain Theory	39
3.2.1	Coordinate Systems	39
3.2.2	Formulation and Derivation	40
3.2.3	Application to Soft Thick Layers	43
3.2.4	Comparison of Finite Strain Results to Classical Theory	44
3.3	Numerical Models used in Thesis	47
3.3.1	Somogyi, 1980	47
3.3.2	Cargill, 1982	50
3.3.3	Comparison of Results from the Two Methods	53
3.4	Other Methods of Analyses	55
3.4.1	Koppula (1970) and Koppula and Morgenstern (1982)	55
3.4.2	Lee and Sills (1981)	56
3.4.3	Finite Element Methods	57
3.4.4	Evaluation of Methods	58
3.5	Experience with the Finite Strain Theory	59
3.5.1	Practical Applications	59

3.5.2	Possible Modifications and or Extensions ..61	61
4.	CONSOLIDATION AND PERMEABILITY TESTS	62
4.1	Equipment	63
4.1.1	Overview	63
4.1.2	Consolidation Portion of the Slurry Consolidometer	66
4.1.3	Permeability Portion of the Slurry Consolidometer	70
4.2	Procedure	72
4.2.1	Overview	72
4.2.2	Step Loading Consolidation Test	75
4.2.3	Constant Head Permeability Test	78
4.3	Test Material	79
4.3.1	Specifications	79
4.3.2	Sampling and Preparation	84
4.3.3	Test Material Description	86
5.	LABORATORY TEST RESULTS	90
5.1	Consolidation Test Results	90
5.1.1	Consolidation Rates	90
5.1.1.1	<u>Oil Sand Tailings Sludge</u>	90
5.1.1.2	<u>Oil Sand Tailings Sludge-Sand Mixes</u>	96
5.1.1.3	<u>Oil Sand Tailings Sludge-Sand Mix with Flocculent</u>	99
5.1.1.4	<u>Comparison of the Self Weight Stages</u>	103
5.1.2	Compressibility Results from the Four Tests	109
5.1.2.1	<u>Oil Sand Tailings Sludge</u>	110
5.1.2.2	<u>Oil Sand Tailings Sludge-Sand Mixes</u>	110

5.1.2.3	<u>Oil Sand Tailings Sludge-Sand Mix with Flocculent</u>	114
5.1.2.4	<u>A Comparison of the Compressibility of the Materials</u>	116
5.2	Permeability Test Results	121
5.2.1	Hydraulic Flow with Time	121
5.2.1.1	<u>Oil Sand Tailings Sludge</u>	121
5.2.1.2	<u>Oil Sand Tailings Sludge-Sand Mixes</u>	128
5.2.1.3	<u>Oil Sand Tailings Sludge-Sand Mix with Flocculent</u>	128
5.2.2	Hydraulic Conductivity with Void Ratio	132
5.2.2.1	<u>Oil Sand Tailings Sludge</u>	132
5.2.2.2	<u>Oil Sand Tailings Sludge-Sand Mixes</u>	138
5.2.2.3	<u>Oil Sand Tailings Sludge-Sand Mix with Flocculent</u>	143
5.2.2.4	<u>Comparison of the Four Tests</u>	143
5.3	Summary of Observations and Conclusions	149
5.3.1	Consolidation and Compressibility	149
5.3.2	Permeability	150
5.3.3	Effect of Sand and Flocculent	152
6.	MODELLING OF SELF WEIGHT CONSOLIDATION TESTS	154
6.1	Introduction	154
6.2	Standpipe #1	157
6.2.1	Input Parameters	157
6.2.2	Comparison of Predicted with Measured Values	161
6.2.2.1	<u>Interface Settlement</u>	161
6.2.2.2	<u>Excess Pore Pressures</u>	166
6.2.2.3	<u>Solids Content</u>	169

6.3 Standpipe #2	173
6.3.1 Input Parameters	173
6.3.2 Comparison of Predicted and Measured Values	174
6.3.2.1 <u>Interface Settlement</u>	174
6.3.2.2 <u>Excess Pore Pressures</u>	177
6.3.2.3 <u>Solids Content</u>	180
6.4 Standpipe #3	182
6.4.1 Input Parameters	182
6.4.2 Comparison of Predicted with Measured Values	185
6.4.2.1 <u>Interface Settlement</u>	185
6.4.2.2 <u>Excess Pore Pressures</u>	187
6.4.2.3 <u>Solids Content</u>	190
6.5 Summary of Observations and Conclusions	192
7. Conclusions and Recommendations	195
7.1 Conclusions	195
7.1.1 Consolidation Parameters	195
7.1.2 Consolidation Theories	198
7.1.3 Consolidation Modelling	199
7.2 Recommendations for Further Research	200
REFERENCES	203
APPENDIX A - Apparatus and Experimental Details	213
APPENDIX B - Consolidation Time Plots	227
APPENDIX C - Excess Pore Pressures	252

List of Tables

Table	Page
3.1 Constants used for Method Comparison Runs	54
3.2 Results of Computer Runs with Common Input	54
4.1 Ten Metre Standpipe Material Properties	81
4.2 Consolidometer Test Material Properties	81
4.3 Consolidometer Test Material Breakdown	88
6.1 Ten Metre Standpipe #1 - Material Breakdown	160
6.2 Soil Input Parameters	160
6.3 Input Data Coefficients of Determination (r^2)	184
6.4 Ten Metre Standpipe #3 - Material Breakdown	184

List of Figures

Figure	Page
2.1 Composition of Oil Sand	7
2.2 Typical Section of Tailings Dyke	11
2.3 Typical Grain Size Distribution of Sludge	12
2.4 Plasticity of Various Mine Waste Sludges	14
4.1 Slurry Consolidometer	64
4.2 Top Cap and Bottom Plate Sections	67
4.3 Compressed Air System for Large Gradients	73
4.4 Slurry Properties Diagram for Standpipe and Consolidometer Test Material	82
4.5 Grain Size Distribution of Standpipe Material	83
4.6 Grain Size Distribution of Test Material	89
5.1 Consolidation of Oil Sand Tailings Sludge	92
5.2 Consolidation of Sludge under 0.9 kPa	93
5.3 Normalized Consolidation, Sludge	95
5.4 Consolidation of 46% Sand Sludge-Sand Mix	97
5.5 Consolidation of 80% Sand Sludge-Sand Mix	98
5.6 Normalized Consolidation, 46% Sand, Sludge-Sand	100
5.7 Normalized Consolidation, 80% Sand, Sludge-Sand	101
5.8 Consolidation of 73% Sand Sludge-Sand Mix with CaCl ₂	102
5.9 Normalized Consolidation, 73% Sand Sludge-Sand with CaCl ₂	104
5.10 Pore Pressure Dissipation, Sludge Sand with CaCl ₂ , $\Delta\sigma' = 6$ kPa, $\sigma' = 11$ kPa	105
5.11 Self Weight Consolidation Strain, All Slurries	106
5.12 Self Weight Consolidation of Sludge Sand Mixes	108

Figure	Page
5.13 Compressibility of Oil Sand Tailings Sludge	111
5.14 Compressibility of 46% Sand Sludge-Sand	112
5.15 Compressibility of 80% Sand Sludge-Sand	113
5.16 Compressibility of 73% Sand Sludge-Sand with CaCl ₂	115
5.17 Compressibility of All 4 Slurries Tested	117
5.18 Compressibility of All 4 Slurries Tested, Fines Void Ratio	118
5.19 Permeability Test on Sludge, e=5.11, i=0.17	123
5.20 Permeability Test on Sludge, e=5.11, i=0.21	124
5.21 Permeability Test on Sludge, e=2.91	126
5.22 Permeability Test on Sludge, e=0.55	127
5.23 Permeability Test on 46% Sand Sludge-Sand, e=1.62, i=0.75	129
5.24 Permeability Test on 46% Sand Sludge-Sand, e=0.95, i=0.39	130
5.25 Permeability Test on 80% Sand Sludge-Sand, e=0.62	131
5.26 Permeability Test on 73% Sand Sludge-Sand with CaCl ₂ , e=1.05	133
5.27 Flow vs. Gradient, Sludge, e=2.91	135
5.28 Flow vs. Gradient, Sludge, e=1.86	136
5.29 Flow vs. Gradient, Sludge, e=0.48	137
5.30 Permeability of Oil Sand Tailings Sludge	139
5.31 Flow vs. Gradient, 46% Sand Sludge-Sand, e=2.03	140
5.32 Permeability of 46% Sand Sludge-Sand	141
5.33 Permeability of 80% Sand Sludge-Sand	142

Figure	Page
5.34 Flow vs. Gradient, Sludge-Sand Mix with CaCl ₂ , e=0.90	144
5.35 Permeability of 73% Sand Sludge-Sand with CaCl ₂	145
5.36 Permeability of All 4 Slurries	146
5.37 Permeability of All 4 Slurries vs. Fines Void Ratio	148
6.1 Ten Metre Standpipe	155
6.2 Standpipe #1 Sludge-Water Interface Settlement	162
6.3 Permeability Input for Standpipe #1	164
6.4 Standpipe #1 Sludge-Water Interface Settlement, Permeability Sensitivity	165
6.5 Predicted Excess Pore Pressure Profiles, Standpipe #1	167
6.6 Comparison of Excess Pore Pressures, Standpipe #1	168
6.7 Predicted Solids Content Profiles, Standpipe #1	170
6.8 Comparison of Solids Content at 850 days, Standpipe #1	171
6.9 Standpipe #2 Sludge Sand Mix-Water Interface Settlement	176
6.10 Predicted Excess Pore Pressure Profiles, Standpipe #2	178
6.11 Comparison of Excess Pore Pressures, Standpipe #2	179
6.12 Comparison of Solids Content at 709 days, Standpipe #2	181
6.13 Standpipe #3 Sludge Sand Mix-Water Interface Settlement	186
6.14 Predicted Excess Pore Pressure Profiles, Standpipe #3	188
6.15 Comparison of Excess Pore Pressures, Standpipe #3	189

Figure	Page
6.16 Comparison of Solids Content at 280 days, Standpipe #3	191
A.1 Calibration of LVDT #1	215
A.2 Calibration of LVDT #2 (kl)	216
A.3 Calibration of Load Cell CS 2 LL Pressure Transducer	218
A.4 Calibration of Load Cell CS 1 RG Pressure Transducer	219
A.5 Pore Pressure Measurement Equipment	221
A.6 Calibration Check Method	221
A.7 Calibration of 35 kPa Diaphragm for Validyne Transducer	222
A.8 Calibration of 140 kPa Diaphragm for Validyne Transducer	223
A.9 Top Cap Friction	225
A.10 Load Cell Stress Readings	226
B.1 Consolidation, Test #1, $\sigma' = 0.22$ kPa (self weight)	228
B.2 Consolidation, Test #1, $\sigma' = 0.45$ kPa	228
B.3 Consolidation, Test #1, $\sigma' = 0.9$ kPa	229
B.4 Consolidation, Test #1, $\sigma' = 1.7$ kPa	229
B.5 Consolidation, Test #1, $\sigma' = 5.0$ kPa	230
B.6 Consolidation, Test #1, $\sigma' = 11.0$ kPa	230
B.7 Consolidation, Test #1, $\sigma' = 25.0$ kPa	231
B.8 Consolidation, Test #1, $\sigma' = 45$ kPa	231
B.9 Consolidation, Test #1, $\sigma' = 100$ kPa	232
B.10 Consolidation, Test #1, $\sigma' = 200$ kPa	232
B.11 Consolidation, Test #1, $\sigma' = 400$ kPa	233
B.12 Consolidation, Test #1, $\sigma' = 650$ kPa	233

Figure	Page
B.13 Consolidation, Test #2, $\sigma' = .45$ kPa (self weight)	234
B.14 Consolidation, Test #2, $\sigma' = 0.54$ kPa	234
B.15 Consolidation, Test #2, $\sigma' = 0.64$ kPa	235
B.16 Consolidation, Test #2, $\sigma' = 1.0$ kPa	235
B.17 Consolidation, Test #2, $\sigma' = 1.75$ kPa	236
B.18 Consolidation, Test #2, $\sigma' = 3.05$ kPa	236
B.19 Consolidation, Test #2, $\sigma' = 6.25$ kPa	237
B.20 Consolidation, Test #2, $\sigma' = 13.0$ kPa	237
B.21 Consolidation, Test #2, $\sigma' = 25.5$ kPa	238
B.22 Consolidation, Test #2, $\sigma' = 50.5$ kPa	238
B.23 Consolidation, Test #2, $\sigma' = 100$ kPa	239
B.24 Consolidation, Test #2, $\sigma' = 200$ kPa	239
B.25 Consolidation, Test #2, $\sigma' = 320$ kPa	240
B.26 Consolidation, Test #3, $\sigma' = 0.75$ kPa (self weight)	241
B.27 Consolidation, Test #3, $\sigma' = 0.85, 0.95, \& 1.3$ kPa	241
B.28 Consolidation, Test #3, $\sigma' = 2.05 \& 3.4$ kPa	242
B.29 Consolidation, Test #3, $\sigma' = 5.8$ kPa	242
B.30 Consolidation, Test #3, $\sigma' = 13.3$ kPa	243
B.31 Consolidation, Test #3, $\sigma' = 25.8$ kPa	243
B.32 Consolidation, Test #3, $\sigma' = 51$ kPa	244
B.33 Consolidation, Test #3, $\sigma' = 100, 150 \& 200$ kPa	244
B.34 Consolidation, Test #3, $\sigma' = 320$ kPa	245
B.35 Consolidation, Test #4, $\sigma' = 0.53$ kPa (self weight)	246
B.36 Consolidation, Test #4, $\sigma' = 1.0$ kPa	246

Figure	Page
B.37 Consolidation, Test #4, $\sigma' = 2.5$ kPa	247
B.38 Consolidation, Test #4, $\sigma' = 5.0$ kPa	247
B.39 Consolidation, Test #4, $\sigma' = 11.0$ kPa	248
B.40 Consolidation, Test #4, $\sigma' = 23$ kPa	248
B.41 Consolidation, Test #4, $\sigma' = 41$ kPa	249
B.42 Consolidation, Test #4, $\sigma' = 86$ kPa	249
B.43 Consolidation, Test #4, $\sigma' = 170$ kPa	250
B.44 Consolidation, Test #4, $\sigma' = 353$ kPa	250
B.45 Consolidation, Test #4, $\sigma' = 463$ kPa	251
C.1 Excess Pore Pressure, Test #1, $\sigma'_{ave} = 0.22$ kPa (self weight)	254
C.2 Excess Pore Pressure, Test #1, $\Delta\sigma' = .23$ kPa, $\sigma' = .45$ kPa	255
C.3 Excess Pore Pressure, Test #1, $\Delta\sigma' = 0.45$ kPa, $\sigma' = 0.9$ kPa	256
C.4 Excess Pore Pressure, Test #1, $\Delta\sigma' = .8$ kPa, $\sigma' = 1.7$ kPa	257
C.5 Excess Pore Pressure, Test #1, $\Delta\sigma' = 3.3$ kPa, $\sigma' = 5$ kPa	258
C.6 Excess Pore Pressure, Test #1, $\Delta\sigma' = 6$ kPa, $\sigma' = 11$ kPa	259
C.7 Excess Pore Pressure, Test #1, $\Delta\sigma' = 14$ kPa, $\sigma' = 25$ kPa	260
C.8 Excess Pore Pressure, Test #1, $\Delta\sigma' = 20$ kPa, $\sigma' = 45$ kPa	261
C.9 Excess Pore Pressure, Test #1, $\Delta\sigma' = 55$ kPa, $\sigma' = 100$ kPa	262
C.10 Excess Pore Pressure, Test #1, $\Delta\sigma' = 100$ kPa, $\sigma' = 200$ kPa	263
C.11 Excess Pore Pressure, Test #1, $\Delta\sigma' = 200$ kPa, $\sigma' = 400$ kPa	264
C.12 Excess Pore Pressure, Test #1, $\Delta\sigma' = 250$ kPa, $\sigma' = 650$ kPa	265

Figure	Page
C.13 Excess Pore Pressure, Test #2, $\sigma'_{v0}=0.53$ kPa (self weight)	266
C.14 Excess Pore Pressure, Test #2, $\Delta\sigma'=.47$ kPa, $\sigma'=1.0$ kPa	267
C.15 Excess Pore Pressure, Test #2, $\Delta\sigma'=1.5$ kPa, $\sigma'=2.5$ kPa	268
C.16 Excess Pore Pressure, Test #2, $\Delta\sigma'=2.5$ kPa, $\sigma'=5.0$ kPa	269
C.17 Excess Pore Pressure, Test #2, $\Delta\sigma'=6$ kPa, $\sigma'=11$ kPa	270
C.18 Excess Pore Pressure, Test #2, $\Delta\sigma'=12$ kPa, $\sigma'=23$ kPa	271
C.19 Excess Pore Pressure, Test #2, $\Delta\sigma'=18$ kPa, $\sigma'=41$ kPa	272
C.20 Excess Pore Pressure, Test #2, $\Delta\sigma'=45$ kPa, $\sigma'=86$ kPa	273
C.21 Excess Pore Pressure, Test #2, $\Delta\sigma'=84$ kPa, $\sigma'=170$ kPa	274
C.22 Excess Pore Pressure, Test #2, $\Delta\sigma'=183$ kPa, $\sigma'=353$ kPa	275
C.23 Excess Pore Pressure, Test #2, $\Delta\sigma'=110$ kPa, $\sigma'=463$ kPa	276

List of Symbols

- A = empirical constant for compressibility relationship
a = lagrangian spacial coordinate
 a_o = upper boundary lagrangian coordinate
 a_v = coefficient of compressibility
B = empirical constant for compressibility relationship
b = bitumen content
 β = function of empirical compressibility constant
C = empirical constant for permeability relationship
 C_c = compression index
 c_v = coefficient of consolidation
D = empirical constant for permeability relationship
 D_R = relative density
 D_{R_b} = relative density of bitumen
 $D_{R_{ss}}$ = relative density of sludge solids
e = void ratio
 e_f = fines void ratio
 e_o = void ratio prior to consolidation
 ϵ = strain
F = fines content
 ϕ = permeability function
g = finite strain coefficient of consolidation
 γ_b = buoyant unit weight
 γ_f = unit weight of fluid phase
 γ_s = unit weight of solid phase
 γ_w = unit weight of water
H = height of slurry H_s = height of sludge solids in slurry

i = hydraulic gradient
 k = hydraulic conductivity (coefficient of permeability)
 k_0 = hydraulic conductivity prior to consolidation
 λ = compressibility function
 M = constrained modulus
 n = porosity
 ψ = permeability function
 p = empirical constant
 q = empirical constant
 s = solids content
 s_0 = solids content prior to consolidation
 σ = total stress
 σ' = effective stress
 σ'_0 = effective stress prior to consolidation
 t = time
 u = excess pore pressure
 u_f = pore pressure
 v = apparent fluid velocity
 v_f = fluid velocity
 v_s = solid velocity
 x = spacial coordinate
 ξ = convective spacial coordinate
 z = material coordinate

1. INTRODUCTION

1.1 Statement of Problem

In surface mining operations, the resulting waste material, tailings, are generally in the form of a slurry. The slurry is eventually contained in some type of pond-dyke arrangement and can cover an area of tens of square kilometres.

In northern Alberta, oil sand deposits are mined and processed to remove the oil from the mineral particles. The tailings are pumped to a containment dyke where the majority of the sand segregates out, leaving the ponds filled with a water - clay - bitumen material termed sludge.

Water is the major portion of the sludge where, after sedimentation, it occupies approximately 10 to 15 times the volume of the mineral solids and bitumen combined. The material, by economic necessity, must rely upon self weight consolidation for its densification. Self weight consolidation is very slow as shown by the high water content of the sludge in the SUNCOR and Syncrude tailing ponds after a number of years of consolidation. The result therefore is a necessity to continually enlarge the containment ponds and dykes to hold the rapidly accumulating large volumes of material.

It is necessary, therefore, to understand the consolidation rates and behaviour of the sludge before an assessment of the effectiveness and feasibility of long

range disposal plans can be made. At the present time, however, there is very limited laboratory or field data available to readily understand or predict the consolidation of the oil sand tailings sludge. The work in this thesis addresses these concerns.

1.2 Objectives of Research Program

The purpose of the work in this thesis is to determine the necessary material properties and analytical procedures to properly analyze the consolidation of the oil sand tailings sludge.

Under this purpose then, the foremost objective of the thesis is to obtain the soil parameters of the sludge which are relevant to its rate and magnitude of consolidation, or more specifically, the permeability (variation of hydraulic conductivity with void ratio) and compressibility (variation of void ratio with effective stress). Involved in determining these values are the development of an appropriate laboratory apparatus and procedure. The equipment will be of general slurry use, not restricted to oil sand sludge.

As additional objectives, tests will also be performed on sludge-sand mixes to determine the effects of the sand on the consolidation parameters (permeability and compressibility). Additionally, tests will be performed on a sludge-sand mix with a chemical flocculent to determine any changes to the consolidation parameters that the flocculent

might induce.

Once the consolidation parameters for the sludge and sludge-sand mixes have been determined, any analysis done using these results should use the proper consolidation theory. Therefore, an examination of consolidation theories and solutions, and in particular those in which large strains and self weight are incorporated, will be carried out in order to determine a useful working consolidation model for oil sand tailings sludge.

Finally, to fulfill the above purpose, it is necessary to examine the ability of the large strain consolidation theory to predict the progress of self weight consolidation of oil sand tailings sludge and sludge-sand mixes using the laboratory data as input. This will be accomplished by attempting to model the consolidation of sludge and sludge-sand mixes in 10 m standpipes.

1.3 Scope of Thesis

The laboratory tests to determine the consolidation parameters are performed on four materials; oil sand tailings sludge, two oil sand tailings sludge-sand mixes, and a sludge-sand mix with a chemical flocculent. The first three materials are, for the purposes of the modelling, similar in constituents to the materials consolidating in 10 m standpipes located in the Civil Engineering laboratory.

The developed laboratory equipment allows for consolidation testing of slurried materials. The yielded

results are sample height (void ratio) versus time, for each stress increment, and void ratio versus effective stress. As well, the equipment allows for permeability tests to be performed such that hydraulic conductivity is determined at various void ratios.

The examination of consolidation theories and solutions focusses on those incorporating large strains and self weight. The finite strain consolidation theory developed by Gibson, England, and Hussey (1967) is investigated in detail. As well, solutions to the theory derived by Somogyi (1980) and Cargill (1982) are also discussed in detail.

The laboratory data is used with the theory to model the consolidation of the tailings slurries in three ten metre standpipes. The comparison is undertaken for the slurry height, density (solids content), and excess pore pressures. The results of the modelling are discussed. Any discrepancies are reviewed and possible explanations presented. A detailed examination of the behaviour of the 10 m standpipes and detailed explanation of any discrepancies, however, are left to further research.

1.4 Organization of Thesis

Literature relevant to the thesis has been surveyed and is summarized in Chapter 2. The Chapter is divided into two main sections. The first contains information on oil sand tailings and the second section concentrates on the testing of slurried materials.

Chapter 3 examines consolidation theories, specifically finite (large) strain consolidation. In this Chapter, the review of consolidation theories leads to an examination of the formulation of finite strain consolidation theory. Solutions that have been presented in the literature are discussed as well as published experience with finite strain consolidation.

The laboratory equipment developed for the consolidation and permeability testing of the sludge is presented in Chapter 4. As well, this Chapter contains a description of the experimental procedure that was used and a description of the material that was tested.

The results of the laboratory tests are given in Chapter 5. Each of the tested materials is looked at with respect to consolidation rates, compressibility, hydraulic flow, and hydraulic conductivity.

Chapter 6 includes the results of the finite strain consolidation theory modelling the consolidation of the sludge and sludge-sand mixes in the 10 m standpipes. Input parameters, which are the results from Chapter 5, are discussed. The comparison examines slurry height, solids content, and excess pore pressures.

Chapter 7 contains a summary of the observations and conclusions that were developed throughout the thesis.

2. LITERATURE REVIEW

2.1 Oil Sand Tailings

2.1.1 Introduction

The Alberta oil sands, which exist in the northern half of the province, consist of four large deposits. The four deposits contain approximately 900 billion barrels of crude bitumen of which it is estimated that 250 billion barrels can be economically exploited to produce a light synthetic crude oil. The four deposits subtend an area of some 48,000 square kilometres (Berkowitz and Speight, 1975).

The Athabasca deposit is the largest of the four main deposits, underlying an area of 23,000 sq. kilometres. This is the only deposit on which commercial oil sand surface mining operations currently exist. The Athabasca deposit is an average of 30 m thick and ranges in thickness from 6 to 90 metres. About 10 % of the deposit has less than 45 m of overburden which has made this deposit economically feasible for surface mining (Berkowitz and Speight 1975). Details of the encompassing geology can be found elsewhere (Berkowitz and Speight, 1975; Isaac *et al.*, 1982).

In situ, the oil sand consists of sand grains, predominantly quartz, covered by a layer of water, which is then enveloped by bitumen. The matrix is portrayed in Figure 2.1 (after Dusseault, 1977). Note the fines in the water layer. In the Athabasca oil sand deposit, the bitumen

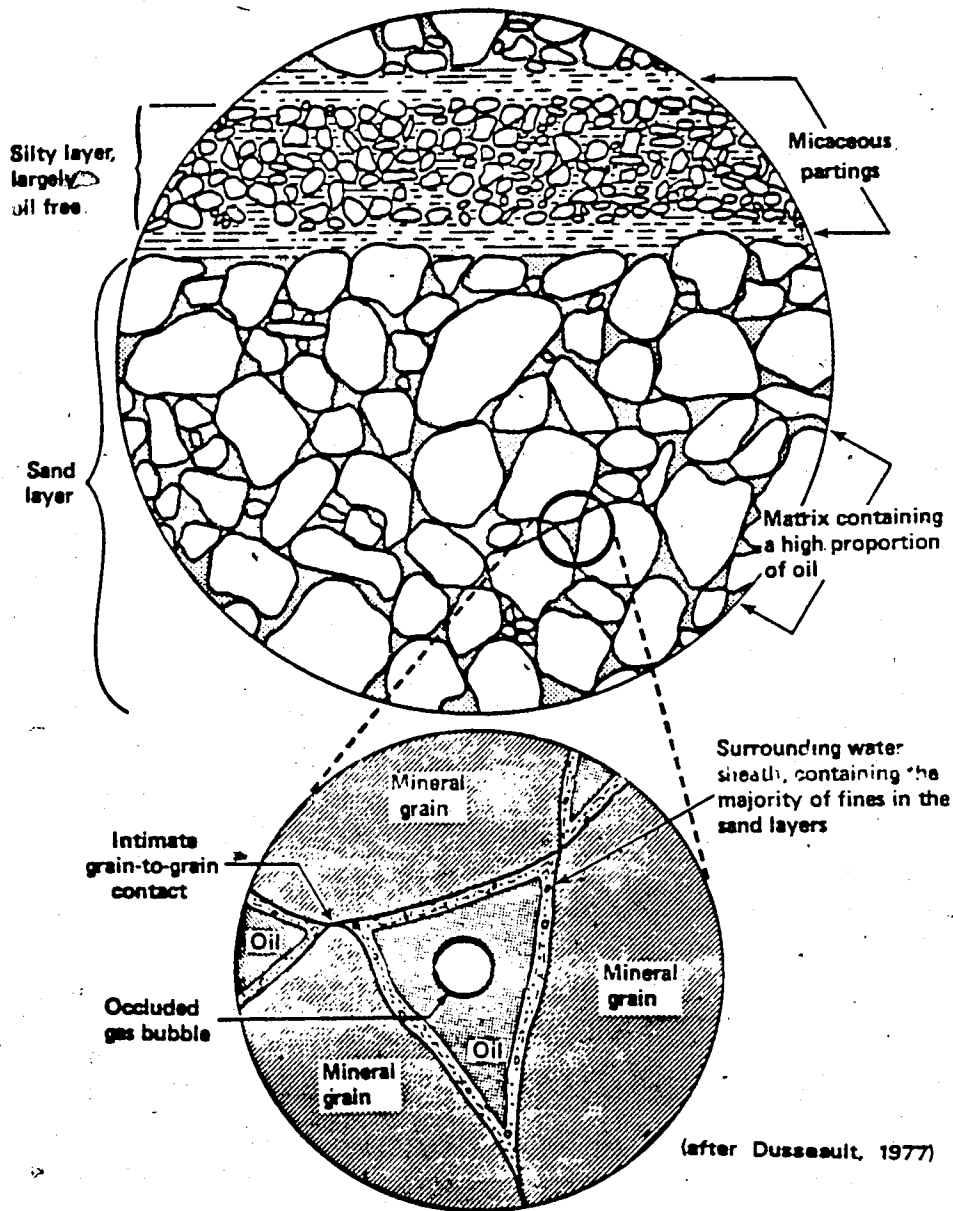


Figure 2.1 Composition of Oil Sand

content (as a percentage of the bulk mass) ranges from 0 to 20 % and averages around 11 %. The amount of water relative to the bulk mass varies from 3 to 6 % and averages about 5 %. The mass of fines (clay and silt size particles), which exist in the oil sand deposit in seams and lenses, averages 14 % of the oil sand mass and the sand averages approximately 70 %. Clay composes approximately 32 % of the fines. If the average mined oil sand is about 10 to 11 % bitumen, then about 90 % of the oil sand (by weight) (plus the bitumen which does not get recovered, is waste to be disposed of (Prasad and Joshi, 1985; Camp, 1977).

2.1.2 Oil Sand Operations

The two oil sand surface mining operations on the Athabasca oil sand deposit (Syncrude Canada Ltd. and Suncor Ltd.) process the oil sand material using the hot water extraction process. In the first stage of the extraction process, known as conditioning, water and steam are mixed with the mined oil sand. Also during this stage chemicals such as NaOH are added to assist in maintaining the pH between 8.0 and 8.5 in order to strip the bitumen from the mineral solids for easy separation in the next stage. However, these conditions cause the clay particles to become well dispersed. In the next stage, called separation, more water is added to the already dilute oil sand to promote the segregation of the sand size particles and the flotation of the bitumen.

The remaining material, known as middlings, is subjected to a final stage called scavenging, for the removal of small amounts of previously unrecovered bitumen. This procedure involves an air injection system. The remainder of the material from this stage combined with the segregated sand from the separation stage (the two materials may already be combined depending on the particular design of the scavenging stage) form the oil sand tailings and are pumped to a disposal area (Camp, 1977, Adam, 1985).

At the Syncrude Canada Limited plant, 1 m³ of oil sand feed requires 1.8 m³ of water for the forementioned extraction process. The tailings stream occupies a volume of more than 2.5 times the volume of the original oil sand (Scott and Dusseault, 1982; Scott, Dusseault, and Carrier, 1985). In a given year, the tailings stream amounts to a volume of approximately 115 million cubic metres (Scott, Dusseault, and Carrier, 1985; Fair and Hanford, 1986).

The disposal area that the tailings are pumped to, consists of a pond of tailings sludge confined by a dyke constructed from the tailings sand. When the tailings arrive at the disposal site, they are pumped into "cells" on top of the dyke, which allows most of the sand to drop out of suspension. The remainder of the material then flows into the pond, this process is called "overboarding". When sufficient sand has been deposited in a cell for construction purposes, the tailings are pumped to a different cell. The loose sand in the filled cell is then

mechanically compacted as the sand builds up. When the material is overboarded, the remainder of the sand segregates out forming a beach and trapping some of the fines while doing so. The beach has an average slope of 5 degrees, where the slope below the water line is steeper than the slope above (Camp, 1977; Dusseault and Scott, 1982). A typical section of the dyke is shown in Figure 2.2.

Approximately 48 million cubic metres of dilute or "thin" sludge (8 % solids content) is formed per year at the Syncrude Canada Ltd. plant (Scott and Dusseault, 1982). Solids content (S) is a ratio of the mass of the sludge solids (bitumen included) to the total mass. A portion of the water is released after the beaching process and initial sedimentation. The tailings at this point occupies a volume approximately 40 % greater than the in situ oil sand (Scott, Dusseault, and Carrier, 1985; Camp, 1977).

2.1.3 Tailings Sludge Description

Typical grain size distribution curves for the tailings stream and the tailings sludge are shown on Figure 2.3 (after Scott and Cymerman, 1984). Approximately one half of the sludge soil particles are in the clay range with more than 90 % of the material being silt or clay size particles. The clay minerals typically consist of 80 % kaolinite, 15 % illite, 1.5 % montmorillonite, 1.5 % chlorite and 2 % mixed clay layers (Roberts, Yong and Erskine, 1980).

after Scott and
Cymerman, 1984

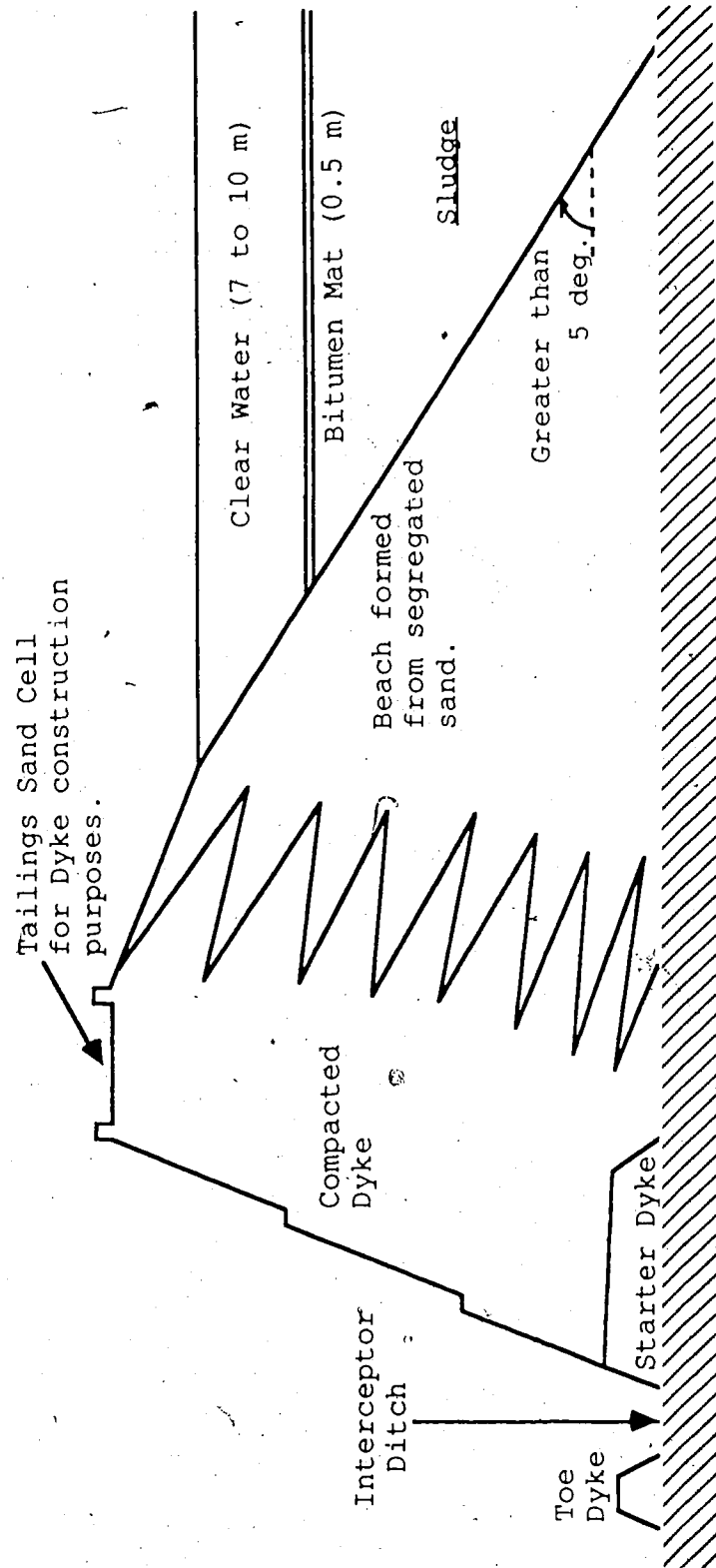


Figure 2.2 Typical Section of Tailings Dyke

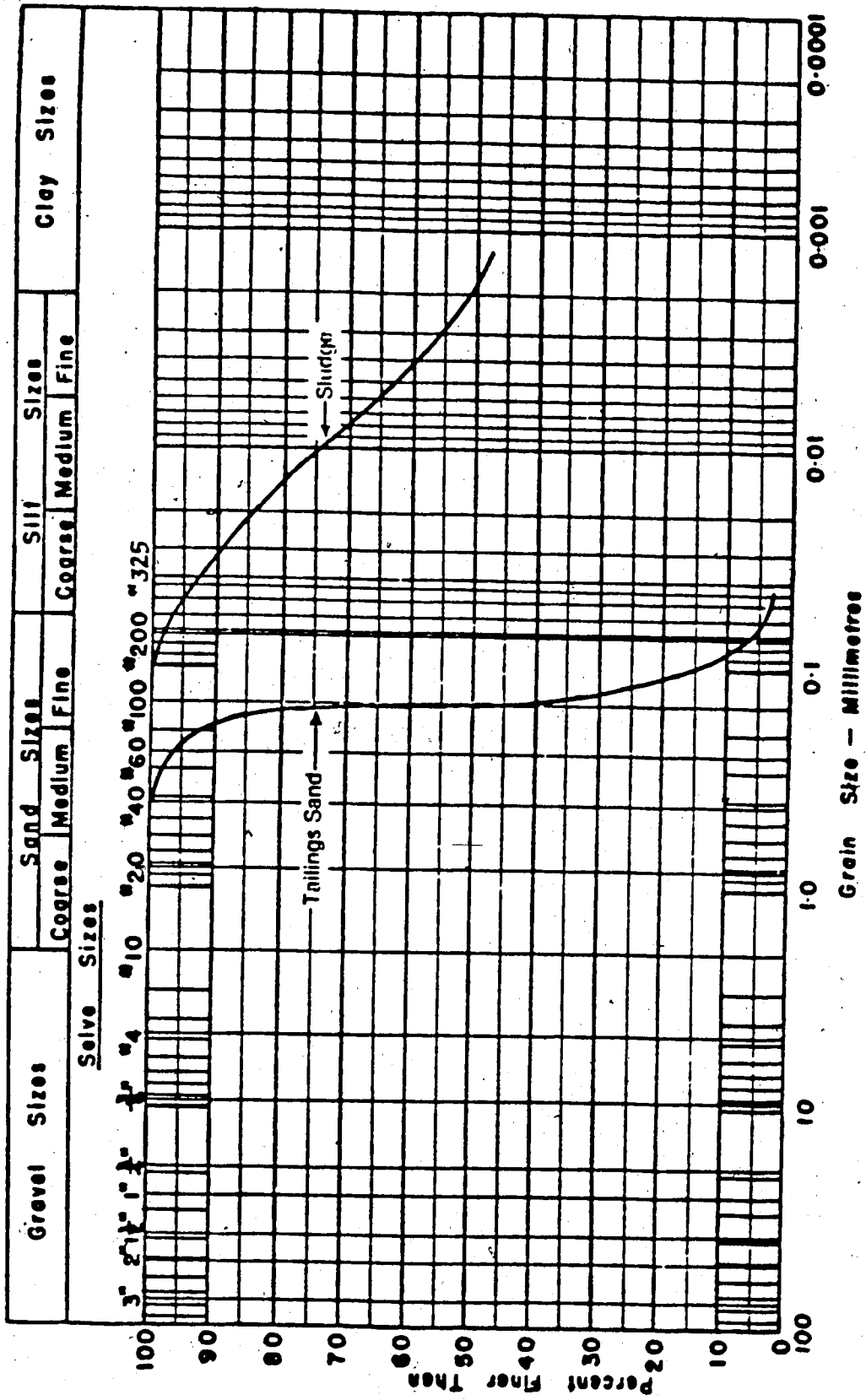


Figure 2.3 Typical Grain Size Distribution of Sludge

The sludge has the consistency of a thick fluid. Sludge which has been in the tailings pond for two years has a solids content of 30 %. Bitumen exists in the sludge as free and adsorbed bitumen (Kessick, 1979). The amount of bitumen (relative to the mass of mineral solids alone) on average is around 16 % (or 30 % by volume), ranges from 2 to 28 %, and is typically greater in finer sludge than coarser sludge (Scott, Dusseault, and Carrier, 1985).

The liquid limit of the sludge ranges from 40 to 80 %, where sludge with higher bitumen contents (usually finer grained sludge) yield the higher liquid limits (Scott, Dusseault, and Carrier, 1985). Figure 2.4 compares the plasticity of oil sand tailings sludge with other mine tailings (after Carrier, Bromwell, and Somogyi, 1983). Phosphate slimes are composed of $1/4$ to $1/3$ clay sized minerals, of which smectite is the primary clay (Carrier, Bromwell, and Somogyi, 1983). The slimes from the China Clay tailings are dominated by kaolinite (Kessick, 1978). The tailings from the processing of bauxite to aluminum, known as the Red Muds, are dominantly sodium alumino-silicate, which comes from kaolinite (Kessick, 1978). When the bitumen from a high bitumen content sludge (28 % by weight) was removed, the liquid limit dropped from 65 to 50 % (Scott and Dusseault, 1980).

A characteristic of oil sand sludge is the gel strength or thixotropic strength that it develops. Measurements of the thixotropic strength of the sludge yield a value of

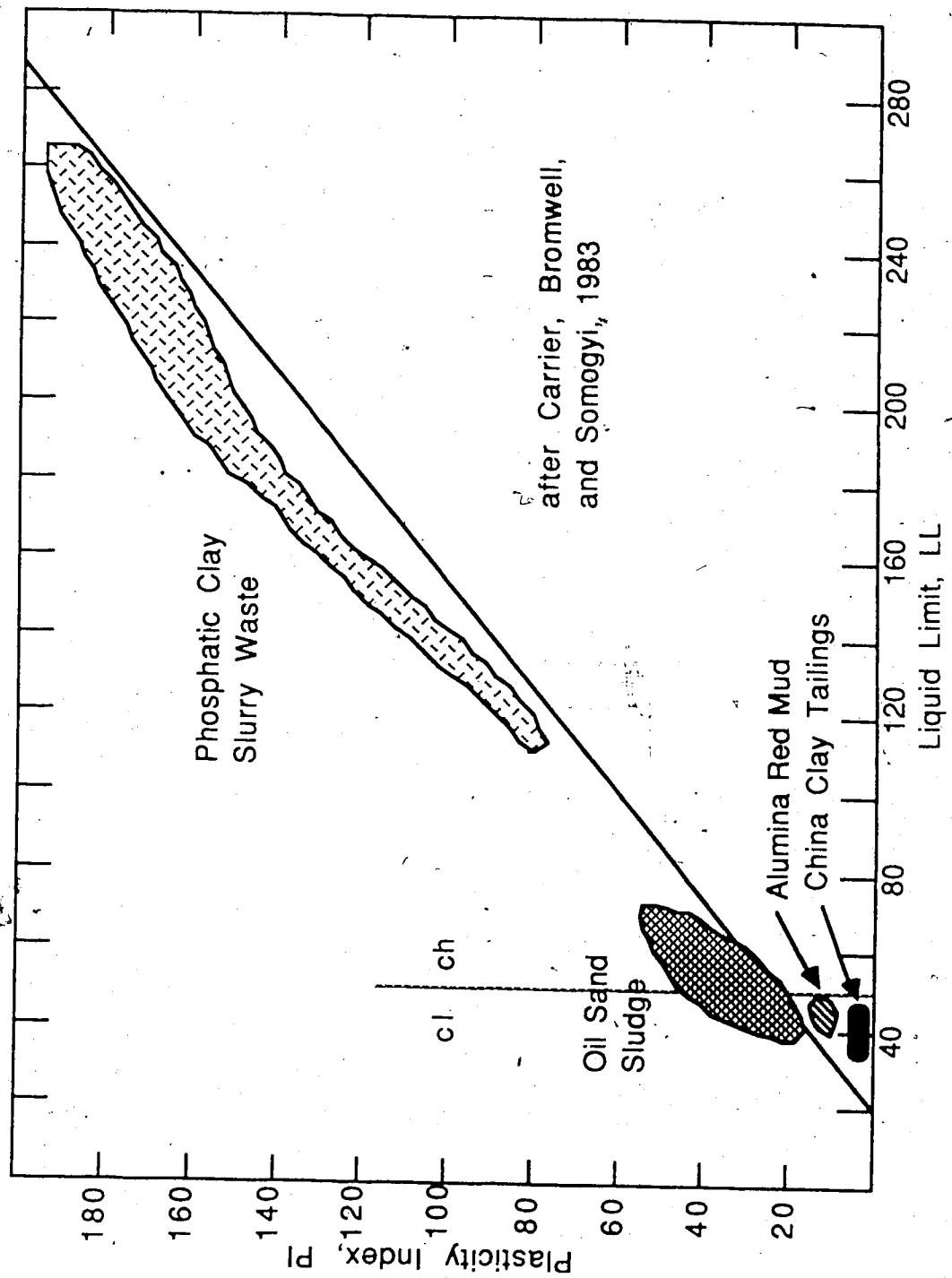


Figure 2.4 Plasticity of Various Mine Waste Sludges

around 13 Pa several days after being remoulded (Scott, Dusseault, and Carrier, 1985; Kessick, 1979). Negative pore pressures, in standpipes containing sludge, are thought to be caused by thixotropy and have been measured in the order of 11 kPa (Scott, Dusseault, and Carrier, 1985). Kolaian and Low (1962) discuss the existence of negative pore pressures in relation to thixotropic gel strength. Not only will the gel formation decrease self weight consolidation in the upper portion of the pond, it will also affect some geotechnical tests performed on the sludge. Atterberg tests, specifically liquid limit, should be performed immediately after mixing the material. Standpipes containing sludge for the purpose of measuring settlement caused by consolidation should be of substantial height so as not to be dominated by the thixotropic effects (Scott, Dusseault, and Carrier, 1985).

2.1.4 Pond Dynamics

As the sludge enters the pond, Dusseault and Scott (1982) propose that it travels on top of the coarse grained beach, through a clear water zone, and into a zone of sedimenting sludge. At this point the sludge separates into a thin sludge density current and a sand density current. The thin sludge having a relative density of around 1.05, and a solids content of about 8 %, travels down the beach in the sedimentation zone, until it reaches a zone of like density. At this point, the thin sludge leaves the beach and

moves towards the center of the pond (Dusseault and Scott, 1982).

Sedimentation is the process in which the solids fall through the ambient fluid, in which stress is not transferred from one particle to another (except through periodical collisions). In the pond, the zone of sedimentation has both Stokian and hindered sedimentation processes which are controlled by fluid viscosity, particle size and shape, and gravity. In this zone, the solids content of the sludge rises from 8 to 20 %, where the density increase arises from the hindered sedimentation region (Dusseault and Scott, 1982; Yong *et al.*, 1982). During sedimentation, some of the free bitumen is released from the sludge and forms a mat on top of the sludge-water interface since the bitumen is slightly denser than water. Most of the bitumen however, is retained with the mineral particles (Dusseault and Scott, 1982).

At a solids content in the range of 15 to 20 %, the sludge solids begin to form a matrix such that stress can be transmitted from one particle to another. After reaching this solids content, any increase in sludge density arises from the process of self weight consolidation (Scott and Dusseault, 1982). This process is controlled by the permeability and compressibility of the matrix, and is induced by the buoyant weight of the particles above the point in question in the matrix. The sludge consolidates to a solids content of 30 % in about two years, which is

relatively fast. The sludge at this point is termed "mature sludge" and has released approximately 65 % of the original water volume. The rate of consolidation from this point is decreased dramatically (Dusseault and Scott, 1982, Yong et al., 1982). Test results combined with field observations led Scott and Dusseault (1980) to conclude that in a properly managed oil sand tailings pond, the sedimentation rate of the sludge will be sufficient, however the problem lies in the consolidation of the sludge.

2.1.5 Sedimentation and Consolidation

In the case of Syncrude Canada Ltd., the bulkiness of the tailings means that the dyke and pond will eventually cover an area of 24 km², and covers areas of mineable oil sand. Environmental considerations such as the prevention of long term seepage of the toxic tailings water as well as the eventual revegetation of the tailings pond area have also contributed to the need of understanding and improving the consolidation behaviour of the sludge (Scott and Dusseault, 1980).

However, as pointed out by Scott and Dusseault (1980), that although sedimentation is not a problem in a properly managed pond, considerable effort has been put into improving the sedimentation of the sludge solids. The settling process of the sludge solids is a combination of a sedimentation process and a consolidation process. When the sedimentation process has deposited sufficient solids to

form a structure such that effective stress can be transferred amongst the particles, then future settlement must be caused by consolidation of the structure.

Chemical additives and changing the sludge pH have been examined to improve the "settling" of the sludge. The optimum pH value, in regards to settling sludge, was found to be 2 by Hocking and Lee (1977). This value corresponds to a point of zero charge for the clay particles. Ripmeester and Sirianni (1981) acknowledged Hocking and Lee's finding, however found that an optimum pH value in the other direction occurred at a pH of 11.3.

Van Olphen (1977) noted two problems in working with chemical agents. The first problem is a tendency for some sols (of which clay is one) to form into a gel upon addition of certain concentration of flocculents. A gel, as defined by Van Olphen (1977), is a system of particles which are agglomerated to one floc extending throughout the available volume. Joshi and Prasad (1985) cited that difficulty when adding lime (CaO or Ca(OH)_2) to oil sand sludge, and commented that water was not released even after 45 days. The second problem mentioned by Van Olphen (1977) is that, when using chemical flocculating agents to improve sedimentation, the product upon completion of sedimentation, the beginning of consolidation, is bulkier than if a flocculating agent were not used.

As mentioned earlier, oil sand sludge without additives possesses a moderate gel or thixotropic strength. Kessick

(1979) stated three conditions necessary for the sludge to form a gel structure at its normal pH. They are 1) the presence of residual bitumen, 2) the presence of a clay bound organic component to confer surface activity on the clay particles, and 3) the clay particles must have been initially well dispersed. Residual bitumen and initial dispersion of the clay particles have been previously discussed. Research (Burchfield and Hepler, 1979, Ignasiak *et al.*, 1982) has shown that clay bound organic compounds do exist and that they are, in part, carboxylic acids.

Scott, Dusseault, and Carrier (1985) show that negligible gel strengths exist in sludges with solids contents less than 20 %. They also state that since the pond is being continually filled, the weight of overlying sludge will dominate the physical stresses starting at a depth of about 3 m. Therefore it is necessary to look elsewhere for other processes causing the mature sludge to consolidate so slowly.

The clay adsorbed organic layer's and bitumen's affinity for water, has been cited by Scott, Dusseault, and Carrier (1985) as a factor in decreasing the sludge's permeability, which determines the rate of consolidation. However, the authors feel the mechanical role of bitumen is more significant. Scott and Dusseault (1980) have shown that bitumen is able to hold mineral grains apart, thereby acting as a solid. In the same study, it was shown that low bitumen sludge behaved similar to kaolinitic slurries dispersed in

NaOH, indicating that sludge can be understood like other soil-water systems. Also, sludge with a high bitumen content was less permeable than low bitumen content sludge. Scott, Dusseault, and Carrier put forth then, that the bitumen allows the soil particles to agglomerate leading to rapid consolidation. Once stress is applied to the sludge structure in the consolidation stage, the bitumen, although treated analytically as a solid, is deformable and able to constrict or cut off flow paths, thereby reducing the permeability. This hypothesis is consistent with the findings from sedimentation and consolidation tests (Scott and Dusseault, 1980) that there is a rapid decrease in the permeability of the sludge once the sludge reaches approximately 30 % solids content.

Another effect that bitumen has on the sludge is that of decreasing the relative density of the sludge solids. The self weight is a factor in the rate of consolidation as well as determining the eventual amount of consolidation. The addition of sand to tailings sludge in order to increase the relative density of the sludge mass is limited, due to sand segregation at moisture contents and sludge sand ratios which would occur in the field (Dusseault and Scott, 1982). However, Lane (1983, 1984) found that by adding lime to the tailings sand, segregation can be prevented. He also found that high density materials can be formed with "relatively high" permeabilities.

2.2 Permeability and Consolidation Testing on Slurries and Soft Clays

2.2.1 Introduction

To understand the consolidation properties of a given soil, laboratory testing is conducted to determine the compressibility (variation of void ratio with stress) and hydraulic conductivity of the soil. For soils undergoing large changes of void ratio, it is necessary to determine the hydraulic conductivity as a function of the void ratio.

2.2.2 Permeability Testing

Permeability evaluation in the laboratory is done either directly or indirectly. The direct method involves forcing a permeant through the soil and monitoring either the rate of flow through the soil, or the hydraulic head changes induced by it. Indirect methods of determining the hydraulic conductivity are done by inverting a consolidation theory and applying it to the data obtained from a consolidation test (Terzaghi, 1943; Lowe, Jonas, and Obrician, 1969).

2.2.2.1 Indirect Methods of Determining Hydraulic Conductivity

The most common method of indirectly determining the hydraulic conductivity is either from the logarithm time plot (Casagrande, 1938) or square root time plot (Taylor, 1948) of the consolidation of a soil under a constant stress

in the standard oedometer test. Olson and Daniel (1981) cite the use of back calculated hydraulic conductivity values as one of the major causes of differing values between field and laboratory permeabilities. For 90 % of reported cases, there was up to a 64 times difference in hydraulic conductivity values. The authors themselves found that for normally consolidated clays, the ratio of measured hydraulic conductivity to back calculated hydraulic conductivity ranged from 0.9 to 5.0.

Pelletier, Olson, and Rixner (1979) ascribed the lower permeability values obtained from Terzaghi's theory to the high strain rates which occur during the test. Lun and Parkin (1985) give other possible test procedural reasons to account for the discrepancy between measured and back calculated hydraulic conductivity. Possible reasons were the length of duration of the previous load increment, and the load ratio increment, which substantially shifted the t_{100} point.

In Tavenas *et al.*'s (1983) study on soft clays, their data indicated that the back calculated values underestimated the measured values up to six times. Their explanation for the differing values lie in the assumptions of Terzaghi's consolidation theory. The assumptions which are most violated, they show, are that of constant permeability, constant compressibility and hence a constant coefficient of consolidation during consolidation. Tavenas *et al.*'s study led them to conclude that indirect methods

are unacceptable in determining the permeability characteristics of natural clays.

2.2.2.2 Direct Methods of Determining Hydraulic Conductivity

The two most widely used methods of directly determining the hydraulic conductivity of a soil are the constant head and falling head permeability tests. The advantage of these two tests is their simplicity in apparatus, procedure and evaluation of the hydraulic conductivity from the test data. The disadvantage of the conventional methods is the length of time required when performing low gradient permeability tests (Olson and Daniel, 1981). With the falling head test, it becomes quite impractical to run low gradient tests. However using large gradients to overcome the test duration problem can lead to other difficulties.

Pane *et al.* (1983) study the problem of large gradients consolidating the soil during the permeability test, and Mitchell and Younger (1967) attribute particle migration during the test to large gradients. To overcome this problem, Olsen (1966) introduced a constant flow test in which water was introduced to the sample at a constant rate by a flow pump and the corresponding pressure difference was measured. At present, the only drawback with this system is in the pump's ability to produce very slow flow rates (Olsen, Nichols, and Rice, 1985).

2.2.2.3 Deviations from Darcy's Law

Darcy's Law (1856) states that the flow discharge velocity (v) is directly proportional to the hydraulic gradient (i) in the soil by a constant (k) known as the hydraulic conductivity or the coefficient of permeability. Although this relationship was presented over 130 years ago, research is still being done to determine its validity for clays. Olsen (1985) stated that possible deviations from Darcy's Law fall under two categories : 1) the relationship between flow and hydraulic gradient is non-linear and 2) the intercept of the flow-hydraulic gradient graph is not at the origin.

Linearity deviations from Darcy's Law in some literature appeared to occur at low hydraulic gradients (Hansbo, 1960; Miller and Low, 1963; Mitchell and Younger, 1967). Also, at high gradients, a trend of increasing hydraulic conductivity with increasing hydraulic gradient seems to be evident for highly plastic clays. To test this trend, Gairon and Swartzendruber (1975) performed a series of permeability tests on a bentonitic clay for a range of void ratios (starting at a gradient of 50). They found that at high void ratios, around 14, a trend of decreasing permeability with increasing gradient occurred. Seepage induced consolidation would probably account for this, since the denser clays showed no deviation from a linear flow-gradient relationship. At lower gradients Olsen, Nichols, and Rice (1985) and Tavenas *et al.* (1983) showed

the validity of Darcy's Law in kaolinitic and Illitic clays respectively. Because of some of the conflicting reports in the literature, Olsen and Daniels (1981) recommended testing at gradients close to those which will occur in the field.

The second type of deviation from Darcy's Law can take either the form of no flow at a finite hydraulic gradient or flow at zero hydraulic gradient. The former was studied by Miller and Low (1963). The threshold gradient, below which no flow occurs, they found, could be up to 45 in bentonitic clays. However, in Mitchell and Younger's (1967) work on kaolinite, they showed that at small gradients a very small flow did occur. The flow was so disproportionally small that it gave the false appearance of having a threshold gradient. Recent work has given conflicting results. Silva, Hetheman and Calnan (1981) state that a small threshold gradient occurs in fine-grained marine sediments (illite and smectite) where as Tavenas *et al.* (1983) show that if a threshold gradient did exist, it would have to be less than 0.07. Other work (Olsen, 1969; Gairon and Swartzendruber, 1975; Olsen, Nichols, and Rice, 1985) has shown the existence of flow at zero gradient. Olsen (1969, 1985) suggests an explanation may be osmotic behaviours induced from within the sample due to chemical reactions changing pore fluid chemistry.

2.2.2.4 Steady State Flow

One phenomena in permeability testing that has received little attention in the literature is the time required until a steady state flow is reached. Olsen, Nichols, and Rice (1985) suggest that the high gradients typically used in laboratory testing mask this characteristic and therefore there has been little mention of it. Many authors have noted in passing the necessity to "wait" before taking readings (eg. Tavenas *et al.*, 1983; Gairon and Swartzendruber, 1975; Miller and Low, 1963), however the most documented work thus far has been performed by Olsen, Nichols, and Rice (1985).

Their work on low gradient testing in kaolinite has revealed that this delay, which increases for increasingly finer soils, can be up to 600 minutes for silty clays. The flow starts off rapid and decreases up to an order of magnitude for silty clays, until a steady state is reached. Gairon and Swartzendruber (1975) noted that the greater the hydraulic gradient, a greater decrease in flow was necessary to reach a steady state condition. As shown by Olsen, Nichols, and Rice (1985) the steady state flows obeyed Darcy's Law. The authors suggest that time dependent changes in either the volume or distribution of pore space in a specimen could account for the phenomena.

2.2.2.5 Summary

Indirect methods of determining hydraulic conductivity have been found to be unacceptable because of experimental (eg. high strain rates) and analytical reasons (Terzaghi

assumptions). When direct methods are used, low gradients must be used since large gradients induce consolidation. The falling head test is impractical with low gradients. Flow pumps are a possibility, but present pumps have difficulty producing extremely slow controlled flows. The constant head test can be used with low gradients, but will result in a long test duration.

Research into the existence of deviations from Darcy's Law, be it a threshold gradient or a nonlinear flow-gradient relationship, have yielded conflicting results and it has therefore been suggested to perform the tests at gradients close to that which will occur in the field. One anomaly of permeability testing which has started to receive some attention is the existence of an initially rapid flow which decreases to a steady state flow after a period of time.

2.2.3 Consolidation Testing

2.2.3.1 Traditional Consolidation Test

To determine the parameters required for the solution of a consolidation problem, consolidation testing has traditionally been coupled with Terzaghi's (1924) theory of one-dimensional infinitesimal consolidation. As mentioned previously, the most common consolidation test is the oedometer test in which a series of constant loads are applied to a sample, and the consolidation with time is observed for each load. This allows one to obtain a relationship between stress and void ratio, coefficient of

compressibility, a_v , a coefficient of consolidation (from the consolidation theory), c_v , and subsequently a hydraulic conductivity value, k .

Difficulties with some of the assumptions involved in the theory as well as problems involved in applying the theory to the test results were briefly discussed earlier. Experimentally, there are two major problems with the test, as discussed by Znidarcic *et al.* (1984). One problem is the length of time for a test to be completed. The other problem is in the determination of the hydraulic conductivity. If one does not want to rely on the back calculated values, permeability testing may cause seepage induced consolidation, as discussed earlier.

2.2.3.2 Improved Consolidation Tests

Other testing techniques have been developed to overcome the time problem of the oedometer test. Such tests include the Constant Hydraulic Gradient (CHG) test (Lowe, Jonas, and Obrician, 1969), the Constant Rate of Deformation (CRD) test (Hamilton and Crawford, 1959; Wissa *et al.*, 1971), and the Constant Rate of Loading (CRL) test. Although these tests are faster than the standard oedometer test, their data is reduced by applying an inversion of the Terzaghi infinitesimal consolidation theory to obtain a compressibility relationship and hydraulic conductivity value, and thus their usefulness is limited by restrictive assumptions (Znidarcic *et al.*, 1984).

In the CHG test, through the use of a feedback system, the loading rate is continually adjusted such that there is a constant gradient within the sample. The assumptions required for the reduction of the data include infinitesimal strain, constant permeability, a linear compressibility relationship and a constant void ratio throughout the sample (Znidarcic *et al.*, 1984). In the CRD test, assumptions include infinitesimal strain, constant coefficient of consolidation, and assumptions regarding the relationships between either the void ratio and time or the void ratio distribution in the sample. Neither of the void ratio relationship assumptions can be validated (Znidarcic *et al.*, 1984).

Other tests reviewed by Znidarcic *et al.*, including the CRL (Aboshi, Yoshikuni, and Maruyama, 1979) and Continuous Loading (Janbu, Tokheim, and Senneset, 1981) tests, have similar assumptions and restrictions. The seepage test, presented by Imai (1979), allows for the determination of void ratio - effective stress and void ratio - permeability relationships without the use of a consolidation theory. The void ratio distribution in the sample is determined by stopping the seepage induced consolidation, and then slicing the sample to determine the void ratio at various locations. However, as pointed out by Znidarcic *et al.* (1984), the void ratio will be altered due to sample rebound.

Except for the seepage test, the forementioned tests with their corresponding analyses have been set up for soils

which relatively obey the assumptions involved in Terzaghi's infinitesimal consolidation theory. However, these tests are not applicable to soft soils such as dredged materials and mine waste slurries which undergo large deformations during consolidation. For such soils several apparatus with corresponding analyses have been proposed.

2.2.3.3 Slurry Consolidation Testing

The Slurry Consolidometer is similar to the oedometer but is designed to accommodate soils which will exhibit large deformations (Salem and Krizek, 1973; Bromwell and Carrier, 1979; Scott, Dusseault, and Carrier, 1986). The test is performed similar to the oedometer test in that the step loading procedure is applied, allowing for a direct determination of stress versus void ratio. A permeability void ratio relationship can be determined by conducting permeability tests on the sample after each increment. Using a load fixing device, described by Scott, Dusseault, and Carrier (1986), seepage induced consolidation can be prevented. Therefore the major difficulty remaining with the procedure is the duration of the test.

Several procedures have been developed to decrease the time involved when doing large strain consolidation testing on clayey soils. However, these procedures involve inverting the complex finite strain consolidation theory (Gibson, England, and Hussey, 1967) and therefore their usefulness is measured by the assumptions used in the inversion process. One such procedure is that presented by Umehara and Zen

(1980, see also Zen and Umehara, 1986). They combine the slurry consolidometer and CRD test procedure with the finite strain consolidation theory as presented by Mikasa (1965). Their analysis requires that a finite strain coefficient of consolidation and compression index be constant throughout the test. Znidarcic *et al.* (1984) state that the assumptions are the cause of the two distinct effective-stress void ratio curves which result from the analysis (from different monitoring devices on the test). Znidarcic *et al.* (1984) present a procedure and analysis of large strain consolidation testing which also employs the CRD technique. Assumptions necessary to their analysis include a constant finite strain coefficient of consolidation over time intervals and negligible self weight of the soil. These assumptions and other difficulties led the above authors to suggest that further work on the analysis portion is necessary.

2.2.3.4 Initial State of Slurried Material

Slurry consolidation tests along with sedimentation tests have revealed several phenomena in sedimentation and self weight consolidating soils, most interesting of which is that surrounding the initial void ratio. Monte and Krizek (1976) proposed a "fluid limit" for a given soil, as the void ratio at the boundary between the sedimenting and consolidating phases. However, Imai (1981) observed that for highly active soils which undergo hindered settling during the sedimentation phase, the initial void ratio at the start

of consolidation is strongly dependent on the initial slurred void ratio. The result of this behaviour is that there exists "countless" compression curves in the low pressure range, less than 0.1 kPa in their study. Above this effective stress there is a unique compression curve. Similar results were reported by Umehara and Zen (1982), Been and Ills (1981), Scully *et al.* (1984), and Salem and Krizek (1973). Imai's study showed however, that kaolinite did not exhibit this behaviour.

2.2.3.5 Summary

The standard oedometer test is developed for small strain consolidation problems and is generally used with small strain theory. Advanced testing techniques such as CHG, CRD, and CRL, which are faster than the oedometer test, also employ an inversion of the Terzaghi infinitesimal consolidation theory to yield usable results, and are thusly restricted by the theory's assumptions. The seepage test does not rely on Terzaghi's theory for consolidation parameters. However, sample rebound at the completion of this test leads to erroneous results.

Slurry consolidometers have been developed which allow for large deformation during consolidation as well as the ability to perform permeability tests on the samples. The tests, however, are slow. Work has been done on combining faster techniques, such as the CRD test, with the slurry consolidometer and inverting a large strain consolidation theory for the results. However, more work is required on

the analytical portion.

Slurry tests have shown that the initial void ratio of the slurry affects the compressibility curve achieved thereafter, for active soils.

3. LARGE STRAIN CONSOLIDATION ANALYSES

To be able to understand and properly model the consolidation of the oil sand tailings sludge, an appropriate consolidation theory should be used.

This Chapter contains a review of the consolidation theories available. Discussion focusses on the necessary developments and extensions relative to slurry consolidation.

The appropriate theory is then looked at in detail with respect to derivation, solution, and usefulness.

3.1 Consolidation Theory Developments

3.1.1 Terzaghi's Theory

In geotechnical engineering, designs based on consolidation and settlement calculations have used the classical one dimensional theory of consolidation derived by Terzaghi (1924). Combining continuity with a flow rate relationship (Darcy's Law), Terzaghi developed the governing equation for one dimensional consolidation,

$$\frac{\partial u}{\partial t} = c_v \frac{\partial^2 u}{\partial x^2} \quad (3.1)$$

where t is time, x is the one dimensional coordinate, u is the excess pore pressure and c_v is the coefficient of consolidation constant defined by

$$c_v = \frac{k (1 + e_0)}{a_v \gamma_v} \quad (3.2)$$

where k is the coefficient of permeability, e_0 is the void

ratio prior to consolidation, γ_w is the unit weight of water and a_v is the coefficient of compressibility ($-\Delta e/\Delta \sigma'$).

Some of the assumptions invoked by Terzaghi on the soil mass, for ease of derivation and solution, were a linear stress-strain (compressibility) relationship, a constant coefficient of permeability, and infinitesimal strain. Infinitesimal strain means that the relative decrease in soil mass thickness due to consolidation, is so small that the volume ratio term $1+e$ can be approximated by $1+e_0$. Those assumptions have given rise to several extensions to the classical theory.

3.1.2 Nonlinearity and Varying Permeability Theoretical Developments

Many authors have undertaken to accommodate a stress-strain relationship different than that posed by Terzaghi, and to account for a not necessarily constant coefficient of permeability. Schiffman and Gibson (1964) addressed the problem of nonlinearity by treating both permeability and compressibility as functions of depth. This indirectly relates the compressibility and permeability to stress since the effective stress changes with depth. The problem is therefore addressed as geometrically nonhomogeneous.

Davis and Raymond (1965) approached the nonlinearity problem by using the stress-strain (or void ratio - effective stress) relationship observed in oedometer

testing,

$$e = e_0 - C_c \log\left(\frac{\sigma'}{\sigma'_0}\right) \quad (3.3)$$

where σ'_0 is the effective stress at e_0 , and C_c is the compression index. Applying this to Terzaghi's derivation, they developed a more general, and complex, one dimensional consolidation equation.

The forementioned extensions are only two of the nonlinear deviations from the classical theory but are representative of the many in that they are infinitesimal strain theories. Such theoretical developments are not valid due to the fact that nonlinear behaviour, and variable permeability would be most pronounced when the strains are large.

For a more complete overview of infinitesimal strain theory extensions, refer to the paper by Olson and Ladd (1979).

3.1.3 Finite Strain Developments

In adapting the classical (infinitesimal strain) theory to large strain problems, Olson and Ladd (1979) and Yong, Siu, and Sheeran (1983) incrementally adjust soil parameters (permeability and coefficient of compressibility) and soil thickness throughout the consolidation process. However, this technique is still an approximation and a more general theory should be sought.

To develop a governing consolidation equation which places no restriction on the amount of strain

(consolidation), McNabb (1960) developed the theory in terms of material coordinates (Ortenblad, 1930). The material coordinate system defines a point in a soil mass by the volume of solid material between that point and a datum. This system has the advantage of allowing a plane in the soil mass to be referenced throughout its movement during consolidation without knowing its exact location. The boundaries are always defined, simplifying the application of the boundary conditions (Gibson, England, and Hussey, 1967).

The consolidation equation McNabb derives is as follows,

$$\frac{\partial e}{\partial t} = - \frac{\partial}{\partial z} \left(\frac{k}{1+e} \frac{\partial \sigma'}{\partial z} \right) \quad (3.4)$$

where z is the material coordinate, and is related to the actual distance ξ by,

$$\xi = \int_0^z (1+e) dz \quad (3.5)$$

The consolidation equation in this form is unrestricted in the amount of strain and in the relationship between k , e and σ' .

Although McNabb's theory represents a turning point in slurry consolidation theory because of the inherent allowance for large deformations and unrestricted soil parameter relationships, the theory is limited because it does not incorporate the self weight of the deposit.

3.1.4 Self Weight Consolidation

The self weight of a thick soft clay layer being consolidated plays a major role in determining the amount and rate of consolidation and is the only consolidation inducing force in conditions such as mine tailings ponds and dredging projects.

McNabb's (1960) lack of self weight applicability limits his finite strain solution to consolidation of soft thin layers where self weight effects are lessened with decreasing thickness. Mikasa (1965) developed a consolidation equation which takes the self weight of the deposit into account. The equation was developed in terms of a consolidation ratio, $(1 + e_0)/(1 + e)$. Gibson, England, and Hussey (1967) also consider self weight when deriving a finite strain consolidation equation.

Pane and Schiffman (1981) show that although the Mikasa (1965) and Gibson, England, and Hussey (1967) solutions were developed independently, the solutions are similar except in one respect, the initial condition. Mikasa's theory inherently assumes that a layer is initially rapidly placed (i.e., instantaneously formed) at a constant void ratio. The Gibson, England, and Hussey theory places no initial restrictions, allowing for a slow deposition process, if required, and is thus the more general solution. Due to its broader applicability and wider usage and acceptance, the remainder of the thesis will mainly refer to the finite strain theory formulated by Gibson, England, and Hussey, and

the next section will examine the formulation in more detail.

3.2 Gibson, England, and Hussey (1967) Finite Strain Theory

3.2.1 Coordinate Systems

As previously discussed, to simplify the handling of the changing vertical distance between soil particles during consolidation, it was necessary to employ an appropriate coordinate system.

Gibson, England, and Hussey (1967) demonstrate the use of three coordinate systems; the Lagrangian, the convective, and the material or reduced coordinate system.

The Lagrangian system refers everything back to a time $t=0$, that is, a soil particle is referenced throughout consolidation by its distance "a" from a datum when time $t=0$. If the upper boundary is located at a_0 , then its Lagrangian coordinate remains a_0 for all time. The standard coordinate system, Eulerian, has particles referenced to planes fixed in space for all time, which is satisfactory for infinitesimal strain problems which state that the thickness of the layer is constant. The upper boundary Eulerian coordinate will be outside the layer for $t>0$ for large strain problems.

When the soil particle at location "a" at time $t=0$ moves, due to consolidation, then its actual distance from the datum at time $t>0$ is now ξ , although its Lagrangian

coordinate is still "a". ξ is the convective coordinate and is a function of a and t. Although working in the convective system would seem more reasonable, the mathematics dictate that the Lagrangian system is more convenient. The convective coordinate is sometimes referred to as the instantaneous Eulerian coordinate (Schiffman, Pane, and Gibson, 1984).

The third system used, material coordinates, was previously introduced under discussion of McNabb's (1960) theory. The material coordinate system is also a mathematically convenient system, and it is in this system that the final governing equation is presented by Gibson, England, and Hussey.

3.2.2 Formulation and Derivation

Gibson, England, and Hussey (1967) employ three pieces of physics in deriving the governing equation; vertical equilibrium, continuity balance, and a fluid flow relationship.

If the weight of a unit of soil is equal to $(n\gamma_f + (1-n)\gamma_s)$, then the vertical equilibrium of the soil mass, in terms of Lagrangian coordinates, is represented by

$$\frac{\partial \sigma}{\partial a} \pm (n\gamma_f + (1-n)\gamma_s) \frac{\partial \xi}{\partial a} = 0 \quad (3.6)$$

where σ is the total vertical stress, "a" is the vertical Lagrangian coordinate (which causes the equation to take the positive sign when measured against gravity), ξ is the convective coordinate, n is the porosity which are functions,

of a and t , and γ_s and γ_f are the densities of the fluid and solid phases respectively.

The continuity balance can be looked at in two parts, continuity for solid phase and continuity for the fluid phase. The continuity of the solid phase is represented by

$$\gamma_s(a,0)(1-n(a,0)) = \gamma_s(1-n)\frac{\partial \xi}{\partial a} \quad (3.7)$$

If the assumption that the fluid and solid phases are incompressible is introduced here, then equation 3.7 becomes

$$(1-n(a,0)) = (1-n)\frac{\partial \xi}{\partial a} \quad (3.8)$$

For the fluid phase continuity, the rate of weight outflow must equal the rate of change of weight of fluid in the element. If the element thickness is δa , then the rate of weight outflow of fluid over the element is $\frac{\partial}{\partial a}(n\gamma_f(v_f - v_s))\delta a$, where v_f and v_s are the velocities of the fluid and solid phases respectively. Equating this to the fluid weight change rate gives an equation of continuity for the fluid phase,

$$\frac{\partial}{\partial a}(n\gamma_f(v_f - v_s)) + \frac{\partial}{\partial t}\left[n\gamma_f\frac{\partial \xi}{\partial a}\right] = 0 \quad (3.9)$$

Equations 3.8 and 3.9 therefore, represent the continuity balance for the problem.

To derive the fluid flow relationship, Gibson, England, and Hussey cast Darcy's Law in terms of relative velocities so that

$$n(v_f - v_s) = -\frac{k}{\gamma_f} \frac{\partial u}{\partial \xi} \quad (3.10)$$

The relationship defining fluid pressure is

$$\frac{\partial u}{\partial \xi} = \frac{\partial u_f}{\partial \xi} \pm \gamma_f \quad (3.11)$$

where u_f is the fluid pressure which is equal to the hydrostatic plus excess pressures. Combining equations 3.10 and 3.11 and making use of the differential chain law leads to an equation for fluid flow,

$$n(v_f - v_s) \frac{\partial \xi}{\partial a} = -\frac{k}{\gamma_f} \left[\frac{\partial u_f}{\partial a} \pm \gamma_f \frac{\partial \xi}{\partial a} \right] \quad (3.12)$$

For mathematical convenience, equations 3.6 (vertical equilibrium), 3.8, 3.9 (continuity), and 3.12 (fluid flow) are converted to material coordinates using the transformation:

$$z(a) = \int_0^a (1 - n(a', 0)) da' \quad (3.13)$$

Combining the continuity equations and presenting all equations in terms of void ratio, the following is achieved:

$$\text{vertical equilibrium } \frac{\partial \sigma}{\partial z} \pm \left[\frac{e\gamma_f + \gamma_s}{1 + e} \right] \frac{\partial \xi}{\partial z} = 0 \quad (3.14)$$

$$\text{continuity } \frac{\partial}{\partial z} \left[\frac{e(v_f - v_s)}{1 + e} \right] + \frac{\partial e}{\partial t} = 0 \quad (3.15)$$

$$\text{and fluid flow } \left[\frac{e(v_f - v_s)}{k(1 + e)} \pm 1 \right] \frac{\partial \xi}{\partial z} + \frac{\partial u_f}{\gamma_f \partial z} = 0 \quad (3.16)$$

Assuming that the soil skeleton is homogeneous, there are no intrinsic time effects (creep, etc.), and permeability and effective stress are functions for void ratio (the latter being for monotonic consolidation only), then equations 3.14, 3.15, and 3.16 combine to form the governing equation for one dimensional consolidation

$$\pm \left(\frac{\gamma_s}{\gamma_f} - 1 \right) \frac{d}{de} \left[\frac{k}{1 + e} \right] \frac{\partial e}{\partial z} + \frac{\partial}{\partial z} \left[\frac{k}{1 + e} \frac{d\sigma' de}{de \partial z} \right] + \frac{\partial e}{\partial t} = 0 \quad (3.17)$$

Schiffman (1980) shows that the classical consolidation theory (Terzaghi, 1924) and nonlinear infinitesimal strain extensions to it are all subsets of equation 3.17. Note that the first term in equation 3.17 represents the effect of the self weight on the consolidation process. If that term was removed, the equation would be the same as that derived by McNabb (1960), eqn. 3.4. (The lack of γ_f in eqn. 3.4 is due to McNabb's neglect of it).

Been (1980) showed that when effective stress is set to zero, the governing equation reduces to Kynch's (1952) theory of sedimentation.

3.2.3 Application to Soft Thick Layers

In the remainder of their paper, Gibson, England, and Hussey focus on solving the governing equation for the special case of thin layers, that is, the self weight of the layer is negligible compared to the load. For this limited case, with additional assumptions, it was still necessary to employ numerical modelling for the solution (however, when the equation was rendered linear, a closed form solution in a form similar to the classical theory form was achieved).

In their 1981 paper, Gibson, Schiffman, and Cargill continued the preceding work to include thick layers. To solve the governing equation for this problem, they defined a finite strain coefficient of consolidation g ,

$$g(e) = - \frac{k(e)}{\gamma_f} \frac{1}{(1+e)} \frac{d\sigma'}{de} \quad (3.18)$$

and a variable

$$\lambda(e) = - \frac{d}{de} \left(\frac{de}{d\sigma'} \right) \quad (3.19)$$

By designating these two variables as constants, the governing equation becomes linear,

$$\frac{\partial^2 e}{\partial z^2} + \lambda(\gamma_s - \gamma_f) \frac{\partial e}{\partial z} = \frac{1}{g} \frac{\partial e}{\partial t} \quad (3.20)$$

The designation of g and λ as constants is one method in which the governing equation can be formulated to be solved, others will be looked at in following sections. As always, the accuracy of a particular method will depend on the accuracy of its approximations and assumptions.

The soil input parameters to the explicit finite difference program used to solve eqn. 3.20 would then be constant values for both g and λ , and void ratios both for the beginning of consolidation and end of consolidation.

Figures in their paper, plotting g and λ vs σ' , show the non-linearity of these functions. The authors acknowledge that they are clearly not constant during consolidation, and thereby provide a point of possible improvement.

3.2.4 Comparison of Finite Strain Results to Classical Theory

Despite the forementioned approximations, results of their analyses and others demonstrate the effect of allowing large strains and self weight on the consolidation analysis.

A prime difference between the Terzaghi and finite strain consolidation results is in the rate of

consolidation. Several authors (Mikasa, 1965; Gibson, Schiffman, and Cargill, 1981; Schiffman and Cargill, 1981) have observed that for a loaded clay layer, the finite strain solution predicts a swifter rate of consolidation (defined as the amount of settlement compared to the final settlement).

Although the rate of consolidation is faster, a surprising second observation noted for consolidation of loaded layers is that the finite strain theory yields higher excess pore pressures, except for a small zone in the center of the layer, at a given degree of consolidation than the conventional theory (Mikasa, 1965; Gibson, Schiffman, and Cargill, 1981). As remarked by Gibson, Schiffman, and Cargill, this has important ramifications on possible effective stress strength analyses.

In the conventional theory, the degree of excess pore pressure dissipation and the degree of settlement with respect to time are the same. However, for a loaded layer, the finite strain theory predicts a settlement rate which is faster than the dissipation rate (Schiffman, Pane, and Gibson, 1984).

Double drainage in a nonlinear finite strain analysis will not be as beneficial as it would in a conventional analysis. This is due to the finite strain theory allowing the non-linear properties of the soil to form a "cake" at the drainage boundary, hindering the drainage (Schiffman, Pane, and Gibson, 1984; Croce et al., 1984).

As the load on the clay layer becomes smaller with respect to the thickness of the deposit, the effect of the self-weight becomes more apparent. Excess pore pressure isochrones from Gibson, Schiffman, and Cargill (1981) show that the finite strain theory predicts higher excess pore pressures in the lower portion than the conventional theory and the reverse in the top end. This skew, for lightly loaded double drained systems, is a result of the self weight being taken into account in the finite strain theory. The infinitesimal strain theory isochrones remained symmetrical.

Consolidation rates predicted by the finite strain theory for lightly loaded clay layers were, as would be expected, faster than those predicted by the conventional theory.

In areas such as mine tailings ponds, dredge deposits, and deltaic formation, comparisons against a linear infinitesimal strain theory (Gibson, 1958) are difficult, since the small strain theory doesn't allow for a change in height from consolidation. However, pore pressures and effective stresses for the two theories were compared, against a normalized height (Schiffman, Pane, and Gibson, 1984; Schiffman and Cargill, 1981). Schiffman and Cargill revealed that for a deposit being formed by sedimentation, the excess pore water pressure predicted by the finite strain theory is less than that predicted by infinitesimal strain theory for low sedimentation rates. As the rates

increased, the finite strain predicted higher excess pore pressures at the bottom of the layer, showing an effect of the self weight. A proper analysis could therefore show a greater effective stress in the deposit than that revealed by conventional analysis (Schiffman and Cargill, 1981).

When modelling a mine tailings pond, Schiffman, Pane, and Gibson (1984) concluded that infinitesimal strain theories are "incapable of reconstructing (or constructing) a rational consistent height time relationship" whereas the finite strain theory as developed by Gibson, England, and Hussey (1967) can be directly used for such a task.

3.3 Numerical Models used in Thesis

As mentioned in section 3.2.3, other methods of solving the governing equation (3.17) have been presented in the literature. Two methods employed in this thesis will now be discussed in general terms. Some of the other available methods will be briefly discussed in the following section.

3.3.1 Somogyi, 1980

The first method to be examined is that presented by Somogyi (1980). Somogyi follows Koppula (1970) in that he reformulates the governing equation in terms of excess pore pressure instead of void ratio, like the classical theory.

Somogyi begins with an equation developed by Koppula (1970) which is a rearrangement of the continuity and fluid flow relationships presented earlier,

$$\frac{\partial}{\partial z} \left[\frac{k}{\gamma_f (1+e)} \frac{\partial u}{\partial z} \right] + \frac{de}{d\sigma'} \frac{\partial \sigma}{\partial t} = 0 \quad (3.21)$$

A time dependent effective stress equation is then presented,

$$\frac{\partial \sigma'}{\partial t} = (D_R - 1) \gamma_f \frac{d(\Delta z)}{dt} - \frac{\partial u}{\partial t} \quad (3.22)$$

where D_R is the relative density of the solids and Δz the material coordinate difference between the surface and the point in question. Δz is time dependent for pond filling problems and equal to zero for quiescent problems.

Combining equations 3.21 and 3.22 leads to a governing equation in terms of excess pore pressure

$$\frac{\partial}{\partial z} \left[\frac{k}{\gamma_f (1+e)} \frac{\partial u}{\partial z} \right] + \frac{de}{d\sigma'} \left[(D_R - 1) \gamma_f \frac{d(\Delta z)}{dt} - \frac{\partial u}{\partial t} \right] = 0 \quad (3.23)$$

The approximation Somogyi then stipulates to handle the nonlinearity is that the $e - \sigma'$ relationship be restricted to the power law form

$$e = A \sigma'^B \quad (3.24)$$

where A and B are curve fitted constants. This leads to a revised governing equation

$$\frac{\partial u}{\partial t} + \frac{\sigma'^\beta}{a} \left(\frac{k}{1+e} \right) \frac{\partial^2 u}{\partial z^2} + \frac{\sigma'^\beta}{a} \frac{\partial \left(\frac{k}{1+e} \right)}{\partial z} \frac{\partial u}{\partial z} = \gamma_b \frac{d(\Delta z)}{dt} \quad (3.25)$$

where $\gamma_b = \gamma_s - \gamma_f$, $a = A B \gamma_f$ and $\beta = 1 - B$. Permeability will also later be forced to take the power law form

$$k = C e^D \quad (3.26)$$

where C and D are constants. The accuracy of the Somogyi method then, will highly depend on the closeness of relationships 3.24 and 3.26 to the true slurry behaviour.

Somogyi uses a fully implicit central finite difference method, because of its stability, to solve equation 3.25. The drawback of this method is that it requires u , σ' , e , and k at the next time increment to solve for u at the current time increment. To overcome this, the current time increment (j) values are substituted for the following time increment ($j+1$) values. The approximation is acceptable when Δt is small enough to ensure little variation in the parameters. Somogyi states that the stability of the implicit method will cause the errors introduced by the approximation to decay. The governing equation in terms of differences becomes

$$S_{i,j} \delta (K_{i,j} + D_{i,j}) u_{i+1,j+1} + (1 - 2S_{i,j} K_{i,j} \delta) u_{i,j+1} + S_{i,j} \delta (K_{i,j} - D_{i,j}) u_{i-1,j+1} = u_{i,j} + \gamma_b \Delta z \quad (3.27)$$

where, $S_{i,j} = \sigma'_{i,j} / a$, $K_{i,j} = k_{i,j} / (1 + e_{i,j})$, $D_{i,j} = 1/4 ((k_{i+1,j} / (1 + e_{i+1,j})) - (k_{i-1,j} / (1 + e_{i-1,j})))$, $\delta = \Delta t / (\Delta z)^2$, i is the material coordinate index, j is the time index, Δt is the time increment, and Δz now represents the material coordinate increment.

At an impermeable lower boundary, $v_s = v_f = 0$, which will cause Darcy's law, eqn. 3.10, to yield $\partial u / \partial z = 0$ which, in terms of central differences, becomes $u_{i+1,j} = u_{i-1,j}$. A permeable lower boundary will simply have the excess pore pressure equal to zero. The upper boundary for a pond filling problem, will be defined by an "immediate solids content" which defines the break between sedimentation and

consolidation. At this solids content a void ratio e_0 , effective stress σ'_0 , and permeability k_0 can be calculated. The excess pore pressure at the surface will be equal to zero.

The initial conditions for the pond filling case must be defined at $t = \Delta t$, not $t = 0$ since it is a trivial case. At $t = \Delta t$, $u = \gamma_b \Delta z$, $\sigma' = \sigma'_0$, $e = e_0$, and $k = k_0$. For a tank or standpipe problem where the initial filling is assumed instantaneous, the void ratio throughout is assumed constant and the excess pore pressure is then equal to the linear buoyant stress distribution, at time $t = 0$.

The governing difference equation, 3.27, combined with the boundary and initial conditions result in a set of simultaneous equations. The effective stress can be obtained from the resulting excess pore pressures, from which void ratios and permeabilities can be derived. Once the void ratios are obtained, the height of the slurry from the material coordinates can be readily obtained.

The soil parameter inputs, with respect to permeability and compressibility are then, the values of the constants A, B, C, and D for the $e - \sigma'$ and $k - e$ relationships, 3.24 and 3.26 respectively. These constants will generally be obtained from the laboratory.

3.3.2 Cargill, 1982

Cargill (1982) keeps the consolidation equation in terms of void ratio, but rewrites the equation in the

following form,

$$\left[\gamma_b \psi(e) + \frac{\partial \phi(e)}{\partial z} \right] \frac{\partial e}{\partial z} + \phi(e) \frac{\partial^2 e}{\partial z^2} + \gamma_f \frac{\partial e}{\partial t} = 0 \quad (3.28)$$

where $\phi(e) = \frac{k(e) \frac{d\sigma'}{de}}{1+e}$ and $\psi(e) = \frac{d}{de} \left[\frac{k(e)}{1+e} \right]$. The terms $\phi(e)$ and $\psi(e)$ represent the nonlinearity of the problem.

Point data relating void ratio to effective stress and permeability are used as input. From the $e-\sigma'$ data and $e-k$ data, $\phi(e)$ and $\psi(e)$ for the point data can be determined by numerical differentiation. To simulate the equation nonlinearity, $\phi(e)$ and $\psi(e)$ can be continually updated by interpolating from the point data ϕ and ψ values for the appropriate void ratio.

In his paper, Cargill uses an explicit finite difference scheme to solve equation 3.28. In terms of differences, equation 3.28 becomes

$$e_{i,j+1} = e_{i,j} - \frac{\Delta t}{\gamma_f} \left[\gamma_b \psi(e_{i,j}) + \left[\frac{\phi(e_{i+1,j}) - \phi(e_{i-1,j})}{2(\Delta z)} \right] \right] \\ \left[\frac{e_{i+1,j} - e_{i-1,j}}{2(\Delta z)} \right] + \frac{\Delta t}{\gamma_f} \phi(e_{i,j}) \left[\frac{e_{i+1,j} - 2e_{i,j} + e_{i-1,j}}{(\Delta z)^2} \right] \quad (3.29)$$

The boundary conditions need now to be represented in terms of void ratio. For a permeable base, $u=0$, which implies that the effective stress is equal to the buoyant stress of the material above it. Knowing the effective stress allows the void ratio to be interpolated from the $e-\sigma'$ data. For an impermeable base, $v_s=v_f=0$ causes the fluid flow relationship (3.17) to eventually yield

$$\frac{\partial e}{\partial z} + \gamma_b / \left(\frac{d\sigma'}{de} \right) = 0 \quad (3.30)$$

and in terms of differences

$$e_{0,j} = e_{2,j} + 2(\Delta z)\gamma_b \left(\frac{de}{d\sigma'}\right)_{e_{1,j}} \quad (3.31)$$

where $e_{1,j}$ is the void ratio at the base, $e_{0,j}$ is a fictitious point Δz below the base and $\left(\frac{de}{d\sigma'}\right)_{e_{1,j}}$ is interpolated from the $e-\sigma'$ data. The top boundary will again be e_0 corresponding to the immediate solids content for the pond filling case.

The initial conditions for the tank (instantaneous filling) problem specifies a constant void ratio throughout. For the pond filling problem, Cargill restricted himself to adding large layers at constant void ratios at various time intervals (i.e., once per year). However, this is easily modified to allow for continual gradual filling and the initial conditions, at $t=\Delta t$, are equal to e_0 .

With the initial and boundary conditions, equation 3.29 can be solved directly to yield the void ratios for the next time step. Once completed, the height of the slurry can be obtained using the material coordinates, and $\phi(e)$ and $\psi(e)$ can then be updated from the $\sigma'-e-k$ data in the manner previously described.

As mentioned earlier, the soil parameter input necessary for this method is a table of effective stress, void ratio, permeability data for the slurry. This type of input does not restrict the shape of the compressibility and permeability curves. The data should cover a large range and have many points to aid in the accuracy of the interpolation procedure.

3.3.3 Comparison of Results from the Two Methods

It is beneficial to determine the discrepancy in output from the Somogyi (1980) and Cargill (1982) methods that is caused by the procedures themselves, not including the differences caused by the differing input requirements.

Eliminating the input differences is possible by substituting the compressibility and permeability power law relationships (3.24 and 3.26), used by Somogyi, into the $\phi(e)$ and $\psi(e)$ terms used by Cargill. Doing this results in

$$\phi(e) = \frac{C e^D}{1 + e} \left[\left(\frac{1}{A}\right)^{1/B} \cdot \frac{1}{B} e^{(1/B-1)} \right] \quad (3.32)$$

$$\psi(e) = \frac{CD e^{(D-1)}}{1 + e} - \frac{C e^D}{(1+e)^2} \quad (3.33)$$

Three sets of parameters (shown in Table 3.1) were used for the compressibility and permeability relationships for the computer program comparison runs. Each run simulated a 10 m depth of slurry which had been instantaneously placed (tank problem). The bottom boundary was impermeable.

For the first set of parameters, the run simulated a consolidation period of 1600 days. The second and third set had a consolidation period of 900 days. The same time and material coordinate increments were used for both programs.

The results, which are shown in Table 3.2, indicate that with similar input, the two methods (Somogyi (1980) and Cargill (1982)) yield virtually identical results with respect to rate and amount of consolidation. When excess pore pressure and solids content against depth are compared, the maximum difference between the two methods that occurs

Table 3.1 Constants used for Method Comparison Runs

Constant	Set #1	Set #2	Set #3
A	28.71	7.256	1.814
B	-.3097	-.2052	-.09929
C	7.43E-11	5.61E-10	2.13E-10
D	3.847	3.927	3.794

Table 3.2 Results of Computer Runs with Common Input

Method	Height of Slurry (m)		
	Set #1	Set #2	Set #3
Somogyi	9.10	8.85	9.27
Cargill	9.10	8.82	9.26

is 0.75% at any given time for all three sets of data.

The difficulty of using laboratory point data for compressibility and permeability will be discussed in a later section. It would seem therefore, that if the power law relationships can satisfactorily describe the slurry behaviour, the Somogyi method will be adequate in modelling the finite strain consolidation.

3.4 Other Methods of Analyses

There have been other methods of solving the governing equations presented in the literature. The methods vary in assumptions, usefulness, and complexity. Some of these methods will be briefly reviewed in this section.

3.4.1 Koppula (1970) and Koppula and Morgenstern (1982)

Koppula and Morgenstern (1982) present analyses and applications based on work by Koppula (1970). As previously noted Koppula rearranges the continuity and fluid flow relationships to derive equation 3.21. To handle nonlinearity, Koppula uses a stress-strain relationship presented by Janbu (1963)

$$\frac{de}{d\sigma'} = \left(\frac{de}{d\sigma'}\right)_0 \left(\frac{\sigma'}{\sigma'_0}\right)^p \quad (3.34)$$

where $\left(\frac{de}{d\sigma'}\right)_0$ is an arbitrary initial value and p is an empirical constant between 0 and -1. If p is kept as -1, as is done by the authors in their applications, then eqn. 3.34 implies that e varies linearly with logarithmic σ' .

The nonlinear permeability is represented by a relationship which is similar in form to 3.34

$$\frac{k}{1+e} = \left(\frac{k}{1+e}\right)_0 \left(\frac{\sigma'}{\sigma'_0}\right)^q \quad (3.35)$$

The compressibility and permeability relationships (3.34 and 3.35), a time variation of effective stress equation, and eqn. 3.21 combine to give a governing consolidation equation of the form

$$\begin{aligned} \left(\frac{\sigma'}{\sigma'_0}\right)^{q-p} \frac{1}{(1+e_0)^2} \frac{\partial^2 u}{\partial z^2} &= \frac{\partial u}{\partial T} - \frac{d(\Delta\sigma)}{dT} - \gamma_f \frac{\partial z}{\partial T} \int_0^z (1+e) dz \\ - \gamma_f \int_0^z \frac{\partial e}{\partial T} dz + \left(\frac{\sigma'}{\sigma'_0}\right)^{q-p} \frac{q}{(1+e)^2 \sigma'} &\left[\left(\frac{\partial u}{\partial z}\right)^2 + \frac{\partial u}{\partial z} \gamma_b \right] \end{aligned} \quad (3.36)$$

where $T = \frac{k_0(1+e_0)t}{\gamma_f (de/d\sigma')_0}$. The authors use an implicit finite difference scheme to solve the equation. Inputs to the program include values for p , q , $\left(\frac{k}{1+e}\right)_0$, $\left(\frac{de}{d\sigma'}\right)_0$ and k_0 , which can be obtained from laboratory data (or field data if available).

3.4.2 Lee and Sills (1981)

To solve the governing equation (3.17), Lee and Sills place severe restrictions on the soil parameters to obtain an equation which is readily solvable.

The compressibility and permeability relationships are required to be linear, and respectively are

$$\sigma' = C_1 - C_2 e \quad (3.37)$$

$$k = \gamma_f k_0 (1 + e) \quad (3.38)$$

where C_1 and C_2 are constants. By substituting 3.37 and 3.38 into 3.17, and making $g(e)$ (3.19) a constant, the governing

equation is reduced to the solvable form

$$\frac{\partial e}{\partial t} = g \frac{\partial^2 e}{\partial z^2} \quad (3.39)$$

The assumptions and restrictions placed by Lee and Sills (1981) are so severe as to virtually negate the theory for practical use.

3.4.3 Finite Element Methods

Monte and Krizek (1976) define the stress-strain relationship in terms of the constrained modulus, M , defined as $\frac{d\sigma'}{de}$ such that

$$M = C_3 + C_4 \epsilon \quad (3.40)$$

$$\text{where } \epsilon = \frac{e_0 - e}{1 + e_0} \quad (3.41)$$

The permeability relationship is given as

$$\frac{k(e)}{1 + e} = C_5 + C_6 e \quad (3.42)$$

where C_3 , C_4 , C_5 , and C_6 are empirical constants.

Substitution of 3.40, 3.41, and 3.42 into the governing equation, leads to (in terms of Lagrangian coordinates)

$$\frac{\partial}{\partial a} \left[\frac{k(e)}{\gamma_f (1+e)} \left(-M(e) \frac{\partial e}{\partial a} + \gamma_b \right) \right] + \frac{1}{1+e_0} \frac{\partial e}{\partial t} = 0 \quad (3.43)$$

For the numerical solution of this equation, Monte and Krizek applied a 'weighted residual' technique which creates a finite element discretization in the spatial variable and finite difference discretization in the time variable.

Yung (1984) applied the finite element program ADINAT (Automatic Dynamic Incremental Nonlinear Analysis of Temperatures) to one dimensional consolidation problems

including finite strain problems. When applying ADINAT to the finite strain theory (Gibson, England, and Hussey, 1967) for thick layers, Yung invoked the same assumptions as Gibson, Schiffman, and Cargill (1981) (see section 3.2.3). There was very good agreement between the results yielded by the finite element program and the results published by Gibson, Schiffman, and Cargill (1981).

3.4/4 Evaluation of Methods

The method presented by Koppula and Morgenstern (1982) has some similarities to Somogyi's method since Somogyi used part of Koppula's (1970) formulation. However, their compressibility and permeability relationships (3.34 and 3.35) are more complex (hydraulic conductivity is related to effective stress as well as void ratio) than Somogyi's (3.24 and 3.26) resulting in a more complex equation (3.36). The method is not lacking in generality, however its use in the literature has been limited.

The method presented by Lee and Sills (1981) is not a very useful method. The linearizing of the finite strain theory for ease of solution makes it nonapplicable to virtually every slurry.

Using finite element methods to model the governing equation (3.17) adds complexity and additional computer time to the analysis. Since finite difference techniques are adequate in modelling the equation (see following section), it is questionable whether using a finite element method is

worth the additional effort. Finite element methods, however, appear promising for use with complex boundary condition problems.

3.5 Experience with the Finite Strain Theory

The intent of this section is to show where the theory has been applied to practical applications in which field monitoring was undertaken to analyze the results from Finite Strain predictions. Also in this section, suggested modifications and enhancements to the theory will be briefly reviewed.

3.5.1 Practical Applications

One of the more controlled field studies was that reported by Glenister and Cooling (1984) on the consolidation of the red muds which result from the Alumina industry. A test pond, 100,000 m² by 15 m deep with four permanent monitoring stations was filled over a period of 29 months. Prior to the filling, laboratory tests were conducted to determine the consolidation and permeability power law coefficients to be used in the finite strain program based on Somogyi (1980). At the end of filling, field testing was undertaken to aid in determining the compressibility parameters. The results from the model showed very good agreement with the monitored solids content and pore pressure profiles.

Florida's phosphate mining industry results in a very high void ratio, slow consolidating clay slurry waste. Considerable work has been done surrounding the consolidation of this material (Bromwell and Carrier, 1979; Carrier, 1982; McVay, Townsend, and Bloomquist, 1986). Somogyi *et al.* (1981) modelled a tank test and an active disposal site of phosphatic clay waste. When their computer program was run with permeability data obtained from the field tests on the tanks and pond themselves, the results showed a good correlation between predicted and actual solids contents for the tanks and heights for the pond. In 1984, Somogyi *et al.* conducted extensive laboratory and field tests to determine the permeability and compressibility characteristics of the phosphatic clay wastes to aid in predicting the behaviour of a test pit 12 m deep by 90 m by 370 m. Agreement between the predicted and actual test pit results (average solids content with time) was finally achieved when seepage at the base of the pit was taken into account in the computer program.

Shiffman, Pane, and Gibson (1984) predicted within 3 % the height of a copper waste slurry in a Bethlehem tailings pond at the 9 year mark. The tailings pond had been subjected to variable filling rates.

As well as mine tailings predictions, finite strain theory has been used to analyze deltaic sediment deposits because of the problems induced by underconsolidation. Koppula (1970, 1985) and Koppula and Morgenstern (1982)

predicted void ratio profiles of deltaic deposits of the continental shelf off the United States with reasonable success, considering the varying conditions over the long time periods involved in forming the deposits which are reflected in the scattered field data.

3.5.2 Possible Modifications and or Extensions

Due to large secondary consolidation strains exhibited by soft deposits (Gibson, Schiffman, and Cargill, 1981), it would seem appropriate that the finite strain theory be extended to include creep rates.

Analyses of tailings ponds which are relatively narrow could benefit from a two or three dimensional finite strain theory. Work has been done towards this end (Somogyi *et al.*, 1984, and Carrier, Bromwell, and Somogyi, 1981).

A multi phase finite strain theory would be of obvious benefit to oil sand sludge analysis as well as highly organic slurries (Schiffman, Pane, and Gibson, 1984). A theory which allows for non gravitational consolidation inducement such as temperature, electrical, or chemical gradients could be of use in certain circumstances (Schiffman, Pane, and Gibson, 1984).

Pañe and Schiffman (1985) proposed an extension to the theory which incorporates the sedimentation process. This would be useful for materials which exhibit a non sharp transition between a dispersion and a soil.

4. CONSOLIDATION AND PERMEABILITY TESTS

The University of Alberta currently has two 10 metre tall - 0.91 metre diameter standpipes containing oil sand tailings sludge and a sludge-sand mix respectively. The standpipes are designated as Standpipes #1 and #3 respectively. The standpipe #3 sludge-sand mix was formed by adding tailings sand to a sludge-sand mix which was previously in the standpipe. This previous sludge-sand mix was designated as 10 m standpipe test #2.

These standpipes represent a very large scale model of a sludge consolidation problem, the next step in size being the actual pond. The benefit of the standpipes is that detailed monitoring of the consolidation process is carried out over the entire height of the mix.

The data obtained from these standpipes therefore allow one to use whatever slurry consolidation data and consolidation theories that are available to model the consolidation that has taken place in the standpipes. To do just that, a set of consolidation tests was performed on material representing that in the standpipes to obtain input data for the finite strain computer program.

This Chapter discusses the equipment and procedures used for the tests as well as the materials used in the tests.

4.1 Equipment

4.1.1 Overview

To use the finite strain theory for modelling or forecasting purposes, it is necessary to establish the permeability and compressibility relationships for the material in question. More specifically, what is required is how the void ratio varies with effective stress and how the permeability varies with the void ratio. Permeability is not solely a function of void ratio (Carmen, 1956), but for predictive purposes, a macroscopic approach towards permeability is reasonable and consistent.

To obtain the compressibility and permeability data required, a large strain slurry consolidometer was used (Figure 4.1). This apparatus allows one to obtain void ratio versus effective stress as well as being capable of conducting permeability tests at various stages. The permeability test capability prevents the need to back calculate the coefficient of permeability to determine a $k-e$ relationship.

A step loading procedure, similar to the oedometer test, was employed due to; its simplicity, the ability to add permeability testing to the procedure at a natural break (i.e., at the end of a consolidation increment), and an inversion of the finite strain theory to obtain the consolidation parameters is not necessary. The lack of employing an inversion technique eliminates the concern over

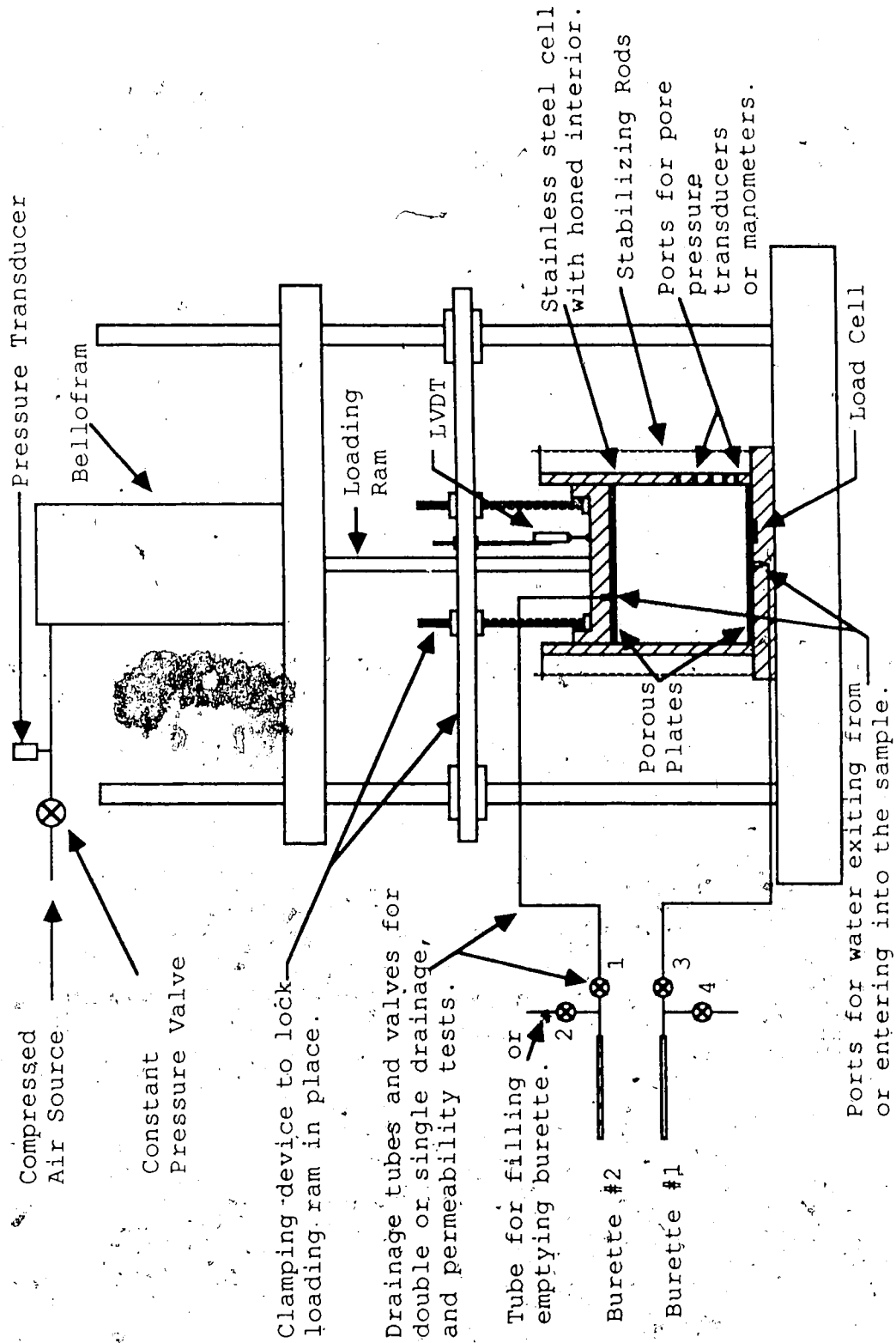


Figure 4.1 Slurry Consolidometer

errors introduced by the assumptions (Znidarcic *et al.*, 1984) necessary to an inversion. However, Somogyi *et al.*, (1984) showed very good correlation between permeability and compressibility parameters for phosphatic clay waste obtained from both step load and CRD tests. The disadvantage of the step load technique, as mentioned in Chapter 2, is the duration of the test.

A constant head technique was chosen for the permeability portion of the test. The constant head test allows for, extremely small head drops (less than 1 cm), as well as the ability to monitor any time effects (Olsen, Nichols, and Rice, 1985). A variable head test is not feasible for either of these two conditions. A constant flow pump might have the ability to produce slow enough flows so as not to induce consolidation, but the flows would be at the extreme bottom end of its range. Again, the major difficulty with the constant head test at low gradients (necessary to prevent consolidation) is the length of time involved per test.

Common to all permeability test methods is the danger of consolidating the slurry during the permeability test, which leads to obvious errors and uncertainties in interpreting the results. Consolidation occurs when the stresses introduced by the seepage force of the permeant is greater than the stress the sample was previously consolidated under. To overcome this problem, a clamping system (details in section 4.1.3) was used to fix the

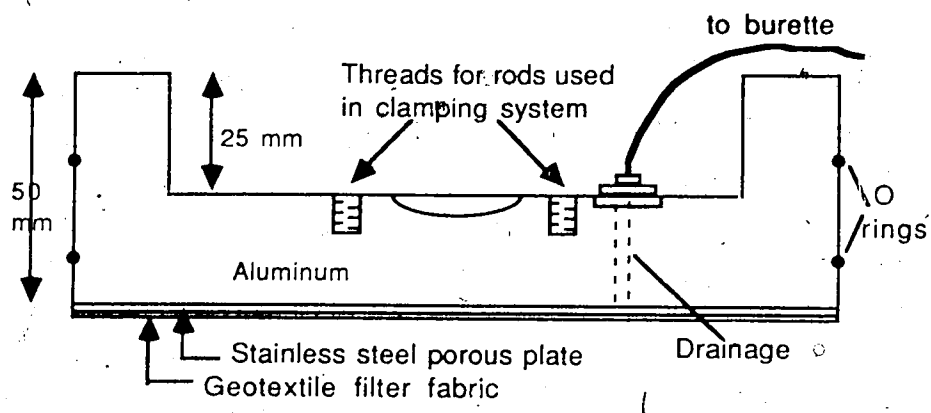
loading cap which sits on the soil, to prevent any movement from occurring. This system then allows a hydraulic gradient to be applied to the sample, up to a gradient where the induced seepage stress is equivalent to the just applied consolidation pressure. Beyond that gradient, prevention of consolidation is not possible.

Four slurry consolidometers were set up, two at the University of Alberta and two at the Syncrude Canada Limited (S.C.L.) research facility. The slurry consolidometers at the S.C.L. research facility were similar to those at U. of A. (Figure 4.1). Differences lay in the size, material used in some components, and no pore pressure ports on the consolidometers at the S.C.L. research facility.

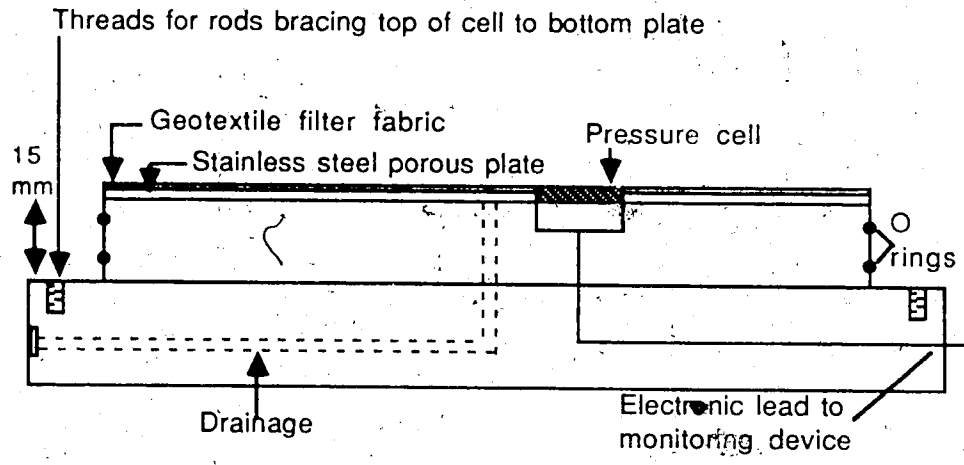
4.1.2 Consolidation Portion of the Slurry Consolidometer

At the U. of A., the cell, the portion of the consolidometers actually containing the sludge, had stainless steel walls with a 203.2 mm diameter honed interior and a 7.45 mm wall thickness. Along a vertical line on one side of the cell, were five 1/16 in. diameter holes to measure the pore pressure, placed at 20, 40, 80, 120, and 160 mm from the bottom. The ports had leads to a Delta P pressure transducer (specifications in Appendix A).

The top (loading) cap and bottom plate (Figure 4.2) were made out of aluminum. Stainless steel was desirable for the cell walls, since scarring from sand grains might allow seepage past the exterior of the top cap if a less durable



TOP CAP



BOTTOM PLATE

Figure 4.2 Top Cap and Bottom Plate Sections

product were used. Since this was not a concern for either the top cap or bottom plate, and weight of the top cap was a concern, aluminum was used. Both the top cap and bottom plates had a network of grooves connecting to external ports to facilitate the transfer of water from the sludge. Stainless steel porous plates were attached to the grooved surfaces, which in turn had a geotextile filter fastened to them (specifications in Appendix A). Geotextiles were used over paper filters because of their durability, which became apparent in a trial run.

The top cap had two "O" rings encircling it. The "O" rings were there to prevent any pore fluid from escaping as well as to minimize friction and aid in stability. The purpose for the raised circumference of the top cap was to increase stability of the cap with a minimum amount of additional weight. Minimizing the top cap weight was a concern for the first applied stress. The bottom plate had a pair of "O" rings around the raised center piece for sealing purposes. The cell body would sit on the bottom plate, surrounding the "O" rings on the raised center area. The cell body was fixed to the bottom plate by four rods which connected the bottom plate to a ring which sat on top of the cell body (see Figure 4.1).

The bottom plate had a pressure cell (see Appendix A for details) mounted in it such that it was flush with the bottom of the cell. The pressure cell aided in determining how much, if any, friction was being created by the soil

along the cell walls.

Since the applied stress range was so great (0.2 to 400 kPa), two types of loading devices were used. For the low stresses (up to 25 kPa) a rod and plate system was used. The required dead weight was placed on a plate which was connected to a rod. The rod, which had a spherical groove, rested on a stainless steel ball which was placed in a groove in the top cap. The ball and groove minimizes any torque being applied to the system. For the higher loads, a compressed air system was used to transfer the force to the loading cap. A Bellofram diaphragm system (specifications in Appendix A) was required to transfer the compressed air pressure to a loading ram, which was also grooved. A regulator and pressure gauge between the bellofram and compressed air source controlled the incoming pressure.

An LVDT (Linear Variable Displacement Transducer, details in Appendix A) with a 50 mm core was used to monitor the travel of the top cap during consolidation.

The data logging of the Electronic components was partly done on a Hewlett Packard 3497A Data Acquisition Control Unit which monitored and recorded the data. Also present were Fluke 8050A Digital Multimeters which gave an immediate read out only, of any of the electronic measuring devices.

The frame supporting the system consisted of a steel channel section on which the cell rested, another steel channel which either supported the bellofram or acted as a

guide for the plate-rod loading system, and four 1/2 in. steel rods separating the two steel sections (see Figure 4.1).

The consolidometers at the S.C.L. research facility were similar to the above description except in the following respects. The inside diameter was 301.5 mm. The cell was made out of aluminum except for the inside walls, which consisted of a teflon lining. The cells also had no pore pressure ports or load cell and the load cap travel was measured by a displacement dial. For a supplemental description of the S.C.L. consolidometers, see Isaac (1987).

4.1.3 Permeability Portion of the Slurry Consolidometer

When performing permeability tests on slurries, the applied hydraulic gradients can cause consolidation to occur during the test (Pane *et al.*, 1983). To overcome this, a clamping device (shown in Figure 4.1) was set up to help prevent consolidation from occurring. The device consisted of a horizontal 50 mm by 50 mm steel bar which was fastened to two vertical frame rods. Two 9.5 mm steel all thread rods were fastened to the top cap, and were allowed to travel vertically through the steel bar through bored holes. To prevent any further movement at the end of the consolidation increment, nuts were then used to clamp the two rods to the steel bar. The LVDT was kept in place to monitor the exact location of the cap throughout the process.

This apparatus ensures that hydraulic gradients could be used up to the value that causes the seepage pressure to equal the previously applied stress, which works out to a maximum head difference (Δh) for each increment of σ'/γ_w . The reason for this is that since the top cap is fixed in space, and the soil beneath it is consolidated under a stress, σ' , the soil will not consolidate unless subjected to a stress (seepage pressure) greater than σ' .

For reasons described in the previous section, a constant head technique was used to evaluate the permeability of the slurry at the fixed void ratio. Because the flows were so small (initially due to the low gradients, later on due to low permeability) it was possible to monitor the flows with horizontal burettes whose inside diameter was small enough to maintain a vertical meniscus. Burettes of the same size were used for monitoring the inflow and outflow, and eliminated any meniscus correction. The burettes used were 5 or 10 ml capacity depending on the expected flow. A third burette, identical to the ones being used, was in the laboratory to monitor evaporation, which turned out to be unobservable over the duration of the tests.

Drainage tubes as shown in Figure 4.1, were used to facilitate draining and filling the lower and upper burettes respectively between permeability test runs.

A digital stopwatch was used to time the flow during the test. The beginning of the test was generally a two

person operation.

In the latter stress increments of the consolidation test, a compressed air system, shown in Figure 4.3, was used to deliver a large gradient to the sample. A pressure regulator controlled the air pressure to the water to be used for the permeability test. A Delta P pressure transducer monitored the pressure sent to the cell.

Permeability test apparatus at the S.C.L. research facility was the same as that just described, except that large gradient tests requiring an air pressure system were not conducted.

4.2 Procedure

4.2.1 Overview

The standard procedure for the consolidation and permeability tests was as follows (details and deviations are covered in the following sections). The slurry was allowed to finish consolidating under its own weight, with the bottom port opened to a head equalling that at the surface to allow for double drainage. Once completed, the top cap was put in the cell and lowered until it reached the sludge-water interface. The top cap was necessary to obtain a seal for the permeability test. Once lowered, the top cap was fixed in place by means of the clamping system previously described.

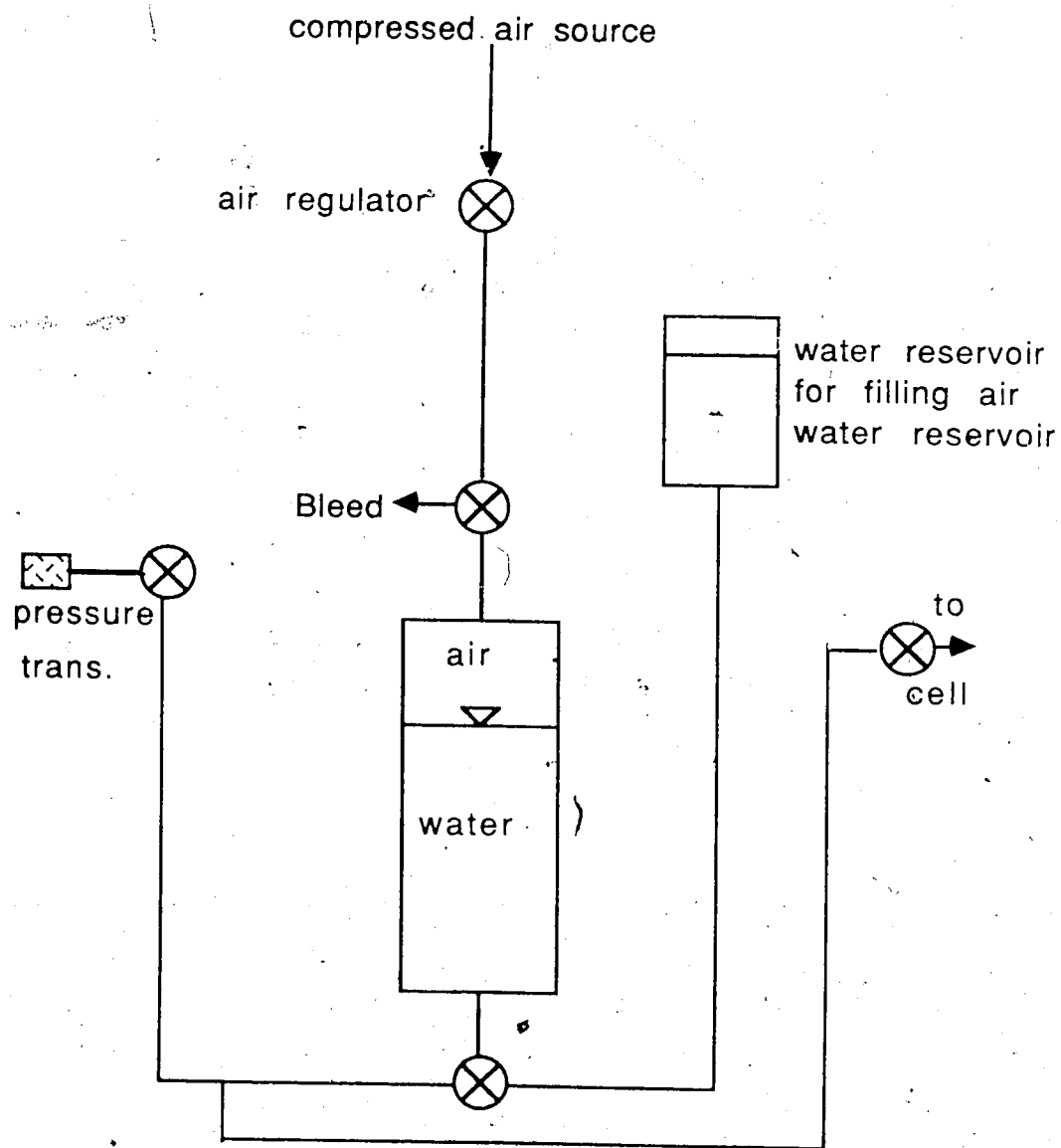


Figure 4.3 Compressed Air System for Large Gradients

Flow for the constant head permeability test for the self-weight stage was upward so as to prevent any consolidation. Once the desired head difference between the inflow and outflow burettes was set, the valves were opened and the flow was monitored in the burette against a stopwatch. Knowing the surface area (A), volume of flow (ΔV), and time period (Δt), the hydraulic conductivity (k) is easily calculated from a rearrangement of Darcy's Law

$$k = \frac{\Delta V \Delta t}{i A} \quad (4.1)$$

where i is the hydraulic gradient equal to the hydraulic head difference (Δh) divided by the height of the sample.

At the completion of the permeability tests, a test for cap friction was performed.

At the completion of the friction test, the required load necessary to give the desired stress plus friction was determined. The top cap was released from the clamping system and the load was applied. The pressure cell in the base of the cell and the pressure transducer attached to pore pressure ports monitored the load and pore pressures respectively, while the LVDT followed the displacement of the surface of the sludge with time. Knowing the amount of solids in the cell, the void ratio is obtained through the following equation

$$e_s = \frac{H - H_s}{H_s} \quad (4.2)$$

where H is the current sample height, and H_s is the height of solids in the sample.

Once it was decided that the consolidation increment was complete, the top cap is clamped and the permeability was determined for the above void ratio and the process is repeated.

4.2.2 Step Loading Consolidation Test

As the general procedure for the step loaded (or controlled stress) consolidation test has been described, this section will focus on some of the details and difficulties involved.

During the self weight consolidation increments, monitoring of the consolidation was done by measuring from the top of the cell to the sludge-water interface with a caliper (accuracy to 0.05 mm). Fortunately the sludge-water interface was sharp and easily discernable allowing for good measurements for all the slurries including the straight sludge material.

The stress value ascribed to the self weight stages was estimated as the average bouyant stress in the sample, taken to be the stress half way down the sample. This was an estimate since the actual effective stress in the slurry would range nonlinearly from the full bouyant stress of the slurry at the bottom to zero at the top. Likewise, the void ratio as calculated by equation 4.2 is slightly in error due to the void ratio varying nonlinearly in the sample. However, the nonlinearity over such a small height is negligible in comparison to the stress ranges that was dealt

with, that the linear assumption within the sample is justified.

The applied stress increments varied for the four tests, but a stress increase equal to the total previous applied stress was aimed for. Factors such as friction (both from the top cap and soil) and pressure system restraints influenced the actual applied stress. The applied stress increments ranged from 0.22 kPa to 650 kPa for the straight sludge, and from 0.2 kPa to 460 kPa for the sand sludge mixtures (see Chapter 5 for more detail).

For all the increments, a double drainage condition was provided to facilitate the consolidation. This was achieved by maintaining the burettes, connected to the drainage ports, at the same height as the slurry surface. Since the initial applied stresses were small, it was necessary during consolidation to continually adjust the burettes to the height of slurry surface, in order to prevent any internal pore pressure from reducing the applied stress in the sealed system.

Another difficulty emphasized by the small load increments was that of the friction between the top cap and cell wall. A series of tests were performed before the cells were filled with the slurry, to determine the static and dynamic friction of the top cap. Supplementary to those tests, friction tests were conducted before the application of each load increment.

For these tests, the top cap was released from the clamping system at the end of the permeability tests. The bottom port was then closed. The burette was then removed from the tube connected to the top port. The tube was raised and water was poured down it until the top cap moved, and the elevation difference between the top cap and the level of water in the tube was then recorded. Knowing the mass and area of top cap, the level of water which it should be able to resist is known, and the difference is attributed to static friction. Dynamic friction was attributed to the steady state difference after the top cap initially moved. The process was repeated for consistency. It was then decided to use the dynamic friction value and to load the sample while the top cap was a few millimetres above the slurry surface, a running start.

The difficulty with the above procedure was the possibility of soil rebound. However, the LVDT readings at the start of the increment were compared with those at the end of the previous increment, and the small rebound was taken into account.

During the test, gas bubbles were observed to be coming from the sample into the tubes connected to drainage ports. The gas was sampled and analyzed, and was found to be virtually all methane. The technique described above of starting the loading with the load cap above the sample aided in clearing the lines. There didn't appear to be any pattern in the amount of gas that would form, or when it

would form.

4.2.3 Constant Head Permeability Test

This section will focus mainly on some of the details of the permeability test.

The permeant used in the permeability tests was either the pore fluid that was forced out during the consolidation or decant from the container of slurry from which the sample was taken. This was done to achieve results consistent with what would be found in the field, since a change in pore fluid chemistry may somewhat affect the permeability.

The gradients applied to the sample ranged from a couple centimetres divided by the sample height to maximum gradient before consolidation would occur. The maximum gradient was defined under discussion of the clamping system in the equipment section. Initially the flow was upward through the sample, in order to use self weight of the material to help prevent consolidation during the permeability run.

Several permeability test runs were performed at each gradient to achieve experimentally consistent results as well as to check the repeatability of some of the initial behaviour. Three situations were occurring; no flow, delayed flow, or initial rapid flow. The no flow state seemed to occur at the lower gradients. The delayed flow condition showed no consistency as to when it would occur. Of the three behaviours, only the initial rapid flow phenomenon

appeared often and with consistency and repeatability and is discussed in detail in Chapter 5. The other two may be caused by gas and are briefly discussed on in Chapter 5.

As was just mentioned, gas formation did occur periodically, causing some problems. The gas formation was a factor which probably introduced some not easily identifiable error into the results.

When the slurry became more like a soil under the higher stresses, high gradient tests became both possible and desirable since it was taking days to produce a few millilitres under the lower gradients. The pressure system, as shown in Figure 4.3, was connected to the cell and, combined with the standard low gradient tests, gradients ranging from 1.0 to 400 were achieved. A series of tests were performed to determine whether the direction of flow affected the results, whether the permeability result at a gradient would change if the gradient was approached from the high or low end, and what the the effect of very large gradients would be (with respect to linearity and Darcy's Law).

4.3 Test Material

4.3.1 Specifications

To model the consolidation of the sludge and sludge-sand mixes in the three 10 m standpipes, it was necessary to obtain compressibility and permeability data

from material similar in bitumen and fines content to the standpipe material. Standpipe #1 contains sludge without admixtures. Standpipes #2 contained and #3 contains sludge with varying amounts of additional sand, and were set up to examine and compare the effects of sand on the consolidation process. Figure 4.4 shows the material breakdown of the mixes in the standpipe on a slurry properties diagram. The fines break is arbitrary and is set at 0.044 mm (#325 sieve). Table 4.1 has some of the standpipe material properties listed. Note that the total solids is taken as the sum of the mineral grains and the bitumen. That is, the bitumen is considered to be a solid in all calculations. The bitumen content is defined as the mass of bitumen over the mass of mineral grains only, to be somewhat geotechnically consistent. The relative density of the sludge solids is a weighted average of the bitumen and mineral portions and is defined as follows

$$D_{R_{ss}} = \frac{b + 1}{b/D_{R_b} + 1/D_{R_s}} \quad (4.3)$$

where b is the bitumen content as defined above, D_{R_b} is the relative density of the bitumen (1.03) and D_{R_s} is the relative density of the mineral grains (2.65). The grain size distribution of the standpipe material is shown in Figure 4.5.

Details on the standpipe testing program are presented in work by Scott and Chichak (1985a, 1985b, 1985c).

Additional to modelling the consolidation of the material in the 10m standpipes, it was desired to examine

Table 4.1 Ten Metre Standpipe Material Properties

	Standpipe #1	Standpipe #2	Standpipe #3
Initial Solids Content	32.4 %	47.8 %	74.8 %
% Sand of Total Solids (by weight)	11 %	45 %	82 %
% Fines of Total Solids (by weight)	89 %	55 %	18%
% Bitumen of Mineral Grains (by weight)	8.6 %	5.6 %	1.6 %
Relative Density of Sludge Solids ($D_{R_{SS}}$)	2.35	2.45	2.59
Bulk Density (kg/m^3)	1221	1388	1810

Table 4.2 Consolidometer Test Material Properties

	Test #1	Test #2	Test #3	Test #4
Initial Solids Content	29.1 %	47.7 %	69.7 %	52.0 %
% Sand of Total Solids (by weight)	8 %	46 %	80 %	73 %
% Fines of Total Solids (by weight)	92 %	54 %	20 %	27 %
% Bitumen of Mineral Grains (by weight)	7.1 %	3.6 %	1.5 %	1.4 %
Relative Density of Sludge Solids ($D_{R_{SS}}$)	2.39	2.51	2.59	2.59
Bulk Density (kg/m^3)	1204	1402	1748	1469

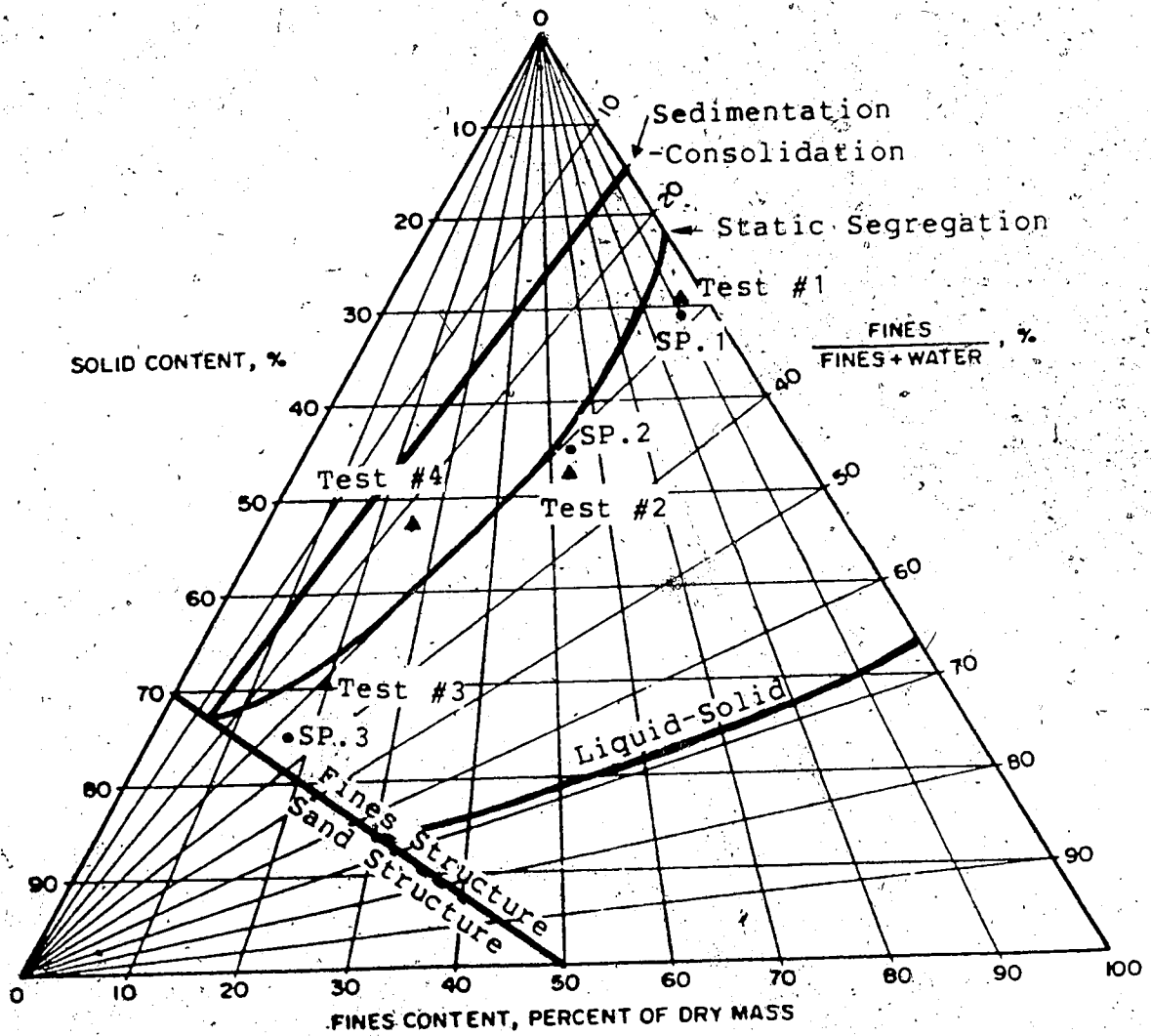


Figure 4.4 Slurry Properties Diagram for Standpipe and Consolidometer Test Material

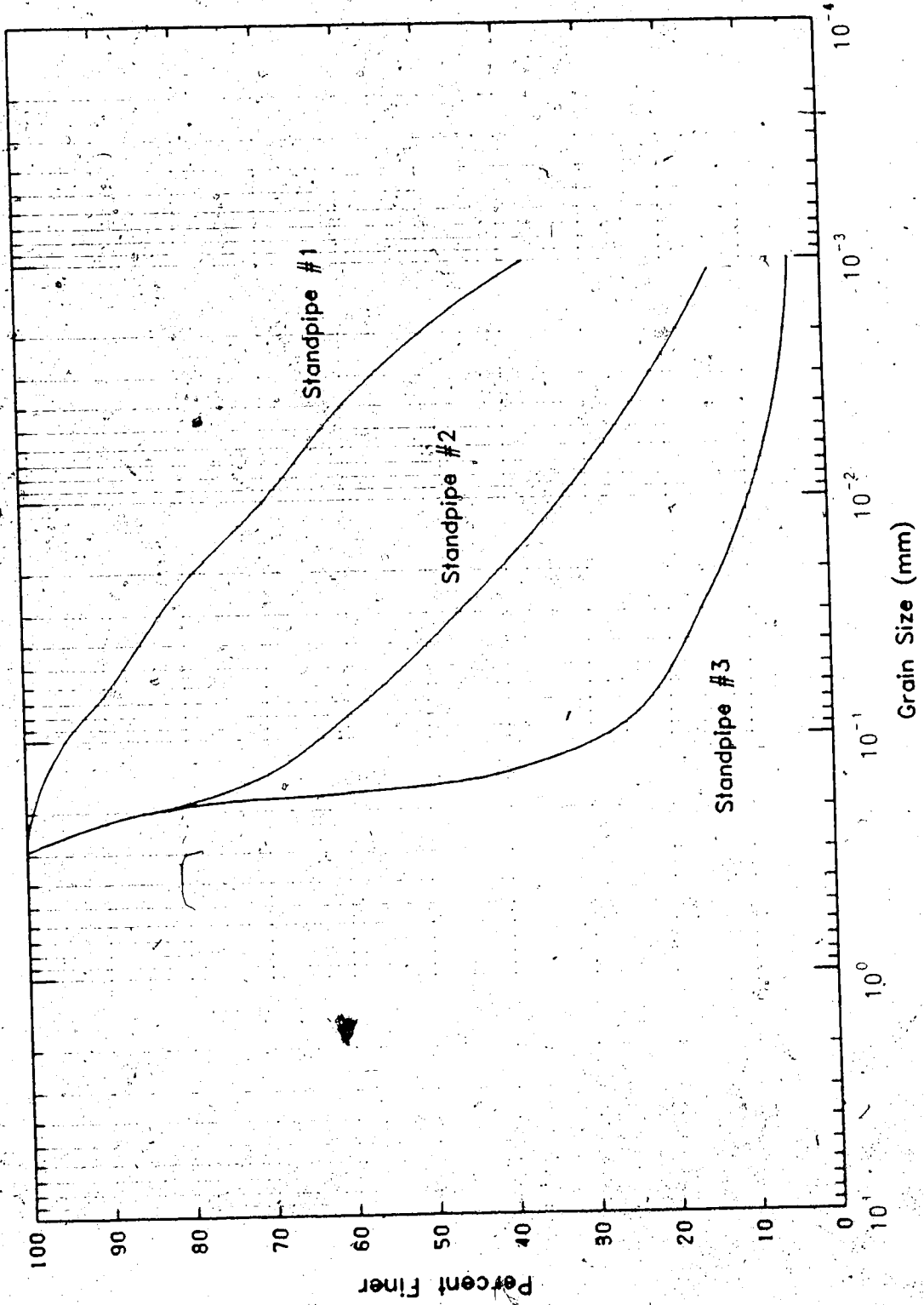


Figure 4.5 Grain Size Distribution of Standpipe Material

the effect of a chemical flocculent on the compressibility and permeability of a sludge-sand mixture.

Chemical flocculents have been suggested (Lane, 1983) for use in enhancing the consolidation of the sludge as opposed to enhancing the sedimentation. The desired quality of a flocculent is not in its ability to improve the consolidation properties of a slurry, but rather its ability to keep sand in suspension. A difficulty in using sand to quicken the consolidation of a slurry is that the sand will segregate out of the slurry when the water content is too high (or solids content too low). However, keeping the material pumpable for transport purposes combined with the moisture content of the slurry and sand make it nearly impossible to achieve a slurry capable of supporting sand. Flocculents help overcome this problem. Therefore a sludge-sand consolidometer test was set up in which CaCl_2 was added to keep the sand in suspension.

4.3.2 Sampling and Preparation.

To obtain test mixes that matched the previously discussed requirements, Syncrude Canada Ltd. provided sludge of about 32 to 34 % solids content. The sludge was taken from the Mildred Lake tailings pond located in northern Alberta on the Athabasca Oil Sand Deposit. The sludge was taken from the centre of the pond, approximately 25 m below the surface, in the "mature sludge" region in 1984. The material was suction pumped up to a barge which then

transferred the material at shore.

When the consolidation test was ready to begin, the sludge was thoroughly mixed in the drum in which it was received, with a mixing blade extension attached to a power drill. This was done to achieve a uniform material throughout the drum. A smaller sample, of known mass and a volume closer to that required, was then extracted and tests were subsequently performed on the material for solids content and bulk density. It was then possible to determine how much additional pond water was required to dilute the sludge to the desired solids content for the sludge with no admixture test. For the sludge-sand tests, tailing sand and pond water were added to achieve the desired mix.

Additional tests were performed on these slurries and, if necessary, additional components were added and index tests redone until the desired mixes were obtained. The calculated amount of CaCl_2 to achieve 250 ppm of solids was then added to one of the sludge-sand mixes that had been set aside for this purpose.

The slurry was poured in the consolidometer and filled to a height of about 23 cm. Desiring to end up with at least several centimetres of compressed material, 23 cm was chosen based on some preliminary compressibility data. The consolidometers with sludge-sand mixes were also filled to this height. The sludge-sand mix with the greatest amount of sand and least solids content was placed more than poured in. However, the mix was still quite mobile and trapping of

air was prevented.

Once the materials were in place, the consolidometers were covered to prevent evaporation, and self weight consolidation then proceeded. Before the load caps were applied, at the end of the self weight stage, it was necessary to remove some of the "free" bitumen which had collected on top of the surface water.

About 9560 cm³ of sludge and sludge-sand mix were put in the U. of A. consolidometers and approximately 16420 cm³ of sludge-sand mix in each of the S.C. consolidometers.

4.3.3 Test Material Description

The oil sand tailings sludge which formed the basis of the tests had a liquid limit of 41% and a plastic limit of 19%, which places it in the medium plastic clay section of the plasticity chart.

The sludge is quite odorous due to the bitumen. The sludge is extremely slick upon touch and the presence of bitumen becomes apparent when attempting to wash the slurry from ones hands.

Of the four tests set up, test #1 contained sludge with no sand admixture and was performed to obtain consolidation properties to model 10 m standpipe #1. Tests #2 and #3 contained sludge-sand mixtures and were performed to obtain consolidation properties to model 10m standpipes #2 and #3 respectively. Test #4 contained a sludge-sand mix and was performed to study the effect of a chemical flocculent.

Properties of the material used in the four tests are listed in Table 4.2 and shown on the slurry properties diagram in Figure 4.4, and a mass/volume breakdown is given in Table 4.3. The mixes generally started at solids contents slightly less than the standpipes they were to model, this was to allow the self weight stage to consolidate through the standpipe starting points. Note that the starting location of test #4, the sludge-sand mix with the chemical flocculent, is in the segregation region. Without the flocculent, the mix would normally have the sand segregate out when at this particular solids content with the particular fines and sand content.

Figure 4.6 shows the grain size distribution for each of the four tests. As can be seen in the Figure, the added tailings sand is predominantly #100 in size.

Table 4.3 Consolidometer Test Material Breakdown

	Test #1		Test #2		Test #3		Test #4	
	Mass g	Volume cm ³	Mass g	Volume cm ³	Mass g	Volume cm ³	Mass g	Volume cm ³
Larger than 0.044 m	28.0	10.6	307.6	116.1	974.7	367.8	557.6	210.4
Finer than 0.044 m	299.1	112.9	337.9	127.5	225.7	85.1	195.7	73.9
Bitumen	23.2	22.6	23.2	22.6	18.0	17.5	10.6	10.3
Water	853.7	853.7	733.3	733.3	529.6	529.6	705.1	705.1
Total	1204	1000	1402	1000	1748	1000	1469	1000

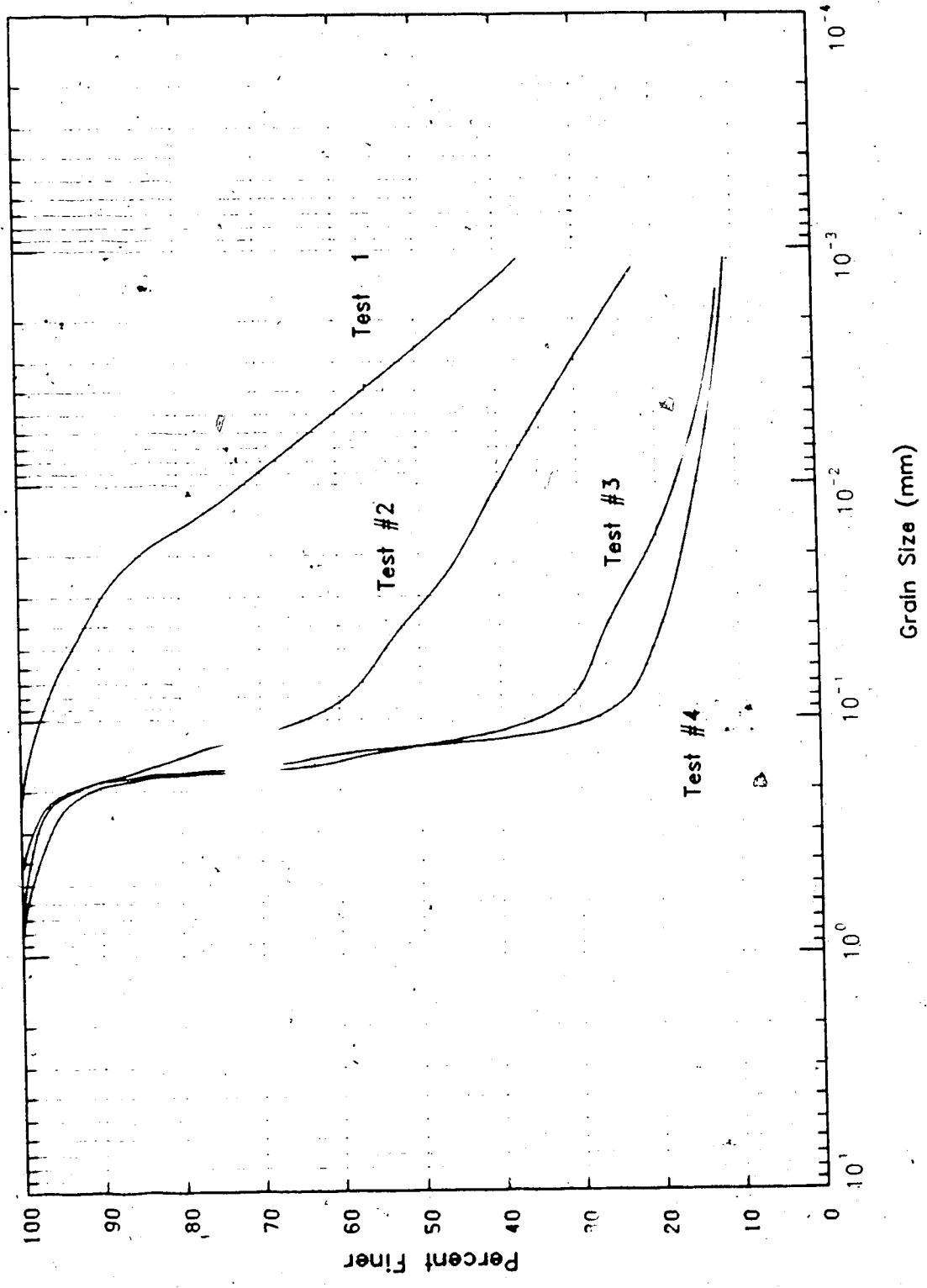


Figure 4.6 Grain Size Distribution of Test Material

5. LABORATORY TEST RESULTS

The results of the consolidometer tests on the four slurry materials are presented in this Chapter, along with associated observations and discussion. The consolidometer tests and the materials tested were discussed in the previous Chapter.

The test results can be broken down into two major categories; consolidation and compressibility results, that is the void ratio versus time and versus effective stress respectively, and the permeability test results.

The parameters required as input for the finite strain analyses are the void ratio versus effective stress data (compressibility), and the hydraulic conductivity versus void ratio data (permeability).

5.1 Consolidation Test Results

5.1.1 Consolidation Rates

5.1.1.1 Oil Sand Tailings Sludge

The oil sand tailings sludge tested has been described in Chapter 4 (see Tables 4.2 and 4.3, and Figures 4.4 and 4.6). The average effective self weight stress was determined to be 0.22 kPa. The effective stresses subjected to the sample, including self weight, were 0.22, 0.45, 0.9, 1.7, 5.0, 11.0, 25.0, 45.0, 100, 200, and 650 kPa.

The duration of the consolidation test and permeability tests was 1 year and 4 months. This time is from the start

of the self weight consolidation stage to the end of the last permeability test of the final stress increment.

Figure 5.1 shows the consolidation time rate plot for all the stresses applied to the sludge. Individual void ratio time plots are given in Appendix B.

For some of the smaller applied increments it was necessary to stop the consolidation before the displacement had levelled out on a logarithm time plot (see Figure 5.1). The reason for stopping the tests was one of practicality. Although, on the log time plot, the material appears to be rapidly consolidating, in reality the material has entered the 10^4 minutes cycle and little change occurs over a period of 1 week (1 week = 10080 minutes). As an example, Figure 5.2 shows the progress of consolidation under 0.9 kPa against linear time. It is obvious that the consolidation is very slowly levelling out, and allowing it to consolidate another week would result in a minor void ratio change (0.04, or 5.9% of the consolidation that increment).

Excess pore pressures at the ports have been plotted and are presented in Appendix C. Some of the results are erratic and are of some but limited value. The early stress increment pore pressure readings are more useful than at the later increments. The values fluctuated with a slight temperature change ($1.5\text{ }^{\circ}\text{C}$) almost synchronously. This suggests that gas, close to the room air existed, although its exact location was never determined. Nevertheless, some of the small plots show reasonable trends of excess pore

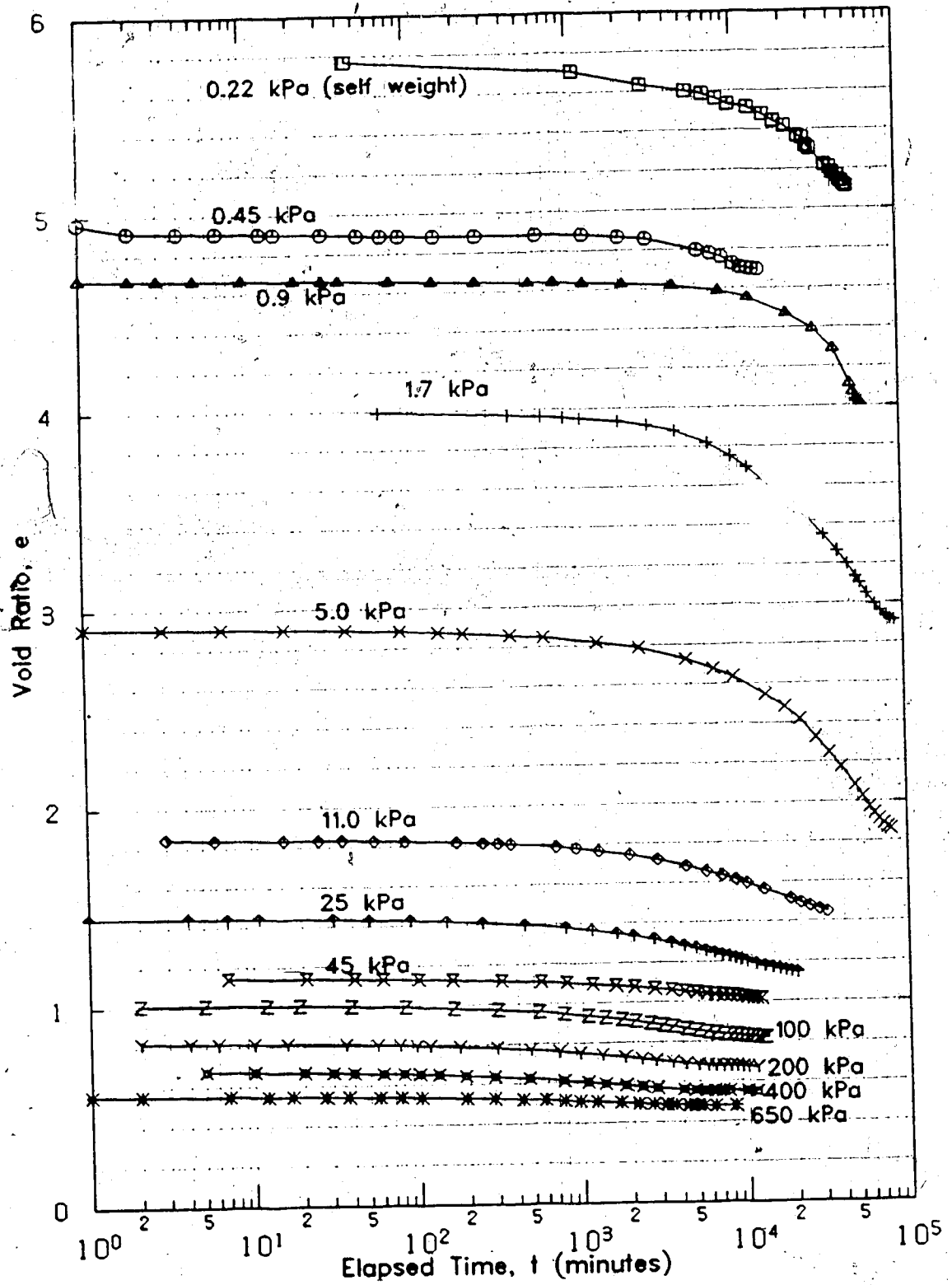


Figure 5.1 Consolidation of Oil Sand Tailings Sludge

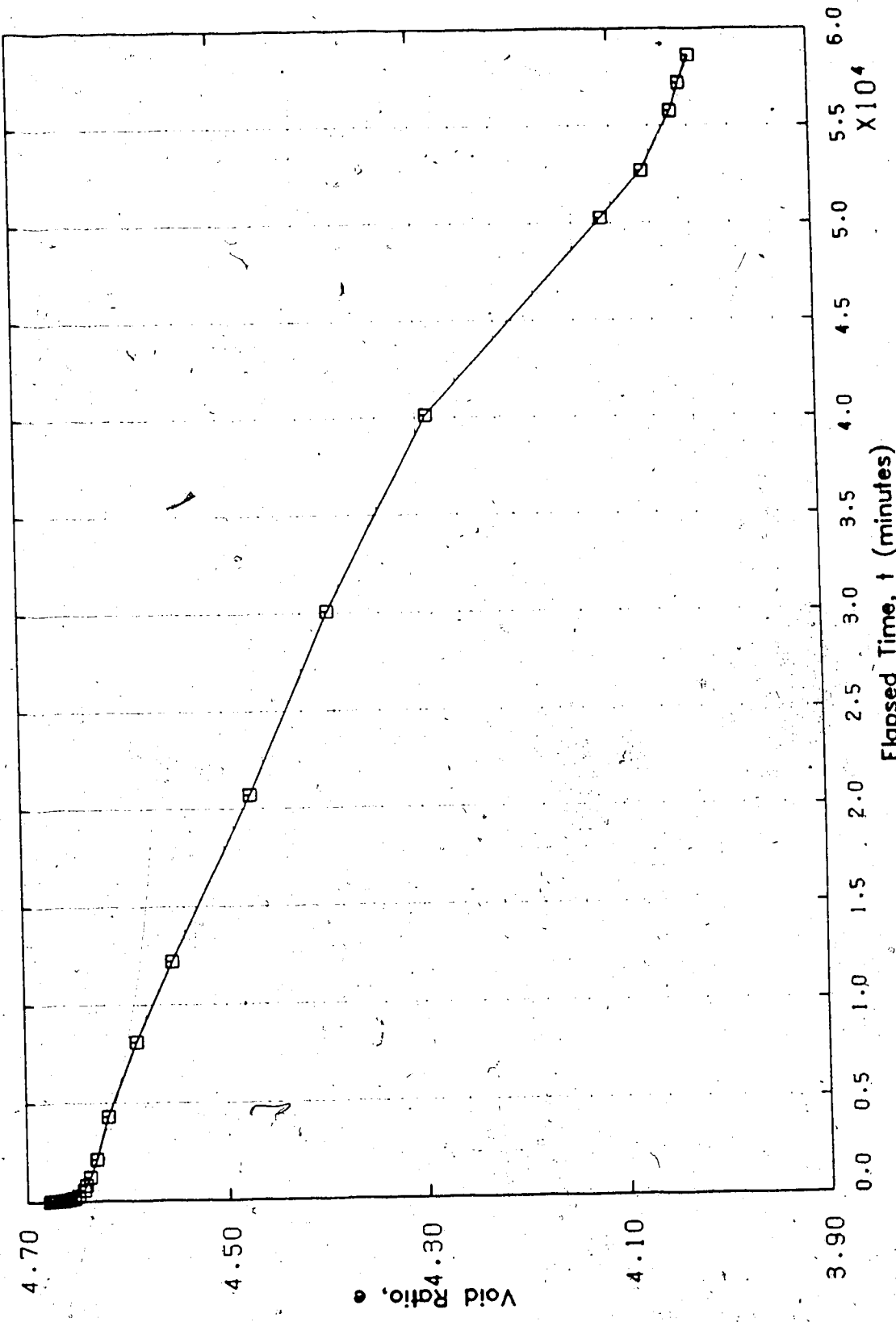


Figure 5.2 Consolidation of Sludge under 0.9 kPa

pressures decreasing from the applied stress increment towards zero at the conclusion of the increment. Several ports indicated a negative excess pore pressure existed at the end of the increment. It is not known if this is another indication of the pore pressure experimental difficulty or an indication of thixotropy. (Negative pore pressures have been observed in the 10 m standpipes and attributed to thixotropy, and Kolaian and Low's (1962) work show negative pore pressures occurring as result of thixotropy). Daily calibration of the pore pressure transducer indicates that a negative excess pressure is definitely being created. See Appendix C for further pore pressure discussion.

Apparent from Figure 5.1 is a shifting left (towards smaller time) of the consolidation curves as the stress increments increase and void ratios decrease. This trend becomes more apparent when comparing the individual curves for 0.9, 25, and 400 kPa (Figure 5.3). The Figure has a normalized void ratio (the change in e for that increment divided by the total change in e for that increment, $\Delta e_i / (e_i - e_{i-1})$) plotted against time. The consolidation curve for the 400 kPa stress increment is, and reasonably so, similar to curves for soil common to geotechnical practice. With the available data, it is not yet known whether this apparent consolidation delay for high void ratio materials under low applied stresses is a function of all slurries or specific to the oil sand tailings sludge.

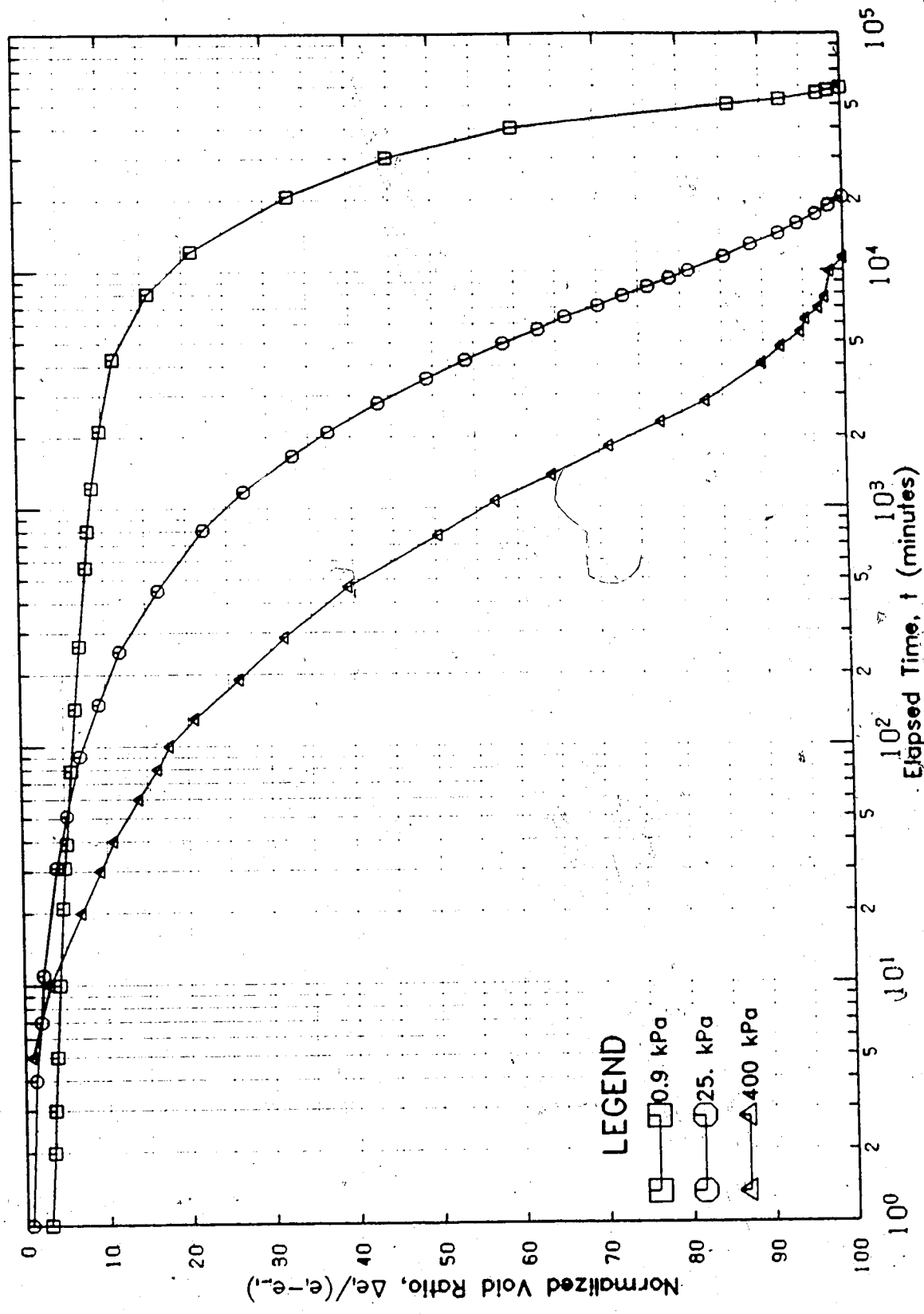


Figure 5.3 Normalized Consolidation, Sludge

5.1.1.2 Oil Sand Tailings Sludge-Sand Mixes

Tests #2 and #3 were performed on sludge with varying amounts of sand, #2 containing 46% sand and #3 containing 80% sand (see Tables 4.2 and 4.3, and Figures 4.4 and 4.6). The average self weight stresses of the mixes were determined to be 0.44 and 0.75 kPa for the 46% sand and 80% sand mixes respectively. The effective stresses subjected to the samples, including self weight were 0.44, 0.54, 0.64, 1.0, 1.75, 3.05, 6.25, 13.0, 25.5, 50.5, 100, 200, and 320 kPa for test #2, and 0.75, 0.85, 0.95, 1.3, 2.05, 3.4, 6.6, 13.3, 25.8, 51, 100, 150, 200, and 320 kPa for test #3.

The duration of the consolidation test and permeability tests was 10 months for each test. This time is from the start of the self weight consolidation stage to the end of the last permeability test of the final stress increment.

Figures 5.4 and 5.5 are summary plots containing all the consolidation increments for tests #2 and #3 respectively. The individual time plots are given in Appendix B.

The consolidometers in which tests #2 and #3 were performed did not have pore pressure ports, and the related data is therefore not available.

The trend that was observed for the sludge material, in which the low stress increment consolidation curves seemed to be delayed compared to the higher applied stress curves (Figure 5.3), is evident for the sludge-sand mixes as well, although it is not as pronounced as it is for the sludge.

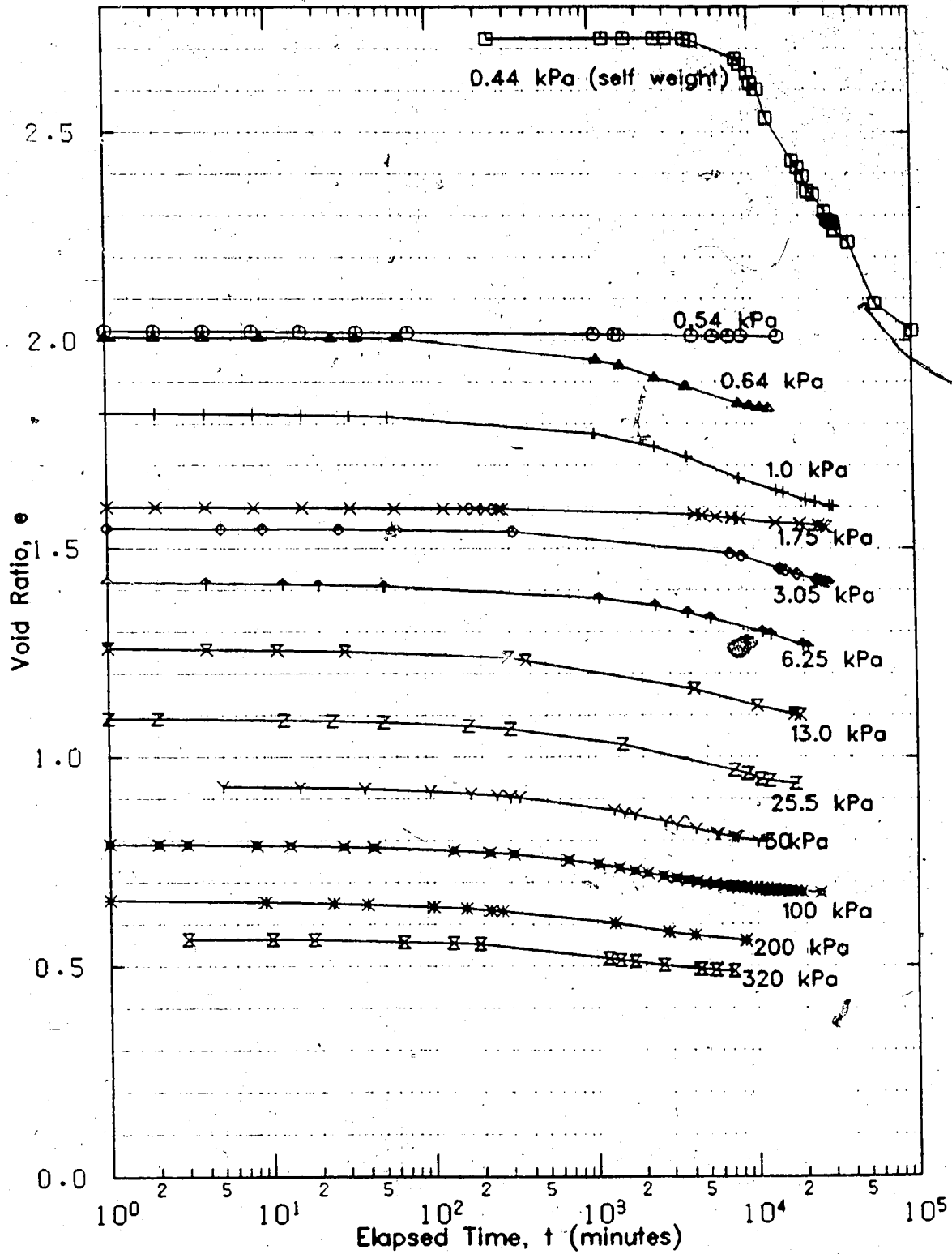


Figure 5.4 Consolidation of 46% Sand Sludge-Sand Mix

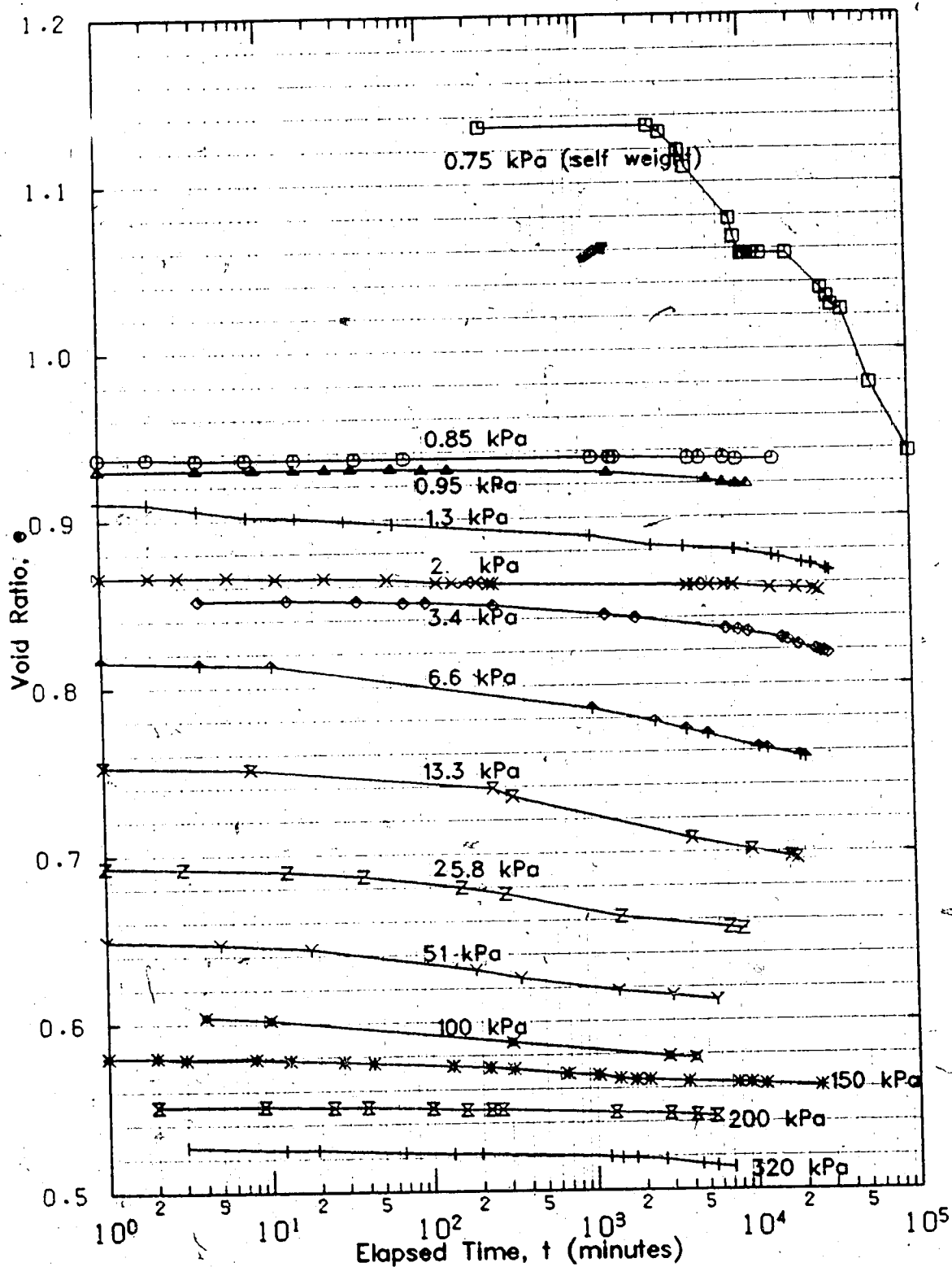


Figure 5.5 Consolidation of 80% Sand Sludge-Sand Mix

Figure 5.6 and 5.7 demonstrate this for the 46% sand and 80% sand sludge-sand mixes respectively, in which the previously defined normalized void ratio is plotted against time. The fact that this trend is evident for the sand sludge mixes tends to suggest that this phenomenon cannot be solely attributed to a thixotropic sludge strength since it would have very little effect on the 80% sand mix.

5.1.1.3 Oil Sand Tailings Sludge-Sand Mix with Flocculent

Test #4 was performed on a 73% sand sludge-sand mix with a chemical flocculent (CaCl_2) for purposes discussed in Chapter 4 (see Tables 4.2 and 4.3, and Figures 4.4 and 4.6 for the material properties). The average effective self weight stress for the mix was determined to be 0.53 kPa. The effective stresses, including the self weight, applied to the sample were 0.53, 1.0, 2.5, 5.0, 11.0, 23, 41, 86, 170, 353, and 463 kPa.

The duration of the consolidation test and permeability tests was 12 months. This time is from the start of the self weight consolidation stage to the end of the last permeability test of the final stress increment.

Figure 5.8 shows the consolidation time plot for all the stresses applied to the sludge-sand mix. Individual void ratio time plots are given in Appendix B.

Again, the trend of the consolidation curves shifting left is apparent, but not as evident as with the sludge (Figure 5.3). Figure 5.9 shows the normalized void ratio

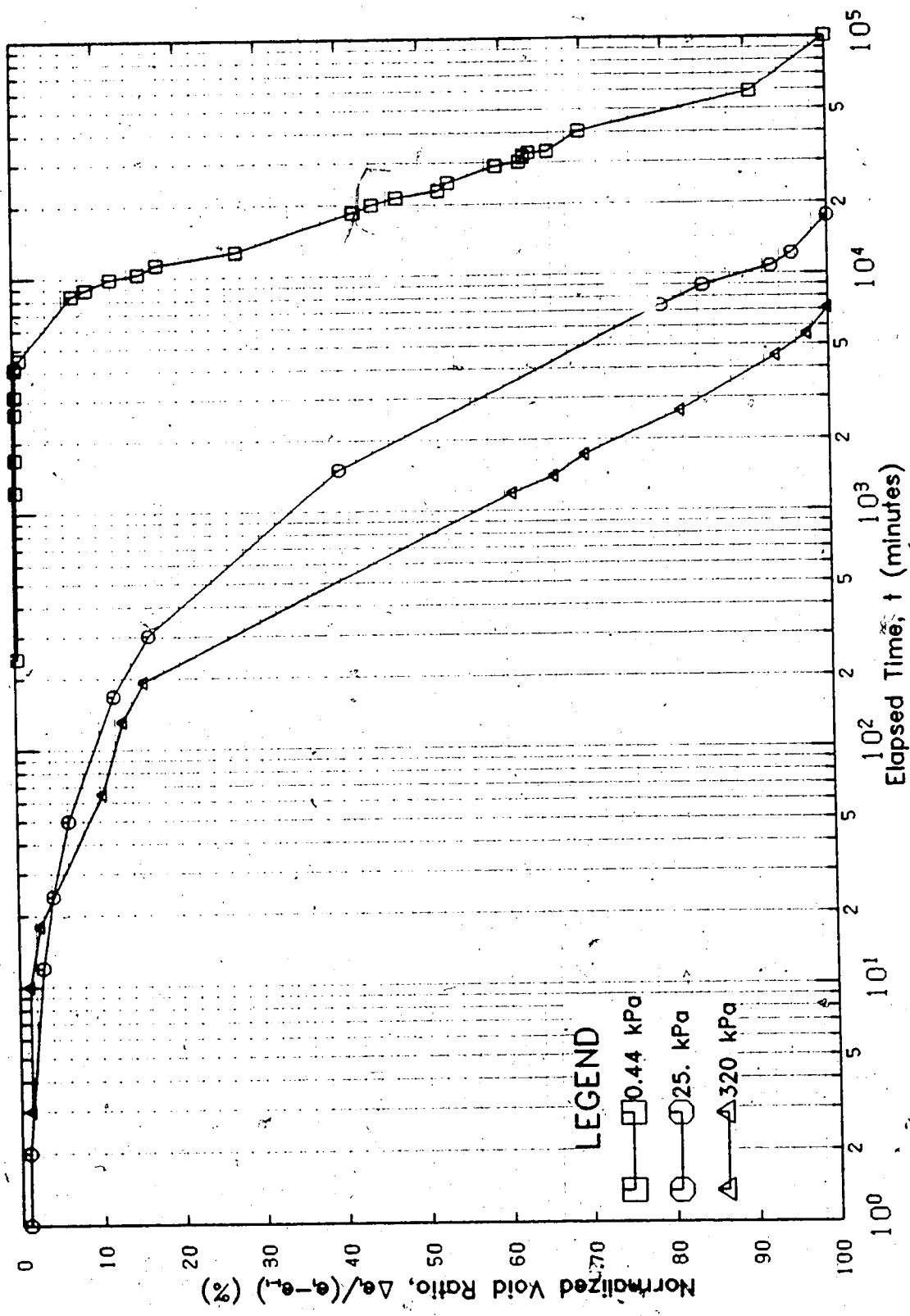


Figure 5.6 Normalized Consolidation, 46% Sand, Sludge-Sand

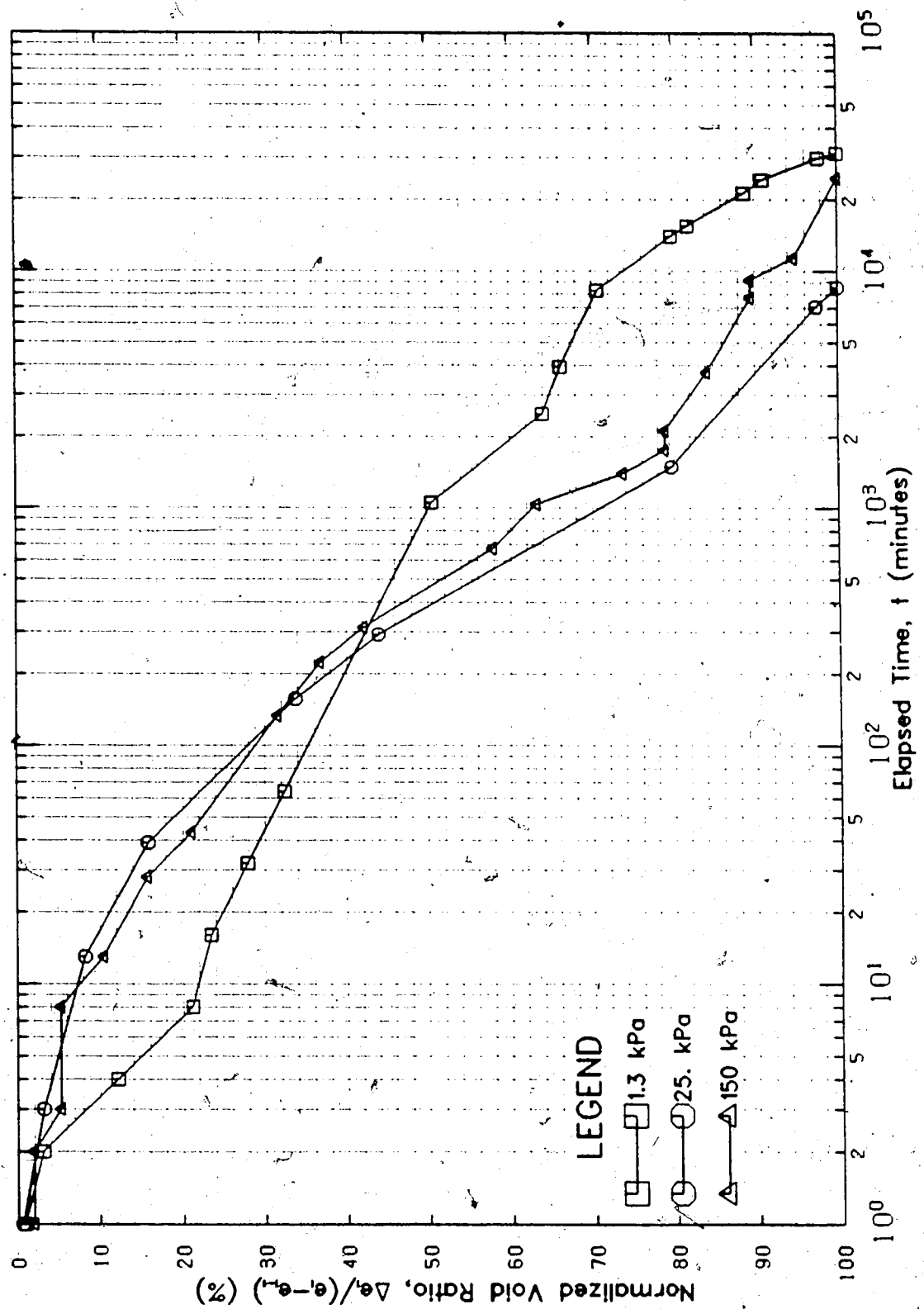


Figure 5.7 Normalized Consolidation, 80% Sand, Sludge-Sand

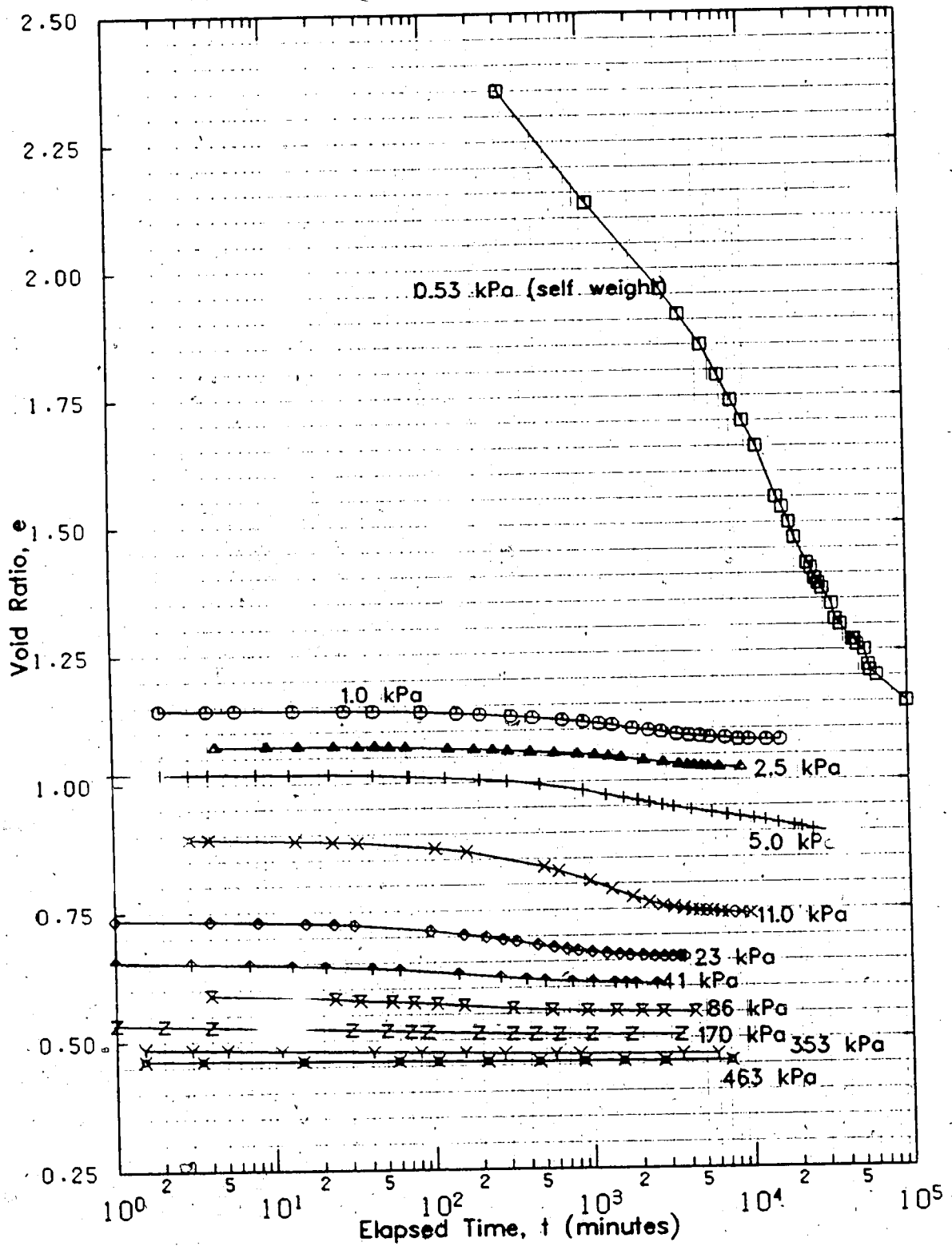


Figure 5.8 Consolidation of 73% Sand Sludge-Sand Mix with CaCl_2

versus time for three increments to illustrate the point.

The consolidometer in which test #4 was carried out in, was equipped with pore pressure ports. Plots of the readings along with some associated discussion is presented in Appendix C. The difficulties described under the discussion of the pore pressure readings for the sludge (section 5.1.1.1) were also encountered in Test #4. However, the results up to the 23 kPa stress level, showed reasonable correlation between pore pressure dissipation and the consolidation progress as can be seen in Figure 5.10.

5.1.1.4 Comparison of the Self Weight Stages

As previously discussed, the reason that a chemical flocculent would be considered in a tailings disposal operation is its ability to prevent sand from segregating out of slurries with low solids content, and thus enhance the self weight consolidation. This enhancing effect can be examined by comparing the self weight consolidation stages of the sludge-sand mix with the flocculent to the self weight stages of the other materials.

Figure 5.11 has the percent consolidation strain plotted against time for the self weight stages for each of the four materials. The important feature to note about the Figure is the percent strain of the flocculent mix compared to the sludge and compared to the sludge-sand mixes.

The flocculent sludge-sand mix has a magnitude of strain, at the end of self weight consolidation, greater than three times that of the sludge material. This result

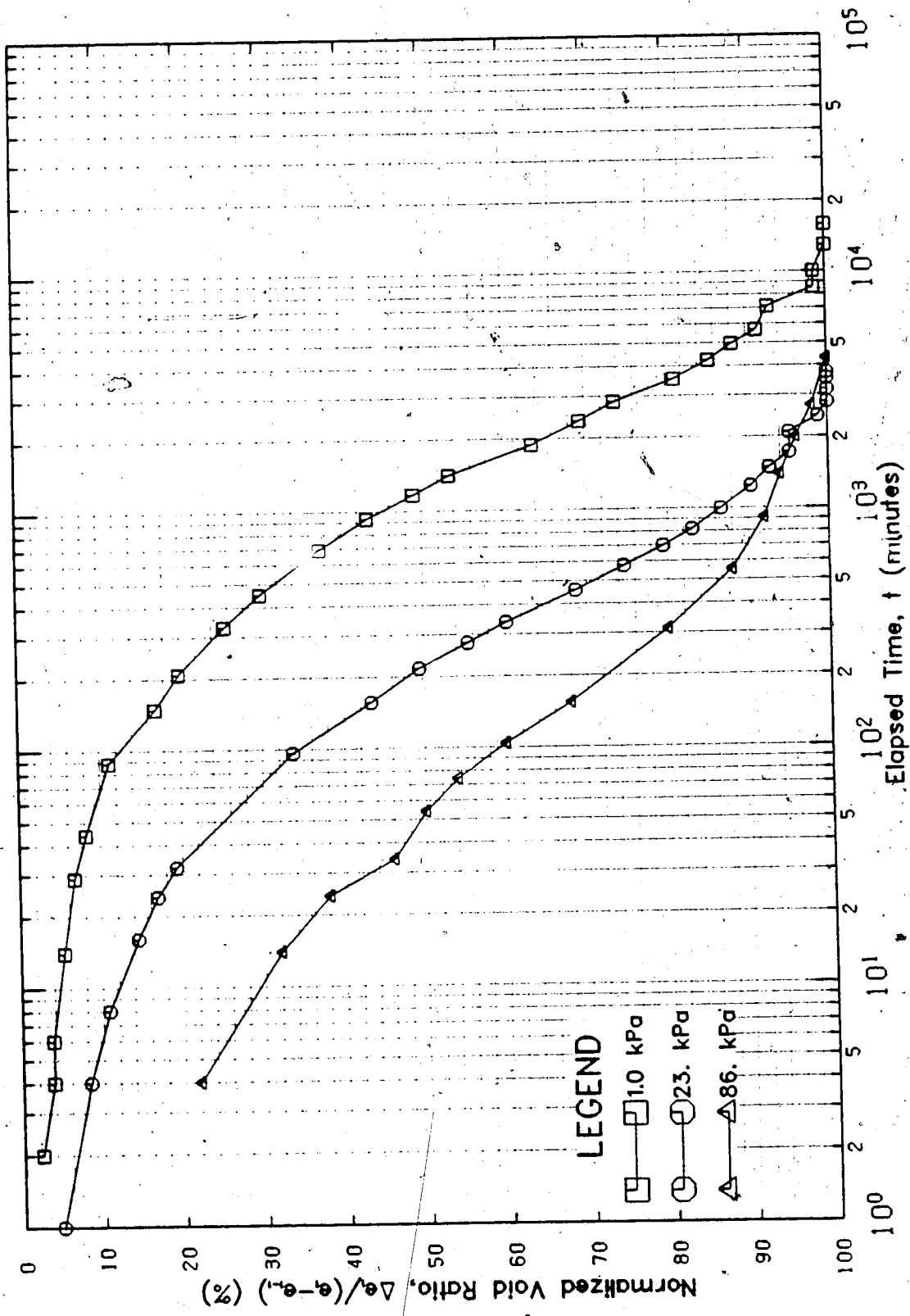


Figure 5.9 Normalized Consolidation, 73% Sand Sludge-Sand with CaCl₂

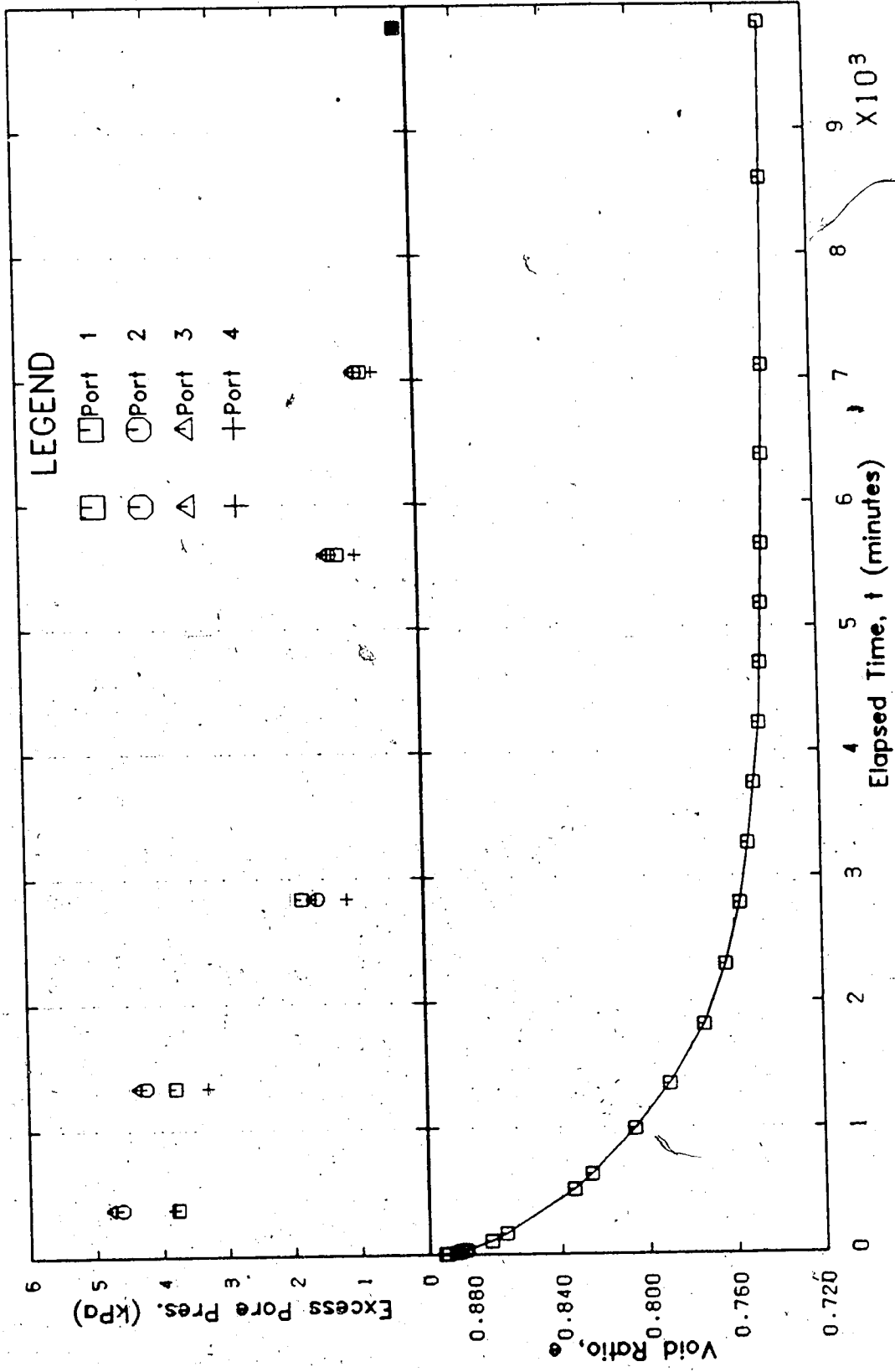


Figure 5.10 Pore Pressure Dissipation, Sludge Sand with CaCl₂, Δσ' = 6 kPa, σ' = 11 kPa

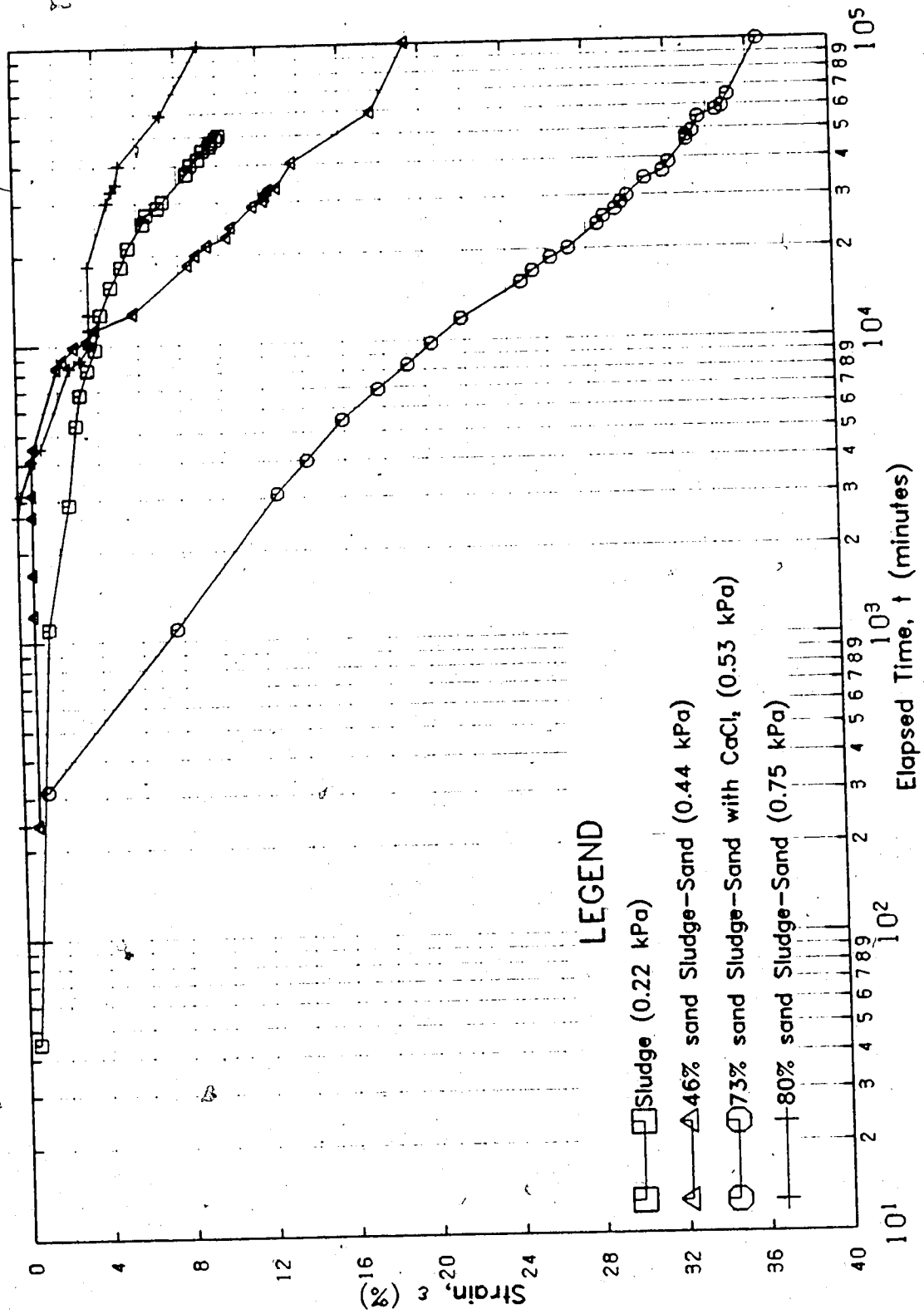


Figure 5.11 Self Weight Consolidation Strain, All Slurries

occurred even though the flocculent sludge-sand mix started off more towards the soil end of the slurry spectrum (solids content(s) = 52%, $e = 2.39$) than the thinner sludge material ($s = 29.1\%$, $e = 5.80$).

A primary reason for the impressive self weight consolidation of the flocculent sludge-sand mix is the relative density of its sludge solids (DR_{ss}). The bitumen in the sludge reduces the relative density of the sludge solids. The addition of sand, provided it is retained as part of the structure, increases the relative density. The DR_{ss} value for the sludge tested (test #1) was 2.39, and the DR_{ss} for the flocculent sludge-sand mix (test #4) was 2.59. Increasing the relative density allows an increase in the self weight stress for the same height of material, from 0.22 kPa for the sludge, to 0.53 kPa for the sludge-sand flocculent mix, thus aiding the self weight consolidation.

It is questionable whether a 2.4 times increase in self weight can be the sole contributor to a 3.6 times increase in consolidation. Figure 5.12 shows that the end point of consolidation of the sludge-sand flocculent mix is consistent with the other sludge-sand mixes, suggesting there is no unique effect from the chemical but that the sand may be having some effect other than that discussed. It is possible that a thixotropic gel strength may be restricting the consolidation progress of the sludge. The presence of sand in large quantities may prevent or reduce the thixotropic strength developed, thus allowing more

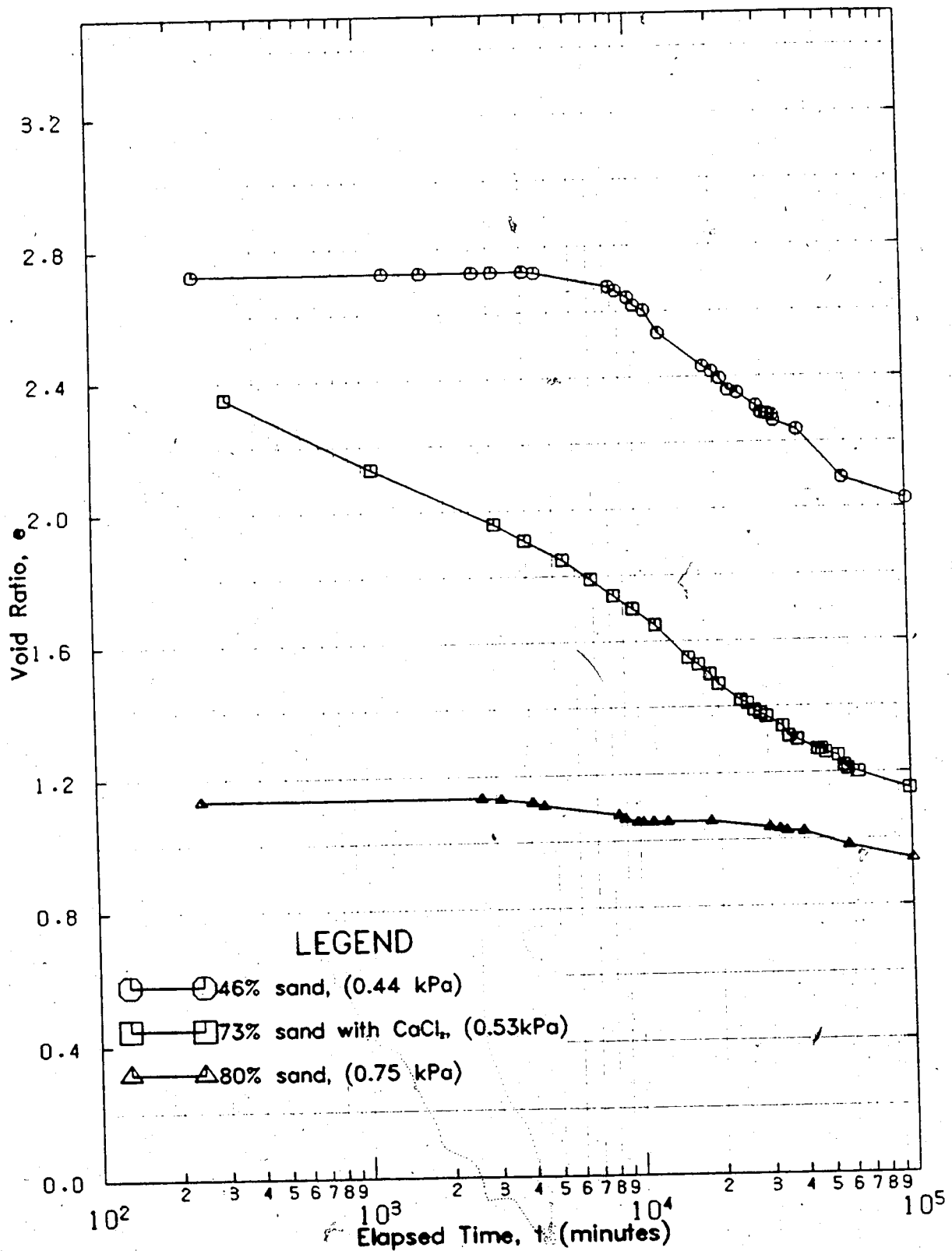


Figure 5.12 Self Weight Consolidation of Sludge Sand Mixes

consolidation. Another possibility is that the increase in relative density of the sludge solids due to the addition of sand could cause yielding of any thixotropic bonding. It is also logical that these two would occur in conjunction with each other. At this stage however, these explanations remain speculative.

The prior discussion on the improved behaviour of the sludge-sand flocculent over that of the sludge material concentrated more on the sand than the chemical flocculent. It was the sand that allows the improved behaviour, but it was the CaCl_2 that allowed the sand to remain in suspension at the low solids content. Figure 5.12 compares the self weight consolidation of the sludge-sand mixes. The end point is consistent with the percentage amount of sand, but the starting point is of interest. As shown in Figure 4.4, the starting point is in the segregating region of the sludge properties diagram. Of interest, is the comparison of the sludge-sand flocculent mix (73% sand) with the similar (80% sand) mix, with respect to magnitude of consolidation.

5.1.2 Compressibility Results from the Four Tests

Of the two major objectives for performing the consolidation, - permeability tests, one was to obtain the void ratio - effective stress, or compressibility, relationship of each material for the purpose of using it as input into the finite strain consolidation program.

5.1.2.1 Oil Sand Tailings Sludge

Figure 5.13 shows the compressibility of the sludge, where the void ratio is plotted against the logarithm of stress. Note that the change in void ratio over the stress range tested is an order of magnitude.

The compressibility data, Figure 5.13, yields a curve with a shape that would be expected, except in the low stress range where a reverse curvature occurs. The data at this end suggests the possibility of Monte and Krizek's (1976) fluid limit which proposes that, as the effective stress tends to zero, the void ratio will tend toward a finite value as opposed to infinity. However, slurry compressibility curves in the literature show the void ratio curvature, at the low stress end, varies from soil to soil (see for example Salem and Krizek, 1973, and Znidarcic *et al.*, 1986). For the sludge in Figure 5.13, with only one test performed on the material, it would be wise not to take the data too literally but to leave an allowance for experimental scatter considering the low stresses involved.

5.1.2.2 Oil Sand Tailings Sludge-Sand Mixes

Figures 5.14 and 5.15 show the compressibility plots for the 46% sand sludge-sand mix and 80% sand mix. With the void ratio plotted against the logarithm of effective stress, the sludge-sand mixes also yield curvilinear plots.

Neither mix displays any definite trend of heading towards a finite void ratio as the stress tends to zero. With only minor scatter in the low stress region, data from

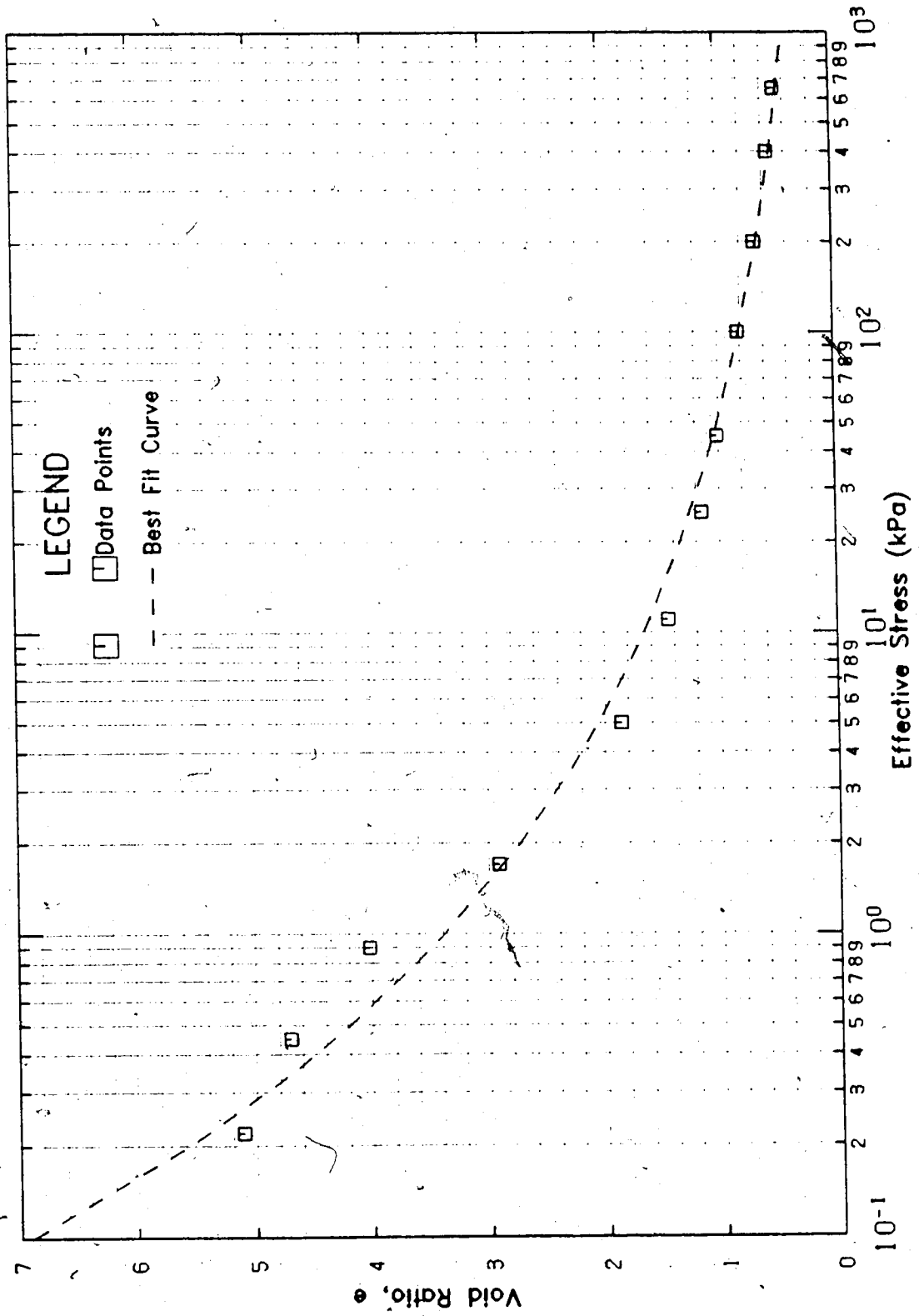


Figure 5.13 Compressibility of Oil Sand Tailings Sludge

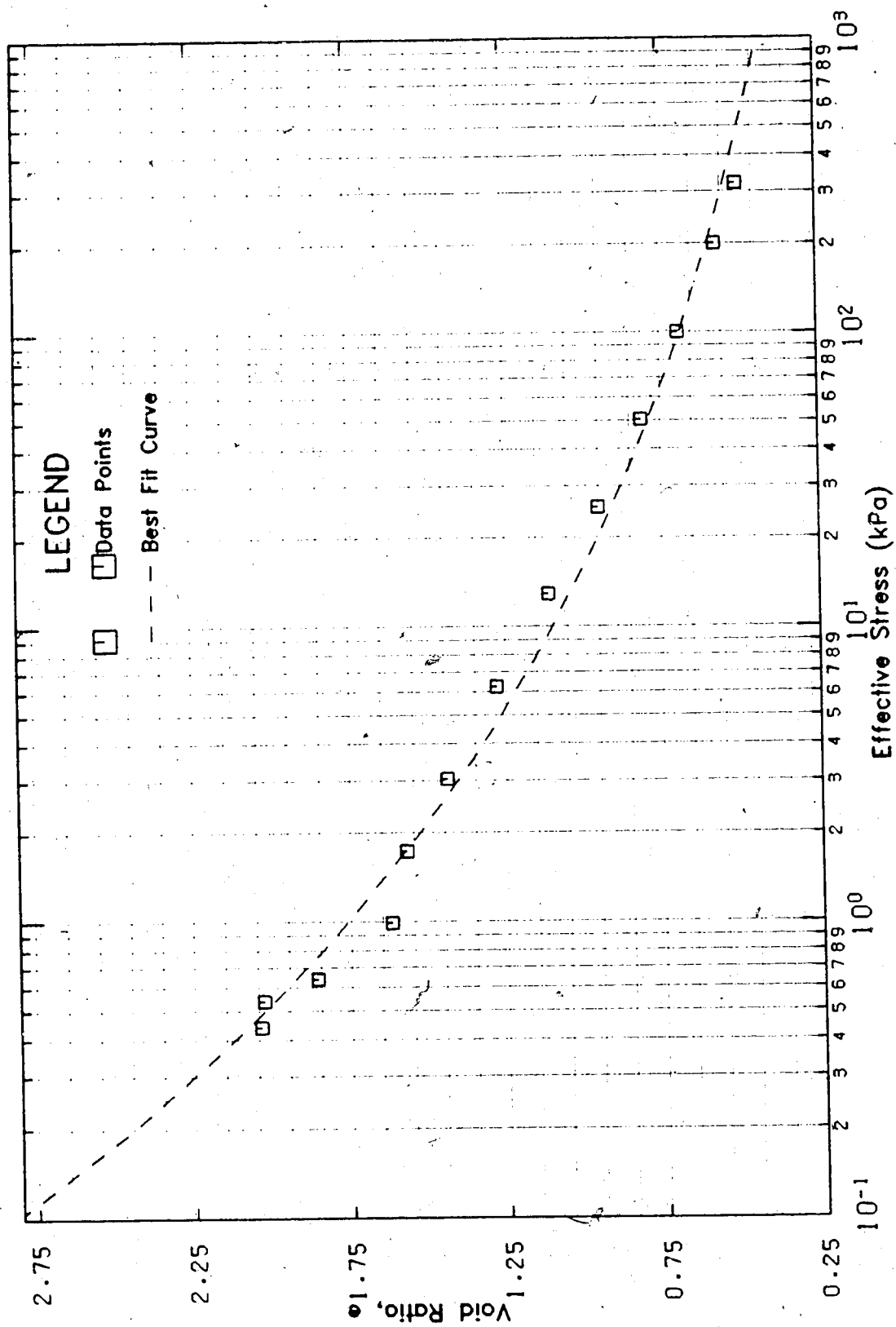


Figure 5.14 Compressibility of 46% Sand Sludge-Sand

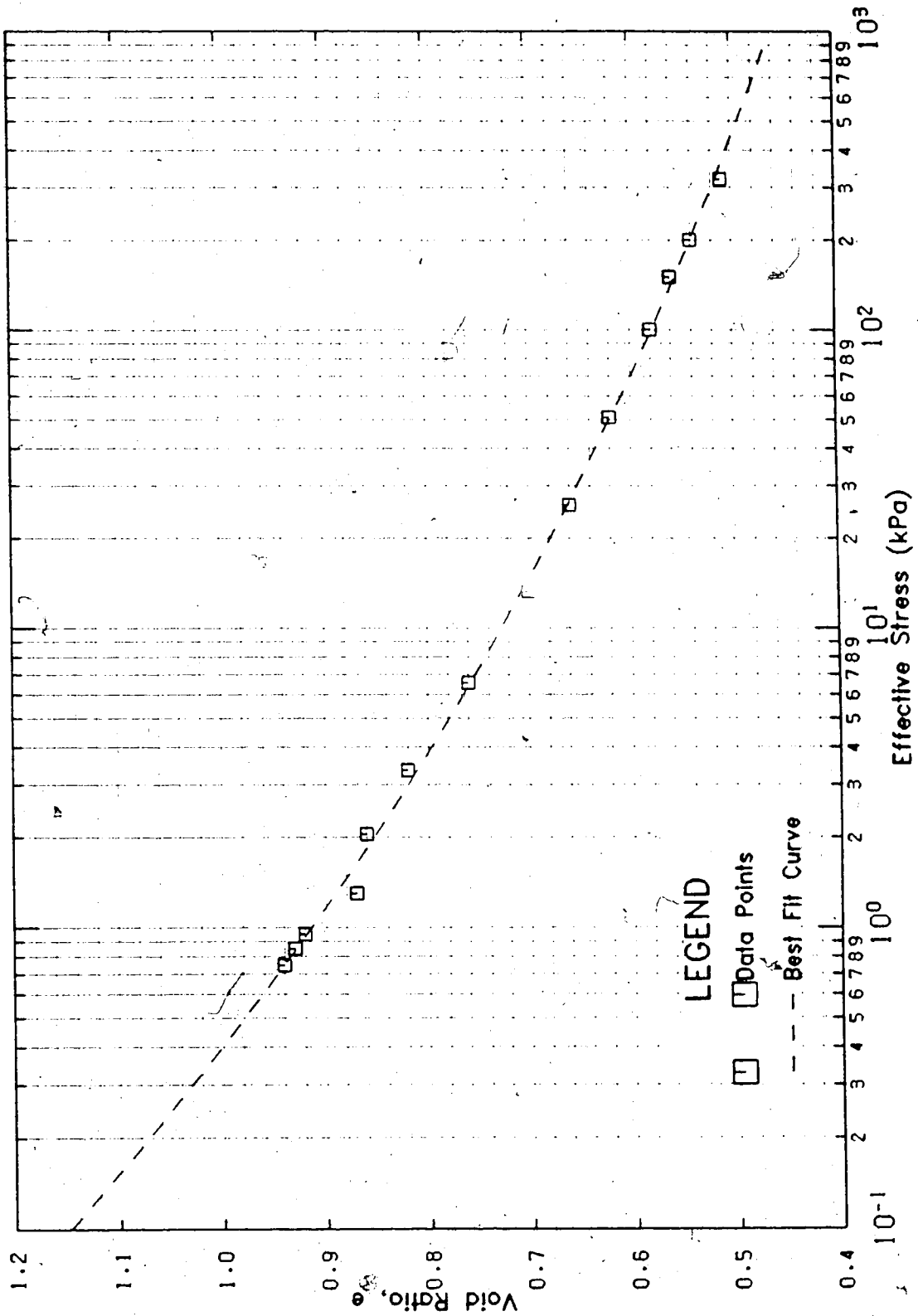


Figure 5.15 Compressibility of 80% Sand Sludge-Sand

both tests appear well behaved.

As would be expected, the change in void ratio over the effective stress range tested is largely affected by the quantity of sand in the mix. Figures 5.14 and 5.15 show that as the percentage of sand increases from 46% to 80%, the change in void ratio over the same stress range is halved, reflecting the 80% sand sludge-sand mix behaving more as a soil than a slurry. Conversely, it is interesting to note the sludge's ability to resist consolidation or compression even when diluted with sand. For example, the 80% sand mix has a void ratio of approximately 0.88 under 1.5 kPa applied stress, whereas the mix with more sludge (46% sand, which is still a significant portion) has a void ratio of 1.65 under the same stress. This will be discussed more in the comparison section (5.1.2.4).

5.1.2.3 Oil Sand Tailings Sludge-Sand Mix with Flocculent

The compressibility plot for the 73% sand sludge-sand mix with the chemical flocculent is given in Figure 5.16. The Figure shows that the data again yields a nonlinear void ratio - logarithm effective stress curve. The data does not suggest a movement towards a finite void ratio as σ' approaches zero (i.e., fluid limit), however mild scatter in the low stress region makes any conclusion in this area difficult.

One item not reflected by Figure 5.16 is the starting location of the slurry ($e=2.39$). Figure 5.16 indicates that

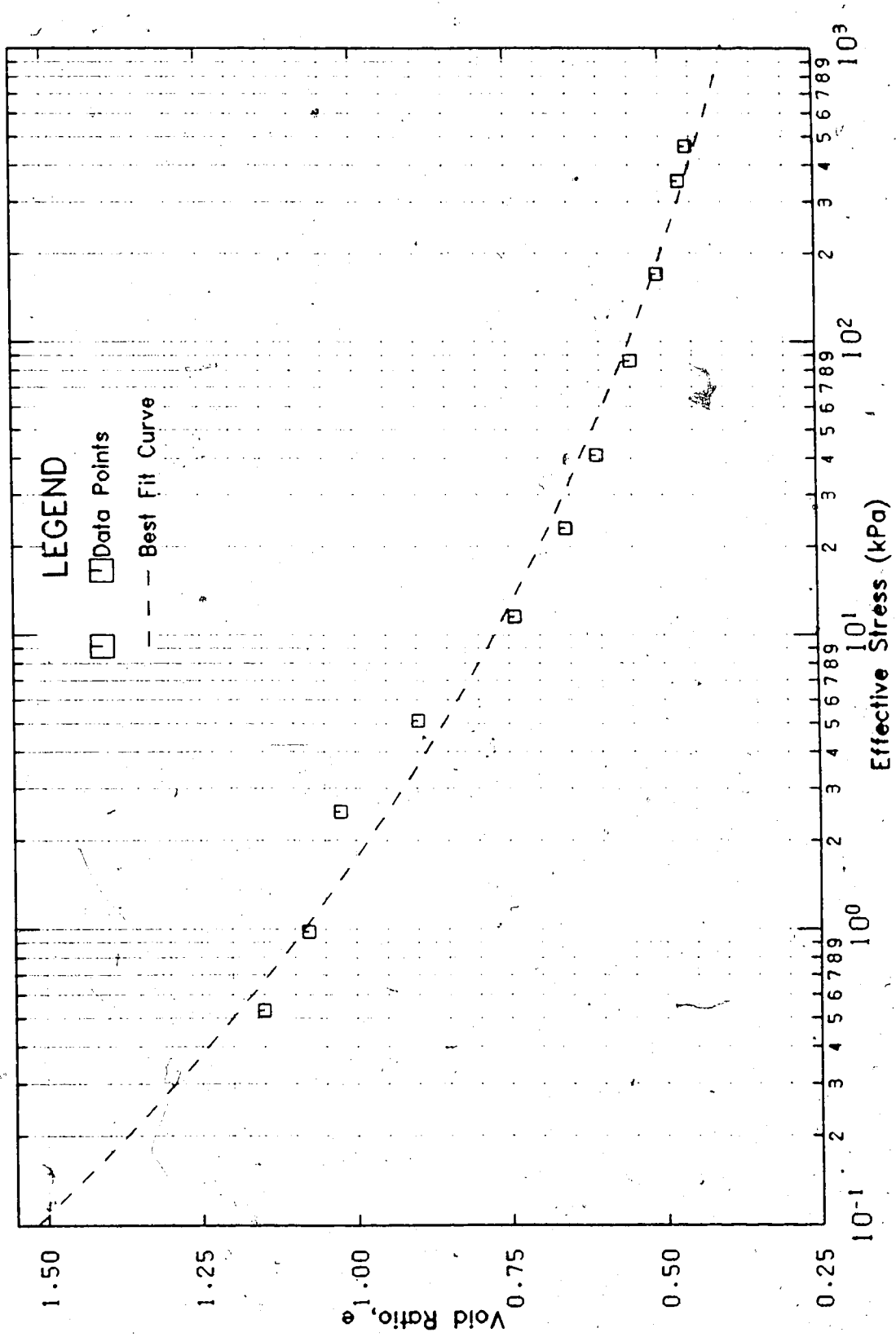


Figure 5.16 Compressibility of 73% Sand Sludge-Sand with CaCl₂

once the slurry has finished consolidating under its own weight from its "unnatural" starting position, the amount of compression henceforth is greatly reduced. The term "unnatural" is used to describe the starting condition of the slurry because without the flocculent, a 73% sand sludge-sand mix could not retain the sand in suspension at a void ratio of 2.39 ($s = 52\%$).

5.1.2.4 A Comparison of the Compressibility of the Materials

A comparison of the compressibility data can reveal more on the behaviour of the sludge, effect of added sand, and the influence of the flocculent. Figure 5.17 shows the compressibility data for the four materials.

The plot shows that as the sand content is increased in the material, the compressibility data becomes more like that of a classical soil, that is a linear $e - \log \sigma'$ plot. This is not merely a result of a smaller overall change in void ratio nor the result of the initial solids content of the slurry as will be presently explained.

With respect to the former, smaller overall void ratio change, Figures 5.14 to 5.16 showed definite curvature in the compressibility data of the sludge-sand mixes. As well, Figure 5.18 shows the fines void ratio plotted against $\log \sigma'$, which brings the data into a common range. The fines void ratio is the void ratio of the material when sand is not considered and is defined as the volume of voids divided by the volume of fines, and is related to the void ratio by

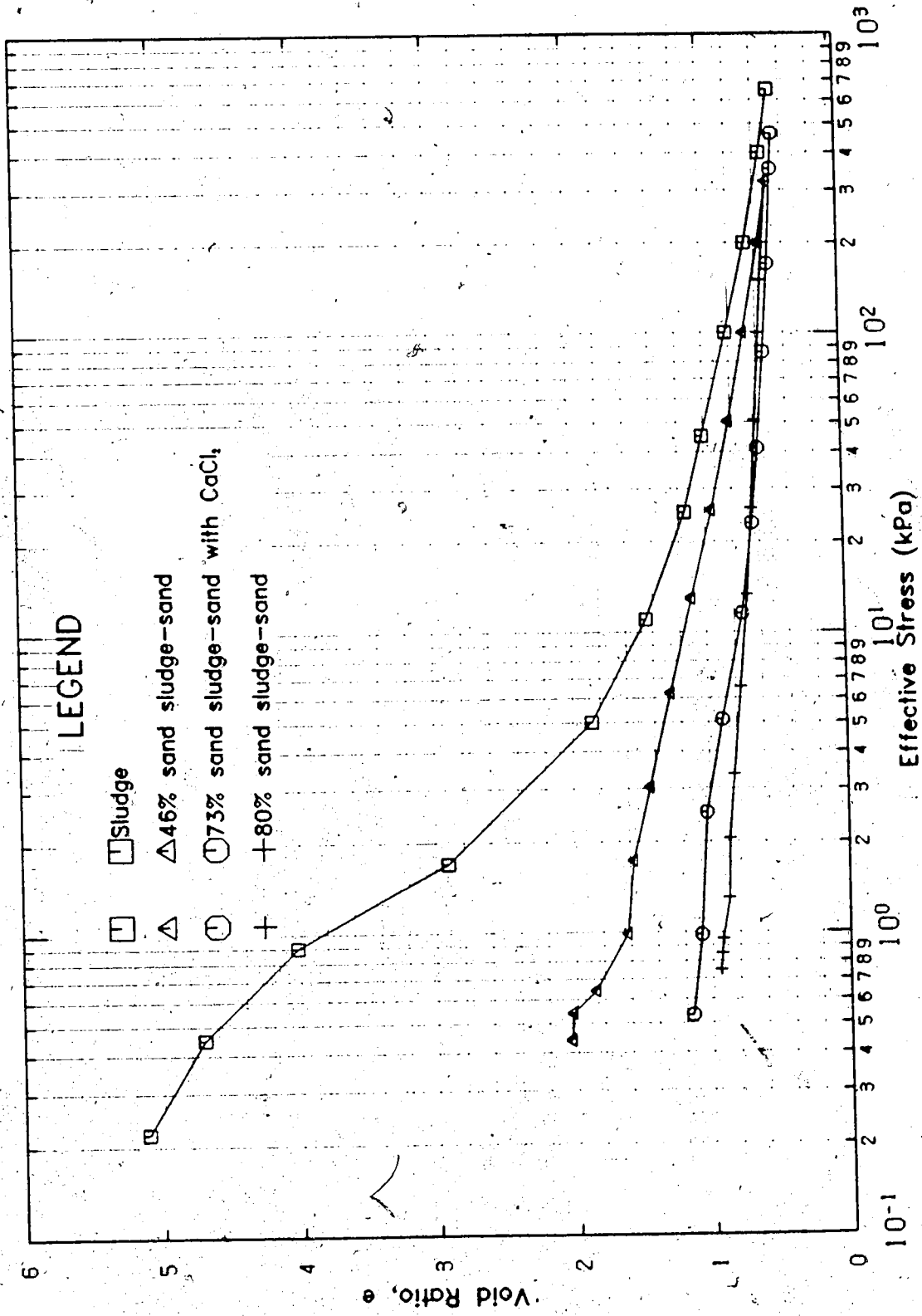


Figure 5.17 Compressibility of All 4 Slurries Tested

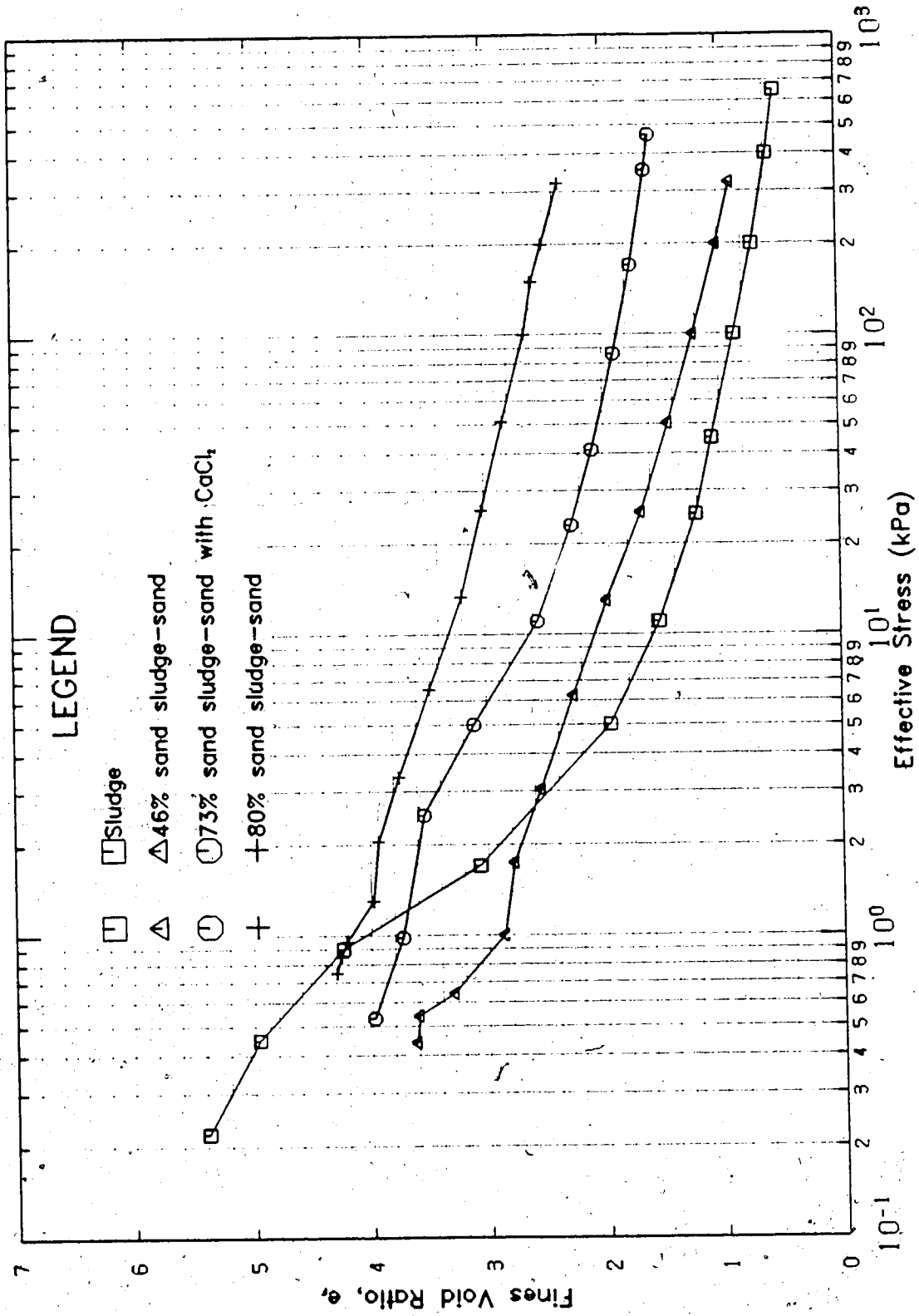


Figure 5.18 Compressibility of All 4 Slurries Tested, Fines Void Ratio

the following,

$$e = F \cdot e_f \quad (5.1)$$

where F is the percentage of fines of the sludge solids and e_f is the fines void ratio. In cases where the relative density of the fines DR_f are different than the total sludges solids DR_{ss} , as in this case since the bitumen is classified as part of the fines, the relationship is

$$e = F \cdot e_f \frac{DR_{ss}}{DR_f} \quad (5.2)$$

Figure 5.18 demonstrates that over a similar fines void ratio change, added sand linearizes the $e - \log \sigma'$ data.

With respect to the slurries' initial condition, the starting void ratio has been shown (eg. Imai, 1981) to affect the compressibility curve of the same material. However, the initial condition of the sludge-sand mix with flocculent negates the possibility of the trend of $e - \log \sigma'$ approaching classical soil plots with increasing sand being a function of the starting void ratio. The cause of the trend therefore lies in the fact that the large quantities of sand are influencing the mixes to behave as normal soils, and effects of the sludge are diluted.

Along the same lines, as has been previously noted in section 5.1.2.2, is the sludge's ability to resist compression and that this ability is decreased with increasing sand content. This is seen in Figure 5.17 where at a given stress, the void ratio is greater for the material with less sand content. This may be partially due

to the initial void ratios of the slurries, but as explained in the preceding paragraph, the initial void ratio of the flocculent sludge-sand mix shows that initial conditions cannot account for all of the consolidation resistance.

Another interesting feature displayed by Figures 5.17 and 5.18 is the behaviour of the sludge-sand mix with the flocculent (test #4). As is seen in both Figures, test #4 is consistent in both shape and location with the other slurries when considering the sand content. This indicates that with respect to compressibility, the chemical flocculent has no affect on the behaviour of the material other than retaining the sand.

Figure 5.17 also illustrates consistency in the behaviour of all the slurries with respect to sand content. This means that it is possible for an engineer to rationally interpolate between the compressibility curves to obtain a curve for a mix with a sand content not investigated. In this respect, Figure 5.17 might be thought of as a "family of curves" for this oil sand tailings. Figure 5.17 also indicates that it may be possible to test only three slurries to obtain a workable family of curves. Obviously any family of curves would be material specific and even site specific for similar materials, such that at a different oil sand mining operation the family of curves would likely be different.

When the fines void ratios are plotted against σ' (Figure 5.18), the curves become colinear above 5 kPa,

possibly reflecting a transition from a slurry to a soil. Although not available, vane shear data above and below this stress would be of some interest.

5.2 Permeability Test Results

The permeability test results will be looked at in two sections; flow with time, and hydraulic conductivity as a function of void ratio.

5.2.1 Hydraulic Flow with Time

According to Darcy's Law the flow discharge velocity is directly related to the hydraulic gradient alone, by a constant, k . However, as has been discussed in section 2.2.2, fine grained soils under low hydraulic gradients demonstrate a time dependent flow discharge (Olson, Nichols, and Rice, 1985). It was also noted that a steady state condition would occur and that the forementioned authors found that the steady state flow obeyed Darcy's Law with respect to a linear gradient-velocity relationship.

In this section, results of some of the permeability measurements are presented to show that the material investigated did indeed display a time dependent flow discharge with a steady state value.

5.2.1.1 Oil Sand Tailings Sludge

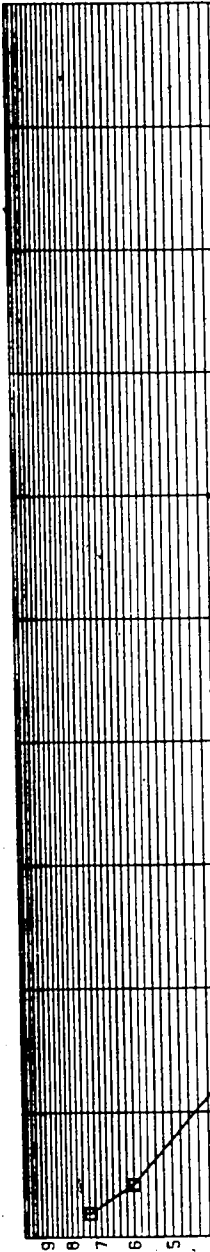
When the permeability tests were first started, a stopwatch was used to obtain flow volume readings with time to obtain an average flow velocity for a particular

gradient, as minor fluctuations were expected. However, when the constant head tests were performed it became apparent that the timed readings were not leading to an average flow velocity but a decreasing flow velocity. Figure 5.19 shows this for a gradient of 0.17 for the sludge at the end of self weight consolidation ($e = 5.11$).

Evident from Figure 5.19 is the approach of the flow velocity to a steady state value. It is the flow velocity at this steady state value then, that would be used to determine the coefficient of permeability (see Olson, Nichols, and Rice, 1985). It is also noted that a falling head test would lead to erroneous results because of this phenomenon.

Several tests were run at certain gradients to check if this phenomenon was repeatable. Figure 5.20 shows the results of one such test. Demonstrated in the Figure is the fact that the trend was repeatable. The tests shown in the Figure were not taken to the steady state condition, but to a time sufficient to check for repeatability. The time between the tests varied from 5 to 10 minutes.

The repeatability of this behaviour suggests that whatever is causing the decrease in flow velocity is triggered by seepage force and is reversible. The bitumen in the sludge might account for this. Although considered as a solid in calculations, the bitumen is not totally rigid and can deform under stress. This deformable quality could allow the bitumen to move to block pore throats while being



10-6

9
8
7
6
5

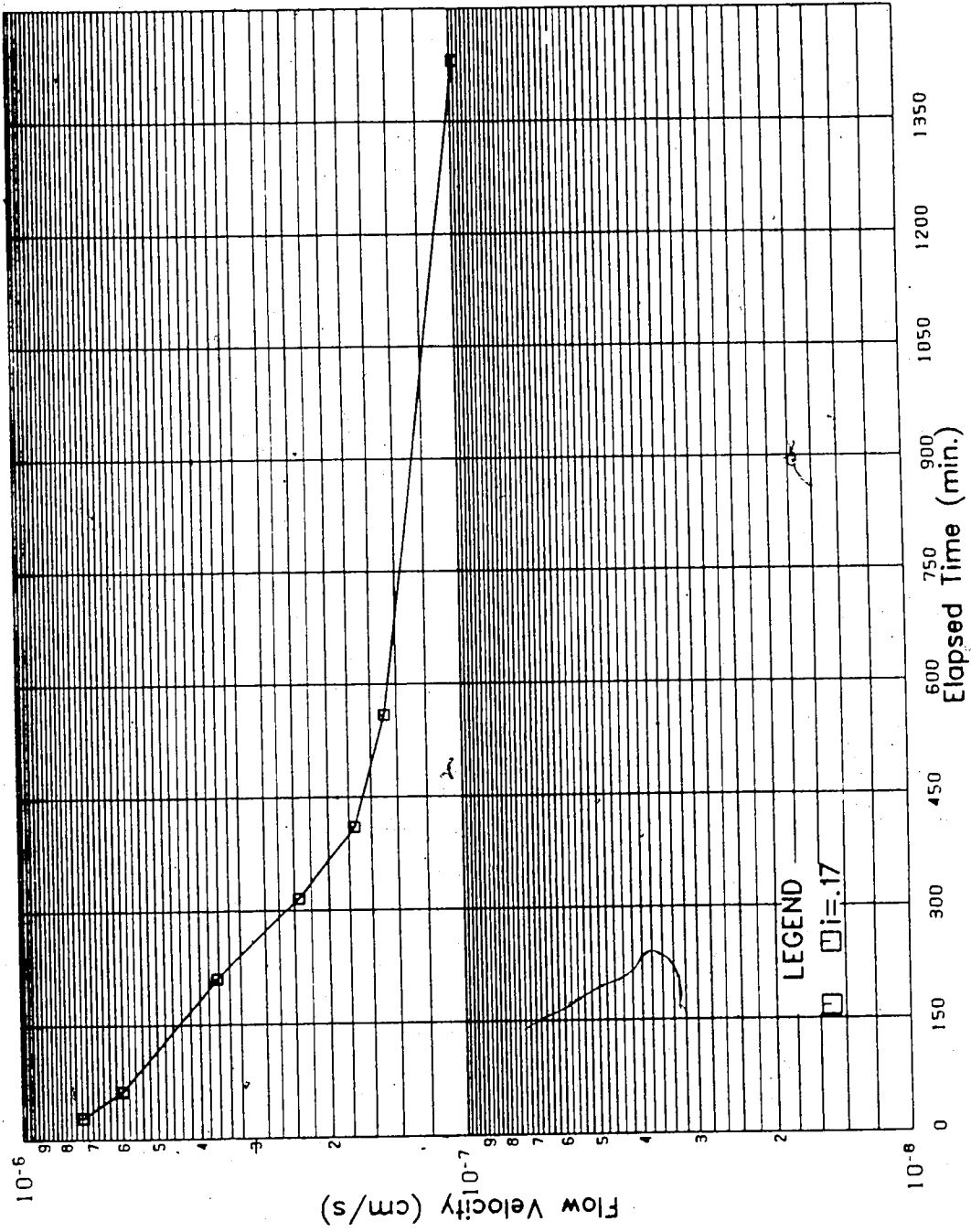


Figure 5.19 Permeability Test on Sludge, $e=5.11$, $i=0.17$

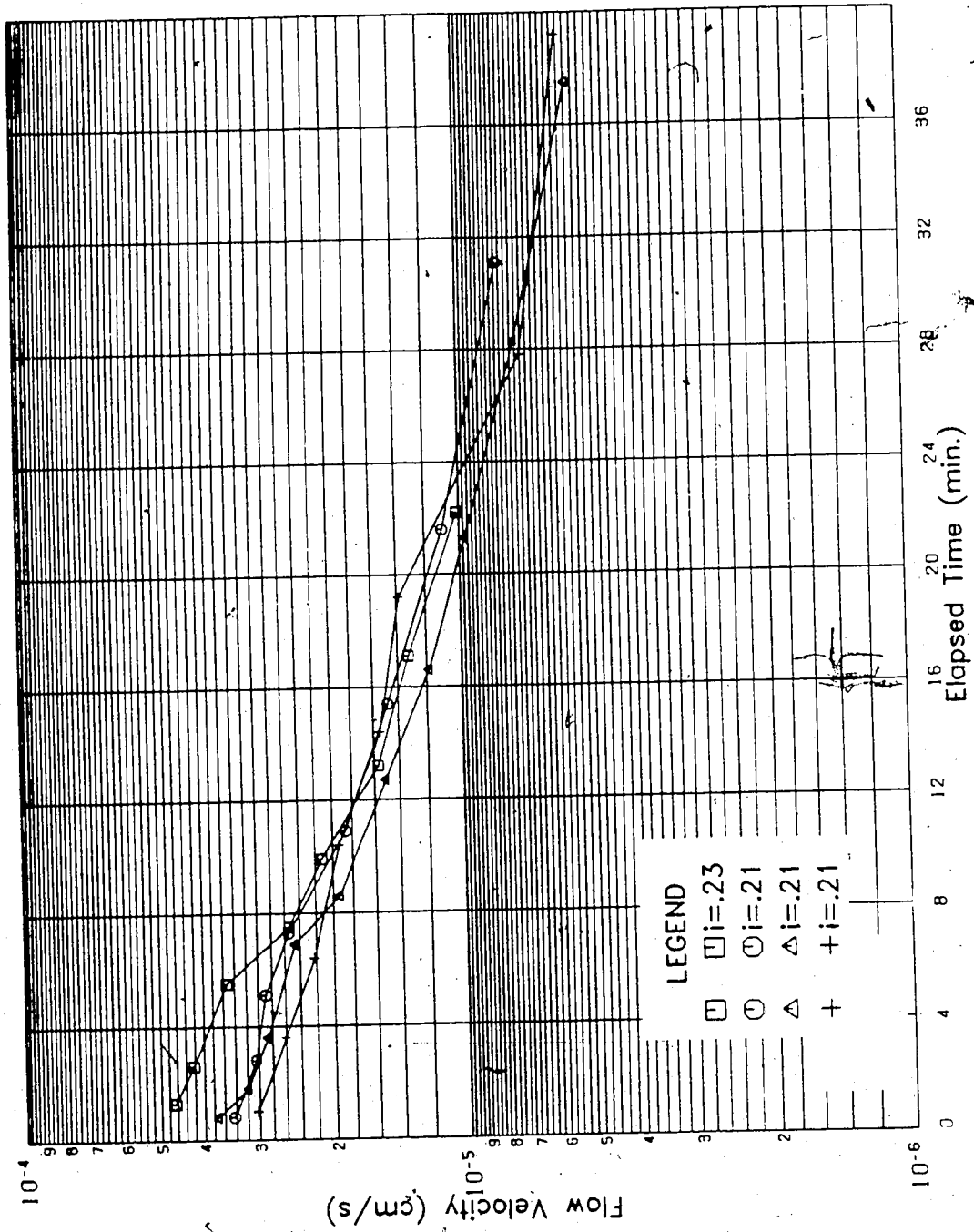


Figure 5.20 Permeability Test on Sludge, $e=5.11$, $i=0.21$

subject to a seepage stress. Once the seepage has stopped, the bitumen would revert to its original position or shape. It is interesting to note however, that the initial condition seems to be reattainable after only 5 to 10 minutes of no flow, even after hours of flow.

Figures 5.21 and 5.22 show some of the permeability test results at void ratios of 2.91 and 0.55 respectively. Evident from those Figures is that the time dependent flow velocity still exists at lower void ratios. However, the drop in flow velocity from initial to steady state becomes less as the void ratio decreases. It would be expected that the drop would be less, since, whether it is the bitumen influencing it or not, at the very low void ratios very little movement of anything (finer particles included) can occur.

Note that in Figure 5.22, the gradients are relatively high (14.6 to 39.4). As the consolidation proceeded, gas being formed created problems. This was borne out in the tests by either no flow occurring or a delay before flow would occur. The problems were predominant in the low gradient tests, whereas the higher gradient tests, being more able to force water through, responded adequately. If the time dependent flow velocity is dependent on moving material, the high gradients in Figure 5.22 may explain why the sludge is still displaying this behaviour at a void ratio of 0.55.

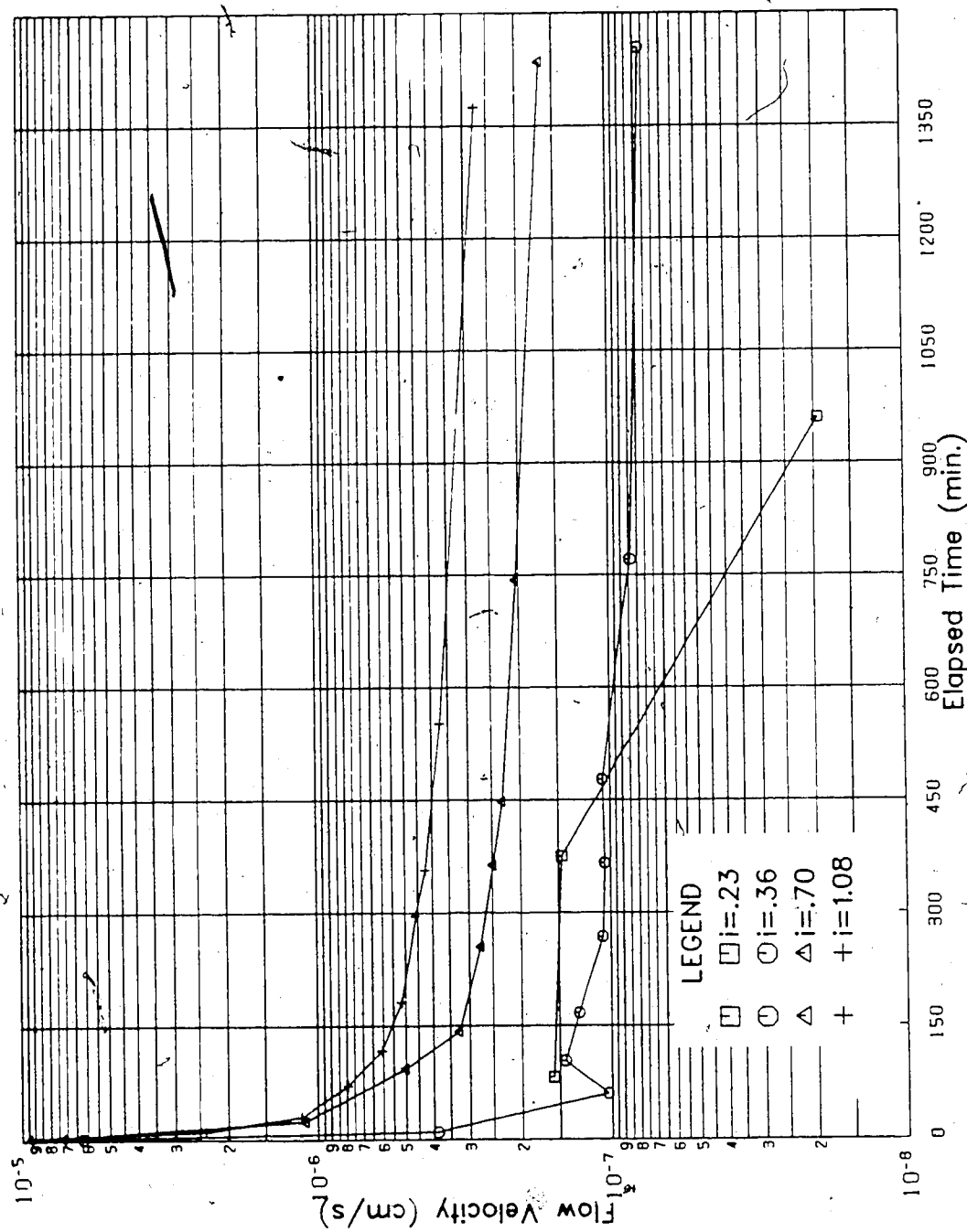


Figure 5.21 Permeability Test on Sludge, $e=2.91$

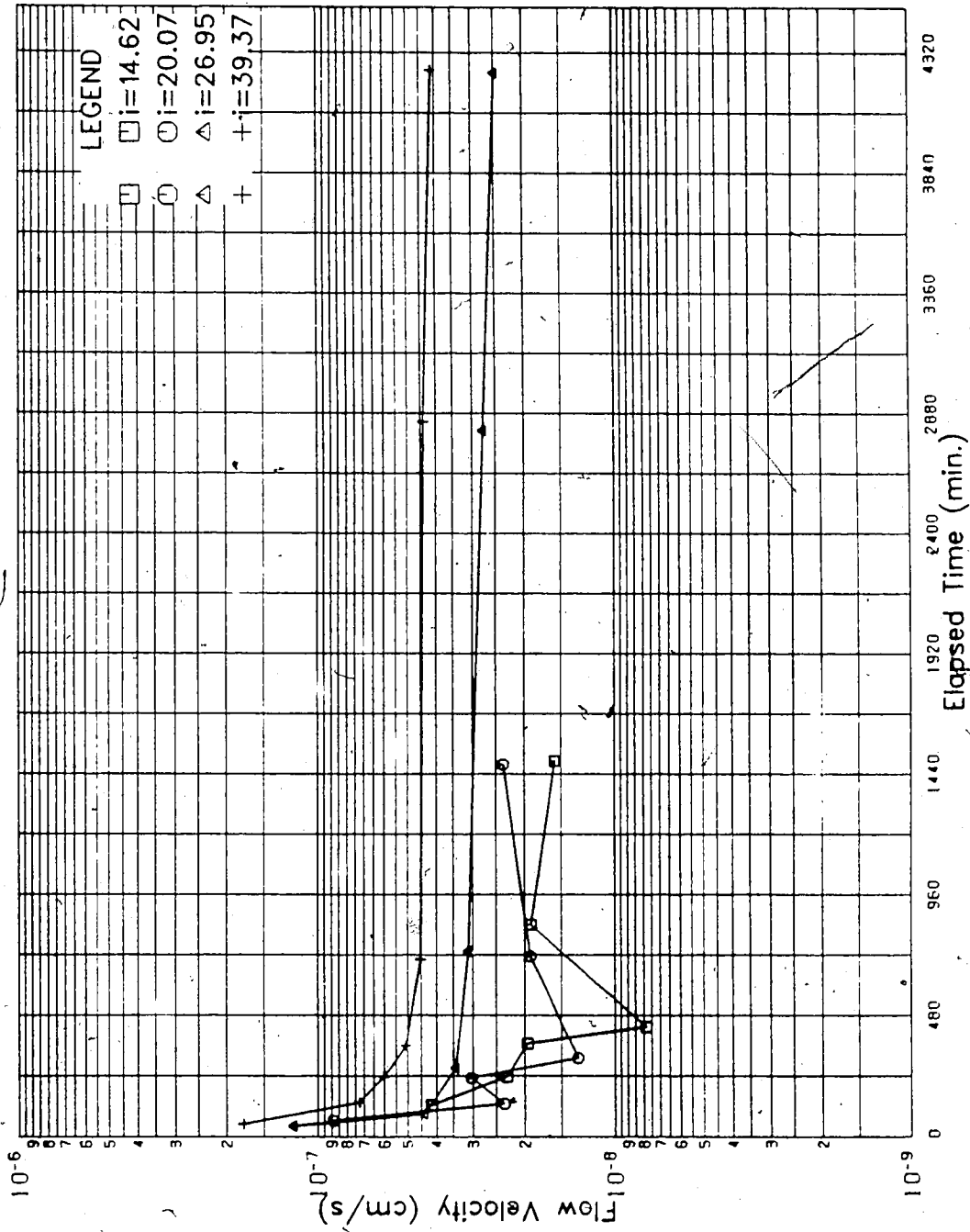


Figure 5.22 Permeability Test on Sludge, $e=0.55$

5.2.1.2 Oil Sand Tailings Sludge-Sand Mixes

The permeability tests on the sludge-sand mixes (46% and 80% sand) were consistently affected by the presence of gas, and erratic flows were thusly produced and recorded.

Figure 5.23 illustrates that, for some of the runs that were not noticeably affected by gas formation for the 46% sand mix, there was still a time dependent flow discharge. The time to a steady state condition appears to be less for the sludge-sand mixture compared to the sludge (100 minutes compared to 600 to 1000 minutes), however there is too much scatter in the results to draw definite conclusions. The drop in flow velocity shown in Figure 5.23 is quite large, however, similar to the sludge, as the consolidation proceeded, the drop decreased. Figure 5.24 shows not only that the drop in flow velocity becomes smaller at lower void ratios but it also demonstrates some erratic flow behavior encountered due to the gas.

Only a mild decrease in flow velocity was displayed by the permeability tests on the 80% sand mix, but the tests were interfered with by gas. Figure 5.25 demonstrates both of these points for the sludge-sand mix.

5.2.1.3 Oil Sand Tailings Sludge-Sand Mix with Flocculent

With respect to the dependence of the flow velocity on time, the 73% sand sludge-sand mix with the flocculent behaved like the other sludge-sand mixes in that it exhibited some time dependence.

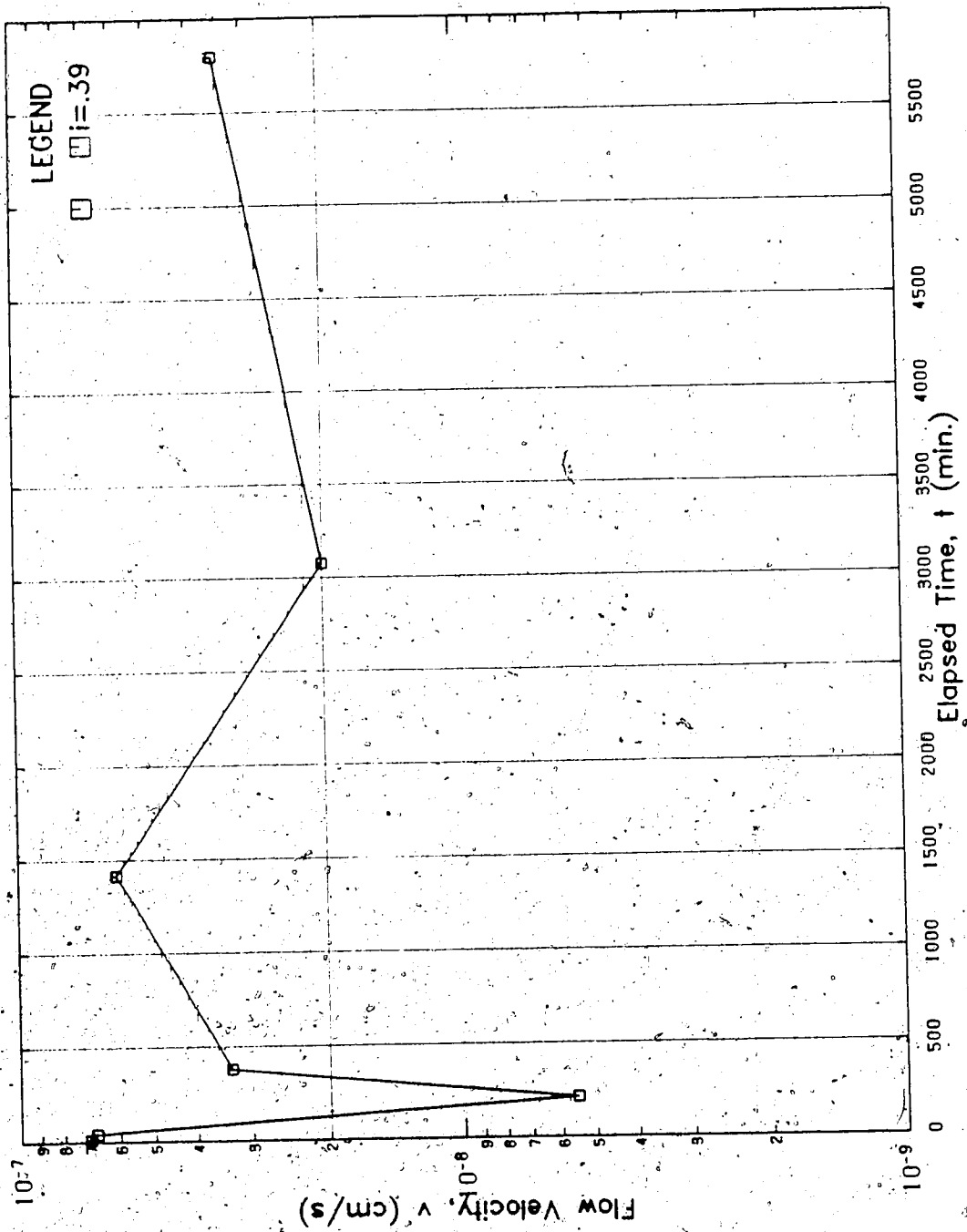


Figure 5.24 permeability Test on 46% Sand Sludge-Sand, $e=0.95$, $i=0.39$

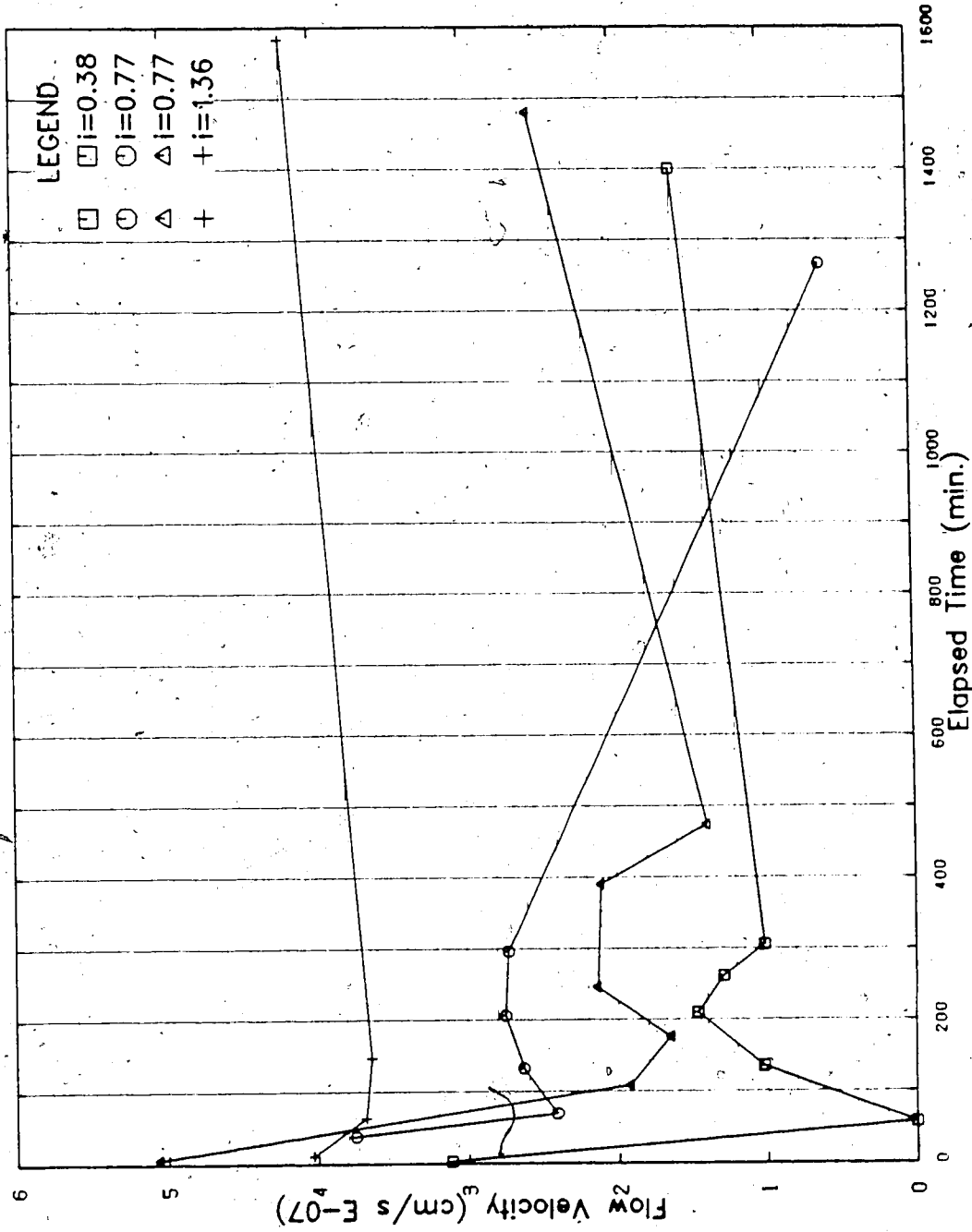


Figure 5.25 Permeability Test on 80% Sand Sludge-Sand, $e=0.62$

Figure 5.26 shows a typical set of runs, and demonstrates that the initial drop (where applicable) is not that large (three times as opposed to 100 times displayed by the sludge). Also shown, once again, is some erratic results influenced by the gas. The Figure shows how the time plots can aid in determining which results deserve more weight, and which results can be discarded. For example, it is obvious from Figure 5.26 that the results from the 0.14 gradient test are questionable.

5.2.2 Hydraulic Conductivity with Void Ratio

The purpose of the permeability tests was to obtain relationships between the hydraulic conductivity and void ratio for each material. The steady state flow velocities were used to determine k at the various void ratios through the relationship

$$k = \frac{v}{i} \quad (5.3)$$

where v is the flow velocity at the steady state condition.

This section presents the hydraulic conductivity values obtained for the four slurries.

5.2.2.1 Oil Sand Tailings Sludge

When the steady state flow velocities were plotted against the gradient to determine a slope (eqn. 5.3), there sometimes arose scatter. In these circumstances, the longer duration tests were given preference. This mainly occurred for the high void ratio tests (greater than 4).

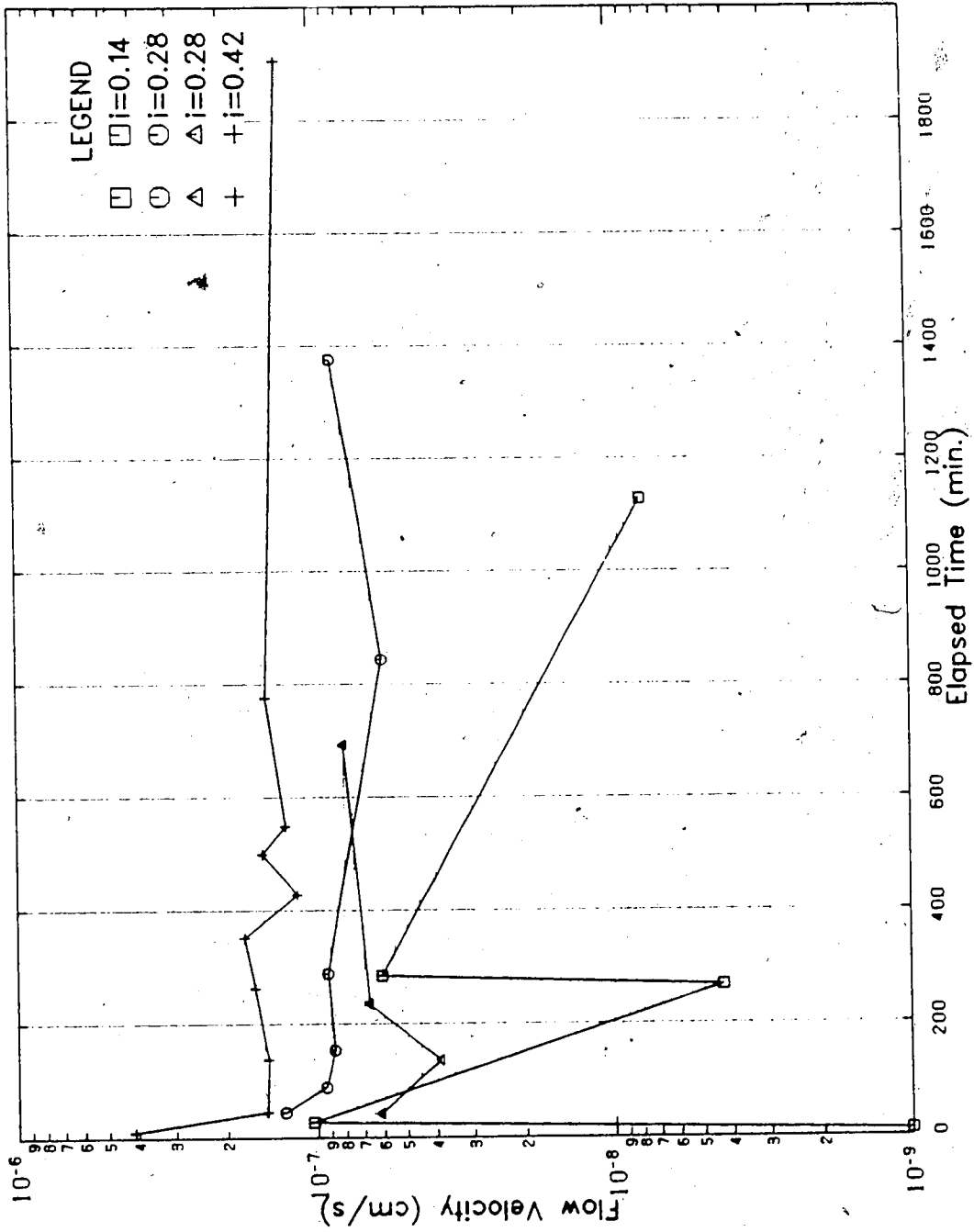


Figure 5.26 Permeability Test on 73% Sand Sludge-Sand with CaCl₂, e=1.05

Figures 5.27 and 5.28 show the velocity-gradient plots for void ratios of 2.91 and 1.86 respectively and are typical of the majority of the plots. To be noted from the plots is that there is no indication of a threshold gradient which is also the case for the other void ratios. The best fit line may intersect one of the axes but no consistent trends existed and the cause can be attributed to experimental scatter.

Figure 5.29 shows the results of a series of permeability tests performed on the sludge to determine the influence of the direction of flow and magnitude of gradient on the hydraulic conductivity. As well, the tests were repeated to check whether the previous gradient being higher or lower had any influence on the conductivity value. As seen in the Figure, it was found that; the direction of flow had no influence on the flow velocity, the flow velocity was only marginally faster when approached from a smaller gradient, and that at unusually large gradients (greater than 200) Darcy's law becomes invalid as the increase in flow velocity becomes less with increasing gradient. The very large velocity most likely caused a migration of fine particles or bitumen to decrease the permeability. It is interesting to note however, that once the peak gradients were reached (twice) and the gradients were then reduced, the flows were virtually the same as before at a given gradient.

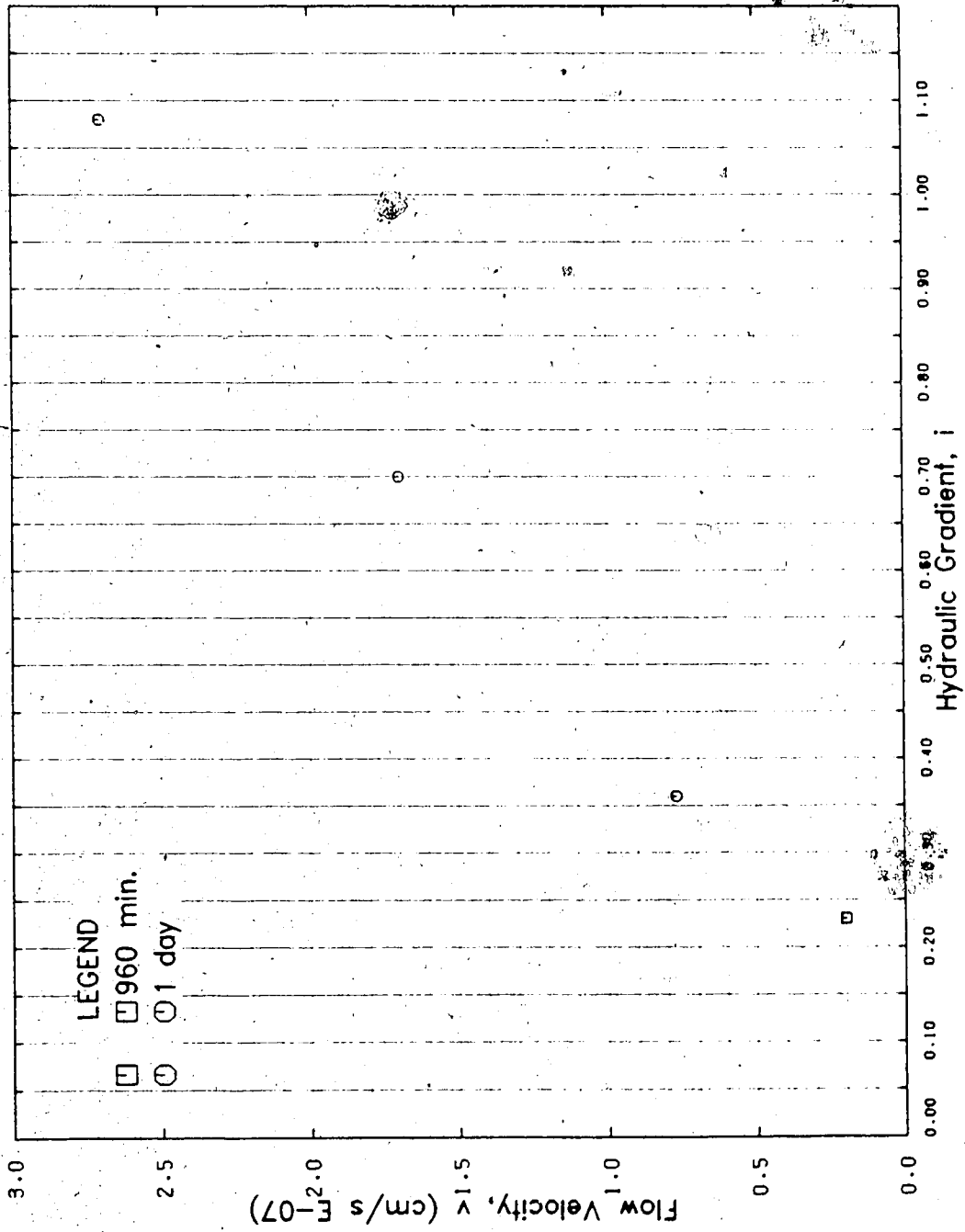


Figure 5.27 Flow vs. Gradient, Sludge, $e=2.91$

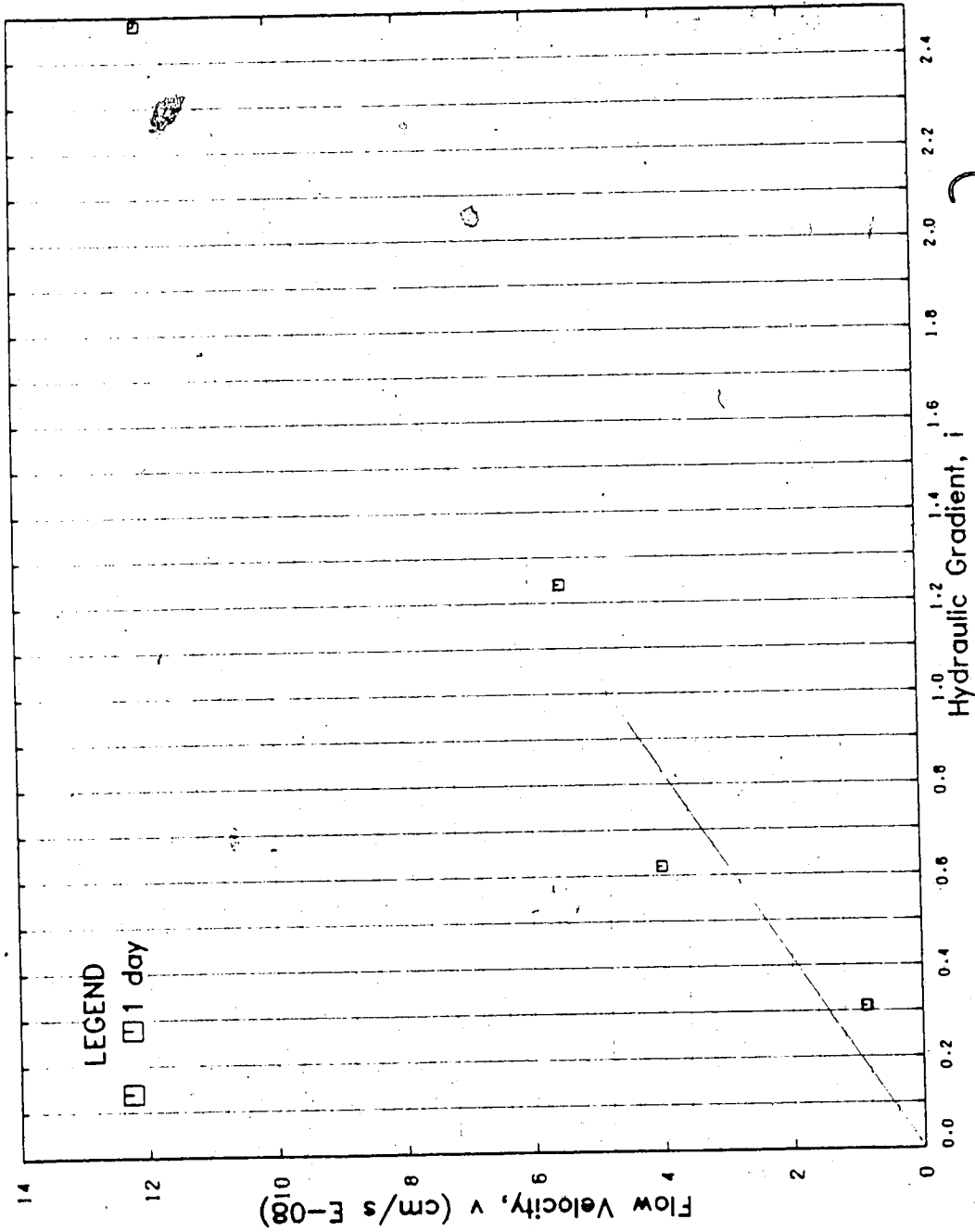


Figure 5.28 Flow vs. Gradient, Sludge, $e=1.86$

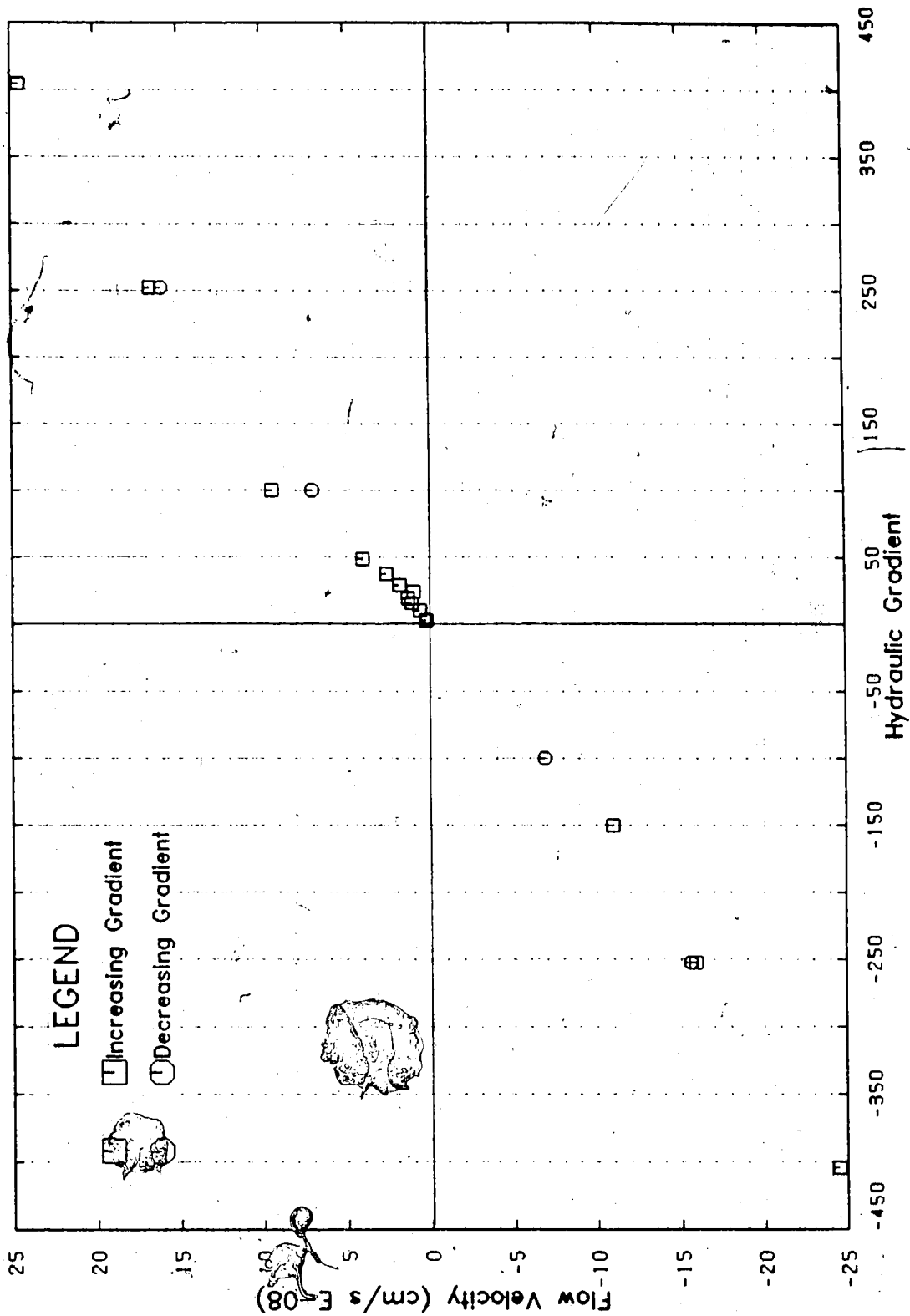


Figure 5.29 Flow vs. Gradient, Sludge, e=0.48

The resulting data, the hydraulic conductivity values, are plotted in Figure 5.30 as a function of void ratio. Note the range which the conductivity values extend through (over 4 orders of magnitude). The values in the high void ratio region reflect the difficulties encountered, as they are slightly scattered. The relationship between $\log k$ and e , over this range, is shown to be definitely nonlinear.

5.2.2.2 Oil Sand Tailings Sludge-Sand Mixes

As described in section 5.2.1.2 the permeability tests on the sludge-sand mixes were regularly interfered with by the formation of gas, and this is reflected in the results. Figure 5.31, a velocity-gradient plot for the 46% sand mix, is typical of the sludge-sand $v-i$ plots with respect to the scatter involved.

The resulting permeability plots, hydraulic conductivity as a function of void ratio, for 46% sand and 80% sand sludge-sand mixes are given in Figures 5.32 and 5.33 respectively. Despite scatter due to the experimental difficulty, the Figures exhibit clear relationships between k and e for the two mixes.

Several items of interest can be noted from the Figures. First, the difficulty of using the actual data as input to a finite strain consolidation program is apparent. The actual data will lead to erroneous results as some higher void ratio conductivities are lower than those at lower void ratios. Second, the benefit of having data over a larger void ratio range than required by the problem is

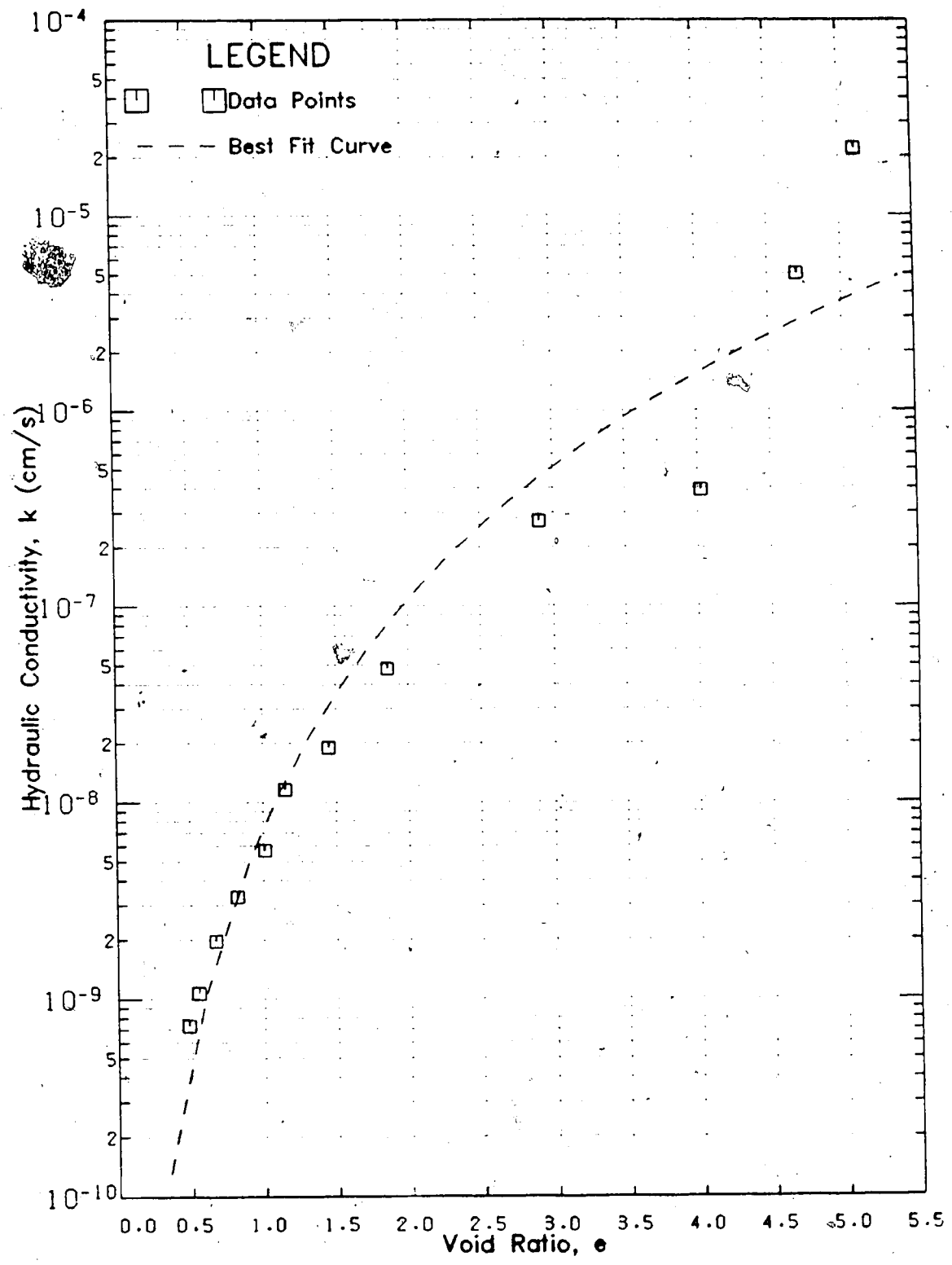


Figure 5.30 Permeability of Oil Sand Tailings Sludge

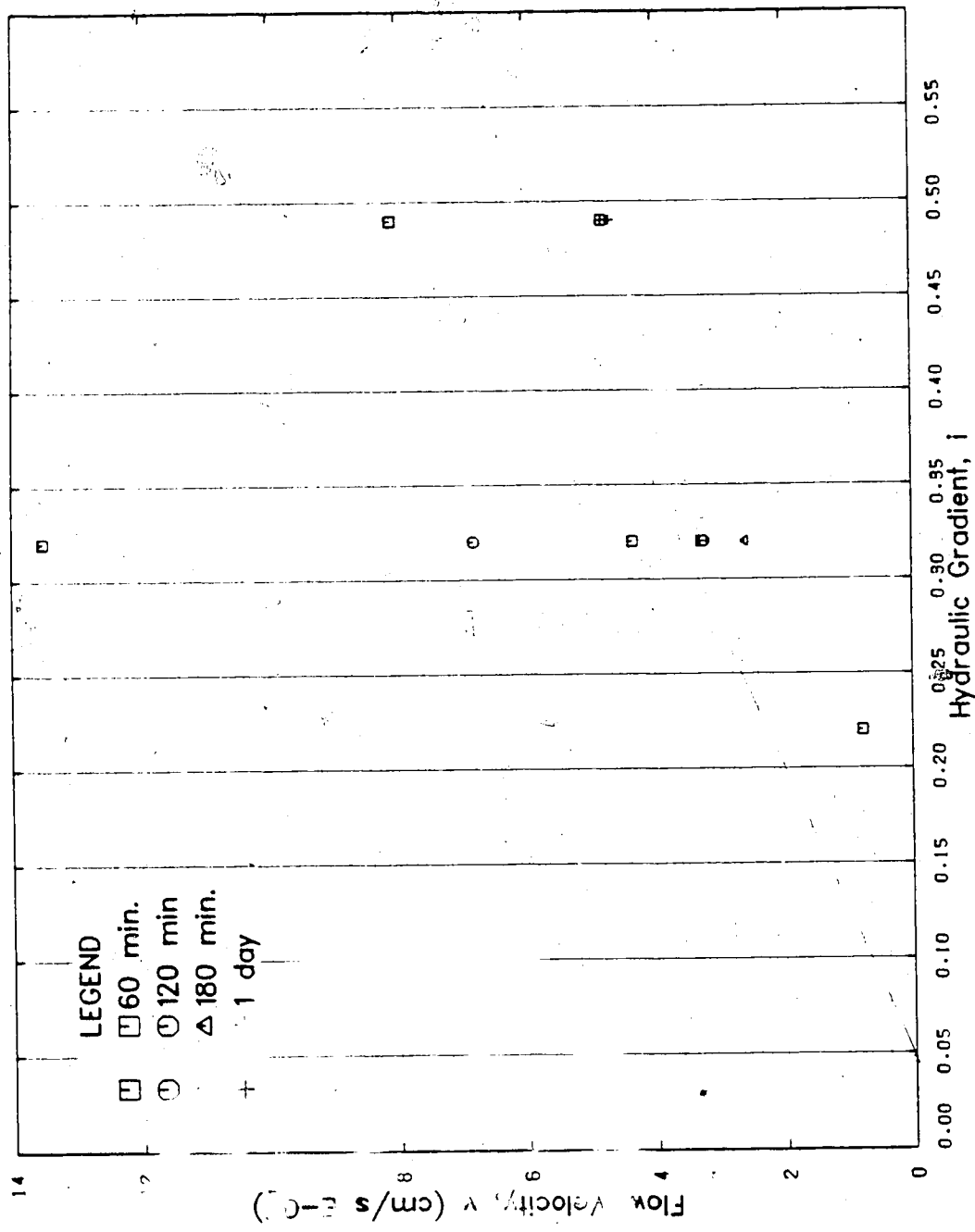


Figure 5.31 Flow vs. Gradient, 46% Sand Sludge-Sat, e=2.03

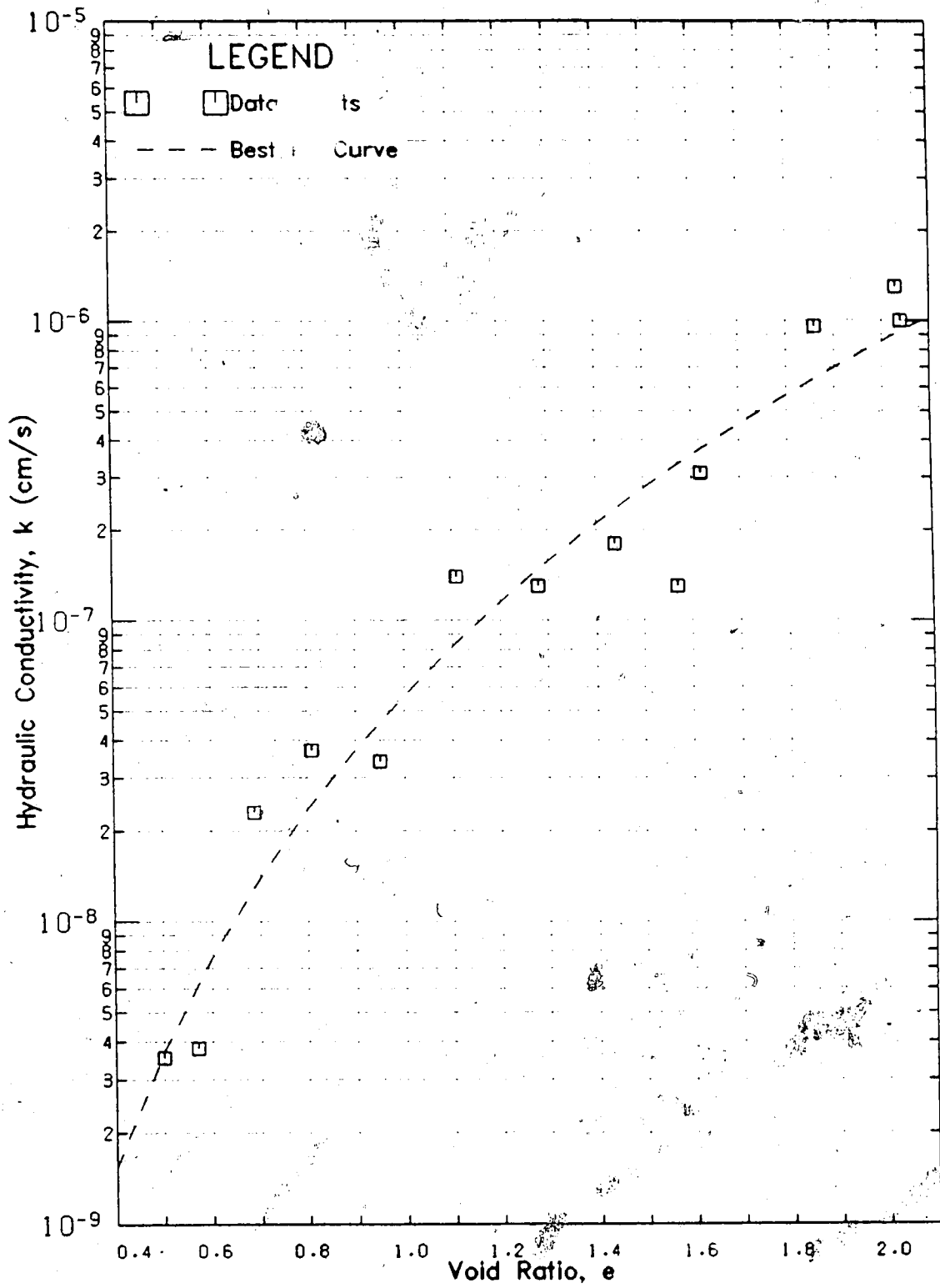


Figure 5.32 Permeability of 46% Sand Sludge-Sand

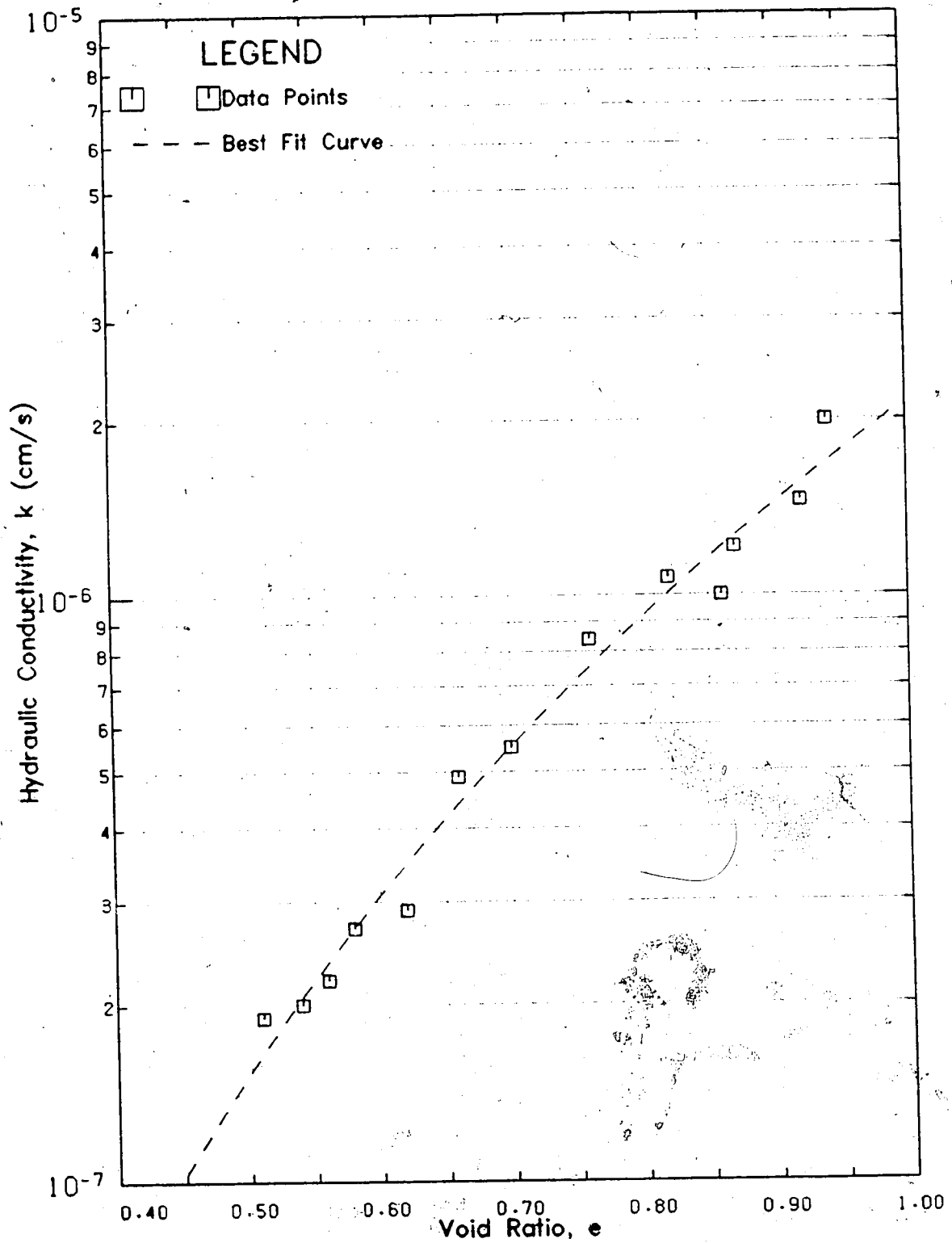


Figure 5.33 Permeability of 80% Sand Sludge-Sand

evident, as the k - e relationship becomes more established.

For the 46% sand mix, the relationship between $\log k$ and e is nonlinear over the void ratio tested (0.5 to 2.05). For the 80% sand mix, the relationship is only mildly nonlinear over the void ratio tested (0.5 to 0.95).

5.2.2.3 Oil Sand Tailings Sludge-Sand Mix with Flocculent

Despite similar problems with gas during the tests, the 73% sand sludge-sand mix with the flocculent yielded relatively linear velocity-gradient plots with minimal scatter. Figure 5.34 is typical of the velocity-gradient plots for the mix with the flocculent.

Although the v - i plots were well behaved, the hydraulic conductivity - void ratio data was still slightly scattered in the high void ratio end. Figure 5.35 shows the resulting permeability data. Again, the Figure exhibits a clear k - e relationship. The relationship between $\log k$ and e is shown to be nonlinear over the void ratio tested.

5.2.2.4 Comparison of the Four Tests

The hydraulic conductivity as a function of void ratio for all four slurries is shown in Figure 5.36. Evident from the Figure is the remarkable consistency of the permeability trends from one mix to the next with respect to the sand/fines content. This pattern, as with the compressibility data, allows one to interpolate permeability values for mixes not tested from the family of curves plot.

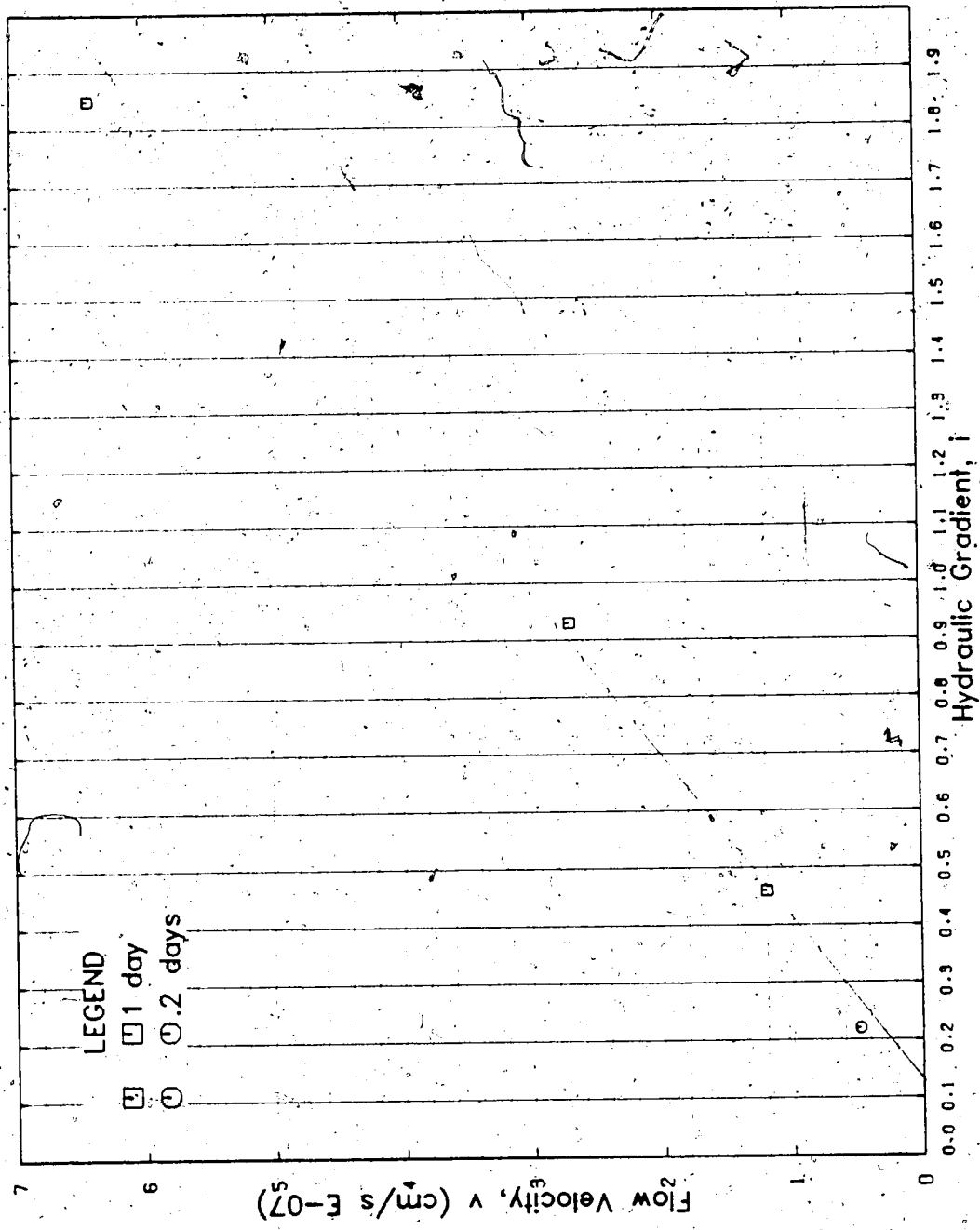


Figure 5.34 Flow vs. Gradient, Sludge-Sand Mix with CaCl_2 , $e = 0.90$

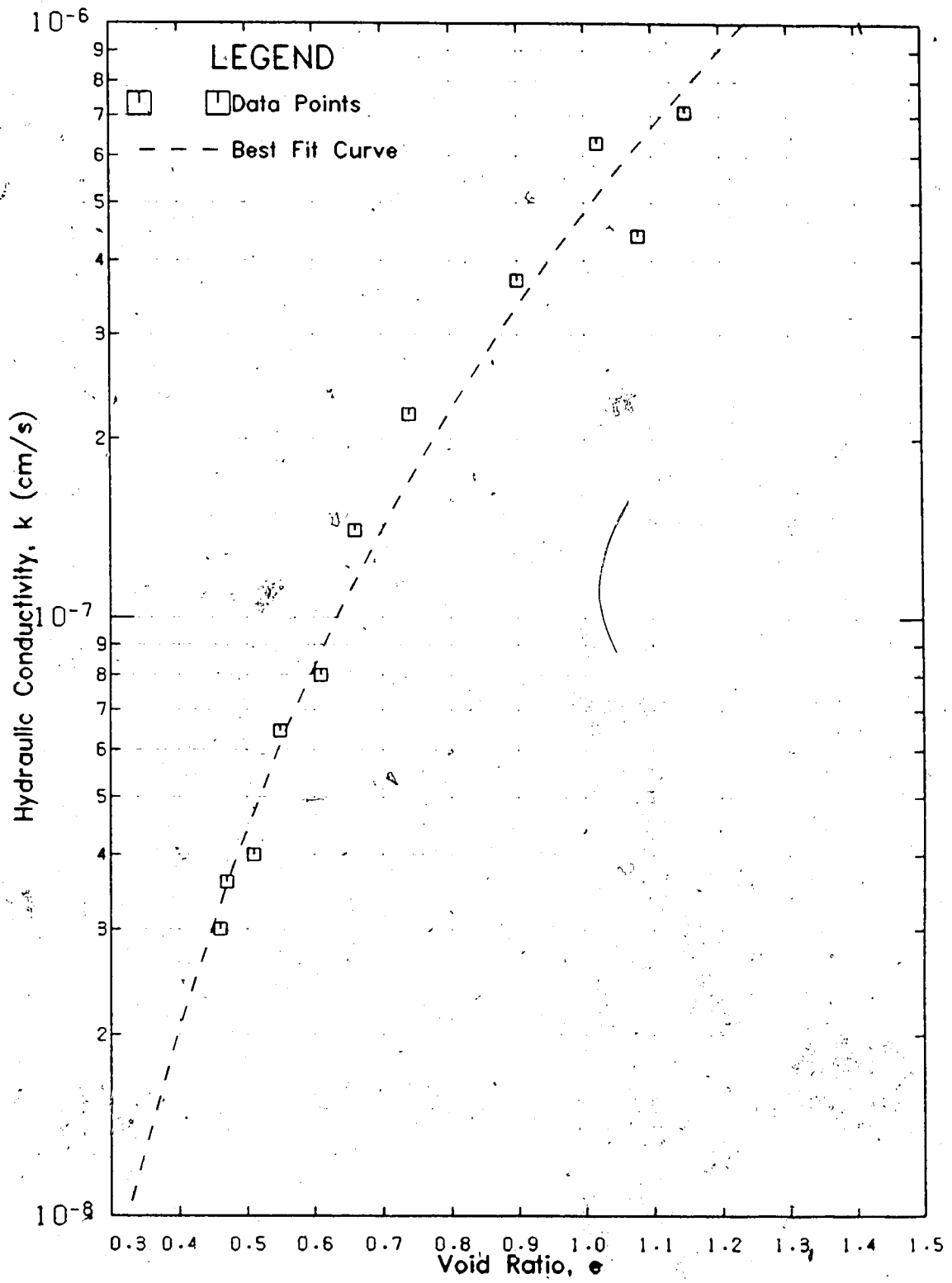


Figure 5.35 Permeability of 73% Sand Sludge-Sand with CaCl_2

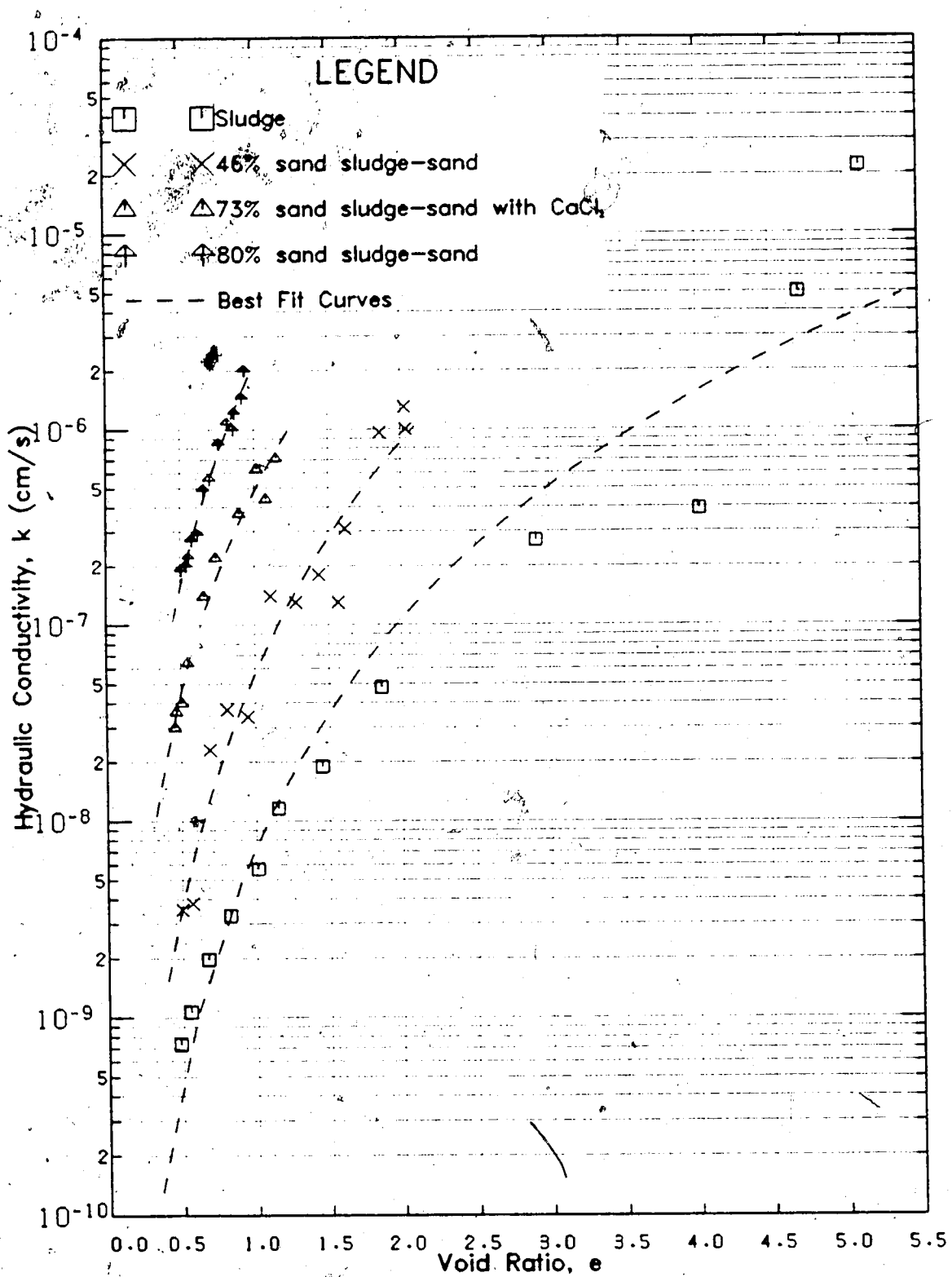


Figure 5.36 Permeability of All 4 Slurries

Also evident from the Figure is the variation of permeability (several orders of magnitude) at a given void ratio. The permeability, at a given void ratio, decreases with increasing fines content. In fact, it is the concentration of fines that governs the permeability and not the sand. This is borne out remarkably well in Figure 5.37 where the hydraulic conductivity is plotted as a function of the fines void ratio. The fact that the data for all four slurries fall on the same line indicates the permeability's dependence on the fines. The sand's influence on the permeability appears only to be as a filler, that is, it decreases the fines concentration for a given volume. For this reason, as is seen in Figure 5.36, the permeability increases with increasing sand content.

Figure 5.37 is a check for internal consistency as well as a reason for confidence in the data. If one or two of the tests would have been off the line or intersect the data then their results would have been somewhat in question. Also, use of the steady state value for flow velocity is validated.

Also shown in Figures 5.36 and 5.37 is that, similar to the compressibility, the flocculent has no effect on the permeability. The 73% sand sludge-sand mix data is completely consistent with the other tests.

The findings of the fines void ratio plot (Figure 5.37) allow a design engineer to do one better than the family of curves plot (Figure 5.36). Now, theoretically only one

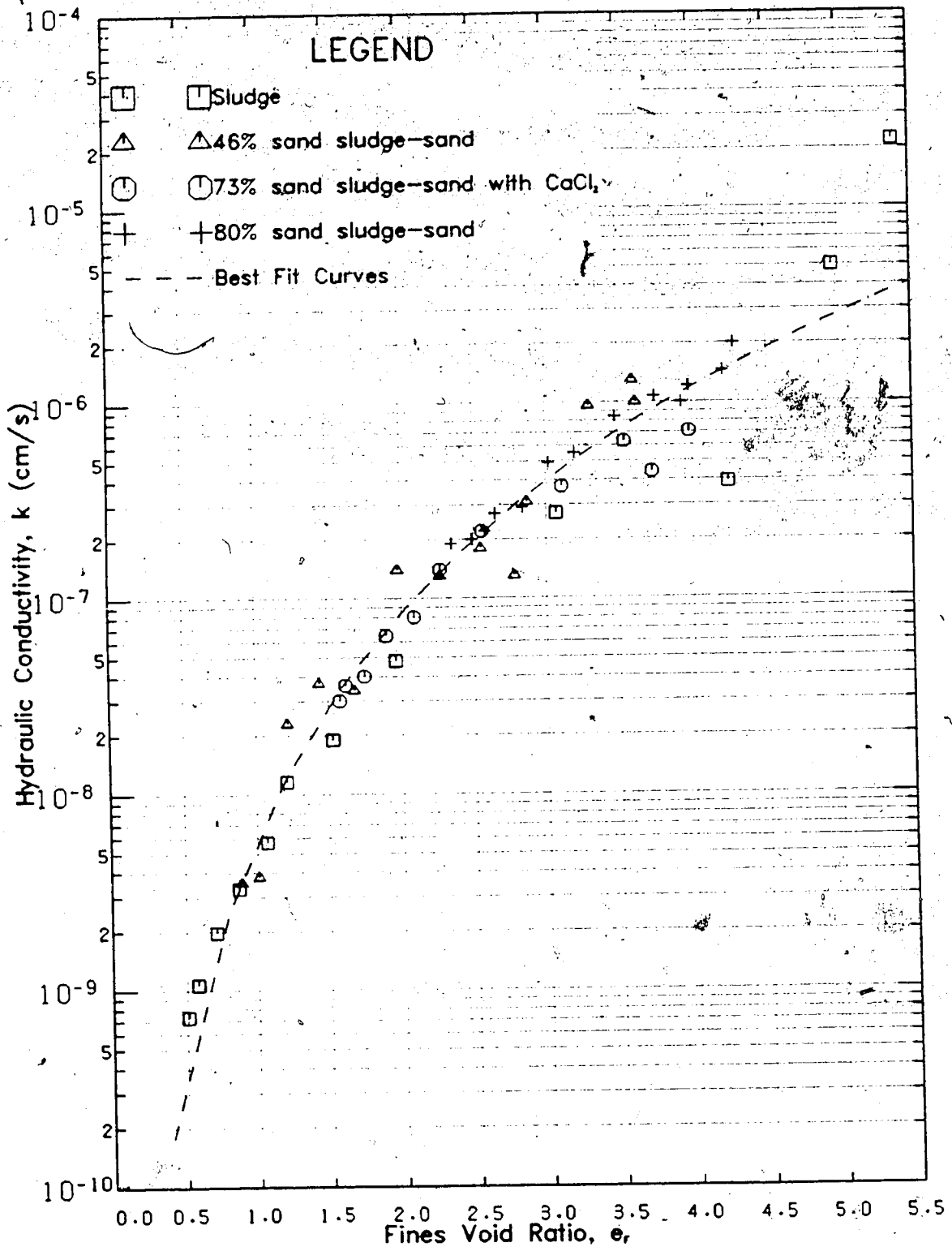


Figure 5.37 Permeability of All 4 Slurries vs. Fines Void Ratio

sludge-sand mix needs to be permeability tested to develop the "family of curves". Since there is a unique $k-e$ relationship for a "family of slurries", a $k-e$ curve can be back calculated for any percentage sand content using equation 5.1 or 5.2. However it would be wise to do at least two tests to develop the $k-e$ relationship, one of which being on the sludge with no admixtures. The same caution given for the compressibility applies, that is, the relationship will be unique to each material and to each mine site.

5.3 Summary of Observations and Conclusions

Due to the wide variety of observations discussed in this Chapter, it would be beneficial to summarize the major findings and conclusions.

5.3.1 Consolidation and Compressibility

The self weight consolidation results of the four tests were affected by both the relative density of the sludge solids and the amount of sludge in the slurry. The D_{r_s} value is increased when sand is added to the sludge, meaning its self weight stress is increased, and logically therefore the amount of consolidation is increased. Although this was shown to be true, Figure 5.12 also showed that the consolidation at the end of the self weight increment was affected by the amount of sand in the mix. That is, as the amount of sludge decreases, the amount of consolidation

increases.

From the consolidation time plots, a trend of delayed consolidation was evident for the lower stress increments (higher void ratios). As the stress increments increased and the void ratios decreased, the delay was lessened and the curves shifted towards smaller time. Although this trend was somewhat evident in sludge-sand mixes, it was more visible in the sludge data.

The compressibility data for all four tests yielded nonlinear $e - \log \sigma'$ curves over the stress ranges tested. The $e - \log \sigma'$ curves began to linearize as the sludge content was decreased by the addition of sand.

The ability of the sludge to resist consolidation and compression even when diluted with sand was again seen, in Figure 5.17. As an example, under a stress of 1.5 kPa a sludge-sand mix with 46% sand (a significant portion) had a void ratio of 1.65 as compared to 0.88 for an 80% sand mix.

The compressibility results yielded a "family of curves" for the oil sand tailings/sludge sand mixes. Not only does this allow one to interpolate compressibility curves for different sand proportions, for this oil sand tailings, it also indicates that for different tailings, only a limited number of tests need to be performed.

5.3.2 Permeability

The permeability tests revealed a time dependent flow discharge with a constant gradient. The flow velocity would

drop up to two orders of magnitude before reaching a steady state value. The time to steady state varied up to 15 hours for the sludge, less for the sludge-sand mixes. The process was repeatable and the initial condition appeared to be reattainable after only a few minutes of no flow, even after hours of flow. The drop in flow velocity decreased with decreasing void ratio. The drop in flow velocity appeared to be less for the sludge-sand mixes than for the sludge for the majority of the cases.

The steady state values were used for the determination of the hydraulic conductivity values. The validity of this method was borne out in relatively linear $v-i$ plots (with some scatter) and consistent $k-e$ plots (as evidenced in Figures 5.36 and 5.37). Because of the presence of gas during the permeability tests, the flow-time plots became valuable tools in determining which results deserved more weight.

The results showed no concrete evidence of the existence of a threshold gradient.

An important finding from the permeability tests was that the relationship between hydraulic conductivity and the fines void ratio was the same for all the slurries. This unique dependence on the fines void ratio indicates the sand does not affect the permeability except to decrease the fines concentration. This is shown in Figure 5.36, where at a given void ratio the hydraulic conductivity increases with increasing sand content. This finding can be used similar to

the "family of curves" of compressibility data, when needing to determine the permeability for certain mixes.

With respect to the large gradient tests conducted (Figure 5.29), it was found that; the direction of flow had no influence on the flow velocity, the flow velocity was only marginally faster when approached from a smaller gradient, and that at unusually large gradients (greater than 200) Darcy's law becomes invalid as the increase in flow velocity becomes less with increasing gradient.

5.3.3 Effect of Sand and Flocculent

The major influences of the sand were to; decrease the sludges role of resisting compression and consolidation, increase the relative density of the sludge solids thereby increasing the self weight stress, linearize the $e - \log_{10} \sigma'$ curve, move the compressibility curve towards the direction of lower void ratio thus causing a smaller void ratio change for a given stress change with increasing sand content, and cause the permeability of a mix to be greater at a given void ratio by decreasing the concentration of fines.

The only effect the chemical flocculent had was to maintain the sand in suspension at a solids content which normally would lead to sand segregation. Figures 5.17 and 5.37 show how the sludge-sand mix with the flocculent yields consistent results with the other slurries with respect to compressibility and permeability respectively once self

weight consolidation is complete. Figure 5.8 shows the effect of keeping the sand in suspension on the self weight consolidation.

6. MODELLING OF SELF WEIGHT CONSOLIDATION TESTS

6.1 Introduction

As has been previously discussed, the geotechnical research program of the Department of Civil Engineering at the University of Alberta has a ten metre standpipe sludge and sludge-sand testing program (Scott, Dusseault, and Carrier, 1986). Details are presented by Scott and Chichak (1985a, 1985b, 1985c).

Oil sand tailings sludge obtained from the Syncrude Canada Ltd. tailings pond was pumped into a standpipe 10 m high and 0.91 m in diameter and allowed to consolidate under its own weight. Sludge-sand mixes were formed by combining sludge with tailings sand and the mix was then pumped into a standpipe and allowed to consolidate under its own weight.

The material description for the three standpipes has been presented in Table 4.1 and Figures 4.4 and 4.5. Standpipe #1 contains sludge without added sand, standpipes #2 and #3 contain 45% and 82% sand respectively. Standpipe #2 was discontinued, and additional sand was added to the material to form the sludge-sand mix for standpipe #3.

The standpipes (Figure 6.1) have pore pressure and sampling ports at various depths. The ports are connected to a pressure transducer and allow excess pore pressure profiles to be determined in conjunction with the sludge-water interface settlement. Sludge samples are extracted from the sampling ports, testing is then performed

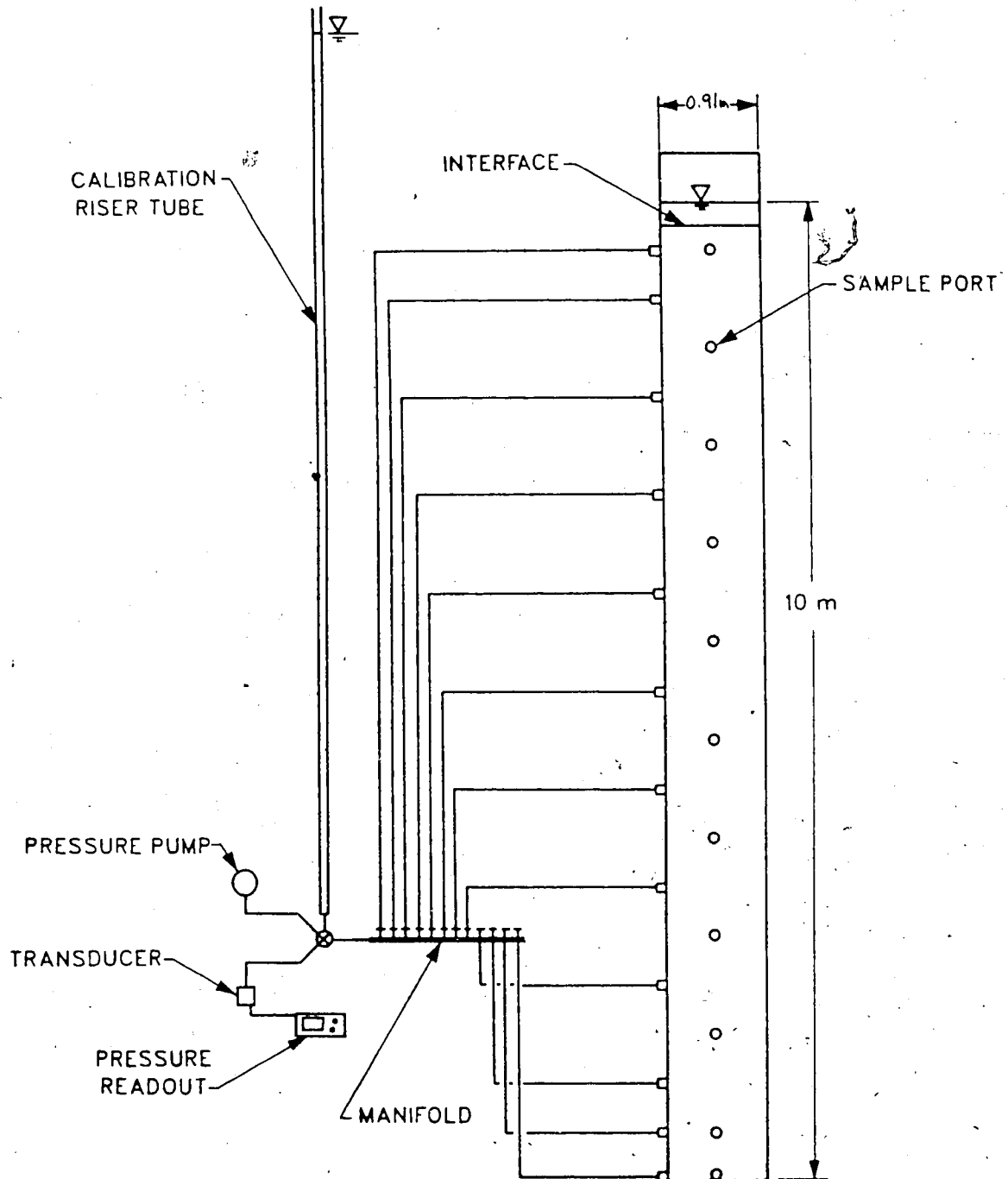


Figure 6.1 Ten Metre Standpipe

and a solids content or density profile can then be determined in conjunction with the interface settlement. These three pieces of data completely describe the progress of the consolidation of the slurry.

Because of the large scale, the monitoring, and the undisturbed environment of these tests, they provide an excellent opportunity to examine the ability of the finite strain consolidation theory to predict the progress of self weight consolidation of oil sand tailings sludge and sludge-sand mixes using laboratory data.

Chapter 3 discussed the finite strain theory in detail as well as presenting some of the analytical procedures used to solve the theory. Two procedures, Somogyi (1980) and Cargill (1982) were discussed in detail. The Cargill method allowed for use of direct laboratory σ' - ϵ - k data, where as the Somogyi method required a best fit power law relationship to describe the data (equations 3.24 and 3.26).

It was shown in Chapter 5 that due to scatter in the results, using direct laboratory data in this circumstance was not feasible and therefore smoothing or a best fit curve was required. It was shown in Chapter 3 that when using the same data, the two methods yielded virtually identical results. Therefore it was decided to use the finite strain consolidation program based on Somogyi (1980) for the analytical work in this Chapter.

The comparison between the theoretical results and measured will be based on the three monitored areas;

interface settlement, excess pore pressure profile, and solids content profile. The intent of this Chapter is not to explain the standpipe data or behaviour of the standpipe slurries, although this is done where relevant, but rather to examine the ability of the finite strain consolidation theory to model the progress of consolidation in the standpipes as measured, in the three forementioned areas. Discussion centers on the accuracy of the prediction and possible explanations are presented where discrepancies occur, however detailed work to account for any discrepancies is left to further research.

6.2 Standpipe #1

6.2.1 Input Parameters

Ten metre standpipe #1 contains oil sand tailings sludge whose properties have been shown in Table 4.1 and Figures 4.4 and 4.5. Slurry consolidometer test #1 was performed to obtain compressibility and permeability data for the sludge to be used in modelling standpipe #1. Tables 4.2 and 4.3, and Figures 4.4 and 4.6 show the material properties. Tables 4.1 and 4.2 show that the two slurries are quite comparable, with the standpipe sludge being slightly finer and having more bitumen than the consolidometer sludge.

The compressibility and permeability input parameters are in the form of four curve fitted constants as described

in Chapter 3 and shown in equations 3.24 and 3.26. Figure 5.13 shows the compressibility plot of the sludge with the best fitted curve. The curve was least squares fitted with a coefficient of determination (r^2) of 0.992, and the relationship is as follows:

$$e = 28.71 \cdot \sigma'^{-0.3097} \quad (6.1)$$

where σ' is in pascals. The high value for r^2 indicates that compressibility data for the sludge lends itself well to a power law relationship like that of equation 3.24.

The permeability data for the tested sludge along with the best fit curve is shown in Figure 5.30. The coefficient of determination was 0.947 and the relationship yielded is as follows:

$$k = 7.425 \times 10^{-11} \cdot e^{(3.847)} \quad (6.2)$$

where k is in m/s. The r^2 value, as would be expected from observing the data, is not as high as for the compressibility data but it still indicates a good correlation to a power law relationship. It is the data in the lower void ratio range (less than 4) which establishes the relationship and contributes to the high r^2 value. It is unfortunate that the data in the higher void ratio range is scattered, since this is the void ratio range through which the analysis will mainly occur. However, the data from the e - k plot (Figure 5.37) for all the data gives confidence to the individual relationships.

Immediately after the 10 m standpipe was filled, samples were taken from the sampling ports and pore pressure measurements were read. The samples were tested for bitumen and solids content. These results along with the pore pressure readings, assuming they reflected the total stress (i.e., zero effective stress condition), were used to obtain a bulk density. A material balance was then performed which showed the existence of gas; 0.69% by total volume (Table 6.1). It was necessary to adjust the relative density of the sludge solids to reflect the gas, and thus, the DR_{ss} value was lowered from 2.35 to 2.27 to account for the 0.69% gas volume.

The final soil parameter necessary to the analysis is the initial condition. It took only several hours to fill the 10 m standpipe and thus can be considered instantaneous when compared to the consolidation period in the analysis (4.6 years). The initial solids content value is 32.4% as determined from the initial samples.

A summary of soil input parameters is given in Table 6.2. The remainder of the problem specific input necessary to the analysis has to do with the consolidation conditions. These include initial height (10 m), analysis time, and lower boundary condition (impermeable).

The initial spatial increment (Lagrangian) was 0.125 m and the maximum allowable time increment for repeatability (found through trial and error) was 5 days.

Table 6.1 Ten Metre Standpipe #1 - Material Breakdown

Material	Mass (kg)	Volume (m ³)
Larger than 0.044 m	43.7	0.0165
Finer than 0.044 m	320.9	0.1211
Bitumen	31.2	0.0303
Water	825.2	0.8252
Gas	0	0.0069
Total	1221	1.000

Table 6.2 Soil Input Parameters

Parameter	Standpipe		
	#1	#2	#3
A (1/Pa)	28.71	7.256	1.814
B	-0.3097	-0.2052	-0.09929
C (m/s)	7.425×10^{-11}	5.606×10^{-10}	2.134×10^{-8}
D	3.847	3.927	3.794
DRss	2.27	2.45	2.54
so (%)	32.4	45.0	74.8

6.2.2 Comparison of Predicted with Measured Values

As previously mentioned, the comparison will be upon three areas; interface settlement, excess pore pressures, and solids content.

6.2.2.1 Interface Settlement

It was found that, similar to the consolidometer tests, the sludge-water interface was discrete and easily discernable (Scott and Chichak, 1985a). The depth was measured by lowering a graduated rod with a circular plate attached at the bottom to "sense" the interface. Results of the measurements are plotted in Figure 6.2.

It is seen from Figure 6.2 that, on the arithmetic time plot, the interface settlement is linear. However there is some deviation from the linear tendency ~~at about~~ at about 800 days, where the consolidation rate decreases slightly. Also of interest in the Figure is a delay in interface settlement in the first four months.

Also shown in the Figure is the result of the finite strain theory using the above input data. Notice that the theory predicts a linear settlement rate even up to the 4.6 year mark. This is a clear indication that the theory predicts the consolidation process for this situation to take decades. The ultimate consolidation predicted by the program is 5.12 m leaving a final height of 4.88 m.

One difference between the predicted and actual settlement is the slight deviation from linear of the actual data. Although the deviation is very small, it is an

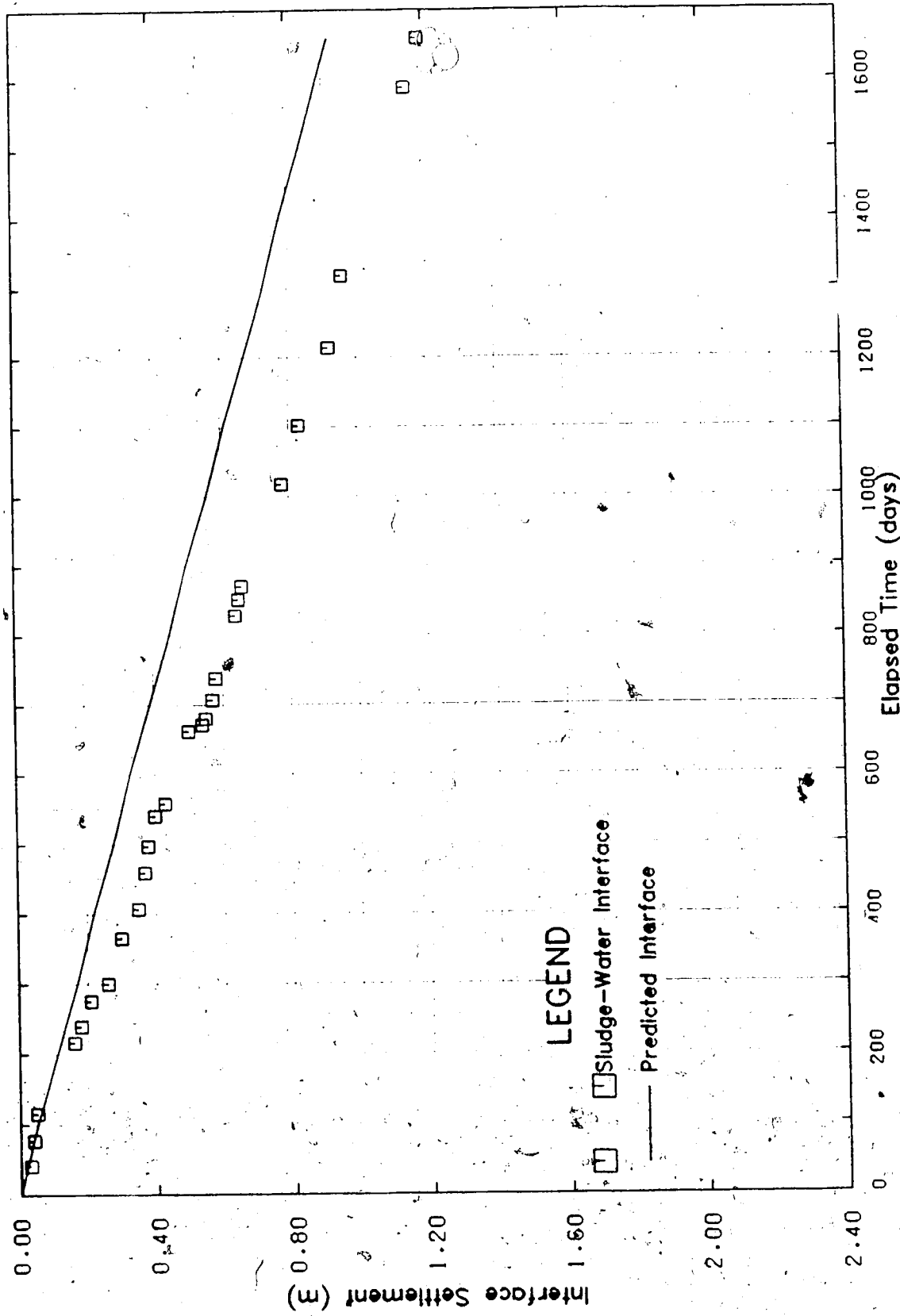


Figure 6.2 Standpipe #1 Sludge-Water Interface Settlement

indication that something not accounted for in the theory, possibly thixotropy, is beginning to retard the consolidation.

The other difference between predicted and actual settlement, which is more apparent than linearity, is the difference in the rate of consolidation. It is evident from Figure 6.2 that the standpipe sludge is consolidating faster than the theory predicts. The quality of fit can be judged better after examining the sensitivity of the analysis to the permeability of the material.

Figure 6.3 shows the shift of the best fit curve when the permeability relationship (equation 6.2) is increased by 50%

$$k = 1.114 \times 10^{-10} \cdot e^{3.847} \quad (6.3)$$

and decreased by 50%

$$k = 3.713 \times 10^{-11} \cdot e^{3.847} \quad (6.4)$$

It is seen from Figure 6.3, that with respect to the overall data, these changes to k are not too drastic. Figure 6.4 has the finite strain output using the permeability from equations 6.3 and 6.4. From Figures 6.3 and 6.4 it is apparent that given the sensitivity of the finite strain output to a relatively minor overall change in permeability, the correlation between the predicted and actual interface is quite reasonable.

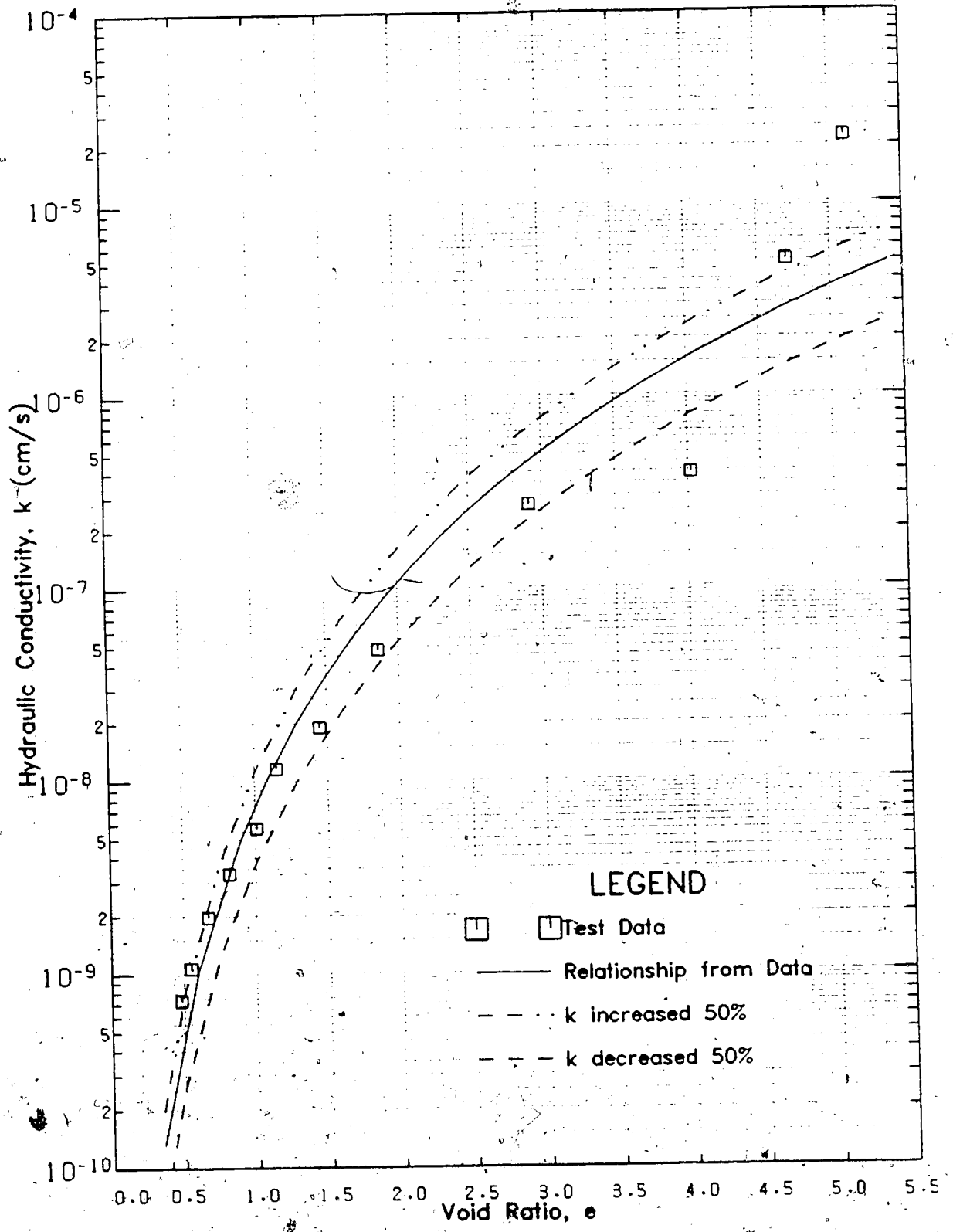


Figure 6.3 Permeability Input for Standpipe #1

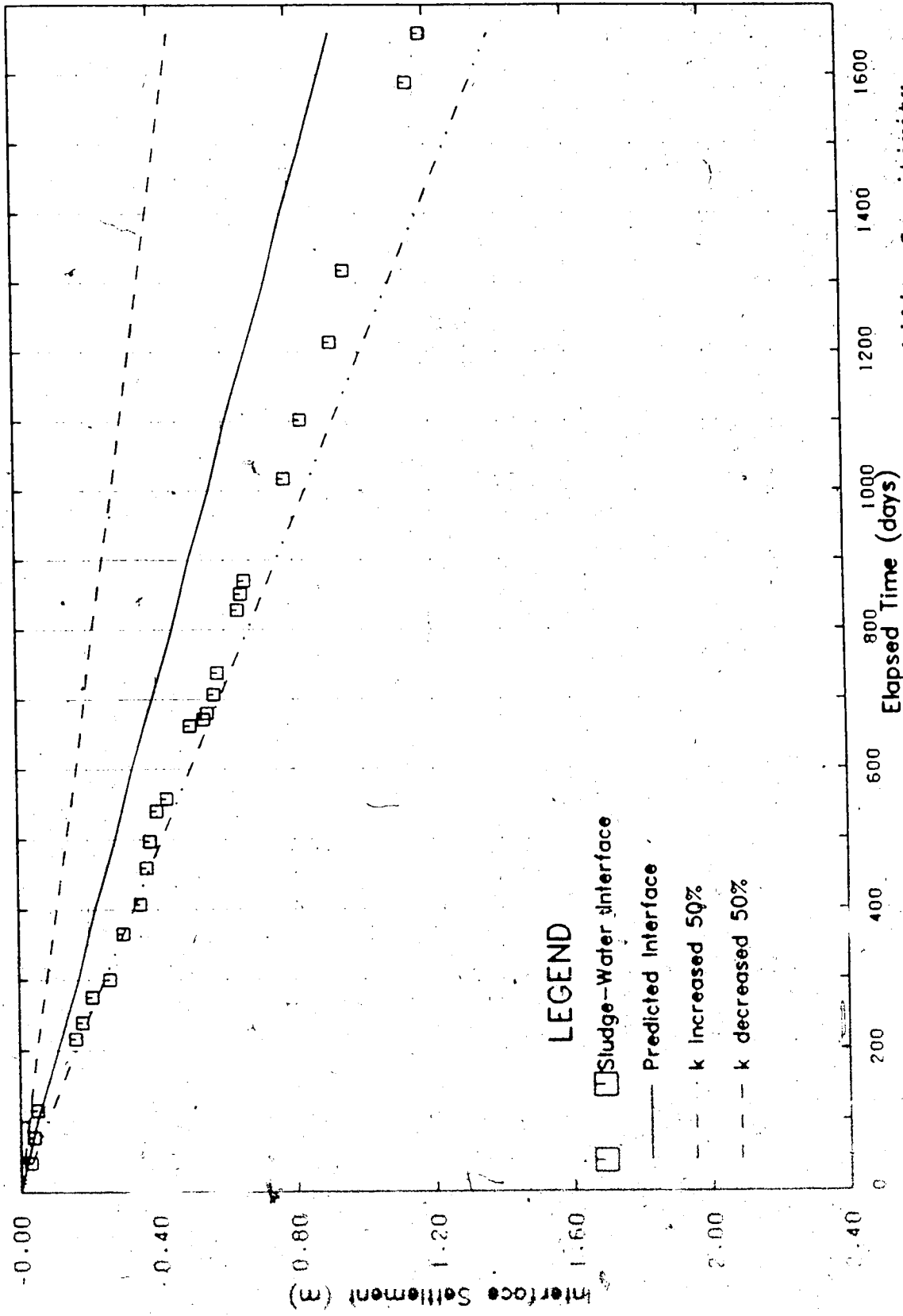


Figure 6.4 Standpipe #1 Sludge-Water Interface Settlement, Permeability Sensitivity

6.2.2.2 Excess Pore Pressures

Pore pressures were measured at ports at various depths along the side of the 10 m standpipe, as shown in Figure 6.1, when interface settlement was measured.

Figure 6.5 shows the excess pore pressure output from the finite strain program for 800, 1600, and 3200 days. Note that the linearity of the curves indicates that the reduction comes only from the surface moving down. It is the curved portion at the bottom of the plot where a reduction in excess pore pressure is due to consolidation. Therefore according to the program, after 1600 days (4.4 years), as seen from Figure 6.5, the sludge will have only a marginal reduction in excess pore pressure due to consolidation, and that, only in the bottom 1.5 metres. Note that at 3200 days, although the profile above the 8.5 m depth appears linear, it is indeed curved, indicating that some consolidation is occurring throughout the standpipe at this time.

When the predicted and measured excess pore pressures are compared, Figure 6.6, it is seen that the measured excess pore pressures do indeed fall along a straight line with some scatter, and that this line is coincidental with the predicted excess pore pressure line. The data, however, does not mimic the curvature at the bottom of the graph as predicted by the finite strain theory. But the difference is within the scatter since the curvature is so small and difficulties were associated with readings from the bottom ports due to a small layer layer of segregated sand (Scott

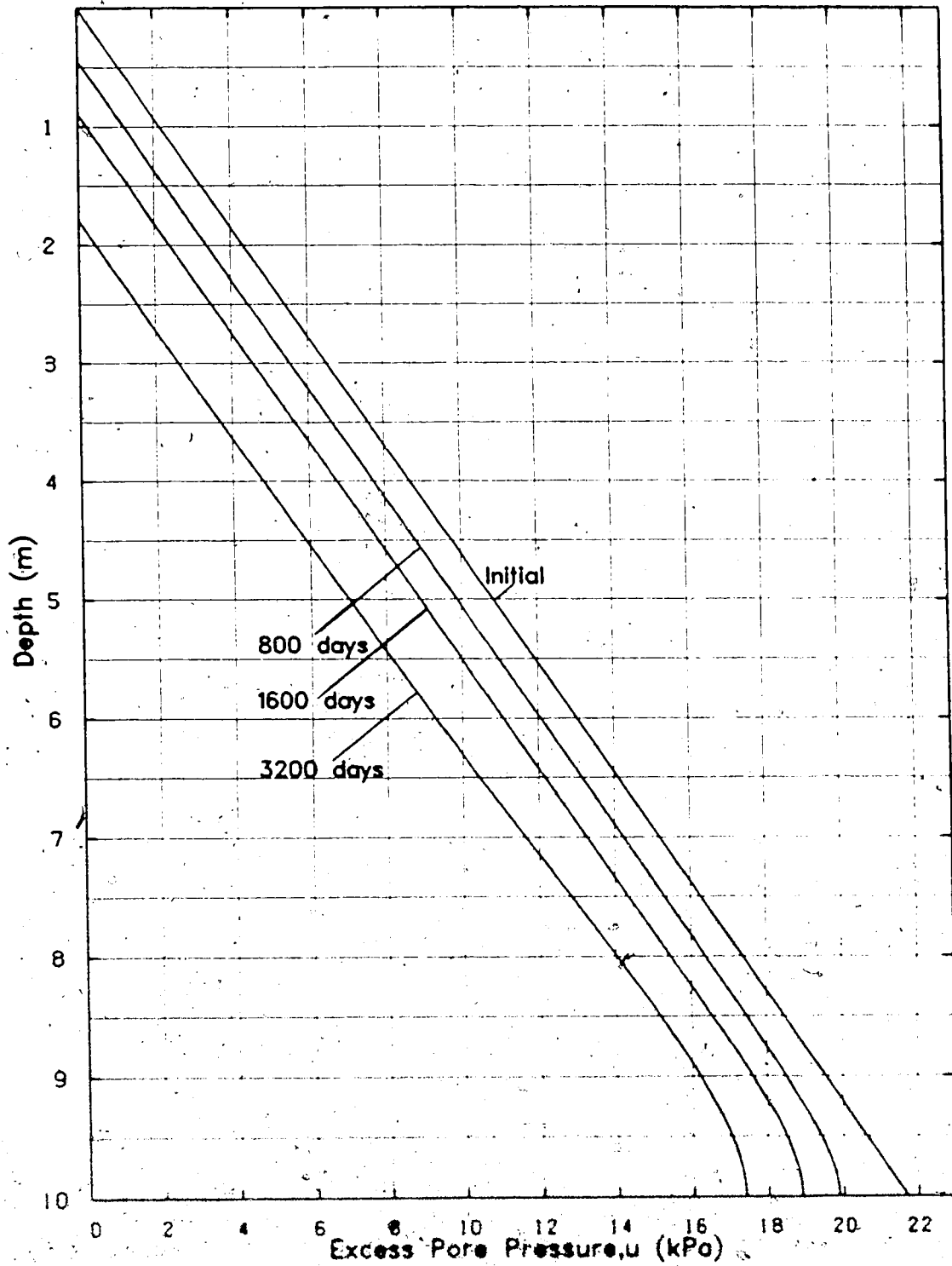


Figure 6.5 Predicted Excess Pore Pressure Profiles, Standpipe #1

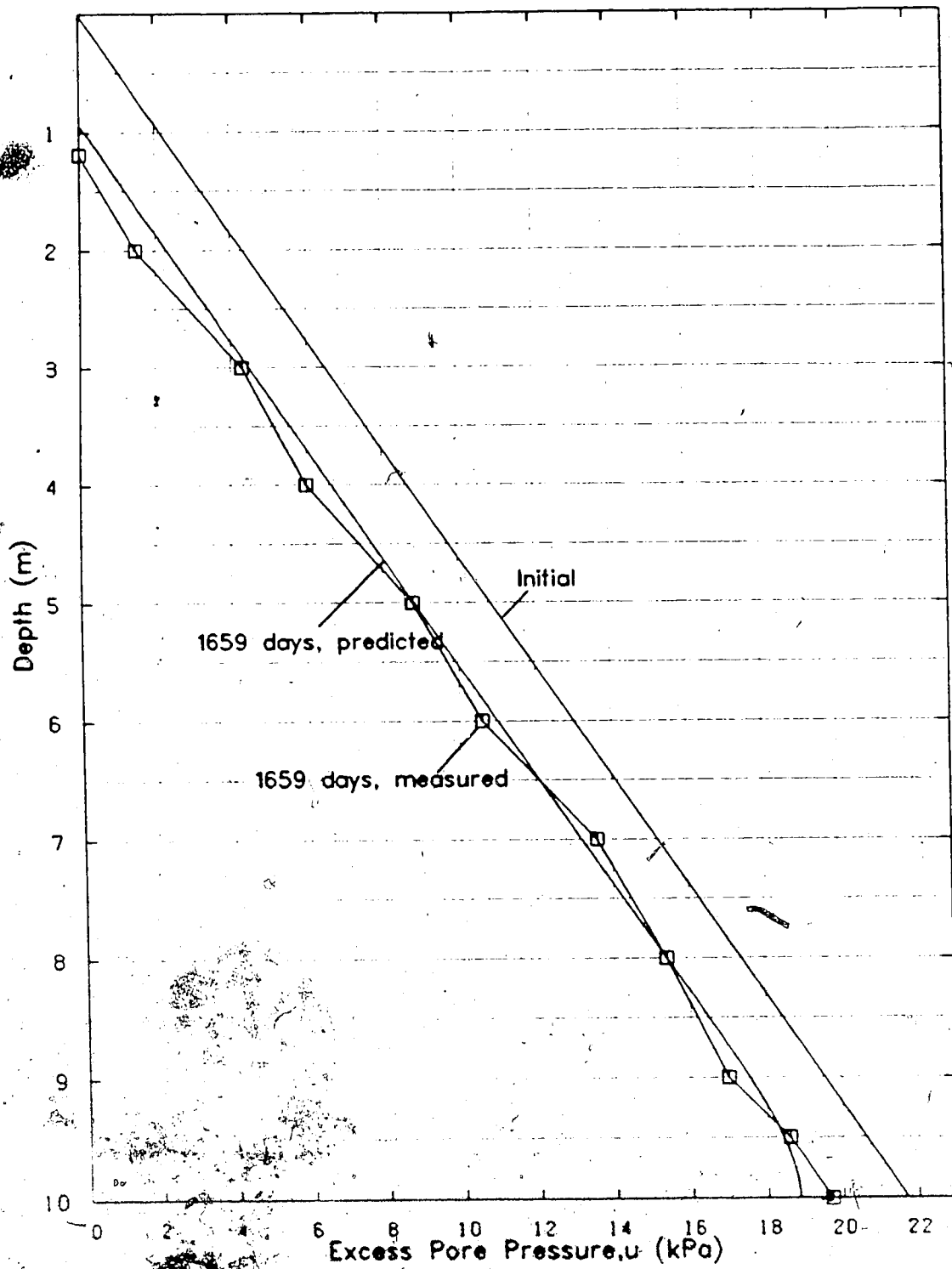


Figure 6.6 Comparison of Excess Pore Pressures, Standpipe #1

and Chichak, 1985a and 1985b). Overall, the prediction of the excess pore pressures is good.

6.2.2.3 Solids Content

Figure 6.7 shows the solids content output from the finite strain program plotted for several time periods. Similar to the predicted excess pore pressure profiles (Figure 6.5), the increase in solids content begins from the bottom, which is to be expected. However, Figure 6.7 reveals more of how the consolidation process is progressing in the upper portions of the standpipe. The 3200 day solids content profile explains the curvature found in the 3200 day excess pore pressure profile.

As previously discussed, samples were periodically taken from the standpipe at certain ports and analyzed for solids, water, and bitumen content. Figure 6.8 shows the results of the measured solids content at the 850 day mark along with the profile predicted by the finite strain program. It is evident that there is a fundamental discrepancy between the measured and predicted solids content profiles.

The predicted solids profile indicates that there should only be an increase in solids content in the bottom portion of the standpipe. However the data shows an increase in solids content along the entire depth of the sludge except for the top 50 cm, where a decrease occurs. The measured data indicates that consolidation is occurring at all depths and not just at the bottom. Therefore, in this

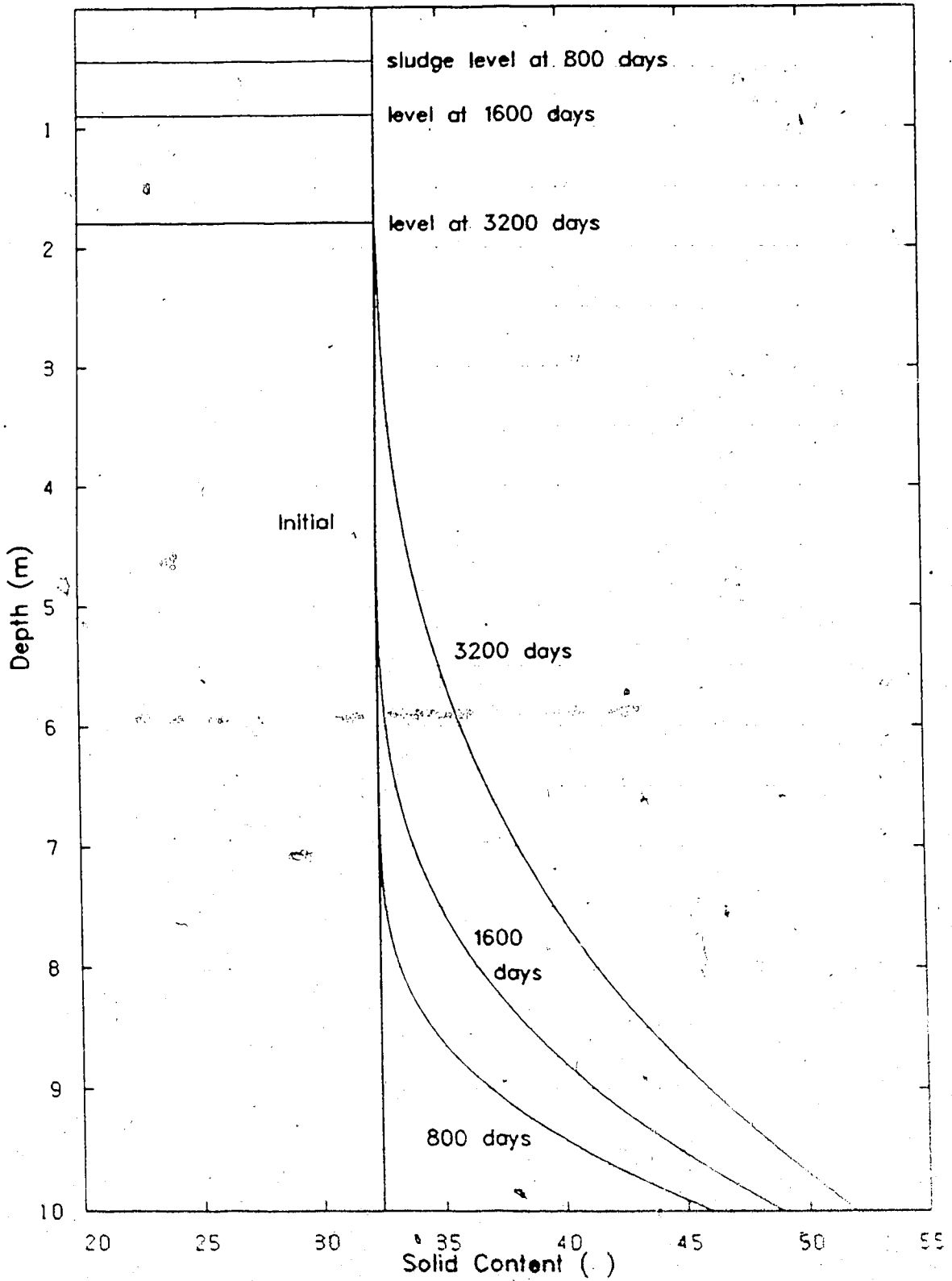


Figure 6.7 Predicted Solids Content Profiles, Standpipe #1

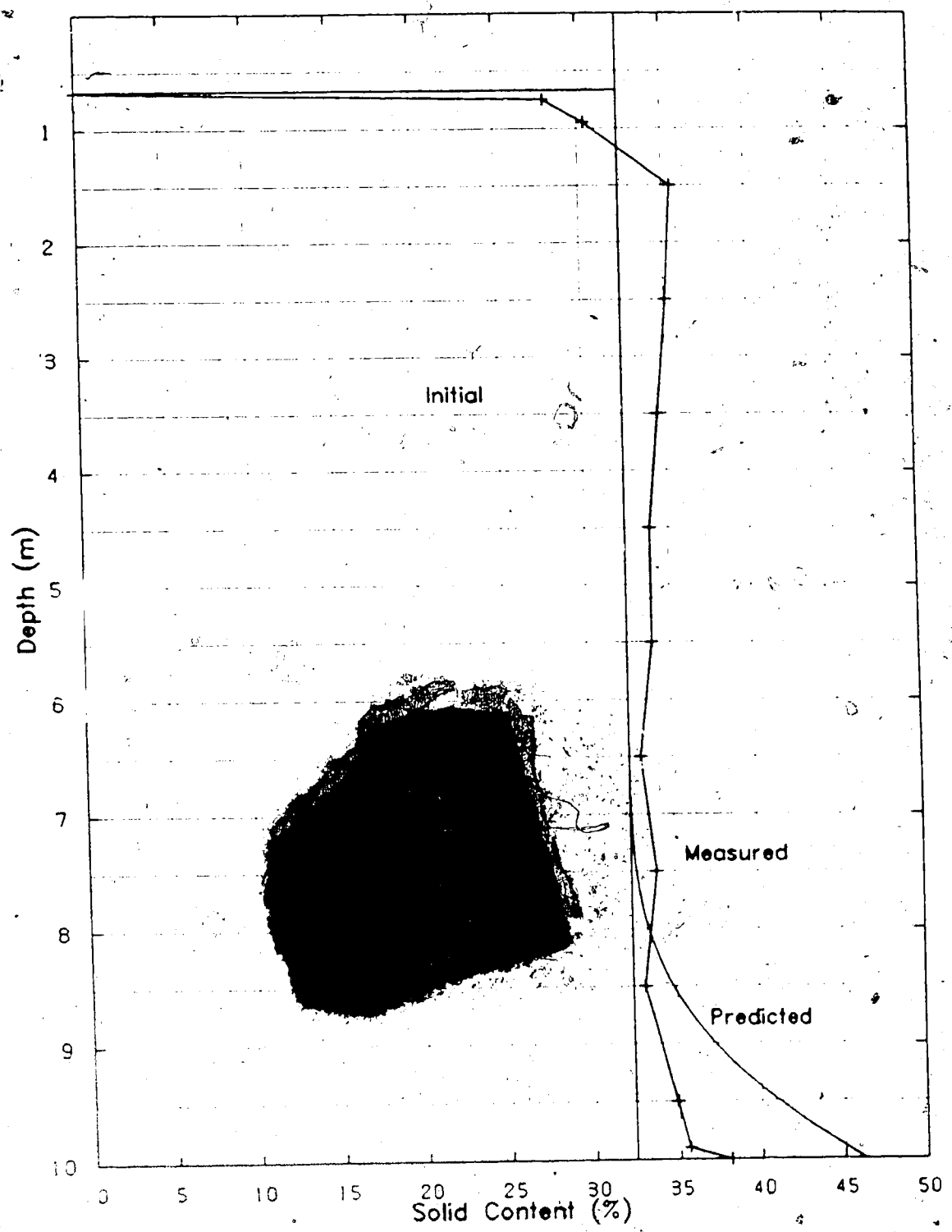


Figure 6.8 Comparison of Solids Content at 850 days, Standpipe #1

circumstance, it is simply not just a matter of the theory not predicting the proper amount, but that there is possibly an additional piece of physics occurring in the standpipe not considered by the theory.

Difficulties in the sampling may be the source of discrepancy. It is possible that gas comes out of solution when the sample is transferred from the in situ pore pressure to atmospheric pressure. The samples from the bottom of the standpipe would be more subject to gas evolution because of the greater difference in pore pressure change, and therefore yield abnormally low densities.

Any explanation for the difference must take into account that there was good correlation between the predicted excess pore pressure profile and the measured profile. Another possibility is that thixotropy may be having an influence and this might in turn cause the interface settlement to be retarded from the predicted linear path as mentioned in 6.2.2.1.

However, before any conclusions can be derived it would be necessary to conduct in situ tests in the standpipe to validate the accuracy of the measured data. Such tests could be an X-Ray technique as employed by Been and Sills (1981) or a nuclear method.

6.3 Standpipe #2

6.3.1 Input Parameters

Ten metre standpipe #2 contained a sludge-sand mix whose properties have been shown in Table 4.1 and Figures 4.4 and 4.5. Slurry consolidometer test #2 was performed to obtain the compressibility and permeability data of the sludge-sand mix to be used in modelling standpipe #2. The slurry consolidometer sludge-sand mix description was given in Tables 4.2 and 4.3, and Figures 4.4 and 4.6. A comparison of Tables 4.1 and 4.2 show that the sand content is similar, however the standpipe sludge-sand had an abnormally high amount of bitumen, which may have some effect on the accuracy of the predictions.

The compressibility and permeability are again the curve fitted constants A, B, C, and D of equations 3.24 and 3.26. Figure 5.14 shows the compressibility plot of the sludge with the best fit curve. The curve was least squares fitted with a coefficient of determination of 0.990 and the relationship is as follows:

$$e = 7.256 \cdot \sigma^{(-0.2052)} \quad (6.5)$$

The high r^2 value indicates once again that compressibility data, in this case for a sludge-sand mix, is well suited to a power law relationship.

The permeability data for the consolidometer sludge-sand along with the best fit curve is shown in Figure 5.32. The coefficient of determination is 0.94 and

the relationship is as follows:

$$k = 5.606 \times 10^{-10} \cdot e^{3.927} \quad (6.6)$$

As with the sludge, the correlation value r^2 is not as high for the permeability data as for the compressibility data, but the value of 0.948 suggests a good fit to the power law relationship.

The relative density of the sludge solids to be used as input for the finite strain program will be that of the standpipe material. The $D_{R_{SS}}$ value of 2.45, is less than the consolidometer sludge-sand $D_{R_{SS}}$, reflecting the higher bitumen content is the standpipe.

The final soil input parameter is the initial solids content. This value for standpipe #2 was found on average to be 45.0%. The summary of soil input parameters is given in Table 6.2.

The analysis period for standpipe #2 is only 2 years as the test was stopped and additional material was added to form the mix for the third standpipe test. The remaining inputs; initial height, lower boundary condition, time increment, and initial spacial increment are the same as for standpipe #1.

6.3.2 Comparison of Predicted and Measured Values

6.3.2.1 Interface Settlement

The depth of the sludge sand mix - water interface was measured in the same manner as described for standpipe #1.

The total duration of the standpipe #2 test was 710 days and the interface data is shown in Figure 6.9. Evident from the Figure is a discrete change in the settlement rate at 225 days. Although the cause for this change in rate remains unknown, Scott and Chichak (1985b) postulate that it is related to the sand segregation which was present in the top 30 cm for the first two days of the test. Since the sludge-sand mix is so close to the segregation boundary (Figure 4.4) they propose, coarse sand particles settling through the fines matrix may have opened drainage channels and may not have been "squeezed" shut until enough consolidation had occurred.

Also shown in Figure 6.9 is the predicted interface output from the finite strain program. Similar to standpipe #1, the predicted interface settlement is linear for the time period analyzed. The theory yields a settlement rate for this sludge-sand mix to be 2.3 times that of the rate predicted for the sludge in standpipe #1. The ultimate settlement predicted by the program will be 4.85 m, which is 0.27 m less than that predicted for standpipe #1.

When the predicted and measured interfaces are compared (Figure 6.9) it is seen that although the theory predicts the settlement at the end of the test to within a few centimetres, it does not model the settlement prior to this. Although the last two months of data appear to follow the predicted interface, that period is too short to be a basis for comparison. Therefore it is to be concluded that past

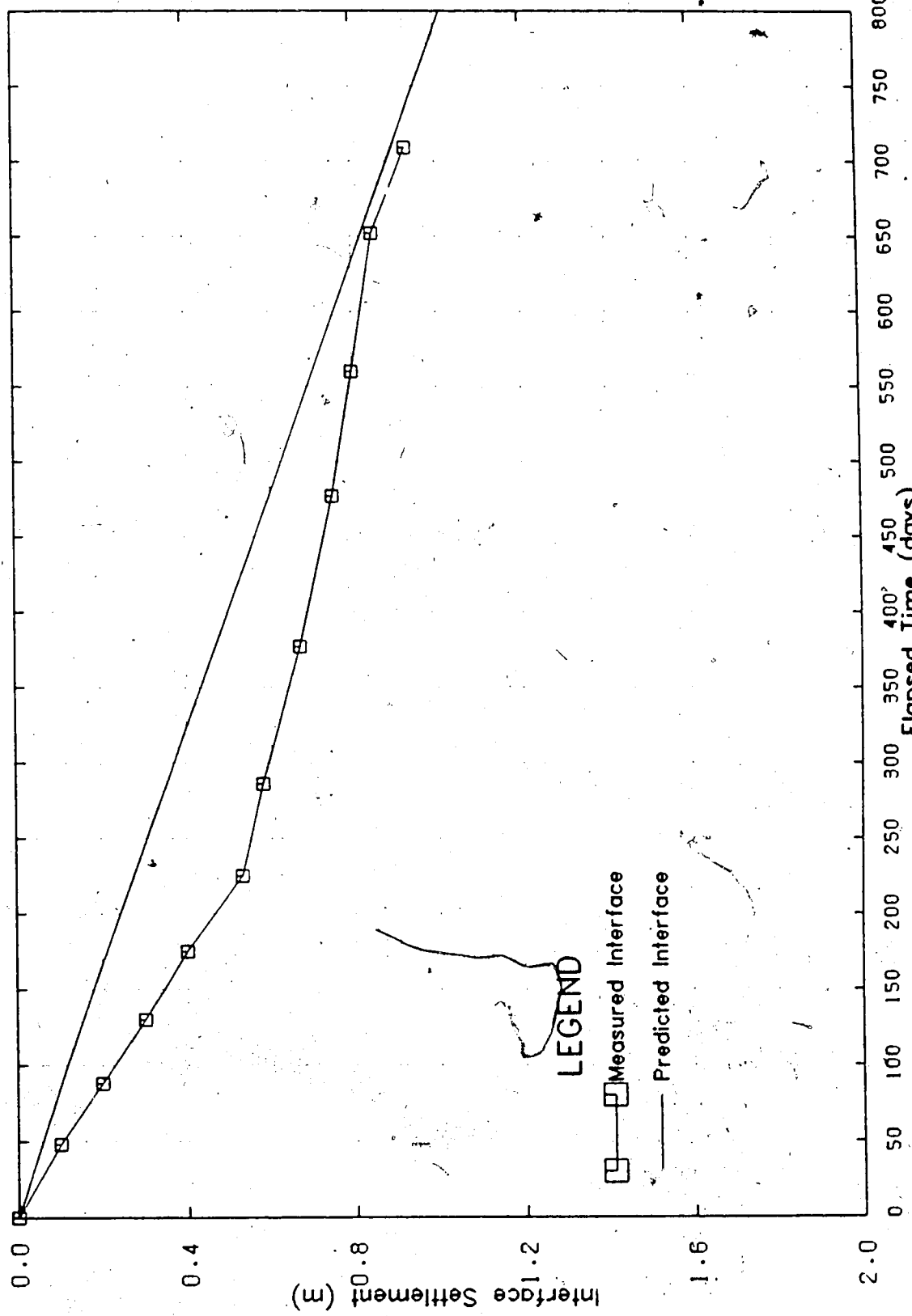


Figure 6.9 Standpipe #2 Sludge Sand Mix-Water Interface Settlement

225 days, the settlement rate predicted is 35% less than the measured.

To have properly modelled the consolidation, the permeability relationship would have had to been increased by 85% up to the 225 day mark (channeling), after which the permeability would have had to been decreased by 35% (from the original).

6.3.2.2 Excess Pore Pressures

The excess pore pressure output from the finite strain program is shown in Figure 6.10 for various times. Evident from the Figure is the curvature in the top (above 8.5 m depth) portion of the profiles, even at 800 days. Also shown is the trend of the top part of the curve to become less steep, representing a greater slurry density, as the consolidation proceeds. This was mildly visible for standpipe #1 in Figure 6.5.

The measured pore pressures at 706 days are shown along with the predicted excess pore pressures for the same time in Figure 6.11. The Figure shows that below 3 metres the measured pore pressures have not dropped an amount consistent with the interface drop, but the excess pore pressures remain parallel with the predicted data. Also shown in the Figure is that similar to standpipe #1, the curvature at the bottom of the standpipe (9.5 - 10 m) is not followed by the data. Therefore, for standpipe #2, the correlation between predicted and measured excess pore pressures is weak.

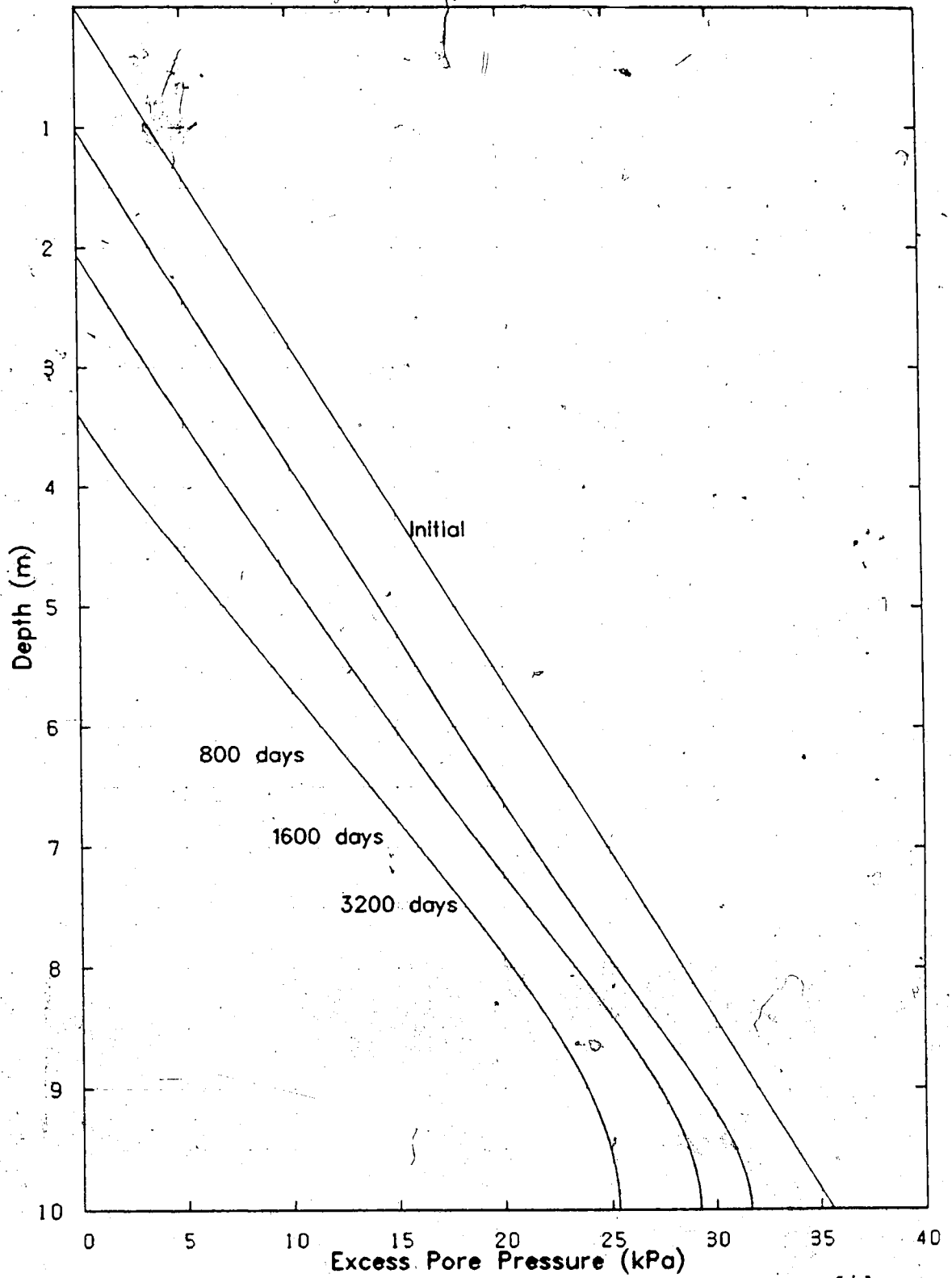


Figure 6.10 Predicted Excess Pore Pressure Profiles, Standpipe #2

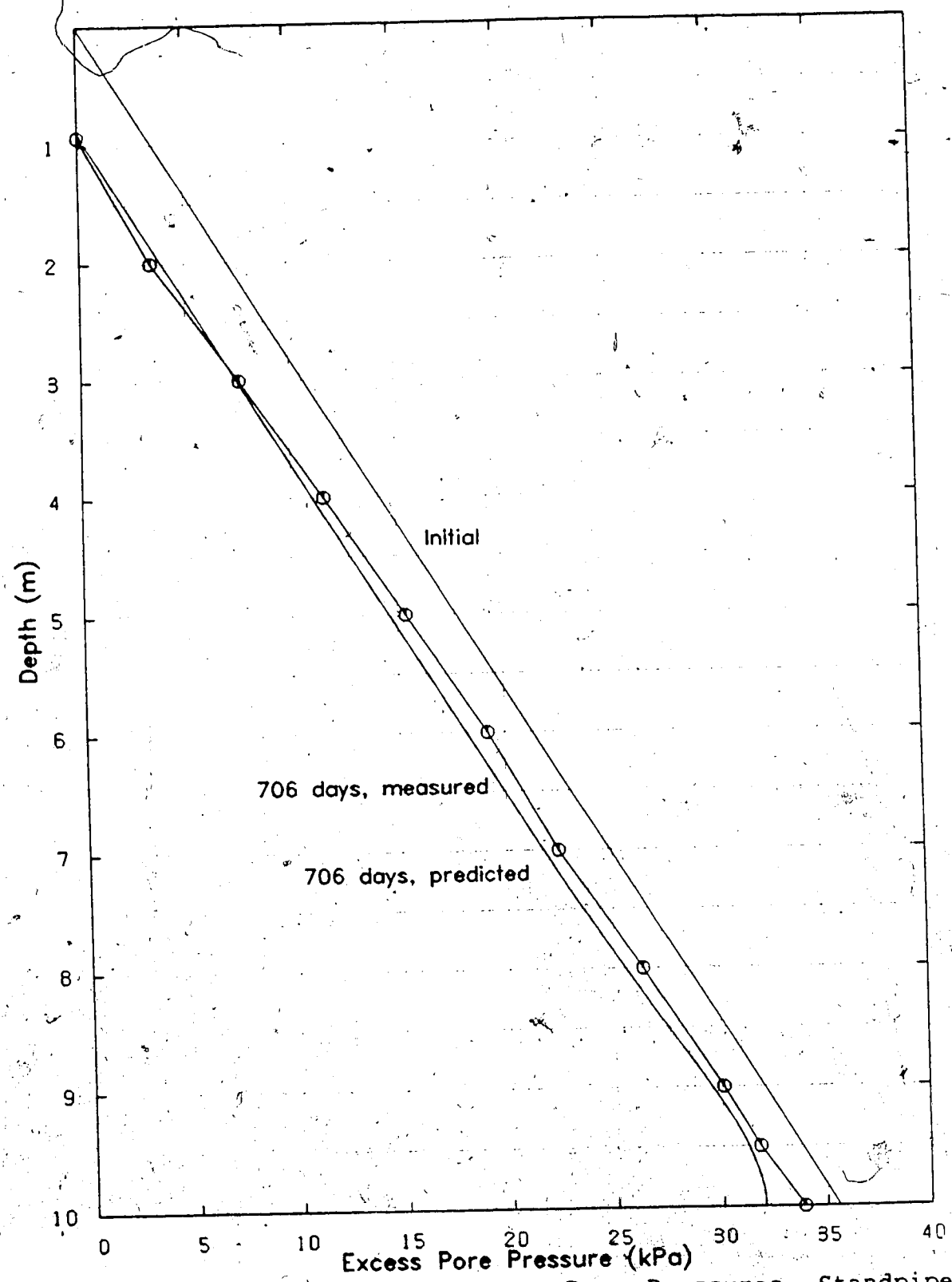


Figure 6.11 Comparison of Excess Pore Pressures, Standpipe

#2

6.3.2.3 Solids Content

Figure 6.12 shows the measured and predicted solids content profiles for standpipe #2 at 709 days. Evident from the Figure is the major discrepancy in the shape of the solids content profile that was also seen in Figure 6.8 for standpipe #1. However in this case the measured solids content data decreases from 50% at 1.5 m to 46% at a depth of 7.5 m before increasing again.

The erratic and inexplicable measured data would suggest problems with the sampling of the material. Although this may be the case, several things should first be noted. First, the sampling procedure was able to show the segregation region in the top 30 cm (Figure 6.12) as well as the large increase in solids content at the base of the standpipe due to a layer of sand that resulted from segregation. Second, the excess pore pressure profile in the top 5 m does lend itself to the solids content profile in question. Note from Figure 6.11 that at 2 m the excess pore pressure dissipation is greater than predicted, but down to 5 m the slope in the measured data reverses, in that it crosses over the predicted line and tends to the initial state.

Physically however, the measured data does not make sense and, as mentioned for standpipe #1, a second method of determining density would be helpful.

The solids content output from the finite strain program, of course, does not predict the measured data, as

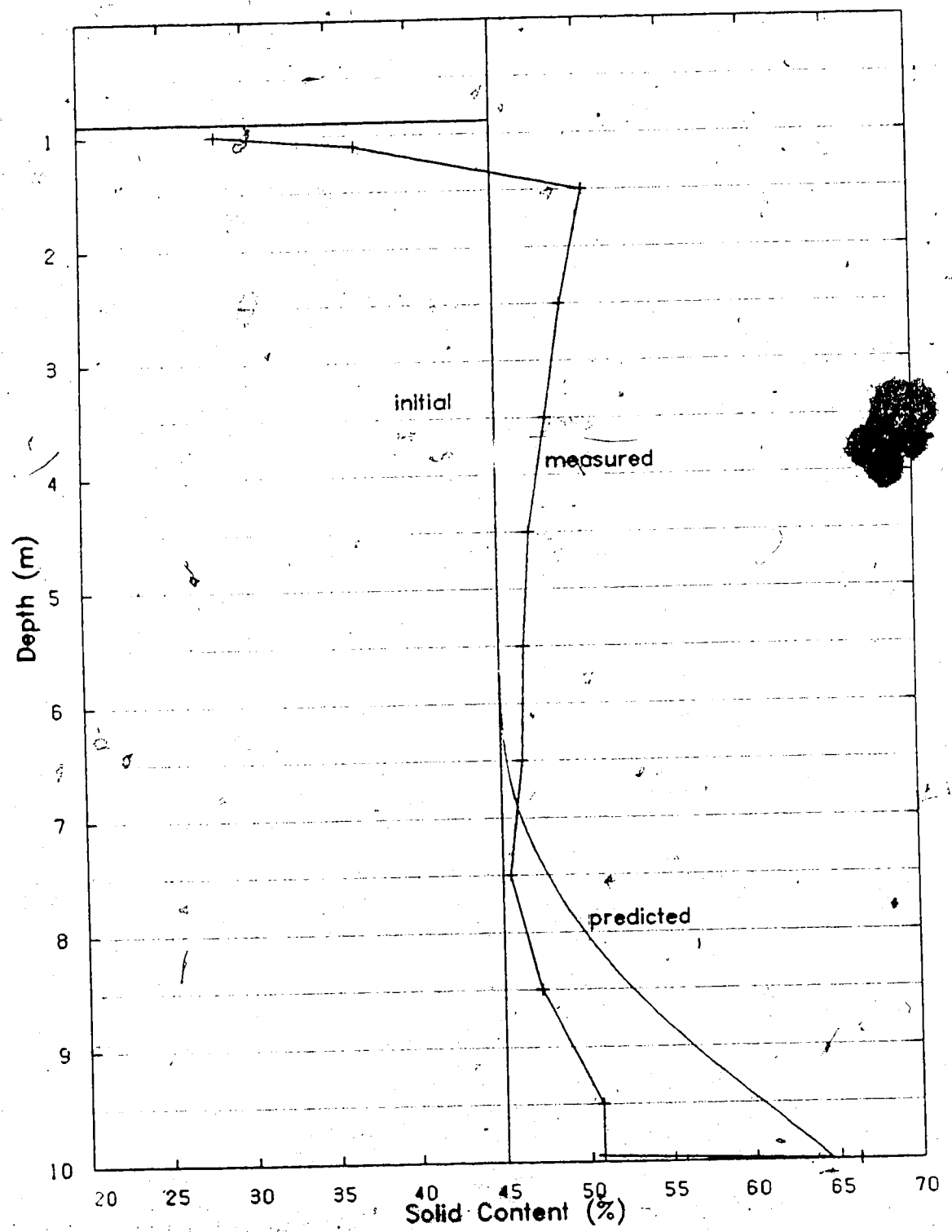


Figure 6.12 Comparison of Solids Content at 709 days, Standpipe #2

it yields a more conventional curve where the increase in solids content begins from the bottom of the standpipe.

6.4 Standpipe #3

6.4.1 Input Parameters

The contents of standpipe #2 were mixed with additional tailings sand to make the sludge-sand mix for the third 10 m standpipe test. The properties of this material have been shown in Table 4.1 and Figures 4.4 and 4.5. Slurry consolidometer test #3 was performed to obtain the compressibility and permeability data of the sludge-sand mix to be used in modelling standpipe #3. The slurry consolidometer sludge-sand mix description was given in Tables 4.2 and 4.3, and Figures 4.4 and 4.6. Tables 4.1 and 4.2 show that the two sludge-sand mixes are virtually identical.

The compressibility data for the sludge-sand mix is shown in Figure 5.15 along with the best fit curve required for determining the input constants A and B of equation 3.24. The curve was least squares fitted with a coefficient of determination of 0.998 and the relationship is as follows:

$$e = 1.814 \cdot \sigma^{(-0.9929)} \quad (6.7)$$

Once again the high value of r^2 (close to a perfect fit) indicates that the compressibility data does follow a power law relationship path.

The permeability data for the consolidometer sludge-sand mix along with the best fit curve are shown in Figure 5.33. The coefficient of determination was 0.981 and the relationship is as follows:

$$k = 2.134 \times 10^{-8} \cdot e^{3.794} \quad (6.8)$$

The high r^2 value indicates that the permeability values obtained in the void ratio range tested are well suited to a power law relationship. Again the permeability data r^2 is less than the compressibility r^2 . Table 6.3 contains a summary of the r^2 values for each standpipe.

In a manner the same as that described for standpipe #1, a material balance was performed using initial measurements and it was determined that there was 1.0 % by volume entrained gas (Table 6.4). To incorporate this into the analysis, as with standpipe #1, it was necessary to reduce the relative density of the sludge solids the appropriate amount. The $D_{r,35}$ value for the analysis then, works out to be 2.54.

The initial solids content for the sludge-sand mix in standpipe #3 was 74.8%. Table 6.2 contains a summary of soil input parameters.

The analysis period for standpipe #3 is 2.5 years. The initial height, lower boundary condition, time increment, and initial spacial increment remain the same as for standpipes #1 and #2.

Table 6.3 Input Data Coefficients of Determination (r^2)

Standpipe	Compressibility	Permeability
#1	0.992	0.947
#2	0.990	0.948
#3	0.998	0.981

Table 6.4 Ten Metre Standpipe #3 - Material Breakdown

Material	Mass (kg)	Volume (m^3)
Larger than 0.044 m	1122.6	0.4232
Finer than 0.044 m	224.3	0.0844
Bitumen	21.9	0.213
Water	461.1	0.4611
Gas	0	0.010
Total	1830	1.000

6.4.2 Comparison of Predicted with Measured Values

6.4.2.1 Interface Settlement

Figure 6.13 shows measured interface settlement data for standpipe #3. Although the data does not display a discrete change in settlement rate as in standpipe #2, there does exist a decrease in settlement rate over the duration of the data. The settlement rate begins to decrease after the first two months, after which the change in this rate begins to lessen as the rate gets close to being constant. This initial fast settlement may be caused by the same mechanism that was postulated for standpipe #2, that is, the formation of channels caused by settling sand increases the permeability until consolidation closes them.

The interface settlement as predicted by the finite strain program is also shown in Figure 6.13. Unlike in standpipes #1 and #2, a slight curvature in the settlement-time line is evident beginning around 700 days. The reason the curvature is evident for this standpipe is that at 700 days, consolidation is about 52 % complete, as the ultimate settlement for standpipe #3 is only 1.13 m. Although the settlement rate is only 65% that of the sludge-sand mix in standpipe #2, standpipe #3's initial condition was 35% more dense, its final condition will be more dense, and it will achieve its final state faster. The predicted rate for standpipe #3 is still 48% faster than the predicted rate for the sludge in standpipe #1.

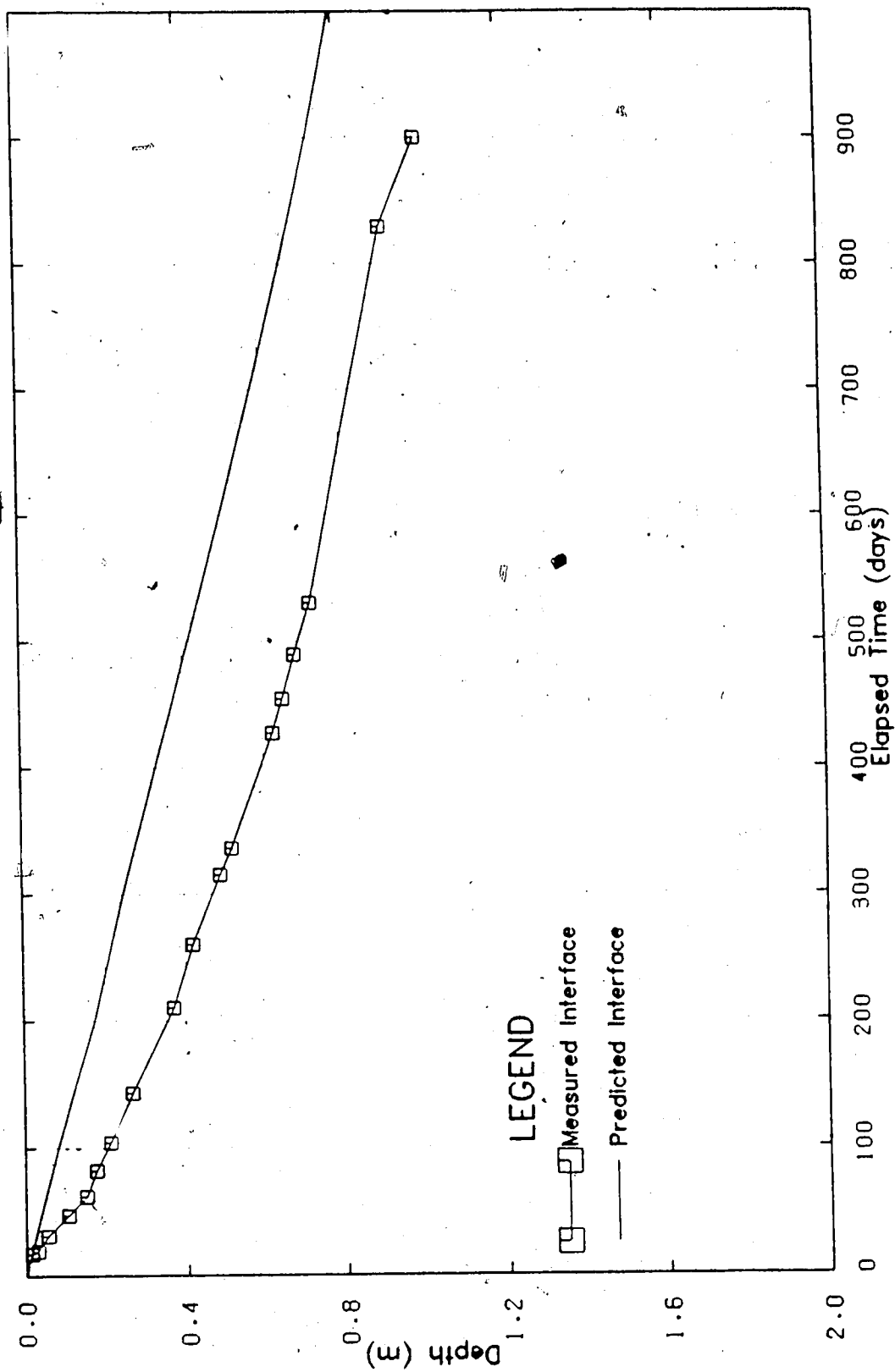


Figure 6.13 Standpipe #3 Sludge Sand Mix-Water Interface Settlement

When the predicted and measured data are compared it is seen that the predicted interface underestimates the measured settlement rate. It is unlikely that the two curves will merge or intersect as with standpipe #2, since at 900 days the measured data is already at 89% consolidation (according to the predicted ultimate settlement) it is the initial (the first 100 days) settlement rate which is not at all modelled by the program and results in the discrepancy between the two interfaces.

6.4.2.2 Excess Pore Pressures

Figure 6.14 shows the predicted excess pore pressure output from the finite strain program for various times. Immediately evident from the Figure is that, unlike the previous two standpipes (Figures 6.5 and 6.10), the shapes of the profiles are more conventional in that as the consolidation progress, the initial slopes of the profiles (as they are plotted) become more steep. The reverse was true of standpipes #1 and #2. This indicates that for standpipe #3, the program predicts the excess pore pressure dissipation to proceed faster than the increase in density. Along with the small amount of settlement also evident from the Figure, the excess pore pressures suggest that the standpipe #3 test is close to a small strain problem.

The measured excess pore pressures are plotted along with their respective predicted excess pore pressures on Figure 6.15. It is seen from the Figure that although the measured data does not lie exactly on the predicted curves,

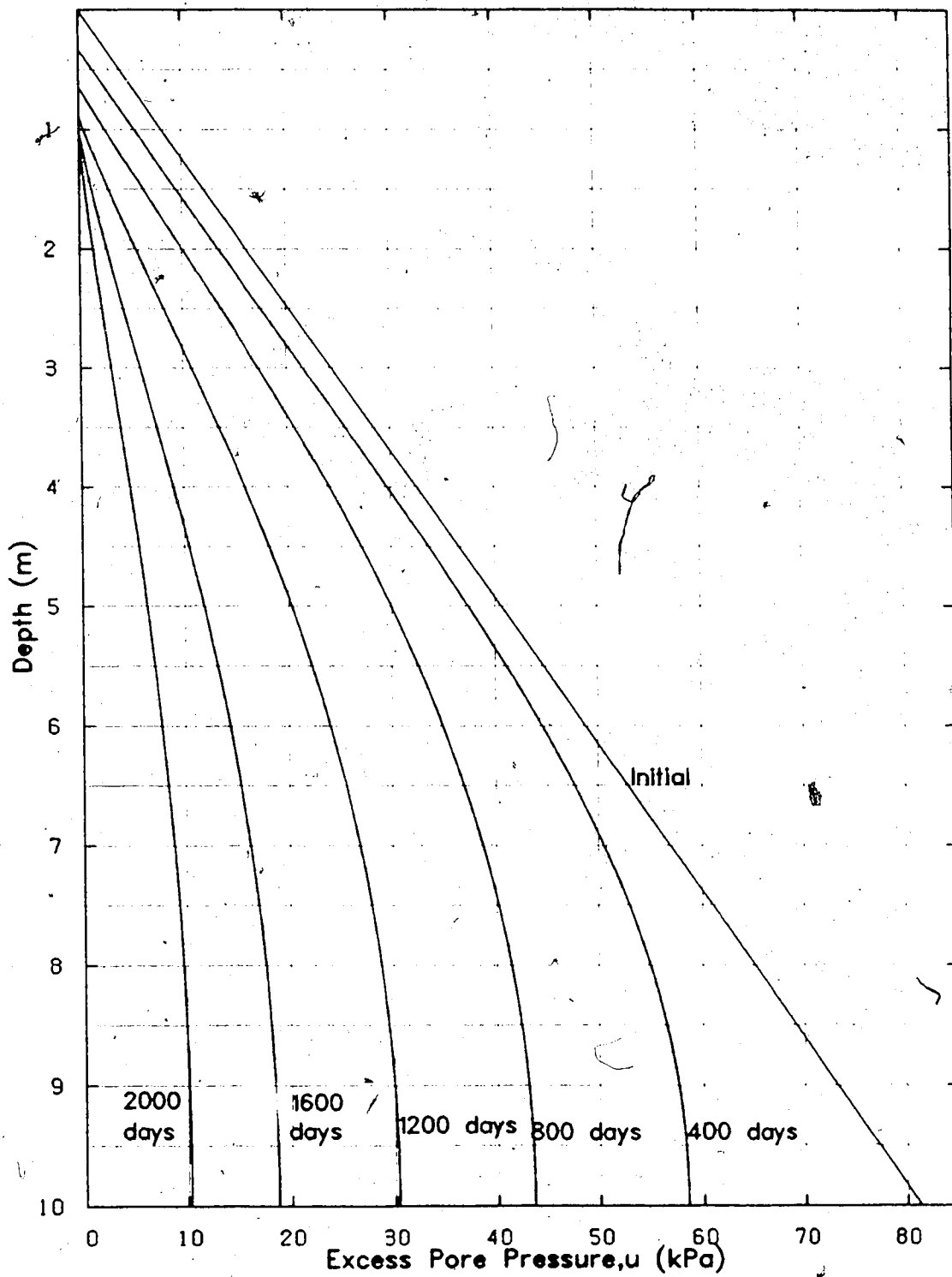


Figure 6.14 Predicted Excess Pore Pressure Profiles, Standpipe #3

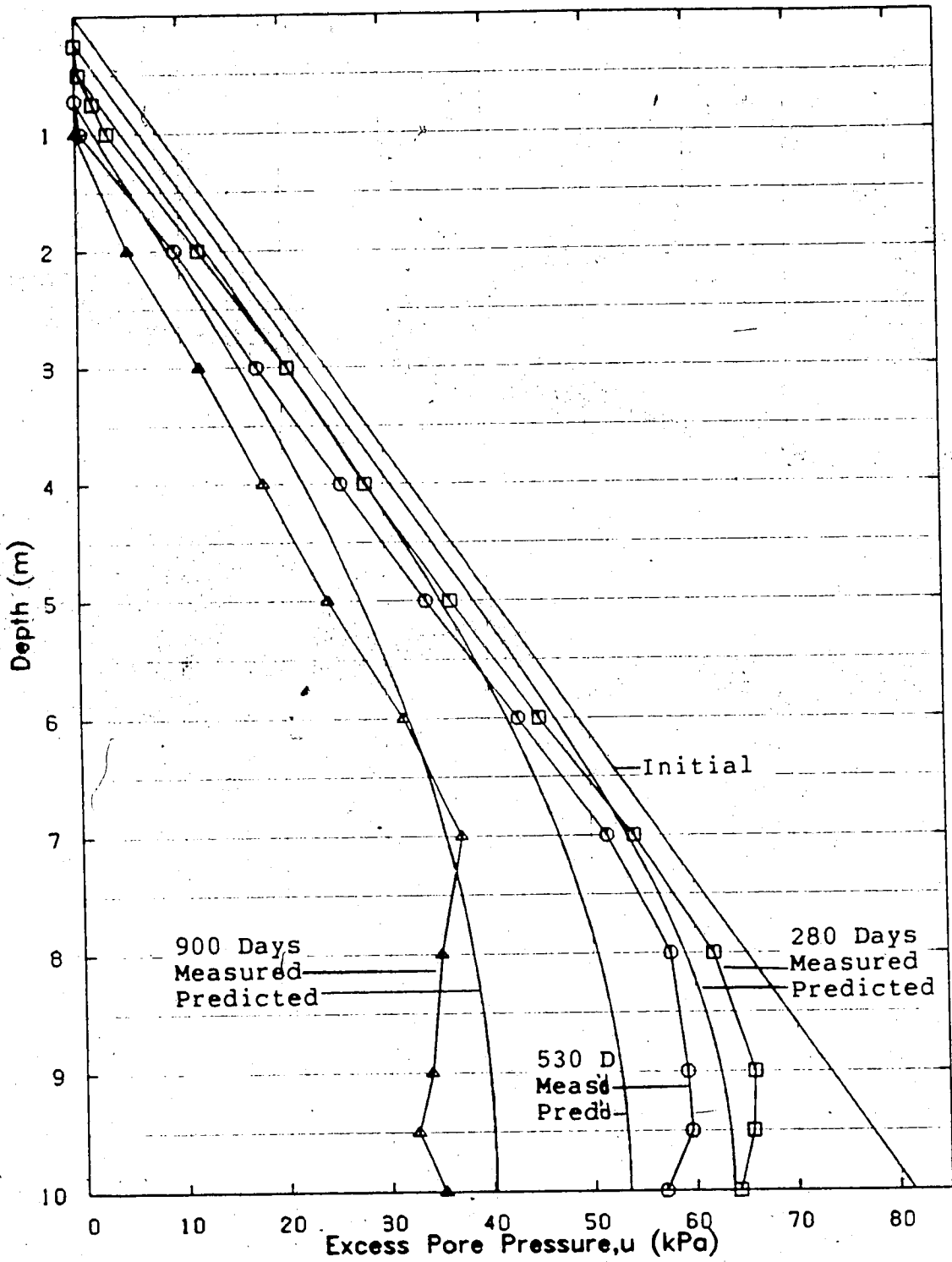


Figure 6.15 Comparison of Excess Pore Pressures, Standpipe

#3

the general shape and location of the data is quite consistent with the predicted. The measured data is exhibiting the features described in the previous paragraph's discussion on the predicted pore pressures regarding profile shape.

6.4.2.3 Solids Content

Due to the initial high density of the material in standpipe #3, sampling and testing for the sludge-sand mix density and solids content was had a lower accuracy than for the other standpipes (Scott and Chichak, 1985c).

The difficulty is reflected in the resulting solids content data as shown in Figure 6.16. The measured solids content at 280 days is shown to be less than the initial solids content which is obviously not the case.

Since the data is incorrect, any prediction cannot be verified. However the predicted solids content profile at 280 days is also shown in Figure 6.16 for completeness. The predicted profile is similar to those for standpipes #1 and #2 (Figures 6.8 and 6.12 respectively) with one exception. An increase in solids content occurs up to the half way mark of the standpipe with only a minor (8%) increase in solids content occurring at the base.

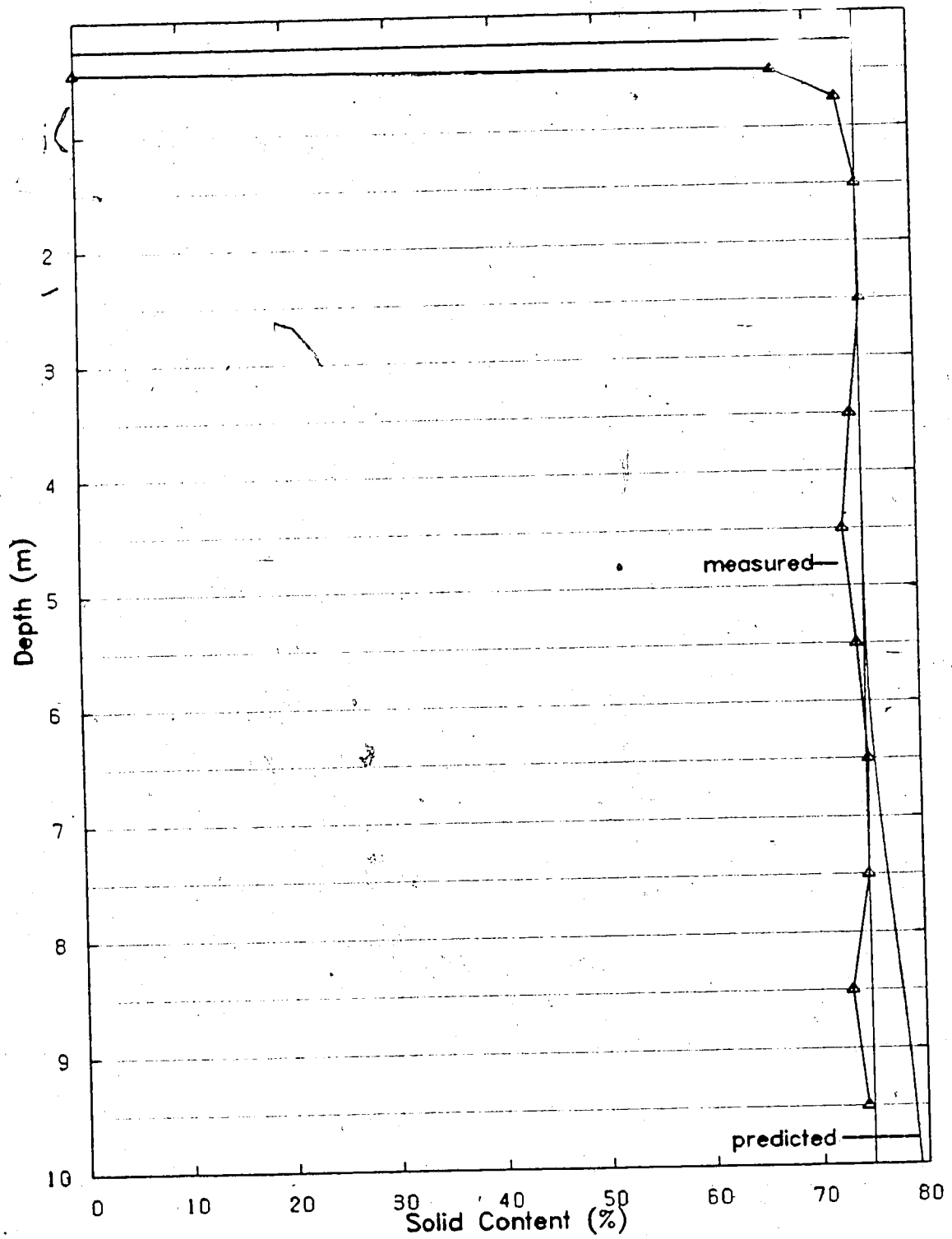


Figure 6.16 Comparison of Solids Content at 280 days, Standpipe #3

6.5 Summary of Observations and Conclusions

A summary of some the observations and conclusions found in the previous discussion in this Chapter will be given in this section.

A finite strain consolidation program based on a solution to the governing equation outlined by Somogyi (1980) was used to model the consolidation progress of the material in the three 10 m standpipes. This method required curve fitted constants based on power law relationships to describe the compressibility and permeability of the slurries (equations 3.24 and 3.26). One of the points of concern would be how well these power law equations actually describe the data. Table 6.3 shows the coefficient of determination (r^2) of the data to a power law fit. The Table shows that the data is well suited to a power law fit with the permeability giving the lowest r^2 values; 0.947 and 0.948 for standpipes #1 and #2 respectively. As discussed in Chapter 5, for some of the relationships, data smoothing was necessary for practical use. Therefore little accuracy was sacrificed using these relationships.

With respect to interface settlement, the theory underestimated the settlement rate. However it was shown for standpipe #1 that a relatively minor change in the permeability relationship (Figure 6.4) could account for the discrepancy. With that consideration, the theory adequately modelled the settlement except for standpipe #2 where a sharp change in the settlement rate occurred. For tailings

pond capacity design purposes, it may be preferred that the settlement is underestimated.

With respect to excess pore pressures, the theory did a good job in modelling the excess pore pressure profiles for standpipes #1 and #3. The standpipe #2 prediction was out as the actual data seemed somewhat inconsistent. Overall the theory predicted the excess pore pressures quite well.

With respect to solids content, the theory did not predict the measured solids content profiles in either shape or magnitude. The solid content measurements for standpipes #1 and #2 showed an increase over the entire depth of the material, but the theory predicts an increase only in the bottom portions with the largest increase at the bottom. It is difficult to determine whether the difference is due to the theory or a problem with the sampling until a second method of obtaining the solids content is developed. The material in standpipe #3 was too dense to obtain good samples for solids content testing with the procedure used, hence the results were not comparable.

It is difficult to assess the meaning of the solids content profiles, however the somewhat successful modelling of the interface settlements and the excess pore pressures lends confidence to using the theory to model the internal behaviour the material. Overall, the finite strain program is close to modelling the 10 m standpipe consolidation behaviour. Perhaps with additional adjusting of the permeability relationship constants to better reflect the

data in the high void ratio end, even better modelling results may have been achieved. However it was the purpose of this Chapter to examine the usability of the theory without prior knowledge, as it would be done in practice. The work in this thesis, however, now allows the data to be adjusted for use in oil sand tailings operations.

7. Conclusions and Recommendations

7.1 Conclusions

7.1.1 Consolidation Parameters

1) The foremost objective of this thesis was met. A laboratory apparatus and testing procedure were successfully developed to perform testing on oil sand tailings sludge, sludge-sand mixes, and a sludge-sand mix with a chemical flocculent, to determine their consolidation parameters.

2) Development of a top cap clamping system permitted permeability testing to be performed on the high void ratio slurries without inducing consolidation.

3) A comparison of the self weight stages for the four slurries tested revealed that the addition of sand to the sludge increased the self weight consolidation by two processes: a) by increasing the relative density of the sludge solids, and b) by diluting the consolidation resisting effects of the sludge.

4) From the consolidation time plots, a trend of delayed consolidation was evident for the lower stress increments (higher void ratios). Although this trend was somewhat evident in sludge-sand mixes, it was more visible in the sludge data.

5) The compressibility data for all four tests yielded nonlinear $e - \log \sigma'$ curves over the stress ranges tested.

The $e - \log \sigma'$ curves tended to linearize as the sludge content was decreased by the addition of sand.

6) The compressibility results yielded a "family of curves" for the oil sand tailings sludge sand mixes. Not only does this allow one to interpolate compressibility curves for different sand proportions, for this oil sand tailings, but it also indicates that for different tailings, only a limited number of tests need to be performed to fully define their compressibility characteristics over a range of grain size distributions.

7) The permeability tests revealed a time dependent flow discharge with a constant gradient. The flow velocity would drop up to two orders of magnitude before reaching a steady state value. The time to the steady state condition varied up to 15 hours for the sludge, less for the sludge-sand mixes.

8) The steady state values were used for the determination of the hydraulic conductivity values. Because of the presence of gas during the permeability tests, the flow-time plots became valuable tools in determining which permeability measurements deserved more weight.

9) The permeability tests, for all four samples, yielded nonlinear $e - \log k$ curves over the void ratio ranges tested.

10) The permeability test results showed no concrete evidence of the existence of a threshold gradient for flow

to commence as has been postulated in the literature.

11) An important finding from the permeability tests was that the relationship between hydraulic conductivity and the fines void ratio was the same for all the slurries. This unique dependence on the fines void ratio indicates the sand does not affect the permeability except to decrease the fines concentration. This finding can be used similar to the "family of curves" of compressibility data, when needing to determine the permeability for certain mixes. As well, this consistency in the measurements gives confidence in using the permeability values determined from the tests.

12) The major influences of the sand in the sludge sand mixes were: a) to enhance compression and consolidation, b) to increase the relative density of the sludge solids thereby increasing the self weight stress, c) to linearize the $e - \log_{10} \sigma'$ curve, d) move the compressibility curve towards the direction of lower void ratio thus causing a smaller void ratio change for a given stress change with increasing sand content, and e) to cause the permeability of a mix to be greater at a given void ratio by decreasing the concentration of fines.

13) The only effect the chemical flocculent had in the sludge-sand mix was to maintain the sand in suspension at a solids content which normally would lead to sand segregation. This ability to keep the sand in suspension resulted in a large amount of consolidation during the self

weight stage. The sludge-sand mix with the flocculent yielded consistent results with the other slurries with respect to compressibility and permeability once self weight consolidation was complete.

7.1.2 Consolidation Theories

1) It was determined that a consolidation theory developed by Gibson, England, and Hussey (1967) was appropriate for the tailings sludge consolidation problem. The theory incorporates finite strains, self weight of the material, and nonlinear soil properties. It has been shown in the literature that Terzaghi's classical consolidation theory and nonlinear infinitesimal strain extensions to it are all a subset of the finite strain theory.

2) It was also determined that analytical solutions to the finite strain's governing equation were best handled by Somogyi (1980) and Cargill (1982). The Cargill solution used laboratory σ' - e - k data as input, where as the Somogyi method required curve fitted constants describing the σ' - e - k data as input. When the same input data was used, it was found that the two methods yielded the same results.

3) Other solutions to the finite strain theory were found to be lacking in generality or were more difficult to employ than the above two methods. Finite element methods, however, appear promising for use with complex boundary condition problems.

4) A survey of the published literature revealed that there has been some success in using the finite strain theory to predict field consolidation problems.

7.1.3 Consolidation Modelling

1) When modelling the consolidation of the slurries in the 10 m standpipes, it was found necessary to use the consolidation parameters in the form of power law curve fitted constants for input to the finite strain computer program. It was shown that these relationships described the laboratory data very well, for both permeability and compressibility.

2) With respect to interface settlement, the theory generally slightly underestimated the settlement rate. However it was shown for standpipe #1 that a relatively minor change in the permeability relationship accounted for the discrepancy. With that consideration, the theory adequately modelled the settlement in all 10 m standpipe tests. For standpipes #2 and #3, after the initial fast settlement which occurred in the standpipes (possibly due to channeling by settling sand), the theory closely models the rate of consolidation.

3) With respect to excess pore pressures, the theoretical calculations were very good in modelling the excess pore pressure profiles for standpipes #1 and #3. The standpipe #2 prediction was not as good as the standpipes measurements seemed somewhat inconsistent. Overall the

theory predicted the excess pore pressures quite well. The successful modelling of the excess pore pressures lends confidence to using the theory to model the internal behaviour the material.

4) With respect to solids content, the theory did not predict the measured solids content profiles in either shape or magnitude. It is difficult to determine whether the difference is due to the theory or a problem with the sampling until a second method of measuring the solids contents in the standpipes is developed.

5) As a general conclusion, the material parameters determined in the laboratory tests in conjunction with the finite strain program were close to modelling the consolidation of the slurries in the three 10 m standpipes.

7.2 Recommendations for Further Research

1) A different consolidation laboratory apparatus and testing procedure should be developed to obtain the desired parameters in a shorter period of time. A logical direction to pursue would be with the CHG, CRD, AND CRL test methods.

2) Additional testing should be done on the tested slurries in the high void ratio region, especially with respect to permeability.

3) More research is required on the time dependent flow discharge measured in the permeability tests to understand the reasons for it and possible implications.

4) Very little is understood in the area of thixotropic gel strength and its effect on consolidation behaviour. Work on this could prove very beneficial to the understanding of the long term consolidation behaviour in tailings ponds.

5) The finite strain consolidation theory should be extended to incorporate the effect of thixotropic gel strength.

6) Additional development of the theory is required to allow for geometrically nonuniform pond shapes and cross sections.

7) It appears necessary to develop a second method of determining the density of the slurries in the 10 m standpipes. A non-sampling procedure, such as, nuclear density measurements would be appropriate.

8) The shear strength of the slurries in the 10 m standpipes should be measured to determine their correlation with effective stress and the magnitude of thixotropic gel strength.

9) The monitoring of the consolidation of the slurries in the 10 m standpipes should continue as sludge consolidation properties can best be determined from such large scale, long term, controlled tests.

10) The test results obtained in this thesis and the finite strain consolidation theory appear applicable to model the consolidation of the sludge in the oil sand tailing ponds. A study to history match the tailing ponds performance should be made. Such a study should vary the

compressibility and permeability values used as input to the computer modelling program. The limits of the parametric study can be evaluated from the results of this thesis.

11) After a successful history matching of the sludge consolidation has been made, the results should be used to predict the long term performance of the ponds.

12) SUNCOR Inc. and Syncrude Canada Ltd. should allow all their tailings pond data to be put into the public domain. The analysis of this data by independent researchers would benefit both companies, future oil sand companies and society in general by contributing to the solution of the oil sand tailings sludge disposal problem.

REFERENCES

- Aboshi, H., Yoshikuni, H., and Maruyama, S., 1979. Constant Loading Rate Consolidation Test. *Soils and Foundations*, Vol. 10, No. 1, March, pp. 43-56.
- Adam, D., 1985. Syncrude's Technology Evolution Since Start-up. Proceedings of 6th annual Advances in Petroleum Recovery and Upgrading Technology, AOSTRA, Edmonton, Alberta, June 6-7, 20p.
- Been, K., 1980. Stress Strain Behaviour of a Cohesive Soil Deposited Under Water. Ph.D. Dissertation, University of Oxford, Oxford, United Kingdom.
- Been, K. and Sills, G.C., 1981. Self Weight Consolidation of Soft Soils: An Experimental and Theoretical Study. *Geotechnique*, Vol. 31, No. 4, pp. 519-535.
- Berkowitz, N. and Speight, J.G., 1975. The Oil Sands of Alberta. *Fuel*, Vol. 54, pp. 138-149.
- Bromwell, L.G. and Carrier III, W.D., 1979. Consolidation of Fine-Grained Mining Wastes. Proceedings of the Sixth Panamerican Conference on Soil Mechanics and Foundation Engineering, Lima, Peru, Vol. 1, pp. 293-304.
- Burchfield, T.E. and Hepler, L.G., 1979. Some Chemical and Physical Properties of Tailings Water from Oil Sands Extraction Plants. *Fuel*, Vol. 58, pp. 745-747.
- Camp, F.W., 1977. Processing Athabasca Tar Sands - Tailings Disposal. *Canadian Journal of Chemical Engineering*, Vol. 55, Oct., pp. 581-591.
- Cargill, K.W., 1982. Consolidation of Soft Layers by Finite Strain Analysis. U.S. Army Engineer Waterways Experimentation Station, Vicksburg, Mississippi, Miscellaneous Paper GL-82-3.
- Carmen, P.C., 1956. *Flow of Gases Through Porous Media*. Academic Press Inc., New York.
- Carrier III, W.D., 1982. Predicting Consolidation of Phosphatic Clay Wastes. Proceedings Consolidation and Dewatering of Fine Particles Conference, University of Alabama - United States Bureau of Mines, Aug., pp. 491-519.
- Carrier III, W.D. and Bromwell, L.G., 1983. Disposal and Reclamation of Mining and Dredging Wastes. Proceedings of the 7th PanAmerican Conference on Soil Mechanics and

Foundation Engineering, Vancouver, Canada, June, Vol. 2, pp. 727-738.

Carrier III, W.D., Bromwell, L.G., and Somogyi, F., 1981. Slurried Mineral Wastes: Physical Properties Pertinent to Disposal. Presented at the ASCE National Convention, St. Louis, October.

Carrier III, W.D., Bromwell, L.G., and Somogyi, F., 1983. Design Storage Capacity of Slurried Mineral Waste Ponds. ASCE Journal of the Geotechnical Engineering Division, Vol. 109, GT2, May, pp. 699-716.

Carrier III, W.D., Scott, J.D., Shaw, W.H., and Dusseault M.B., 1987. Reclamation of Athabasca Oil Sand Sludge. Proceedings of Geotechnical Practice for Waste Disposal '87, GT Division of ASCE, Ann Arbor, MI., June, pp. 377-391.

Casagrande, A., 1938. Notes on Soil Mechanics - First Semester. Harvard University (unpublished), 129p.

Croce, P., Pane, V., Znidarcic, D., Ko, H.Y., Olsen, H.W., and Schiffman, R.L., 1984. Evaluation of Consolidation Theories by Centrifuge Modelling. Proceedings of the Conference on Applications of Centrifuge Modelling to Geotechnical Design, University of Manchester, United Kingdom, pp. 380-401.

Darcy, H., 1856. Histoire Des Fontaines Publique de Dijon. Dalmont, Paris, pp. 590-594.

Davis, E.H. and Raymond, G.P., 1965. A Non-Linear Theory of Consolidation. Geotechnique, Vol. 15, pp. 161-173.

Dusseault, M.B., 1977. The Geotechnical Characteristics of Oil Sands. Ph.D. Thesis, University of Alberta, Edmonton, Canada.

Dusseault, M.B. and Scott, J.D., 1982. Characterization of Oil Sand Tailings Sludge. Proceedings of Short Course on Consolidation Behaviour of Fine Grained Waste Materials, Bromwell Engineering, Denver, Colorado, Oct., 35p.

Fair, A.E. and Hanford, T.G., 1986. Overview of the Tailings Dyke Instrumentation Program at Syncrude Canada Ltd.. Proceedings of the International Symposium on Geotechnical Stability in Surface Mining, Calgary, Alberta, Nov. 6-7, pp. 245-253.

Gairon, S. and Swartzendruber, D., 1975. Water Flux and Electrical Potentials in Water-Saturated Bentonites. Proceedings of the Soil Science Society of America, Vol. 39, No. 5, pp. 811-817.

- Gibson, R.E., 1958. The Progress of Consolidation in a Clay Layer Increasing in Thickness with Time. *Geotechnique*, Vol. 8, pp. 171-182.
- Gibson, R.E., England, G.L., and Hussey, M.J.L., 1967. The Theory of One-Dimensional Consolidation of Saturated Clays, I, Finite Non-Linear Consolidation of Thin Homogeneous Layers. *Geotechnique*, Vol. 17, pp. 261-273.
- Gibson, R.E., Schiffman, R.L., and Cargill, K.W., 1981. The Theory of One-Dimensional Consolidation of Saturated Clays, II, Finite Non-Linear Consolidation of Thick Homogeneous Layers. *Canadian Geotechnical Journal*, Vol. 18, pp. 280-293.
- Glenister, D.J. and Cooling, D.J., 1984. Gravity Underdrainage as an aid to the Consolidation of Red Mud Residue from the Alumina Industry. Fourth Australia-New Zealand Conference on Geomechanics, Perth, pp. 198-202.
- Hall, E.S. and Tollefson, E.L., 1984. Stabilization and Destabilization of Mineral Fines-Bitumen-Water Dispersions in Tailings from Oil Sands Extraction Plants that use the Hot Water Process. *Canadian Journal of Chemical Engineering*, Vol. 60, No. 6, Dec., pp. 812-821.
- Hamilton, J.J. and Crawford, C.B., 1959. Improved Determination of Preconsolidation Pressure of a Sensitive Clay. *Papers on Soils - 1959 Meetings, American Society for Testing and Materials, Philadelphia, STP 254*, pp. 254-271.
- Hansbo, S., 1960. Consolidation of Clays with Special Reference to the Influence of Vertical Sand Drains. *Swedish Geotechnical Institute Proceedings, Stockholm, No. 18*, pp. 41-61.
- Hocking, M.B. and Lee, G.W., 1977. Effect of Chemical Agents on Settling Rates of Sludges from Effluent of Hot-Water Extraction of Athabasca Oil Sands. *Fuel*, Vol. 56, July, pp. 325-333.
- Ignasiuk, T.M., Kotlyar, L., Longstaffe, F.J., Strausz, O.P., and Montgomery, D.S., 1982. Separation and Characterization of Clay from Athabasca Asphaltene. *Fuel*, Vol. 62, March, pp. 353-362.
- Imai, G., 1979. Development of a New Consolidation Test Procedure Using Seepage Force. *Soils and Foundations*, Vol. 19, No. 3, Sep., pp. 45-60.
- Imai, G., 1981. Experimental Studies on Sedimentation Mechanism and Sediment Formation of Clay Materials.

- Soils and Foundations, Vol. 21, No. 1, March, pp. 7-20.
- Isaac, B.A., 1987. Slurry Consolidation Tests for Oil Sands Overburden and Sludge Wastes. M.Eng. Report, University of Alberta, Edmonton, Canada, 96 p.
- Isaac, B.A., Dusseault, M.B., Lobb, G.D., and Root, J.D., 1982. Characterization of the Lower Cretaceous Overburden for Oil Sands Surface Mining within Syncrude Canada Ltd. Leases Northeast Alberta, Canada. Proceedings of the IV International Congress, International Association of Engineering Geology, New Delhi, India, Vol. 2, Theme 1, pp. 371-384.
- Janbu, N., 1963. Soil Compressibility as Determined by Oedometer and Triaxial Tests. Proceedings, European Conference on Soil Mechanics and Foundation Engineering, Weisbaden, Vol. 1, pp. 19-25.
- Janbu, N., Tokheim, O., and Senneset, K., 1981. Consolidation Tests with Continuous Loading. Proceedings of the Tenth International Conference on Soil Mechanics and Foundation Engineering, Vol. 1, pp. 645-654.
- Kessick, M.A., 1978. Clay Slimes from the Extraction of Alberta Oil Sands, Florida Phosphate Matrix and Other Mined Deposits. Waste Treatment, Feb., 9p.
- Kessick, M.A., 1979. Structure and Properties of Oil Sands Clay Tailings. Journal of Canadian Petroleum Technology, Vol. 18, No. 1, Jan-March, pp. 49-52.
- Kolaian, J.H. and Low, P.F., 1962. Thermodynamic Properties of Water in suspensions of Montmorillonite. Proceedings of the Ninth National Conference on Clays and Clay Minerals, Pergamon Press, Monograph 11, Earth Science Series, pp. 519-535.
- Koppula, S.D., 1970. The Consolidation of Soil in Two-Dimensions and with Moving Boundaries. Thesis presented to the University of Alberta, Edmonton, Canada, in partial fulfillment of the requirements for the degree of Doctor of Philosophy.
- ©Koppula, S.D., 1985. Consolidation of Marine Sediments: A Case Study. Eighth South East Asian Geotechnical Conference, Kuala Lumpur, Malaysia, pp. 1-1 to 1-7.
- Koppula, S.D. and Morgenstern, N.R., 1982. On the Consolidation of Sedimenting Clays. Canadian Geotechnical Journal, Vol. 19, pp. 260-268.
- Kynch, G.J., 1952. A Theory of Sedimentation. Transactions of the Faraday Society, Vol. 48, pp. 166-176.

- Lane, S., 1983. Lime Coagulation and Stabilization of Total Oil Sands Tailings. Proceedings of the 34th Annual Technical Meeting of the Canadian Institute of Mining and Metallurgy, Banff, Alberta, May, Preprint, Paper 83-34-33, 17p.
- Lane, S., 1984. Dry Disposal of Whole Oil Sands Tailings. Environment Canada, May, pp. 66-79.
- Lee, K. and Sills, G.C., 1981. The Consolidation of a Soil Stratum, Including Self Weight effects and Large Strains. Numerical and Analytical Methods in Geomechanics, Vol. 5, No. 4, pp. 405-428.
- Lowe, J., Jonas, E., and Obrician, V., 1969. Controlled Gradient Consolidation Test. ASCE Journal of the Soil Mechanics and Foundation Division, Vol. 95, SM1, Jan, pp. 77-97.
- Lun, P.T. and Parkin, A.K., 1985. Consolidation Behaviour Determined by the Velocity Method. Canadian Geotechnical Journal, Vol. 22, pp. 158-165.
- McVay, M., Townsend, F., and Bloomquist, D., 1986. Quiescent Consolidation of Phosphatic Waste Clays. ASCE Journal of the Geotechnical Engineering Division, Vol. 112, GT11, pp. 1033-1049.
- McNabb, A., 1960. A Mathematical Treatment of One-Dimensional Soil Consolidation. Quarterly Journal of Applied Mathematics, Vol. 17, No. 4, Jan., pp. 337-347.
- Mikasa, M., 1965. The Consolidation of Soft Clay - A New Consolidation Theory and Its Application. Japan Society of Civil Engineers, Synopsis of J.S.C.E. Prize Papers for 1964 in Civil Engineering in Japan, pp. 21-26.
- Miller, R.J. and Low, P.F., 1963. Threshold Gradient for Water Flow in Clay Systems. Proceedings of the Soil Science Society of America, Vol. 27, No. 6, pp. 605-609.
- Mitchell, J.K. and Younger, J.S., 1967. Abnormalities in Hydraulic Flow Through Fine-Grained Soils. Permeability and Capillarity of Soils, American Society for Testing and Materials, Philadelphia, STP 417, pp. 106-139.
- Monte, J.L. and Krizek, R.J., 1976. One-Dimensional Mathematical Model for Large-Strain Consolidation. Geotechnique, Vol. 26, No. 3, pp. 495-510.
- Olsen, H.W., 1966. Darcy's Law in Saturated Kaolinite. Water Resources Research, Vol. 2, No. 6, pp. 287-295.

- Olsen, H.W., 1969. Simultaneous Fluxes of Liquid and Charge Through Saturated Kaolinite. Proceedings of the Soil Science Society of America, Vol. 33, No. 3., pp. 338-344.
- Olsen, H.W., 1985. Osmosis: A Cause of Apparent Deviations from Darcy's Law. Canadian Geotechnical Journal, Vol. 22, pp. 238-241.
- Olsen, H.W., Nichols, R.W., and Rice, T.L., 1985. Low Gradient Permeability Measurements in a Triaxial System. Geotechnique, Vol. 35, No. 2, pp. 145-157.
- Olson, R.E. and Daniel, D.E., 1981. Measurements of Hydraulic Conductivity of Fine-Grained Soils. Permeability and Ground Water Contaminant Transport, American Society for Testing and Materials, Philadelphia, STP 746, pp. 18-64.
- Olson, R.E. and Ladd, C.C., 1979. One Dimensional Consolidation Problems. ASCE Journal of the Geotechnical Engineering Division, Vol 105, GT 1, Proceeding Paper 14330, pp. 11-30.
- Ortenblad, A., 1930. Mathematical Theory of the Process of Consolidation of Mud Deposits. Journal of Mathematics and Physics, Vol. 9, No. 2, pp. 73-149.
- Pane, V., Croce, P., Znidarcic, D., Ko, H.W., Olsen, H.W., and Schiffman, R.L., 1983. Effects of Consolidation on Permeability Measurements for Soft Clay. Geotechnique, Vol. 33, No. 1, pp. 67-72.
- Pane, V. and Schiffman, R.L., 1981. A Comparison Between Two Theories of Finite Strain Consolidation. Soils and Foundations, Vol. 21, No. 4, pp. 81-84.
- Pane, V. and Schiffman, R.L., 1985. A Note on Sedimentation and Consolidation. Geotechnique, Vol. 35, No. 1, pp. 69-72.
- Pelletier, J.H., Olson, R.E, and Rixner, J.J., 1979. Estimation of Consolidation Properties of Clay from Field Observations. Geotechnical Testing Journal, Vol. 2, No. 1, pp. 34-43.
- Prasad, B.D. and Joshi, R.C., 1985. Tailings Pond Bitumen Extraction and Sludge Solidification. Third International Conference on Heavy Crude and Tar Sands, UNITAR/UNDP Information Centre for Heavy Crude and Tar Sands, Long Beach, California, July 22-31, Preprint, Vol. 2, 17p.
- Ripmeester, J.A. and Sirianni, A.F., 1981. Recovery of Water

- and Bitumen from the Athabasca Oil Sands Tailings Ponds. Canadian Journal of Petroleum Technology, Jan-March, pp. 131-133.
- Roberts, J.O.L., Yong, R.N. and Erskine, H.L., 1980. Surveys of Some Tar Sand Sludge Ponds; Results and Interpretations. Proceedings of Applied Oilsands Geoscience 1980 Conference, Edmonton, Alberta, June 11-13, 46p.
- Salem, A.M. and Krizek, R.J., 1973. Consolidation Characteristics of Dredging Slurries. ASCE Journal of the Waterways, Harbors and Coastal Engineering Division, Vol. 99, WW4, pp. 439-457.
- Schiffman, R.L., 1980. Finite and Infinitesimal Strain Consolidation. ASCE Journal of the Geotechnical Engineering Division, GT2, Vol. 106, Proceedings Paper 15193, pp. 203-207.
- Schiffman, R.L. and Cargill, K.W., 1981. Finite Strain Consolidation of Sedimenting Clay Deposits. Proceedings of the Tenth International Conference on Soil Mechanics and Foundation Engineering, Stockholm, Sweden, Vol. 1, pp. 239-242.
- Schiffman, R.L. and Gibson, R.E., 1964. Consolidation of Nonhomogeneous Clay Layers. ASCE Journal of the Soil Mechanics and Foundation Division, Vol. 90, SM5, Sep., pp. 1-30.
- Schiffman, R.L., Pane, V., and Gibson, R.E., 1984. The Theory of One-Dimensional Consolidation of Saturated Clays, IV, An Overview of Nonlinear Finite Strain Sedimentation and Consolidation. Sedimentation/Consolidation Models - Prediction and Validation, American Society of Civil Engineers, New York, pp 1-29.
- Scott, J.D. and Chichak, M.F., 1985a. Large Sludge Stand Pipe Consolidation Test 1, Progress Report to February, 1985. Sludge Stand Pipe Testing Contract Agreement C2919-55 for Syncrude Canada Ltd., June, 60p.
- Scott, J.D. and Chichak, M.F., 1985b. Large Sludge Stand Pipe Consolidation Test 2, Final Report. Sludge Stand Pipe Testing Contract Agreement C4884-55 for Syncrude Canada Ltd., June, 62p.
- Scott, J.D. and Chichak, M.F., 1985c. Large Sludge Stand Pipe Consolidation Test 3, Progress Report to September, 1985. Sludge Stand Pipe Testing Contract Agreement C4884-55 for Syncrude Canada Ltd., June, 46p.
- Scott, J.D. and Cymerman, G.J., 1984. Prediction of Viable

- Tailings Disposal Methods. Sedimentation/Consolidation Models - Prediction and Validation, American Society of Civil Engineers, New York, pp. 522-544.
- Scott, J.D. and Dusseault, M.B., 1980. Behaviour of Oil Sand Tailings. Proceedings of the 33rd Canadian Geotechnical Conference, Calgary, Alberta, 35p.
- Scott, J.D. and Dusseault, M.B., 1982. Behaviour of Oil Sand Tailings Sludge. 33rd Annual Technical Meeting of the Petroleum Society of the Canadian Institute of Mining and Metallurgy, Calgary, Alberta, June, Paper no. 82-33-85, 19p.
- Scott, J.D., Dusseault, M.B., and Carrier III, W.D., 1985. Behaviour of the Clay/Bitumen/Water Sludge System from Oil Sands Extraction Plants. Journal of Applied Clay Science, Vol. 1, No. 2, July, pp. 207-218.
- Scott, J.D., Dusseault, M.B., and Carrier III, W.D., 1986. Large Scale Self-Weight Consolidation Testing. Consolidation of Soils: Testing and Evaluation, American Society for Testing and Materials, Philadelphia, STP 892, May, pp. 500-515.
- Scully, R.W., Schiffman, R.L., Olsen, H.W., and Ko, H.Y., 1984. Validation of Consolidation Properties of Phosphatic Clay at Very High Void Ratios. Sedimentation/Consolidation Models - Prediction and Validation, American Society of Civil Engineers, New York, pp 158-181.
- Silva, A.J., Hetherman, J.R., and Calnan, D.I., 1981. Low Gradient Permeability testing of Fine-Grained Marine Sediments. Permeability and Ground Water Contaminant Transport, American Society for Testing and Materials, Philadelphia, STP 746, pp. 121-136.
- Somogyi, F., 1980. Large Strain Consolidation of Fine Grained Slurries. Presented at the Canadian Society for Civil Engineering, Winnipeg, Manitoba, May 29-30.
- Somogyi, F., Carrier III, W.D., Lawver, J.E., and Beckman, J.F., 1984. Waste Phosphatic Clay Disposal in Mine Cuts. Sedimentation/Consolidation Models - Prediction and Validation, American Society of Civil Engineers, New York, pp 545-564.
- Somogyi, F., Keshian, B., Bromwell, L.C., and Carrier III, W.D., 1981. Consolidation Behaviour of Impounded Slurries. Presented at Annual Spring Convention, ASCE, New York.
- Tavenas, F., Leblond, P., Jean, P., and Leroueil, S., 1983.

- The Permeability of Natural Soft Clays: part I, Methods of Laboratory Measurement. Canadian Geotechnical Journal, Vol. 20, No. 4, pp. 629-644.
- Taylor, D.W., 1948. Fundamentals of Soil Mechanics, John Wiley and Sons, New York.
- Terzaghi, K., 1924. Die Theorie der Hydrodynamischen Spannungserscheinungen und ihr Erdbautechnisches Anwendungsgebiet. Proceedings of the First International Congress of Applied Mechanics, Delft, The Netherlands, Vol. 1, pp. 288-294.
- Terzaghi, K., 1943. Theoretical Soil Mechanics. John Wiley and Sons, New York, 227p.
- Umehara, Y. and Zen, K., 1980. Constant Rate of Strain Consolidation for Very Soft Clayey Soils. Soils and Foundations, Vol. 20, No. 2, pp. 33-65.
- Umehara, Y. and Zen, K., 1982. Consolidation Characteristics of Dredged Marine Bottom Sediments with High Water Content. Soils and Foundations, Vol. 22, No. 2, June, pp. 40-54.
- Van Olphen, H., 1977. An Introduction to Clay Colloid Chemistry. John Wiley and Sons, Wiley-Interscience, 2nd ed., New York, 318p.
- Wissa, A.E.Z., Christian, J.T., Davis, E.H., and Heiberg, S., 1971. Analysis of Consolidation at Constant Strain Rate. ASCE Journal of the Soil Mechanics and Foundation Division, Vol. 97, SM10, pp. 1393-1413.
- Yong, R.N., Sheeran, D.E., Sethi, A.J., and Erskine, H.L., 1982. The Dynamics of Tar-Sand Tailings. Proceedings of the 33rd Annual Technical Meeting of the Canadian Institute of Mining and Metallurgy, Calgary, Alberta, June, Preprint, Paper 82-33-42, 6p.
- Yong, R.N., Siu, S.K.H., and Sheeran, D.E., 1983. On the Stability of Suspended Solids in Settling Ponds. Part I, Piece-Wise Linear Consolidation Analysis of Sediment Layer. Canadian Geotechnical Journal, Vol. 20, No. 4, Nov., pp. 817-826.
- Yung, F.P., 1984. Application of the Finite Element Program 'ADINAT' to One Dimensional Consolidation. Thesis submitted at the University of Alberta in partial fulfillment of a Master of Science Degree, Edmonton, Canada, 265p.
- Zen, K. and Umehara, Y., 1986. A New Consolidation Testing Procedure and Technique for Very Soft Soils.

Consolidation of Soils: Testing and Evaluation, American Society for Testing and Materials, Philadelphia, STP 892, May, pp. 405-432.

Znidarcic, D., Croce, P., Pane, V., Ko, H.W., Olsen, H.W., and Schiffman, R.L., 1984. The Theory of One-Dimensional Consolidation of Saturated Clays, III, Existing Testing Procedures and Analyses. Geotechnical Testing Journal, Vol. 7, No. 3, Sept., pp. 123-133.

Znidarcic, D., Schiffman, R.L., Pane, V., Croce, H.Y., Ko., H.Y., and Olsen, H.W., 1986. The Theory of One-Dimensional Consolidation of Saturated Clays: part V, Constant Rate of Deformation Testing and Analysis. Geotechnique, Vol. 36, No. 2, pp. 227-237.

APPENDIX A - Apparatus and Experimental Details

Equipment Details

Diaphragm Air Cylinder

To transfer the air pressure from the air source to the loading ram, a diaphragm air cylinder from Bellofram Corporation was used. The particular models used had the following specifications.

Type:	SS
Size:	36
Series:	F
Rod:	BP
Bore:	6.8 in
Stroke:	6.0 in

Detailed specifications as well as an explanation of how the diaphragm works are available from the manufacturer.

Geotextile Filter

In the U. of A. consolidometers, a melded geosynthetic fabric by ICI Fibres was used. The fabric had the following manufacturer given specifications.

Fabric Name:	Terram 1500
Thickness:	1.0 mm
Porometry	.076 mm
Permeability	.035 m/s

The Consolidometers at the Syncrude Canada Limited (S.C.L.) laboratory had a nonwoven geosynthetic fabric by Rhone-Poulenc fibres. The fabric had the following manufacturer given specifications.

Fabric Name:	Bidim U24
Thickness:	
Under .5 kPa:	1.9 mm
Under 200 kPa:	0.8 mm
Porometry:	
Under .5 kPa:	0.094 to 0.059 mm
Under 200 kPa:	0.050 to 0.028 mm
Permeability:	
Under 2.0 kPa:	3×10^{-3} m/s
Under 200 kPa:	7×10^{-4} m/s

Additional specifications are available from the manufacturers.

Surface Displacement Measuring Equipment

The travel of the top caps in the U. of A. consolidometer was measured by a Hewlett Packard Linear Varying Displacement Transducer (LVDT). The model for both consolidometers was a 24 DC DT-1000 which had a 50mm displacement range. The LVDTs were calibrated using a high precision micrometer, the results of which are shown in Figures A.1 and A.2.

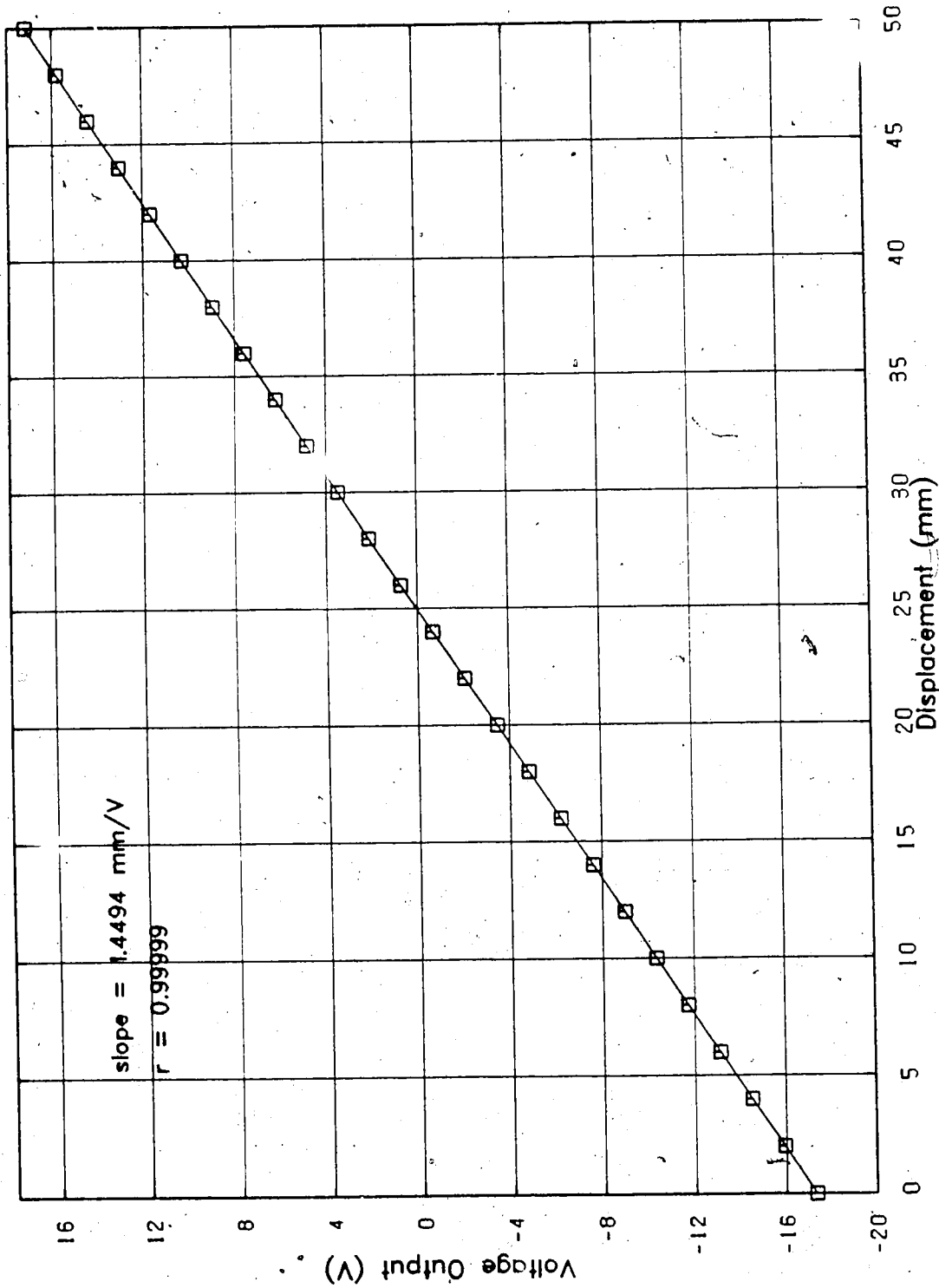


Figure A.1 Calibration of LVDT #1

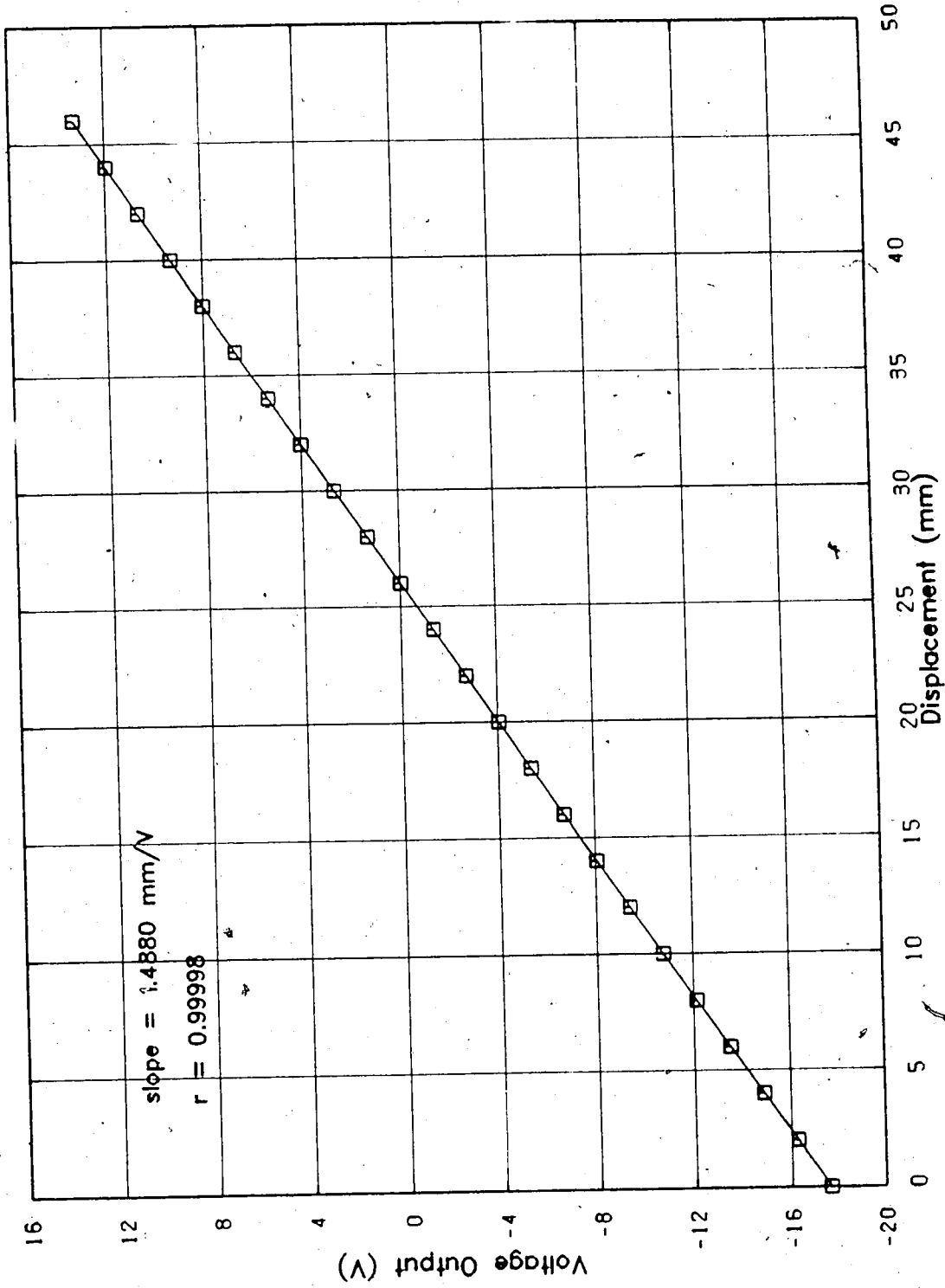


Figure A.2 Calibration of LVDT #2 (k1)

Dial gauges were used to measure top cap travel in the S.C.L. consolidometers. The gauges used were made by Wykeham Farrance Eng. Ltd. and had 0.001 inch divisions.

Specifications on either product are available from their manufacturers.

Load (Pressure) Cell

The load being applied to the sample in the U. of A. consolidometers was monitored with a DJ Transbar pressure transducer from DJ Instruments Incorporated.

In the consolidometer with test material #1, a series 200, CS 2 LL (maximum 4200 kPa) pressure transducer was used. The calibration of the load cell in the low stress range (0 to 30 kPa) was undertaken by subjecting the cell to a known height of water and then obtaining the corresponding voltage output from a signal conditioner. Above this stress, a water pressure was applied to the consolidometer in an identical manner as that shown in Figure 4.3, and a corresponding voltage output was again obtained. The results of the calibration are shown in Figure A.3.

The other U. of A. consolidometer (Test #4) had a series 100, CS 1 RG (maximum 420 kPa) pressure transducer installed in the base. The calibration for this load cell was the same as that previously described and the results are shown in figure A.4.

It was determined that the CS 1 RG was the better transducer for the testing involved in this thesis even

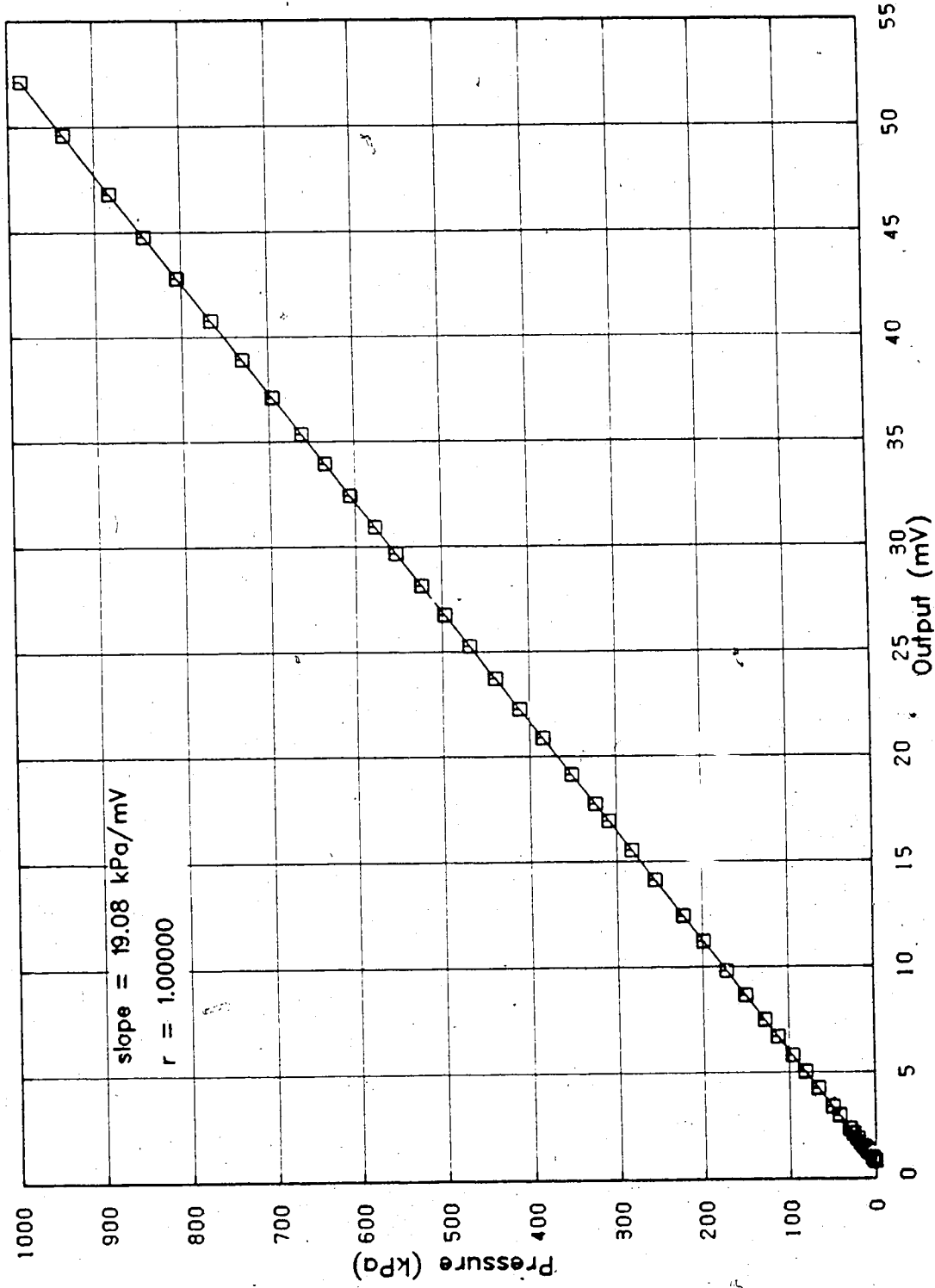


Figure A.3 Calibration of Load Cell CS 2 LL Pressure Transducer

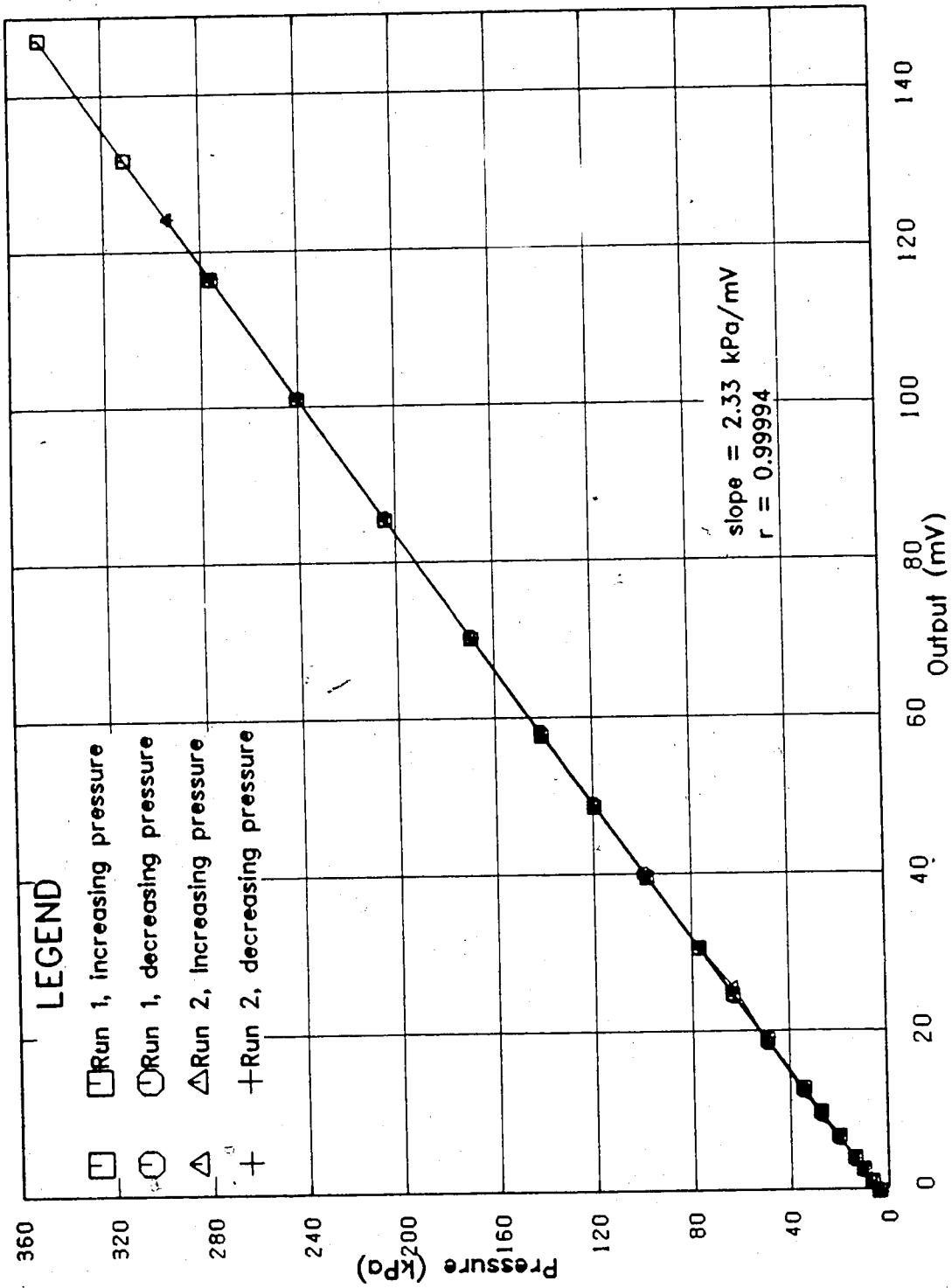


Figure A.4 Calibration of Load Cell CS 1 RG Pressure Transducer

though its range was significantly less than the CS 2 LL. This was based on the fact that the CS 1 RG was easier to install than the CS 2 LL (with respect to flush mounting). Also, pressures above 400 kPa are not necessary for the sludge problem.

Detailed specifications available from the manufacturer.

Pore Pressure Measuring Equipment

The two U. of A. consolidometers were equipped with 5 pore pressure ports each. The lines from the ports led to Whitey ball valves and then to a Validyne Δp pressure transducer as shown in Figure A.5. Before a series of pore pressure measurements were taken, a quick (rough) calibration was done to ensure that the related equipment was functioning properly. Figure A.6 shows the simple set up for this procedure.

The pressure transducer used was a Validyne Eng. Corp. Multirange Δp transducer, model DP15TL. This type of transducer allows for different pressure ranges to be used with only one transducer. This is accomplished by substituting different range diaphragms into the transducer when required. The calibration of the transducer with the different diaphragms was done with a Deadweight Tester Pressure Balance from Pressurements Ltd. (U.K.), type M1900-3. The results of the calibration for the two diaphragms used are shown in Figures A.7 and A.8.

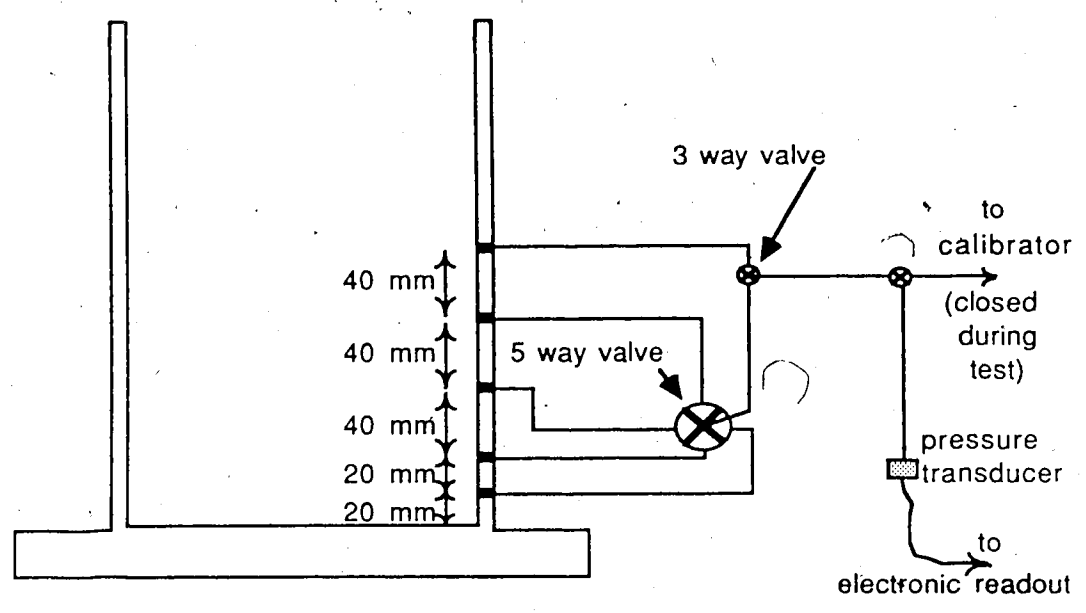


Figure A.5 Pore Pressure Measurement Equipment

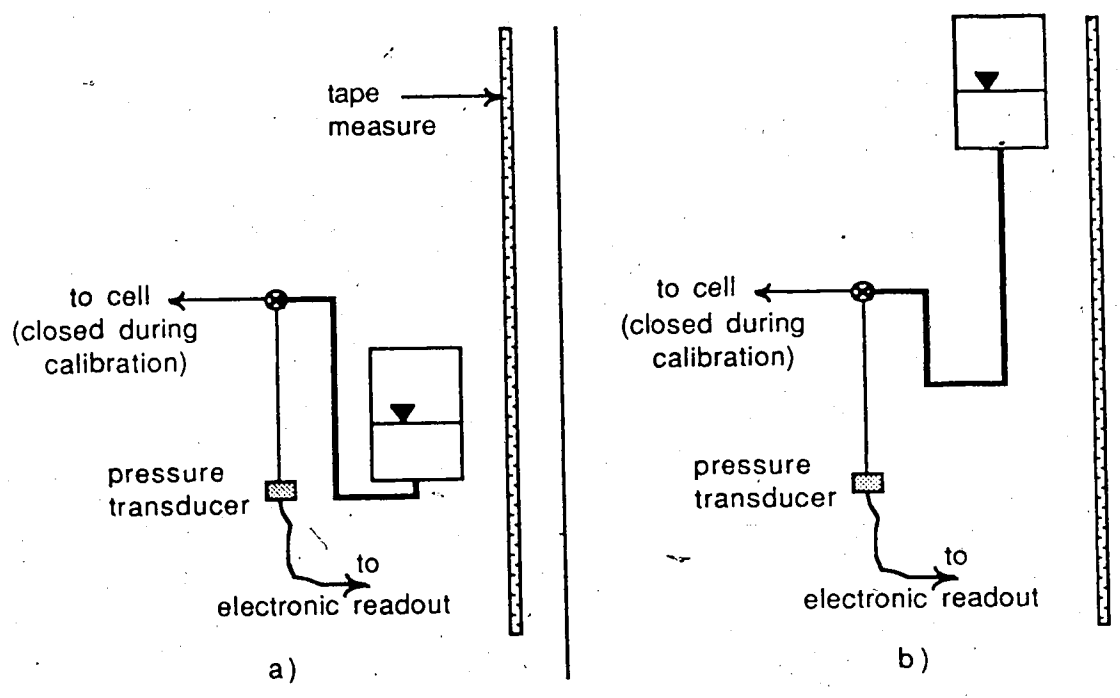


Figure A.6 Calibration Check Method

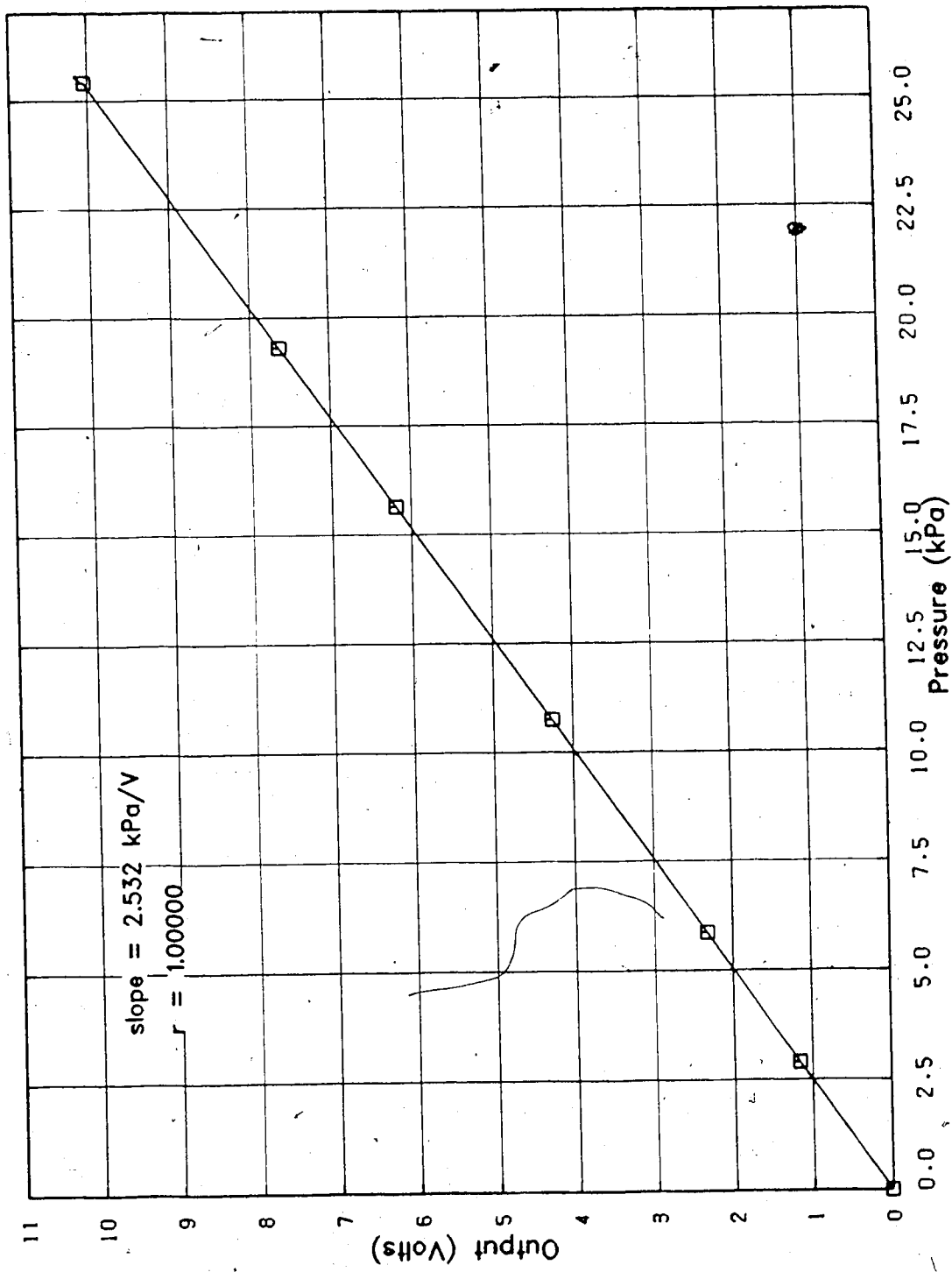


Figure A.7 Calibration of 35 kPa Diaphragm for Validyne Transducer

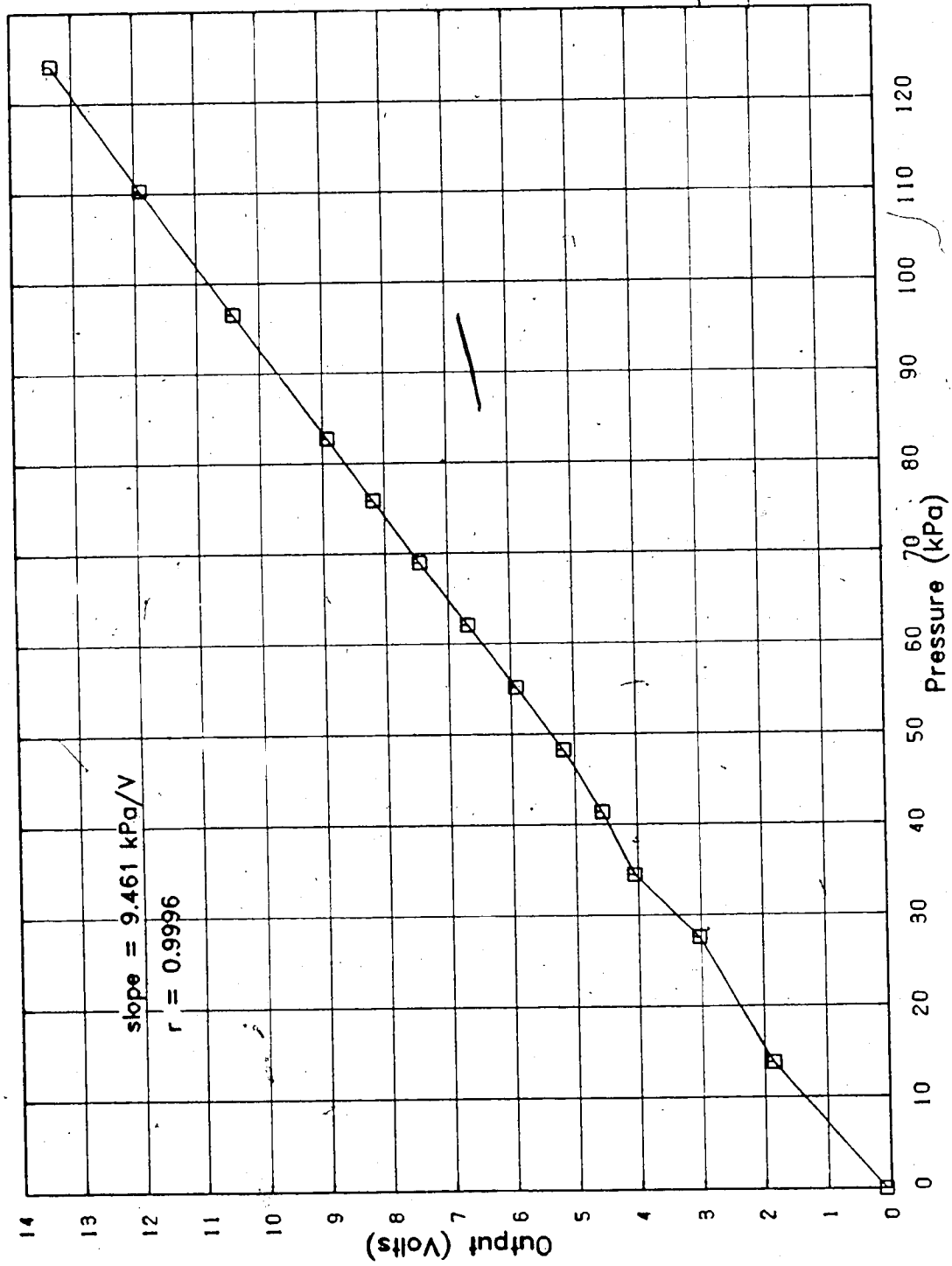


Figure A.8 Calibration of 140 kPa Diaphragm for Validyne Transducer

Detailed specifications on any of the mentioned equipment can be obtained from the respective manufacturers.

Procedural Details

Top Cap Friction

As discussed in Chapter 4 (4.2.2), tests were performed before a stress was applied to the sample to determine how much additional load would be required to overcome the top cap friction. The results at the various stress increments are shown in Figure A.9.

Soil Friction

For the two consolidometers with load cells in the base, it was possible to compare the applied stress (at the top of the sample) to the stress being received at the bottom of the sample. When the stress at the top was greater than the at the bottom, the difference was attributed to soil friction along the wall of the cell.

Figure A.10 shows applied stress values compared to the load cell stress value. Notice that for Test #4, from 50 kPa onwards there is an increasing difference between the two values. For calculations purposes, the stress for those increments was taken as the average of the stress at the top and at the bottom of the sample (i.e., soil friction was assumed to be linear along the height of the sample).

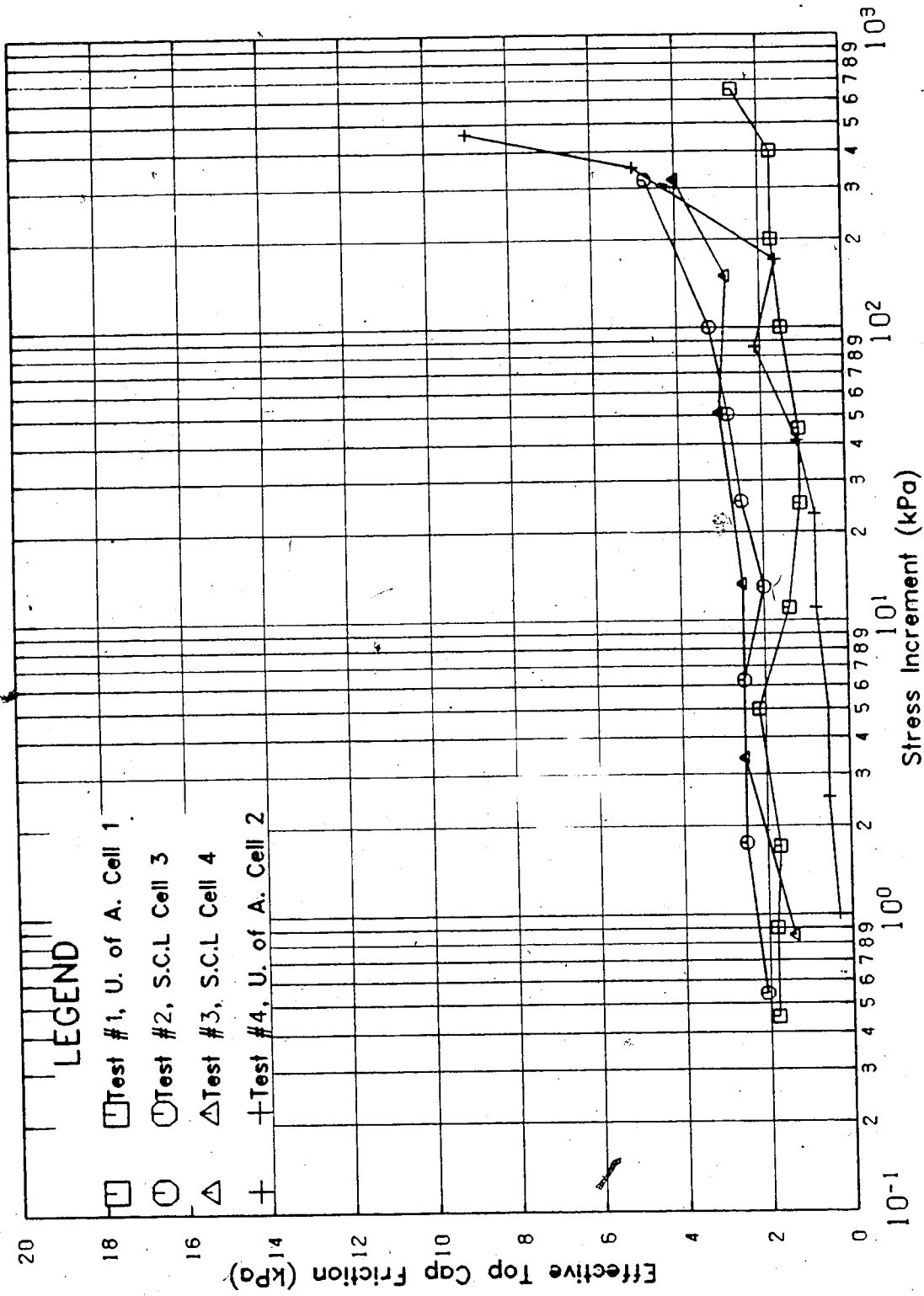


Figure A.9 Top Cap Friction

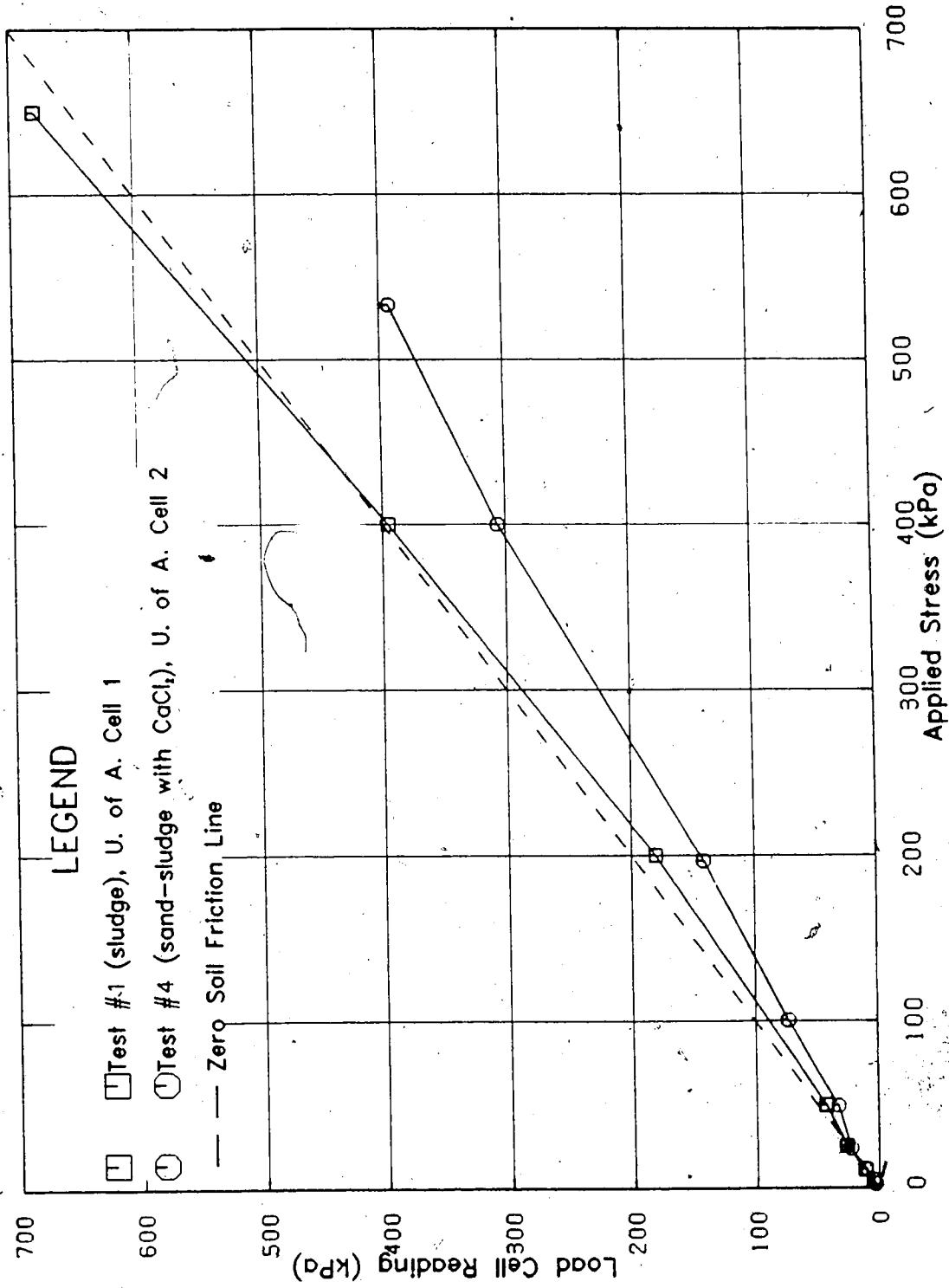


Figure A.10 Load Cell Stress Readings

APPENDIX B - Consolidation Time Plots

This Appendix contains the consolidation time plots for each stress increment in each of the four tests. The test material has been described in detail in Chapter 4 and is categorized below.

Test #1	Oil Sand Tailings Sludge
Test #2	46% Sand Sludge-Sand Mix
Test #3	80% Sand Sludge-Sand Mix
Test #4	73% Sand Sludge-Sand Mix with CaCl_2

The plots for Tests 1, 2, 3, and 4 begin on pages 228, 234, 241, and 241 respectively.

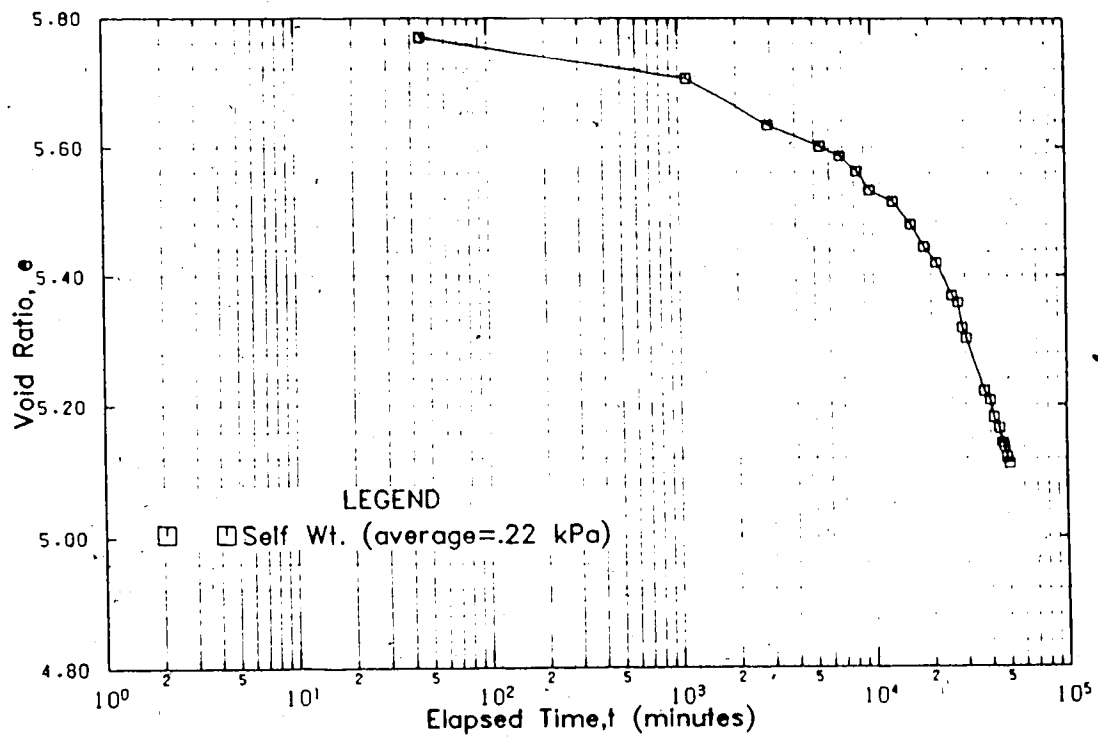


Figure B.1 Consolidation, Test #1, $\sigma' = 0.22$ kPa (self weight).

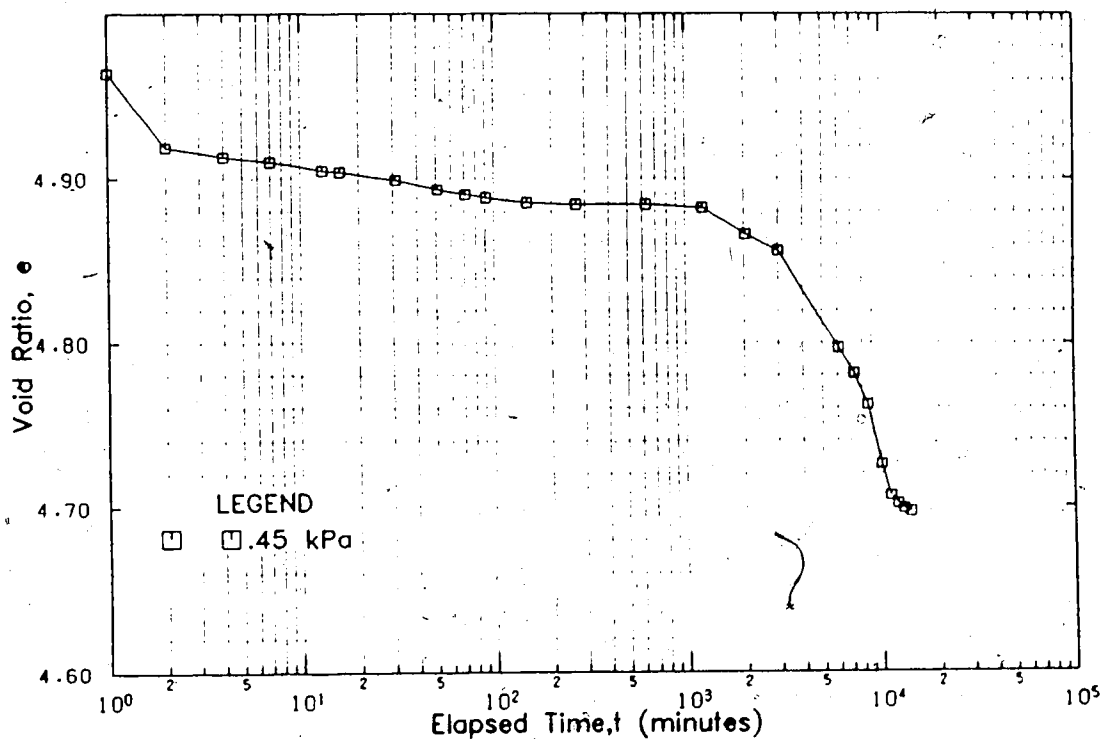


Figure B.2 Consolidation, Test #1, $\sigma' = 0.45$ kPa

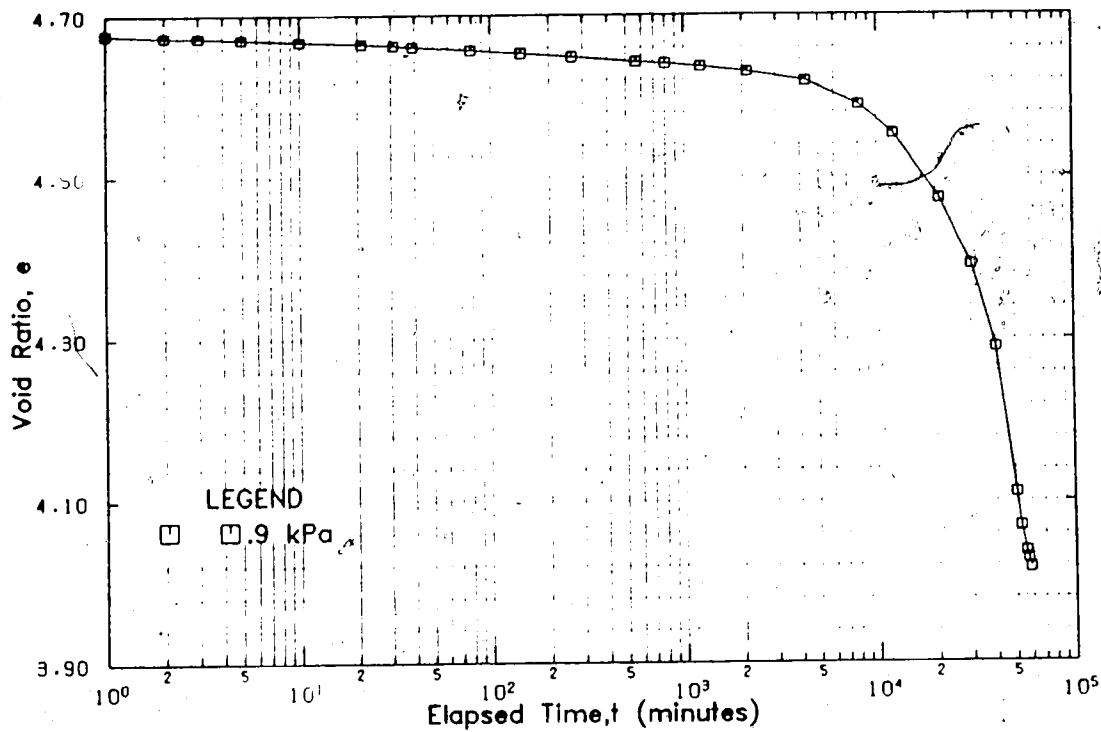


Figure B.3 Consolidation, Test #1, $\sigma' = 0.9$ kPa

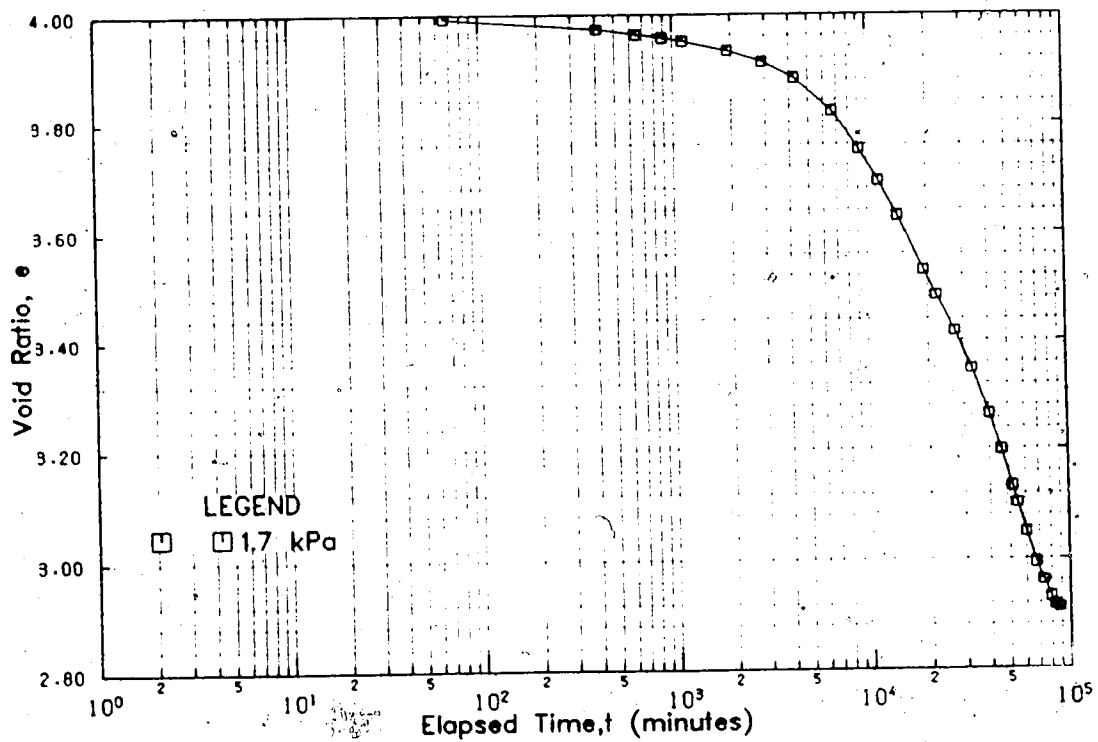


Figure B.4 Consolidation, Test #1, $\sigma' = 1.7$ kPa

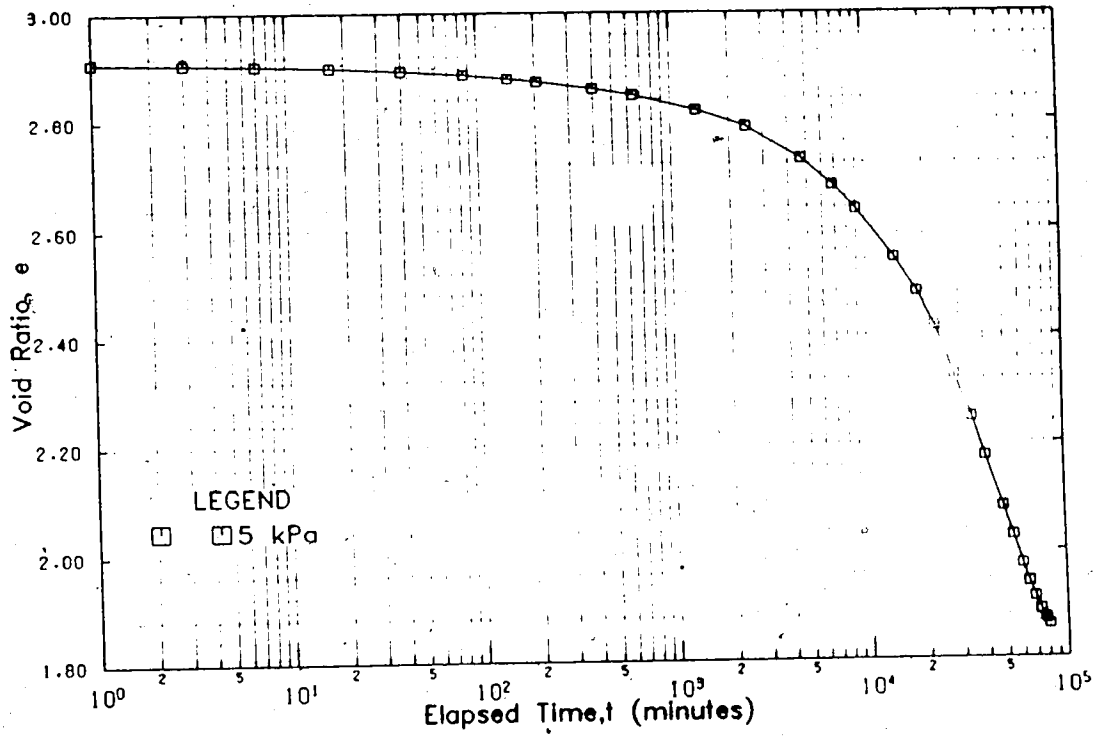


Figure B.5 Consolidation, Test #1, $\sigma' = 5.0$ kPa

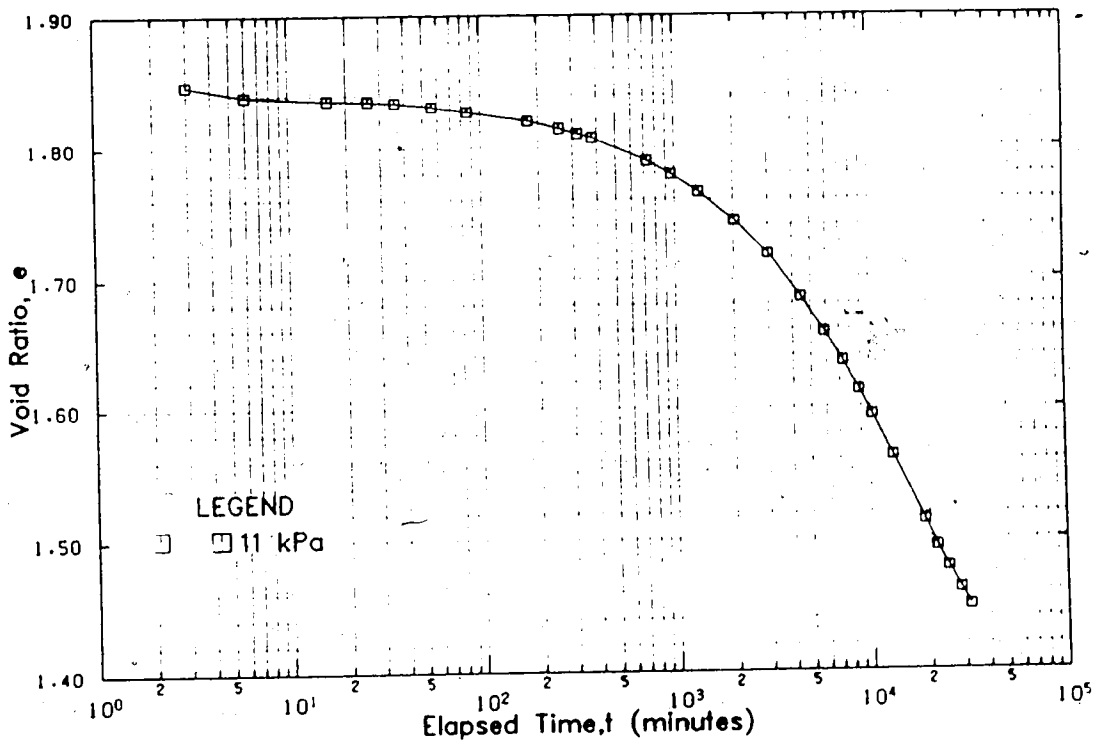


Figure B.6 Consolidation, Test #1, $\sigma' = 11.0$ kPa

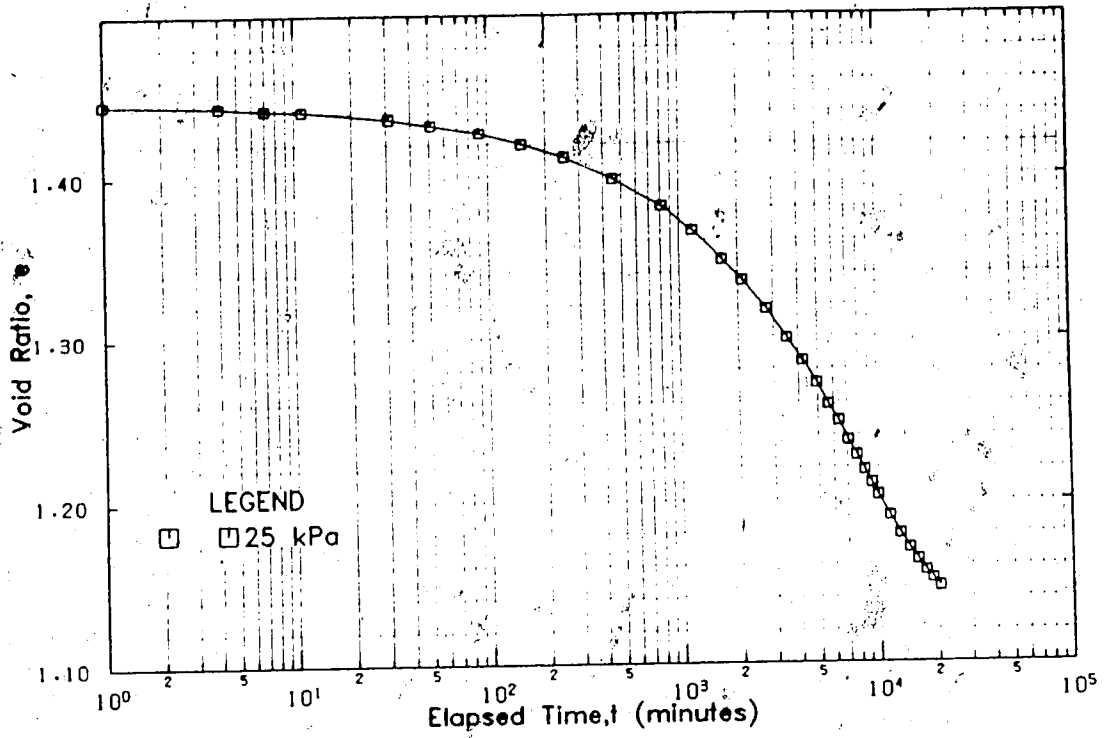


Figure B.7 Consolidation, Test #1, $\sigma' = 25.0$ kPa

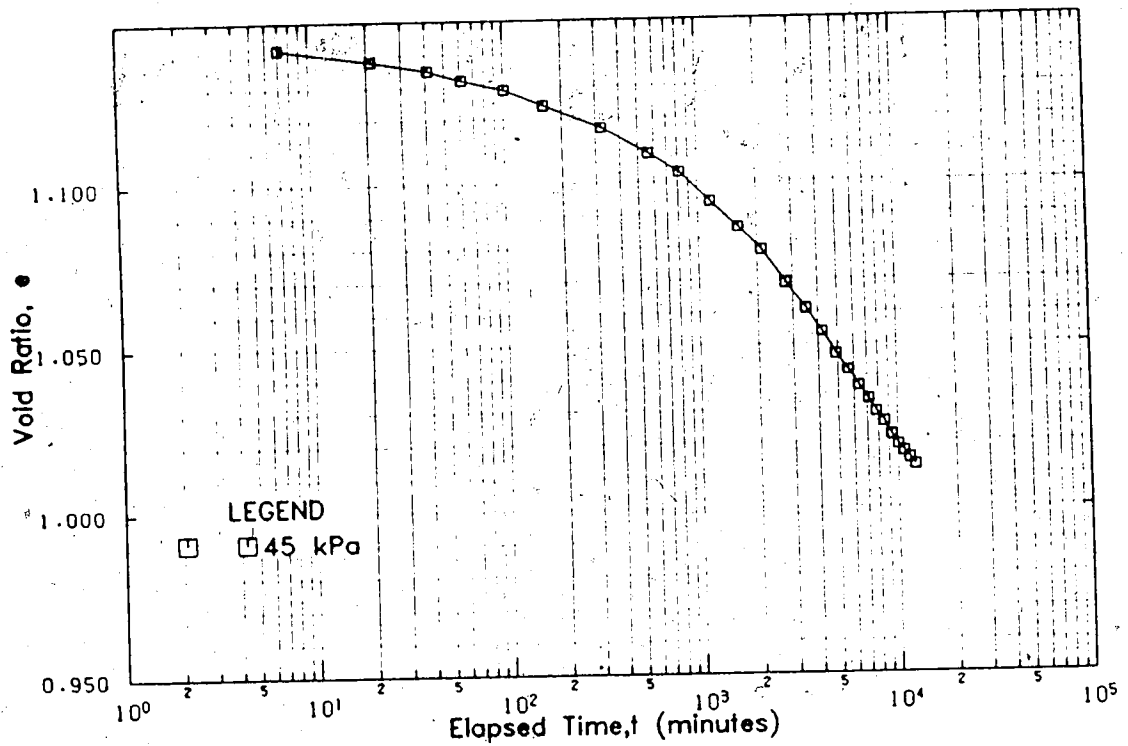


Figure B.8 Consolidation, Test #1, $\sigma' = 45$ kPa

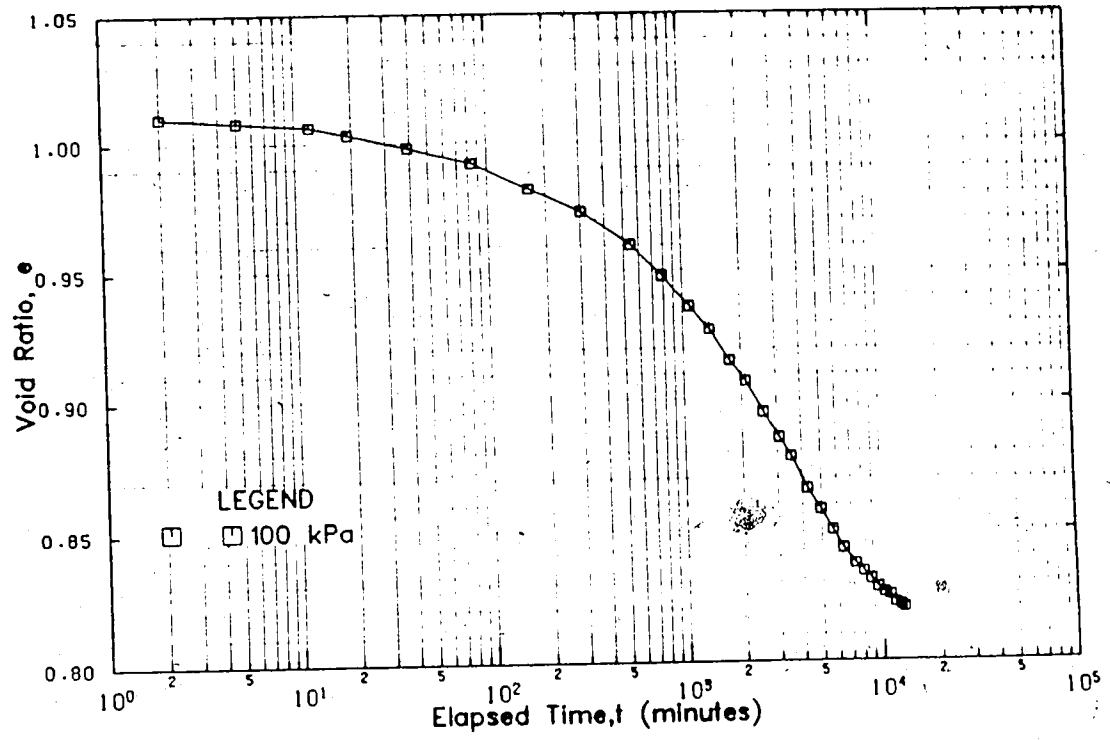


Figure B.9 Consolidation, Test #1, $\sigma' = 100$ kPa

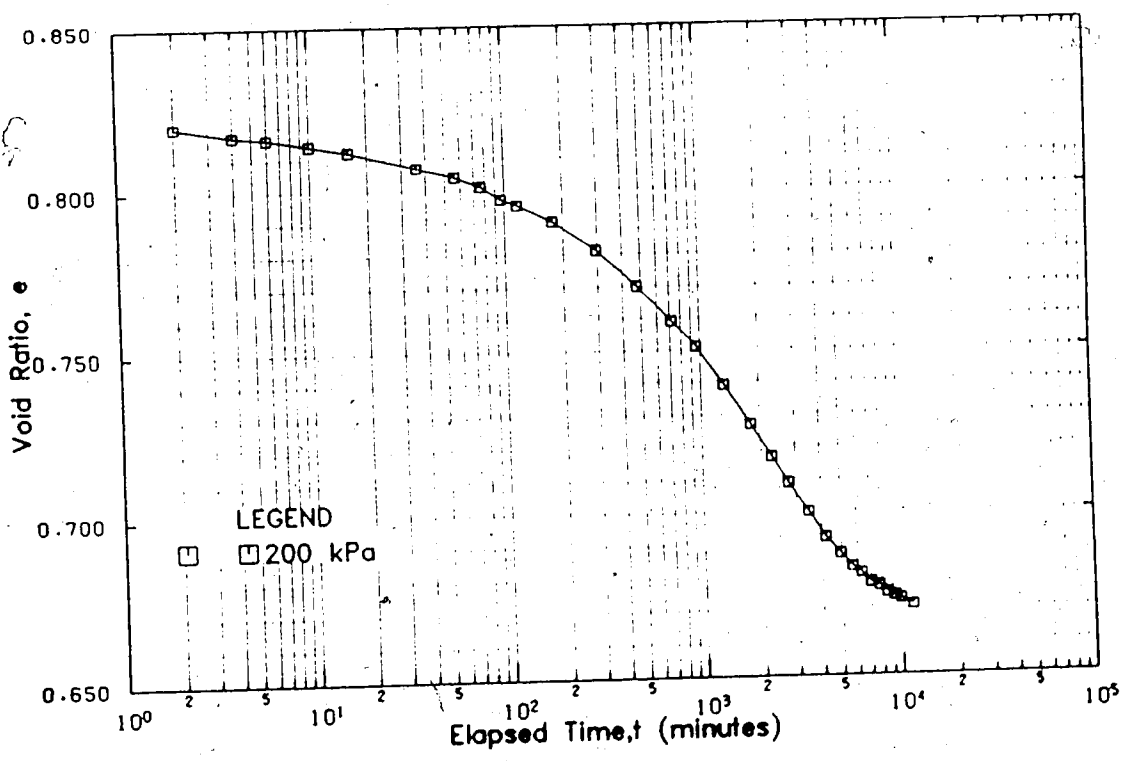


Figure B.10 Consolidation, Test #1, $\sigma' = 200$ kPa

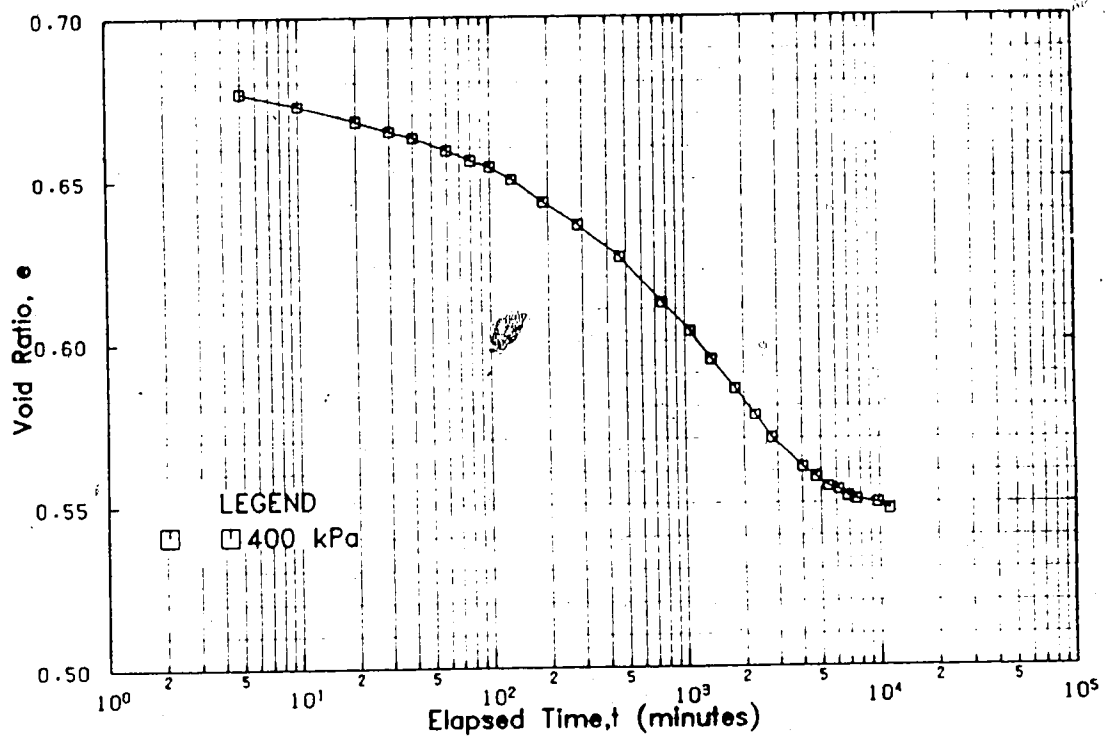


Figure B.11 Consolidation, Test #1, $\sigma' = 400$ kPa

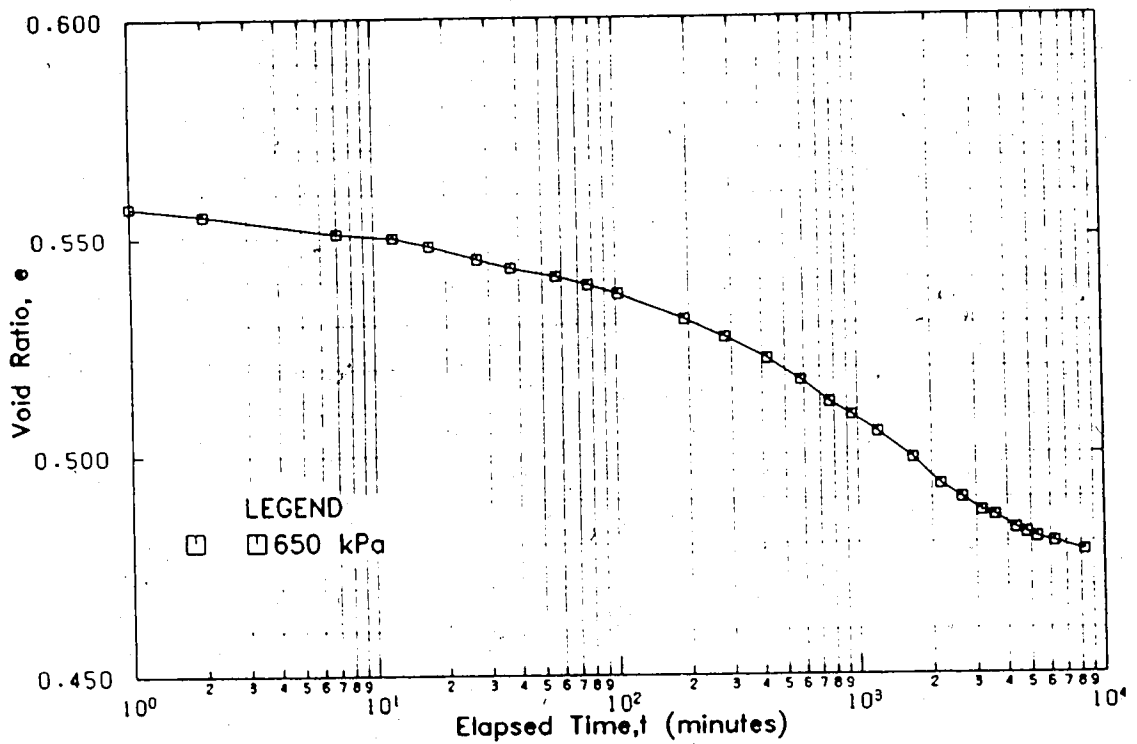


Figure B.12 Consolidation, Test #1, $\sigma' = 650$ kPa

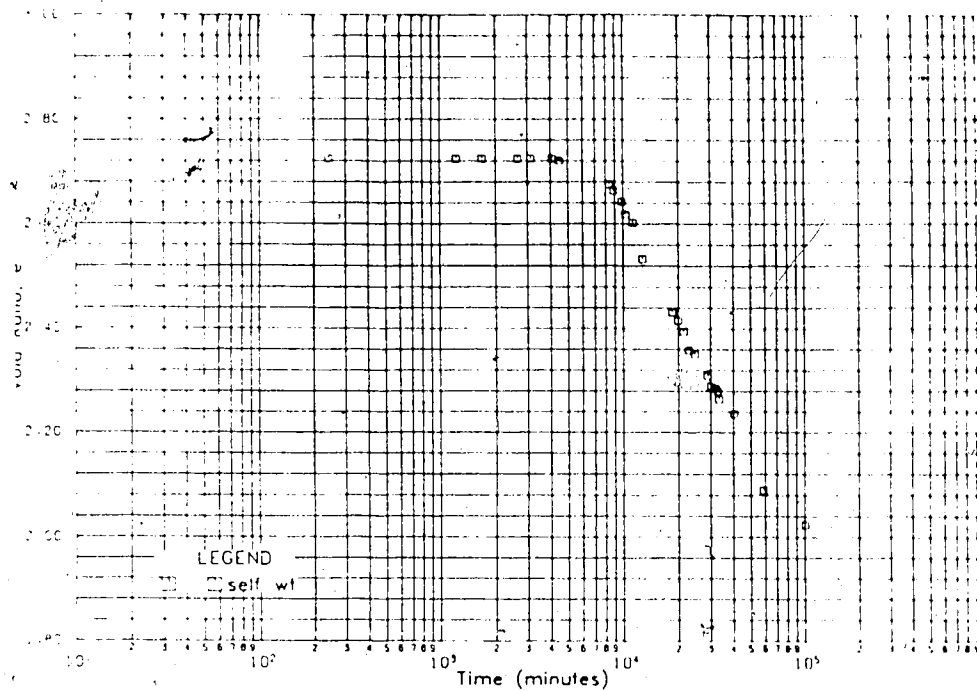


Figure B.13 Consolidation, Test #2, $\sigma' = 0.45$ kPa (self weight)

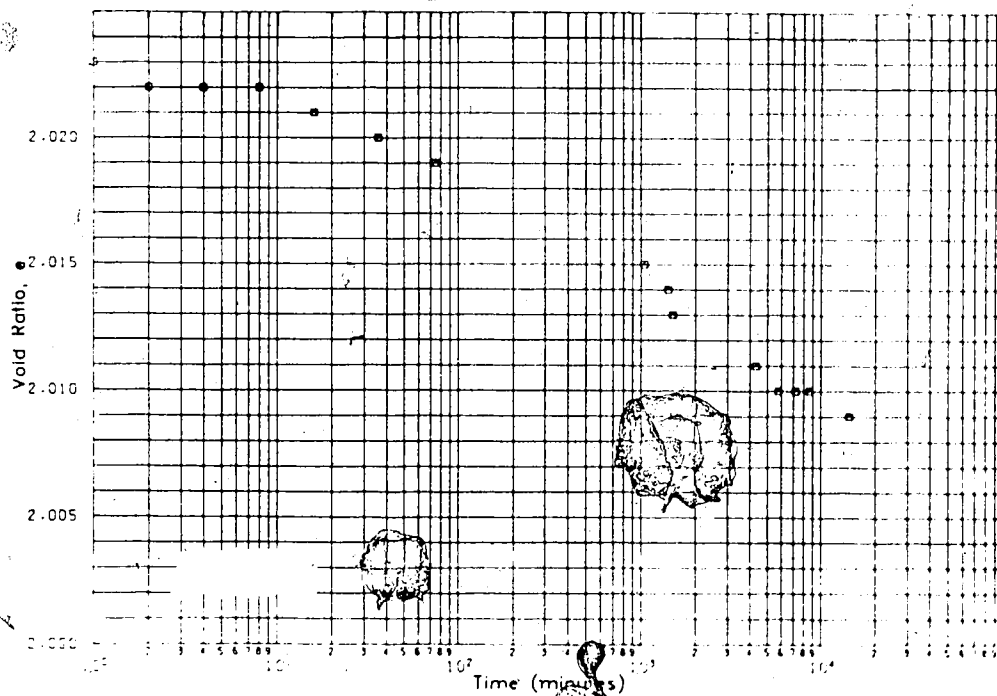


Figure B.14 Consolidation, Test #2, $\sigma' = 0.54$ kPa

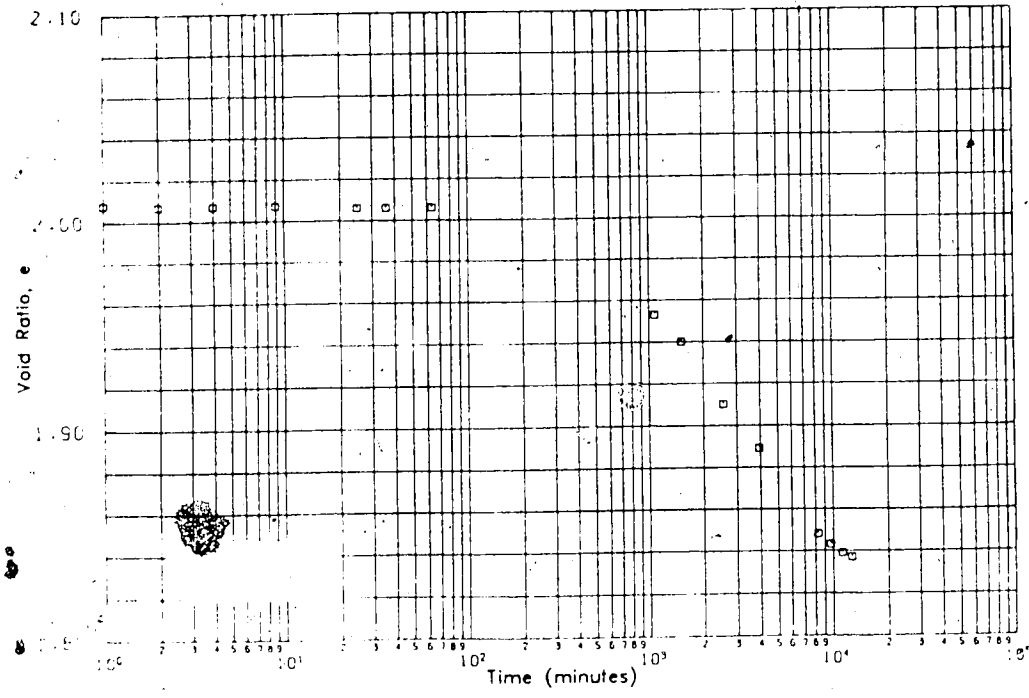


Figure B.15 Consolidation, Test #2, $\sigma' = 0.64$ kPa

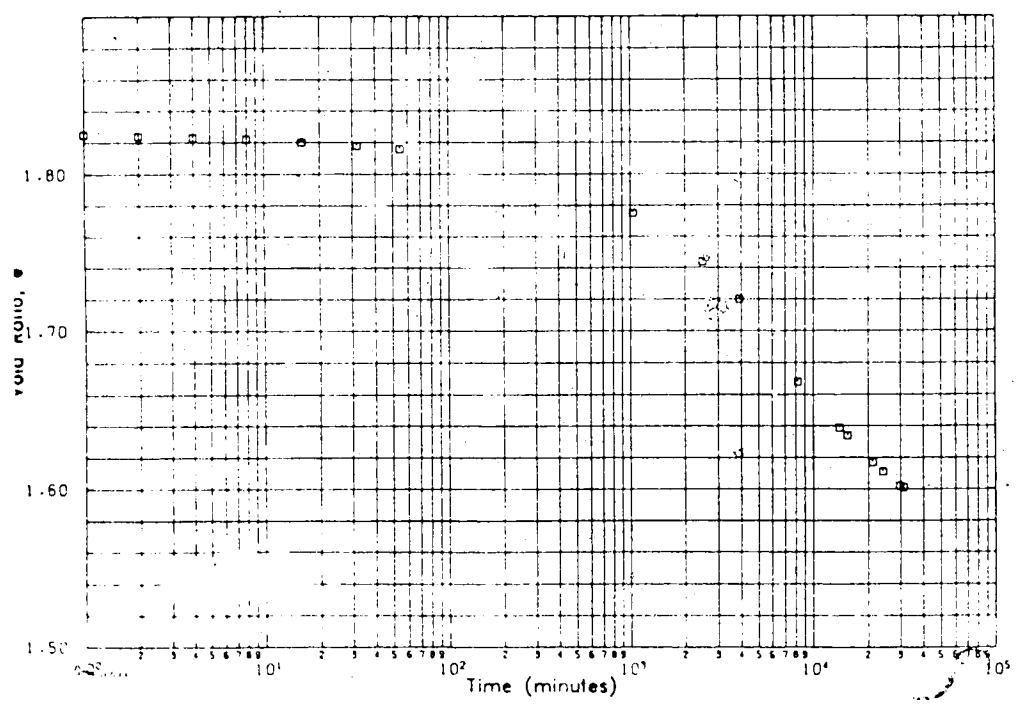


Figure B.16 Consolidation, Test #2, $\sigma' = 1.0$ kPa

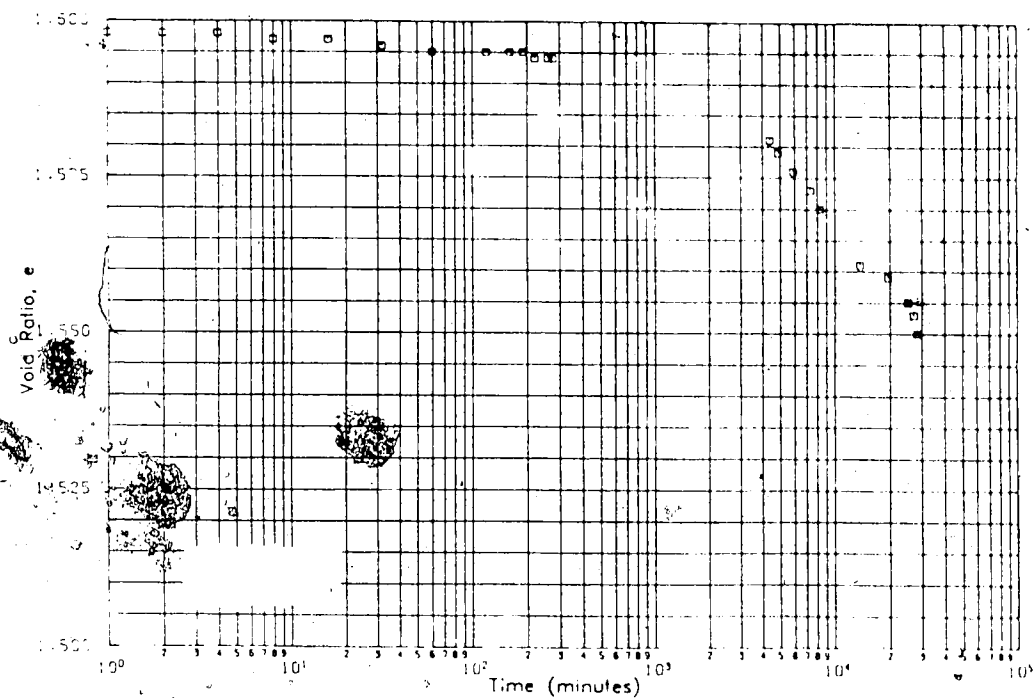


Figure B.17 Consolidation, Test #2, $\sigma' = 1.75$ kPa

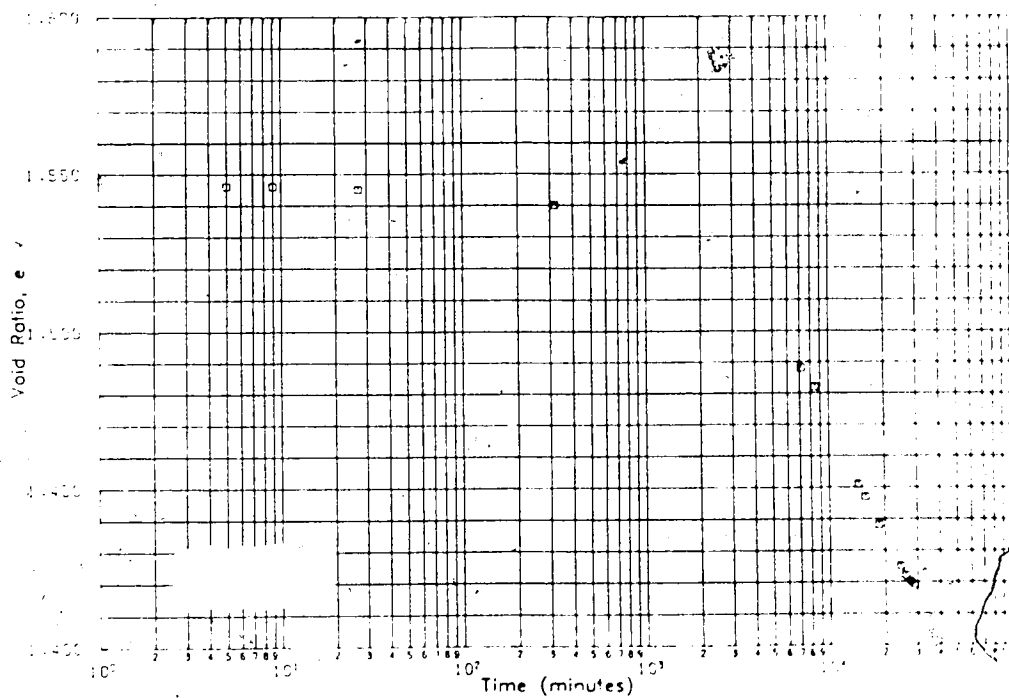


Figure B.18 Consolidation, Test #2, $\sigma' = 3.05$ kPa

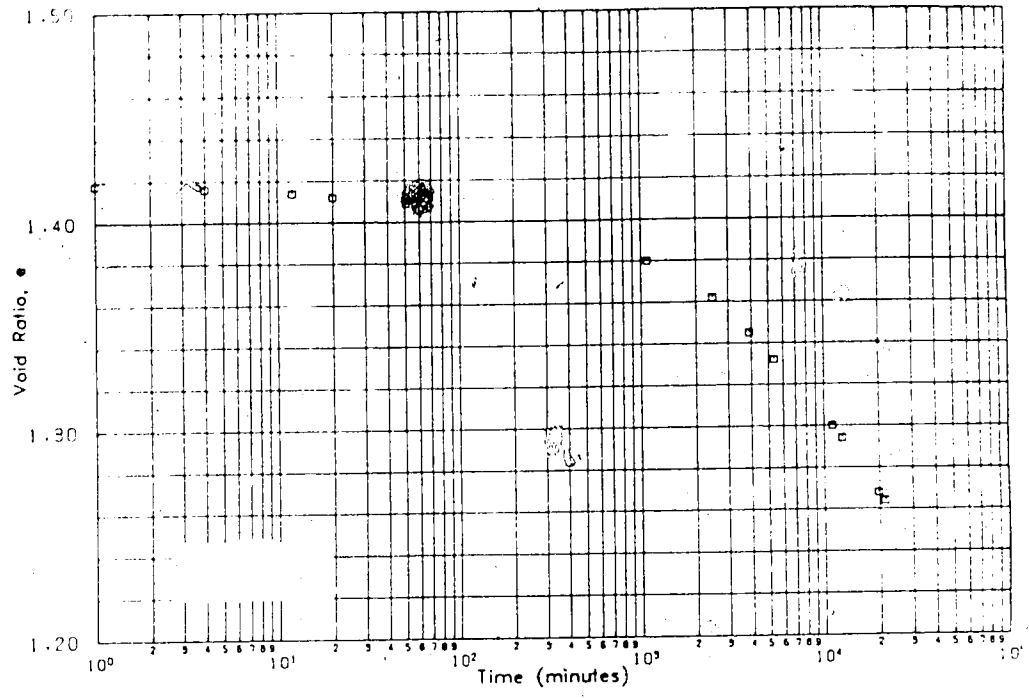


Figure B.19 Consolidation, Test #2, $\sigma' = 6.25$ kPa

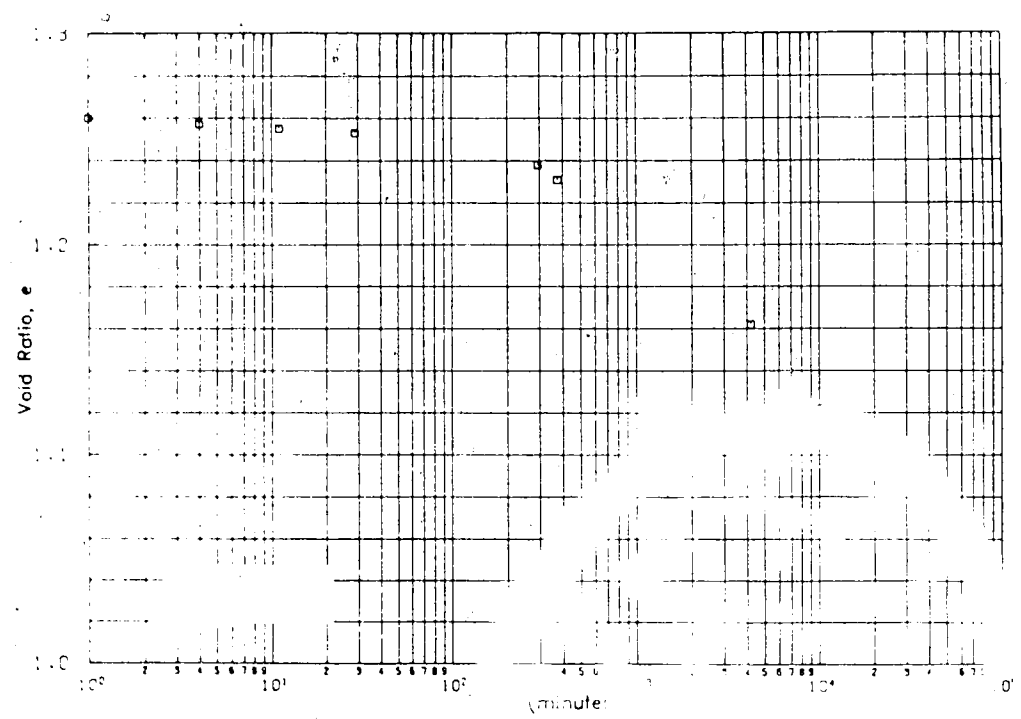


Figure B.20 Consolidation, Test #2, $\sigma' = 13.0$ kPa

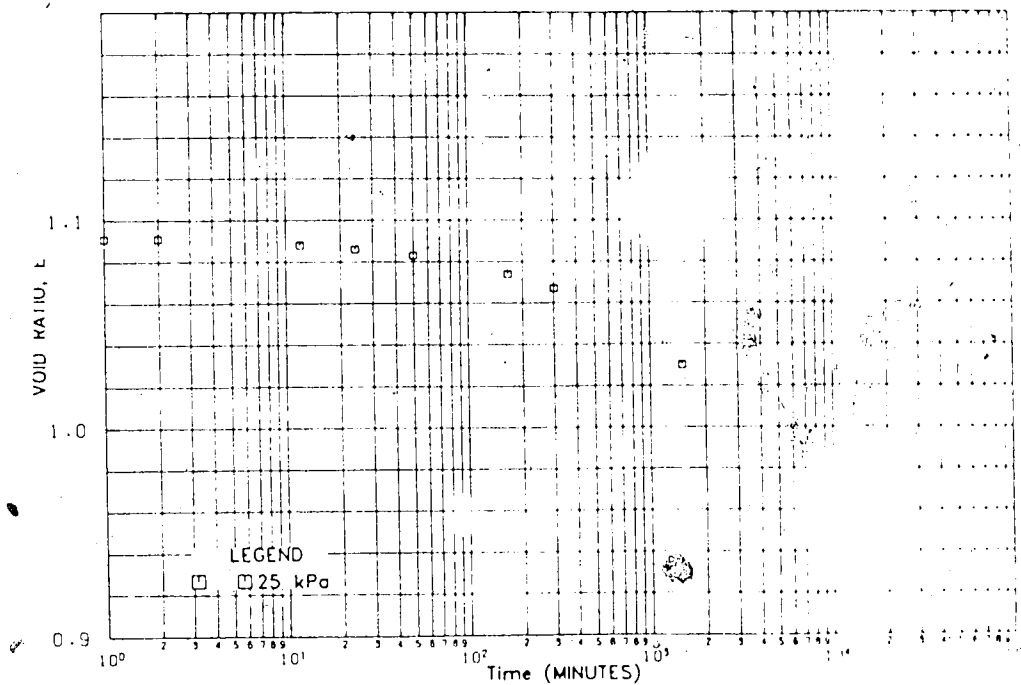


Figure B.21 Consolidation, Test #2, $\sigma' = 25.5$ kPa

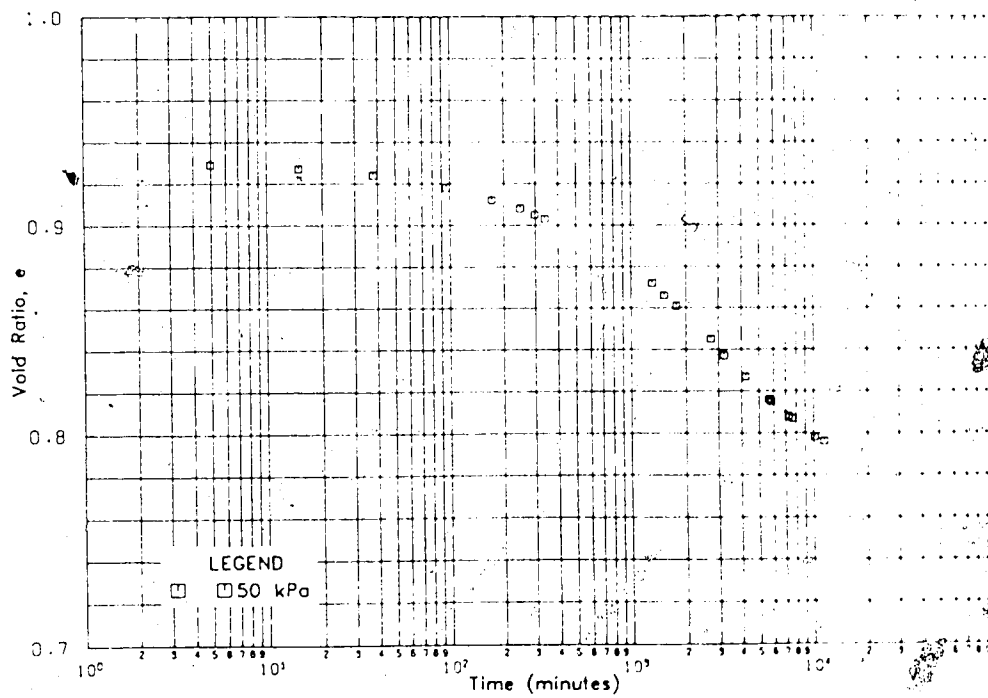


Figure B.22 Consolidation, Test #2, $\sigma' = 50.5$ kPa

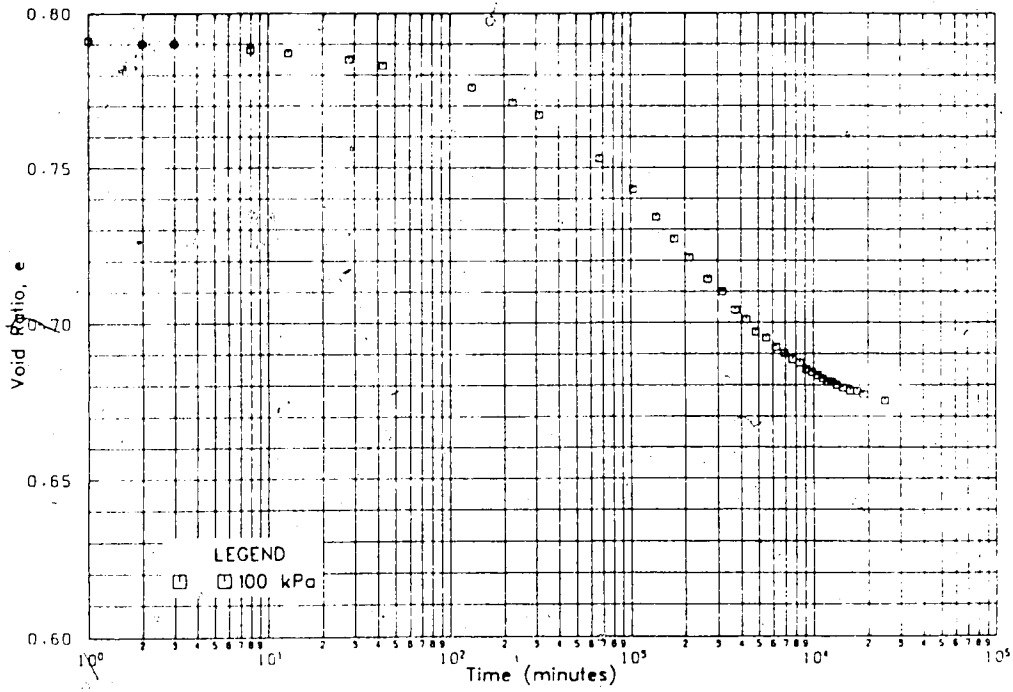


Figure B.23 Consolidation, Test #2, $\sigma' = 100$ kPa

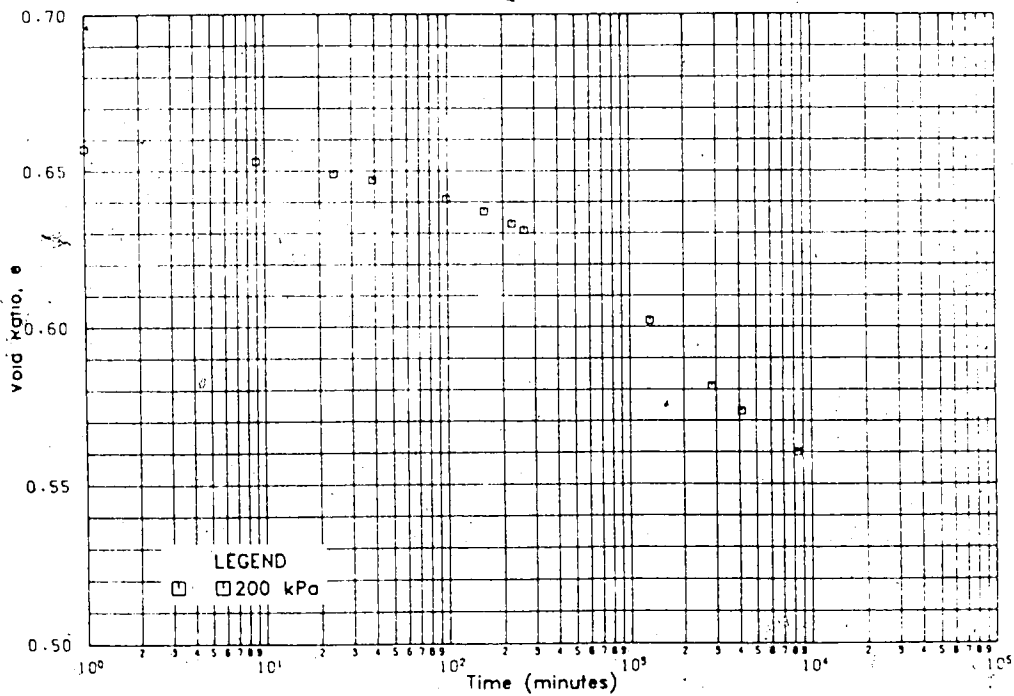


Figure B.24 Consolidation, Test #2, $\sigma' = 200$ kPa

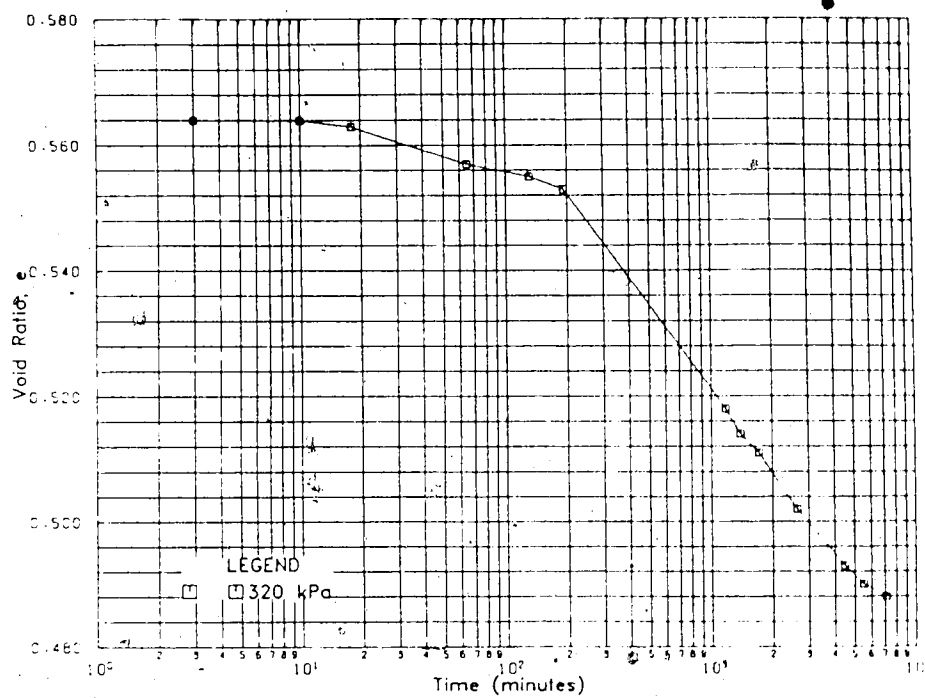


Figure B.25 Consolidation, Test #2, $\sigma' = 320$ kPa

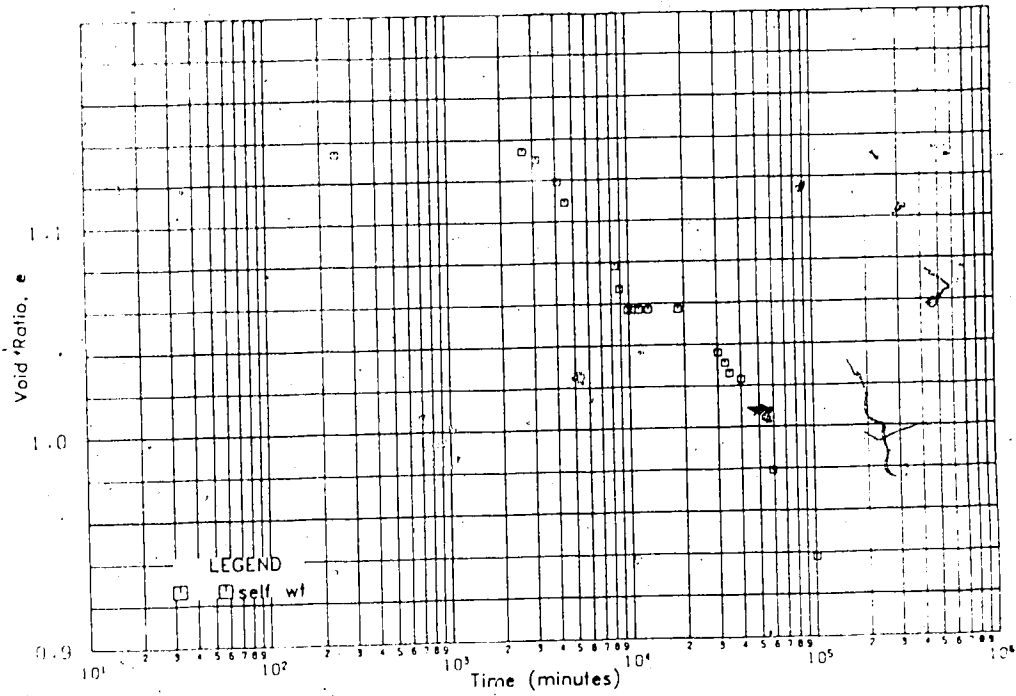


Figure B.26 Consolidation, Test #3, $\sigma' = 0.75$ kPa (self weight)

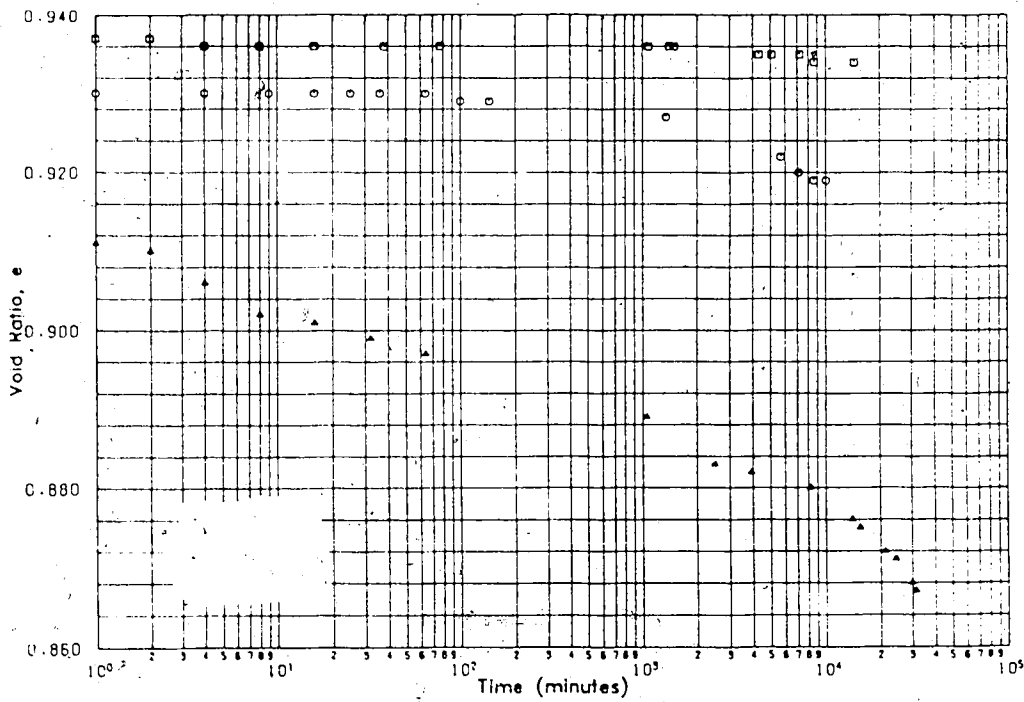


Figure B.27 Consolidation, Test #3, $\sigma' = 0.85, 0.95, \& 1.3$ kPa

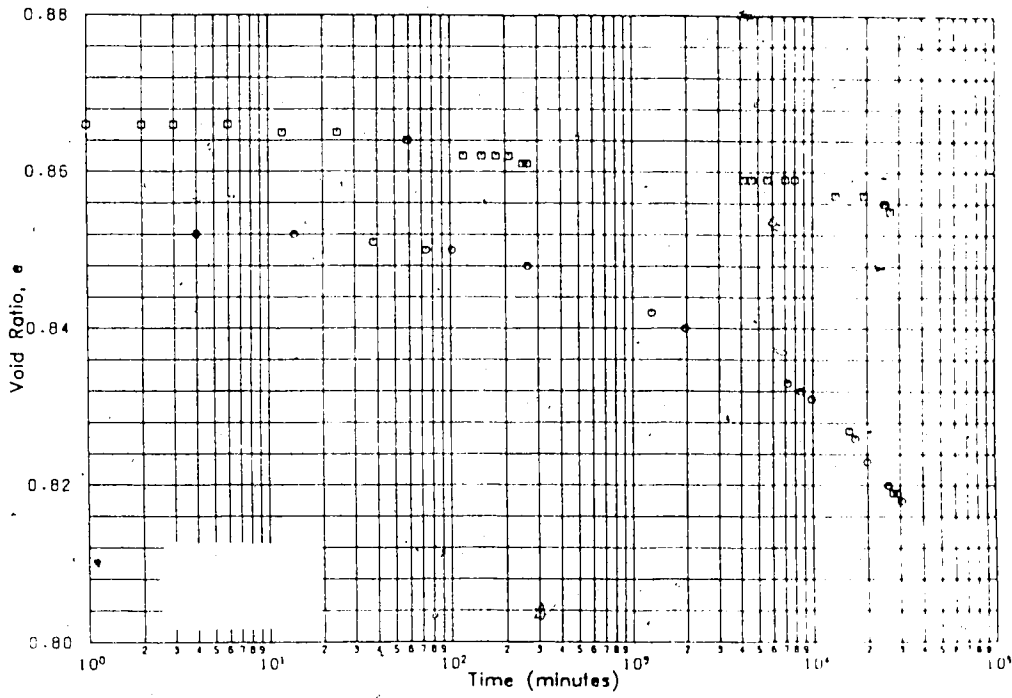


Figure B.28 Consolidation, Test #3, $\sigma' = 2.05$ & 3.4 kPa

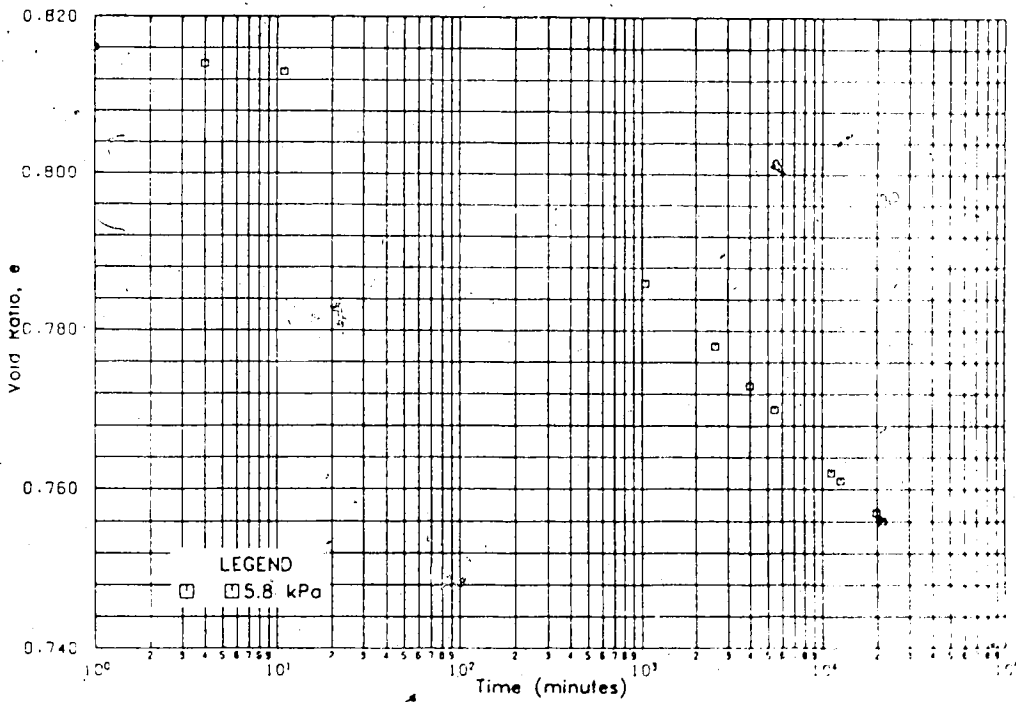


Figure B.29 Consolidation, Test #3, $\sigma' = 5.8$ kPa

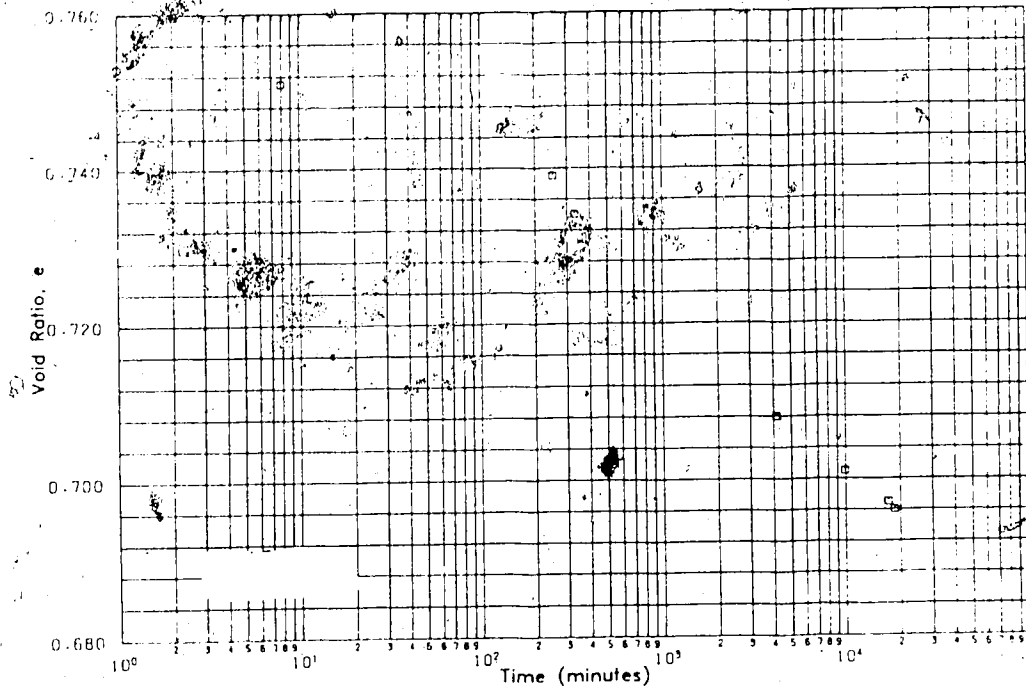


Figure B.30 Consolidation, Test #3, $\sigma' = 13.3$ kPa

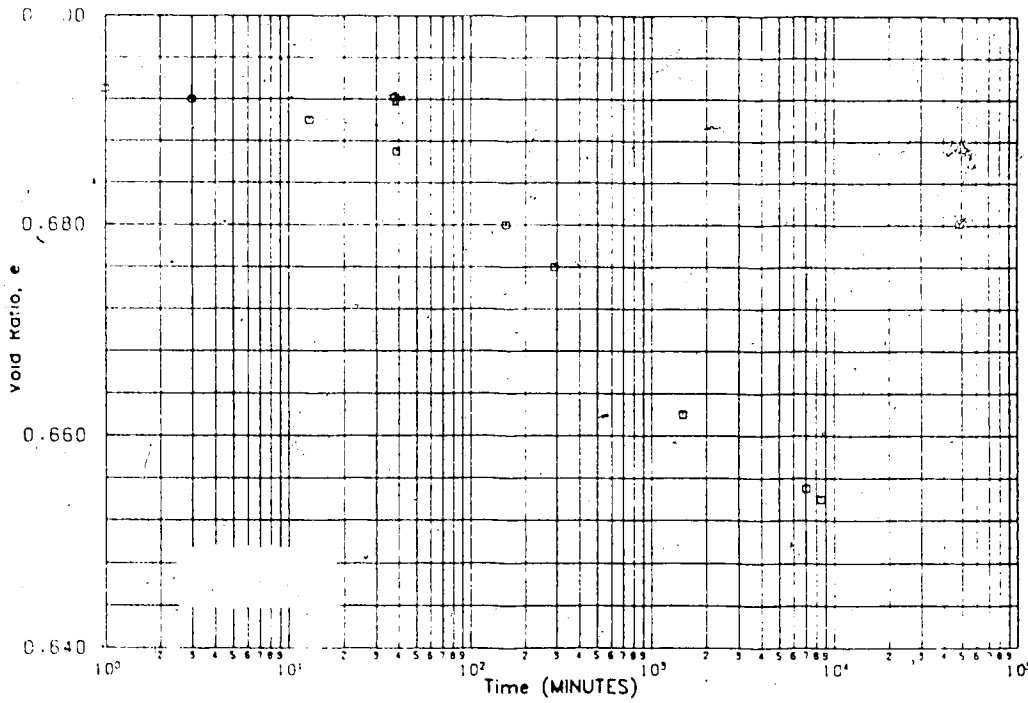


Figure B.31 Consolidation, Test #3, $\sigma' = 25.8$ kPa

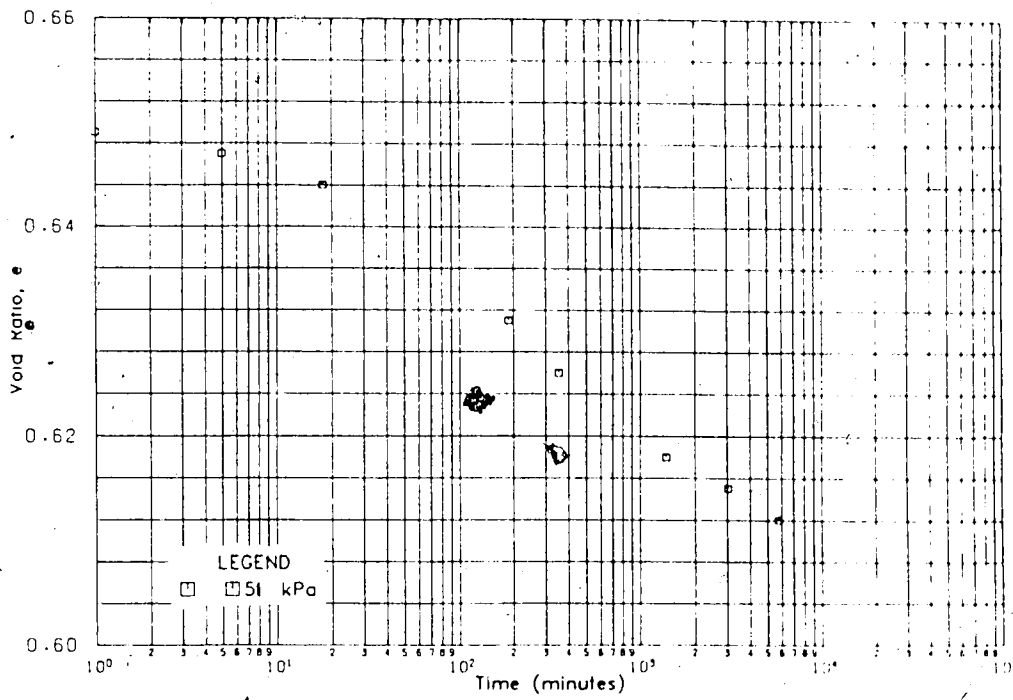


Figure B.32 Consolidation, Test #3, $\sigma' = 51$ kPa

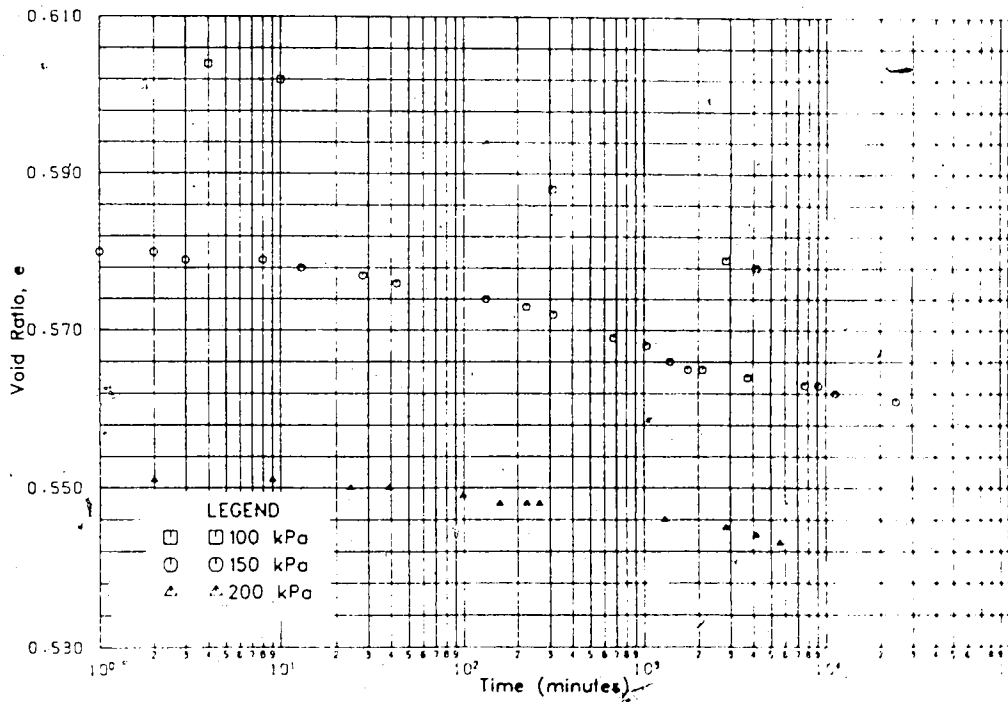


Figure B.33 Consolidation, Test #3, $\sigma' = 100, 150$ & 200 kPa

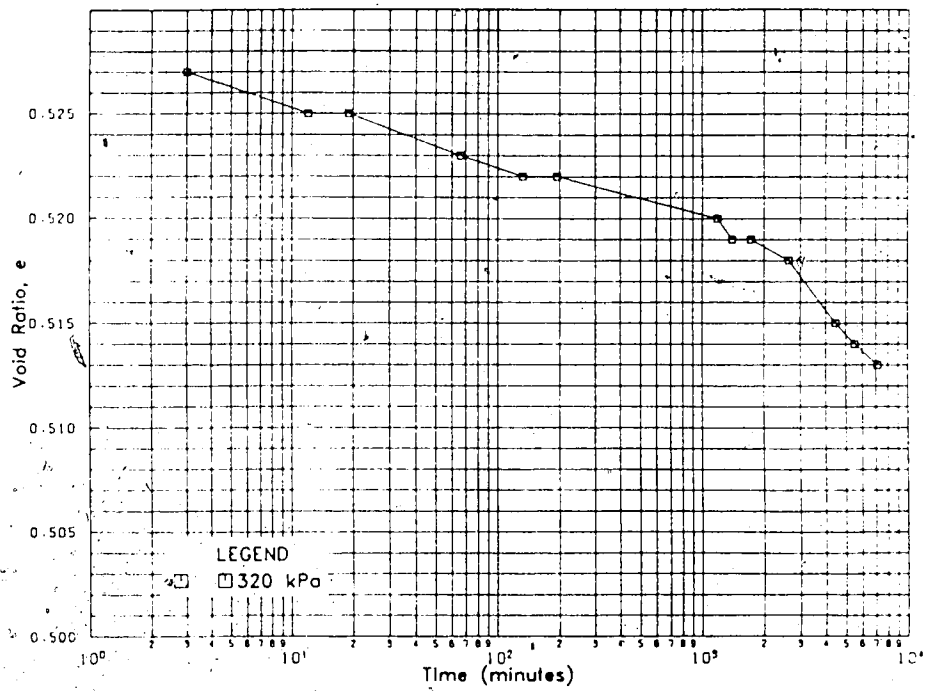


Figure B.34 Consolidation, Test #3, $\sigma' = 320$ kPa

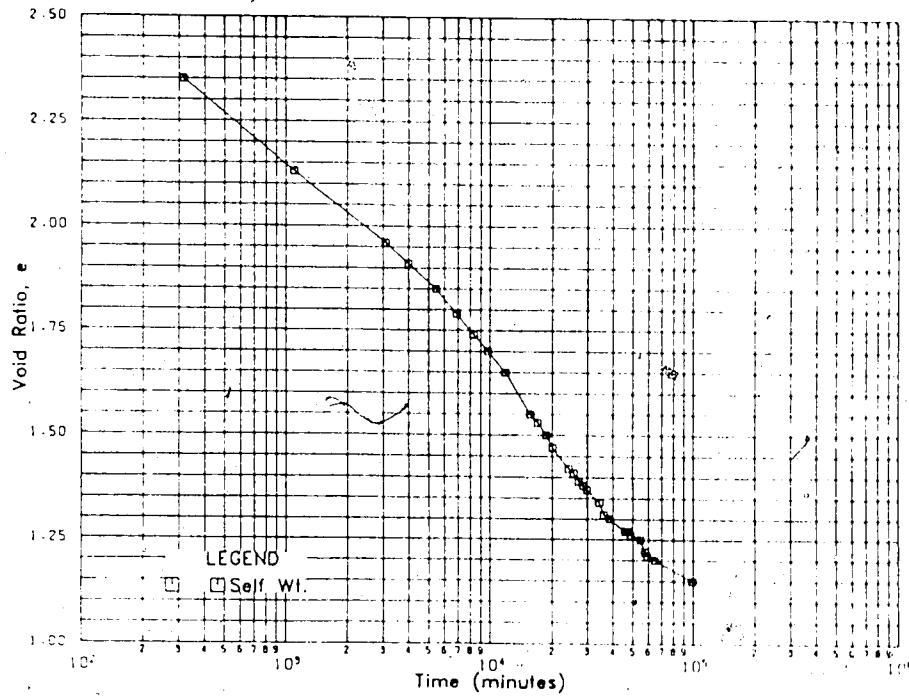


Figure B.35 Consolidation, Test #4, $\sigma' = 0.53$ kPa (self weight)

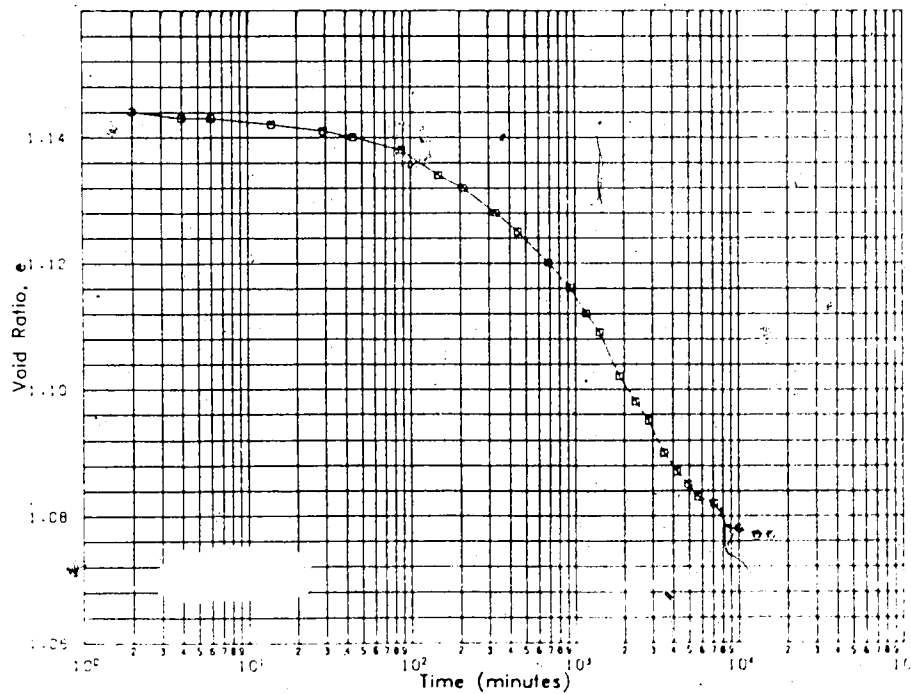


Figure B.36 Consolidation, Test #4, $\sigma' = 1.0$ kPa

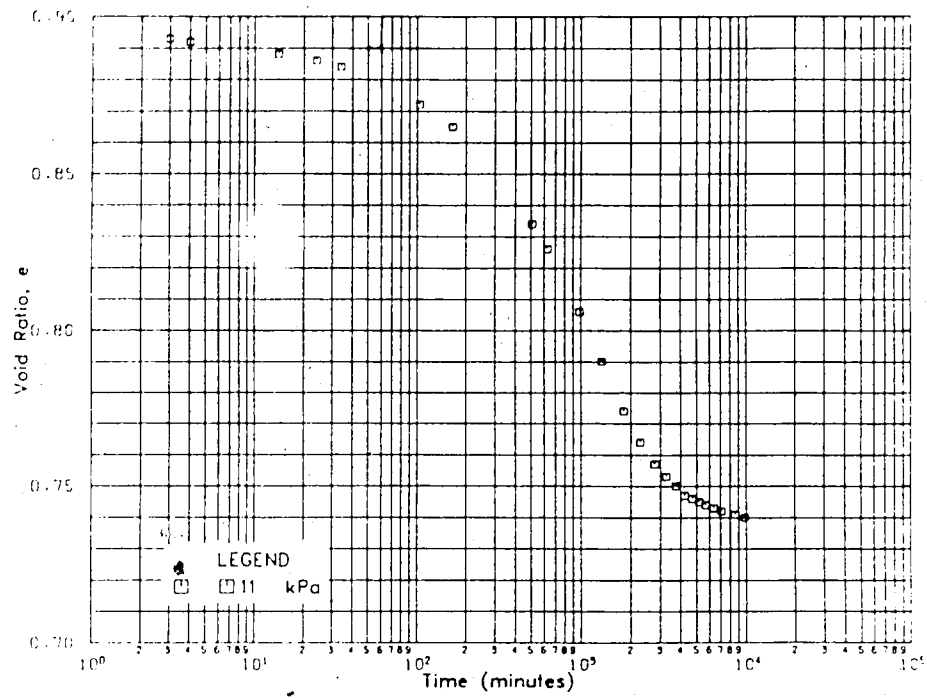


Figure B.39 Consolidation, Test #4, $\sigma' = 11.0$ kPa

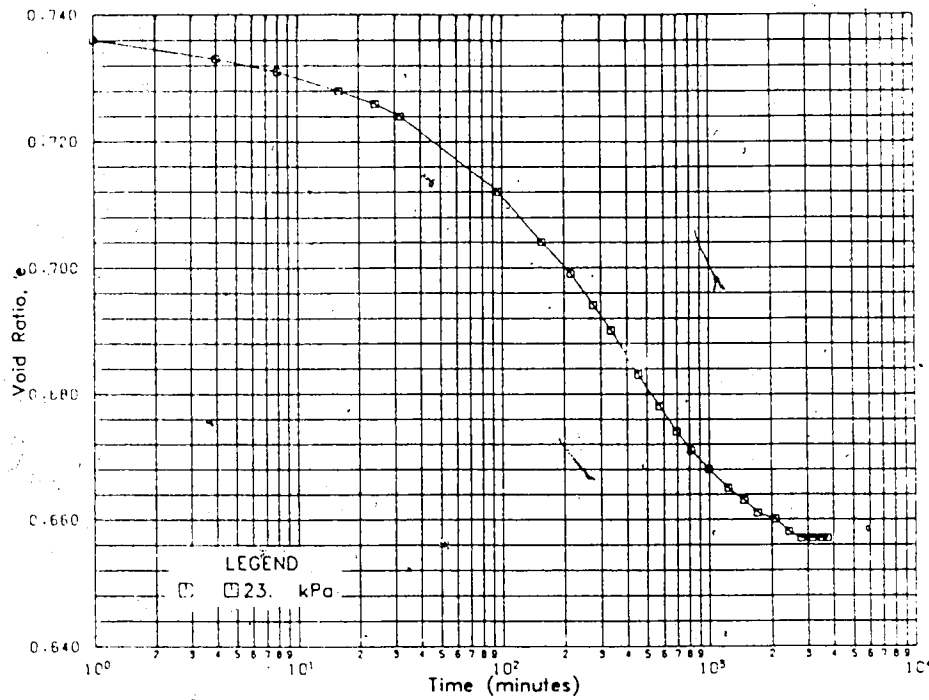


Figure B.40 Consolidation, Test #4, $\sigma' = 23$ kPa

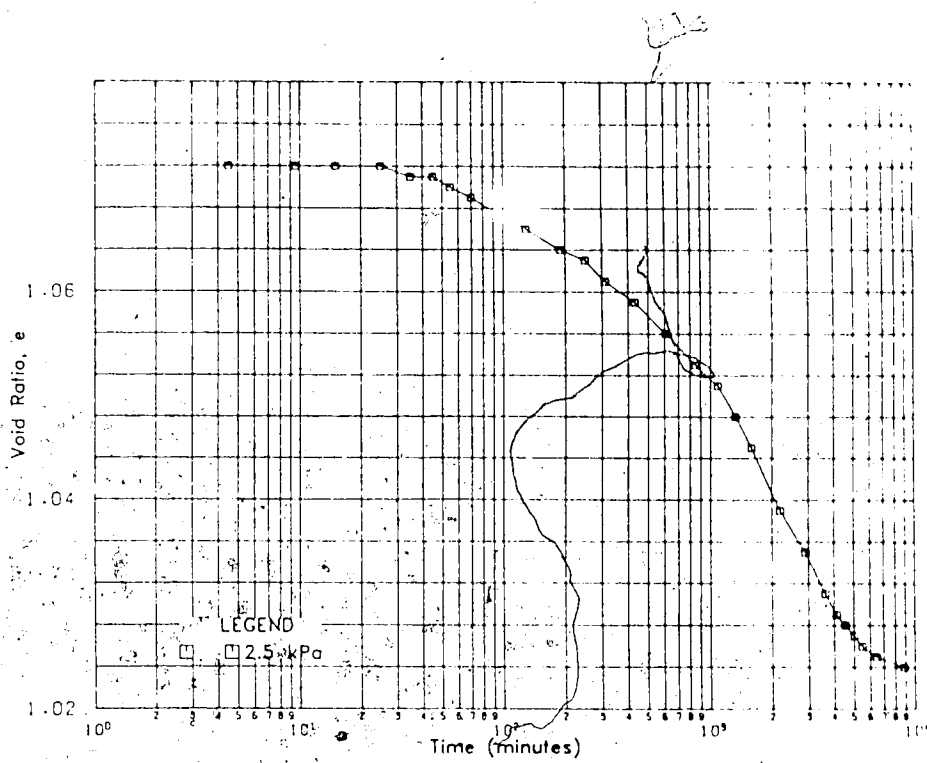


Figure B.37 Consolidation, Test #4, $\sigma' = 2.5$ kPa

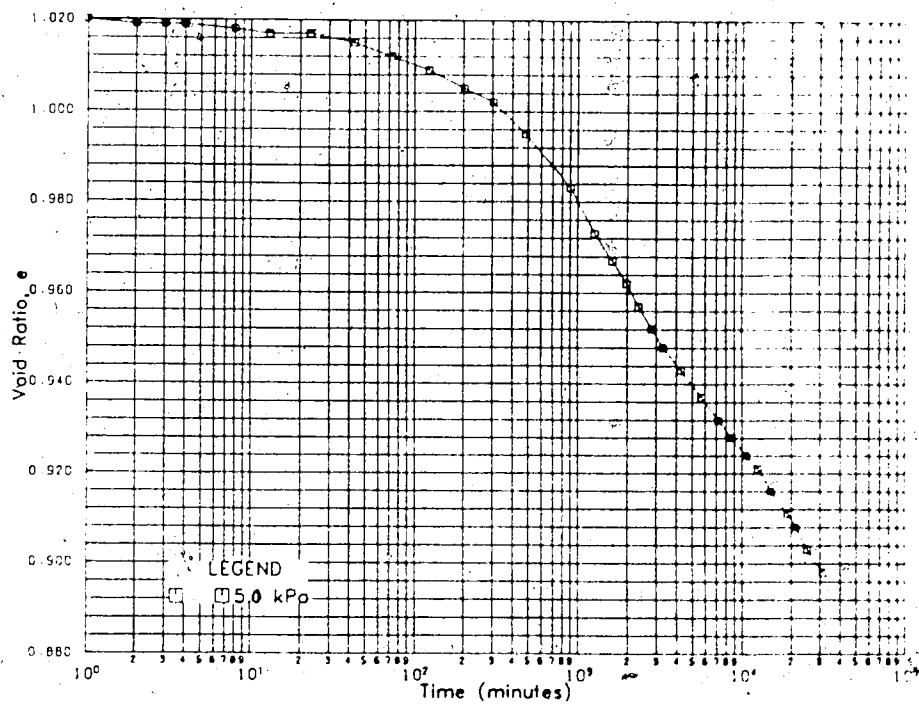


Figure B.38 Consolidation, Test #4, $\sigma' = 5.0$ kPa

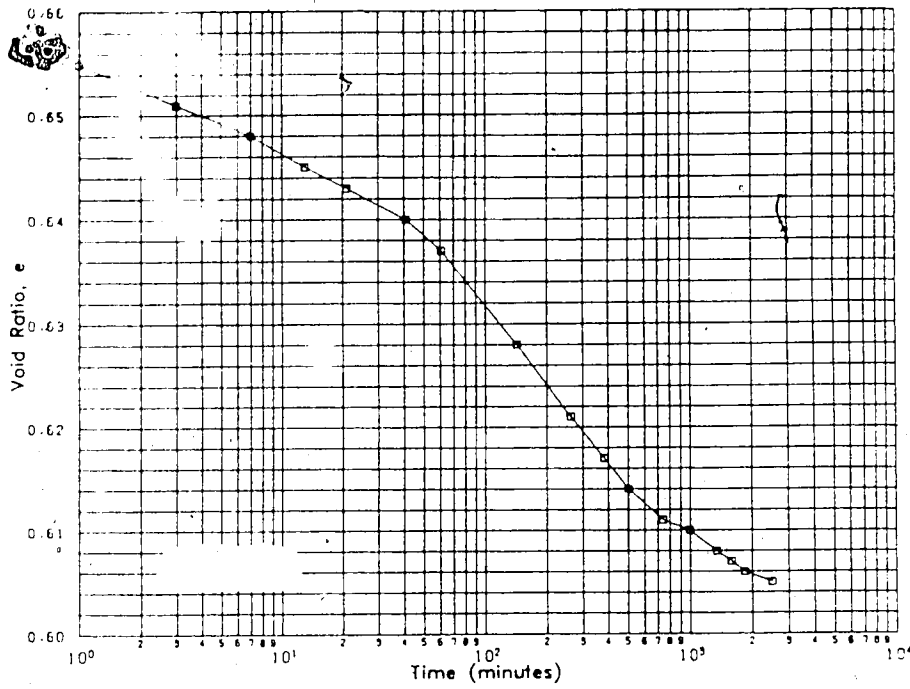


Figure B.41 Consolidation, Test #4, $\sigma' = 41$ kPa

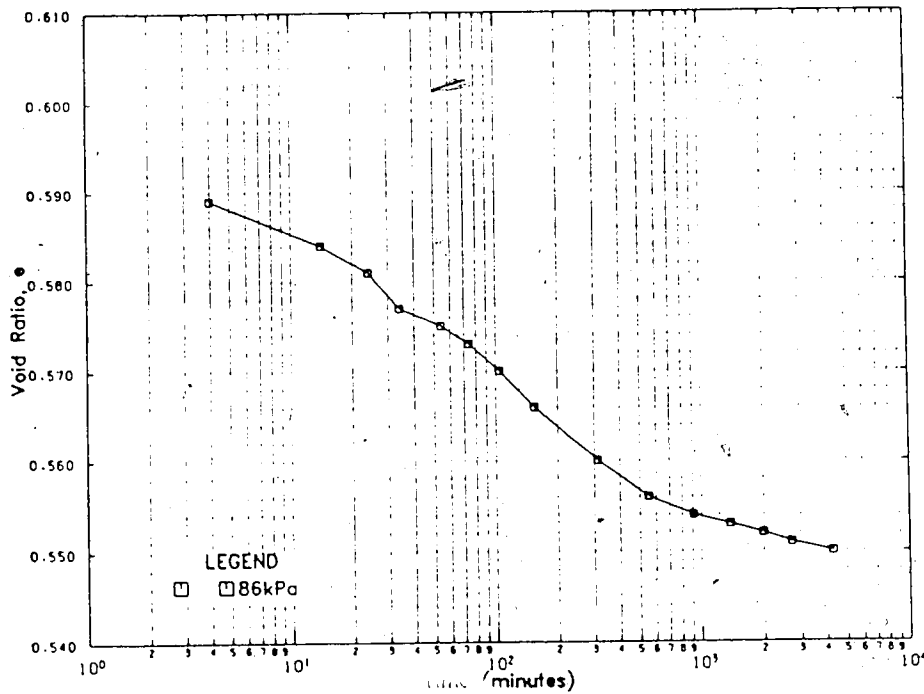


Figure B.42 Consolidation, Test #4, $\sigma' = 86$ kPa

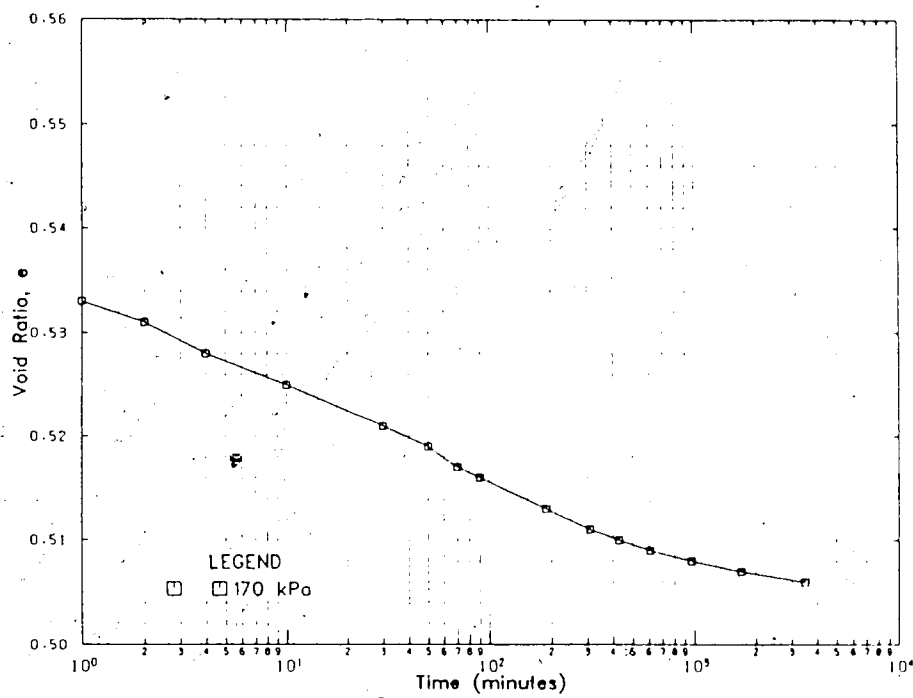


Figure B.43 Consolidation, Test #4, $\sigma' = 170$ kPa

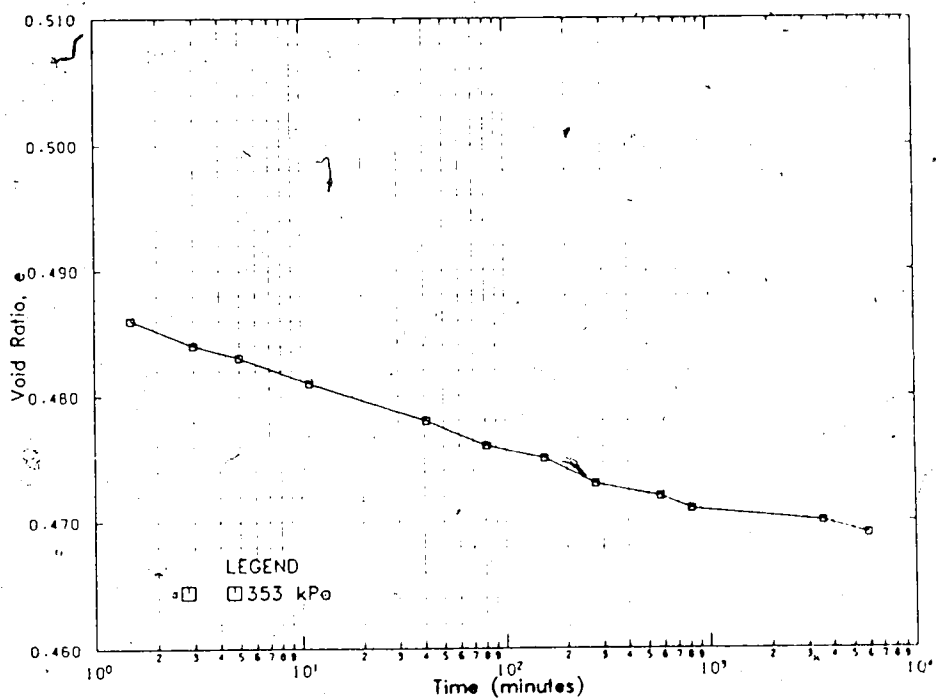


Figure B.44 Consolidation, Test #4, $\sigma' = 353$ kPa

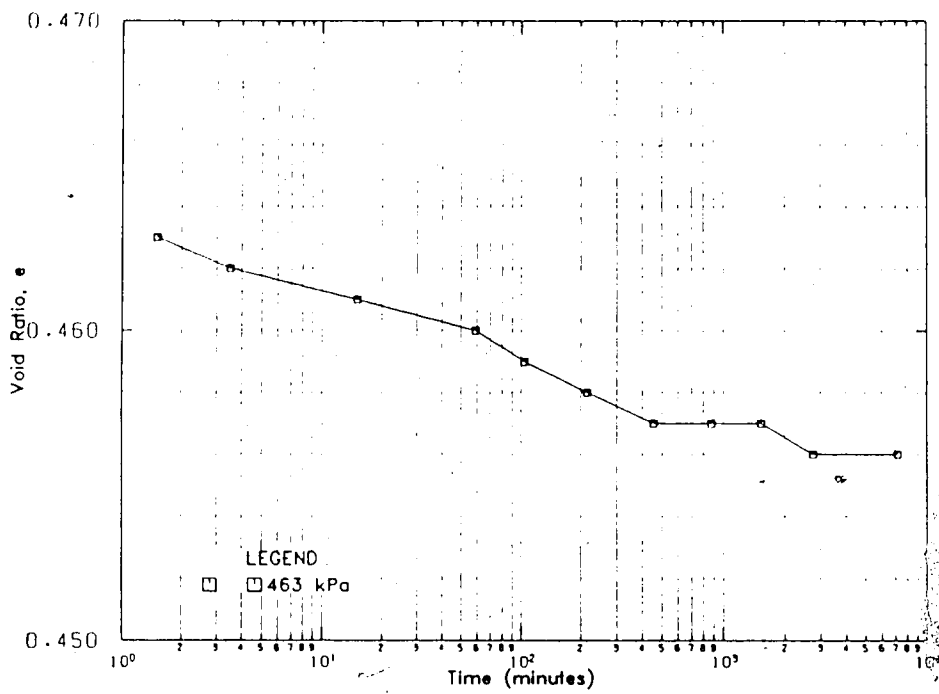


Figure B.45 Consolidation, Test #4, $\sigma' = 463$ kPa

APPENDIX C - Excess Pore Pressures

This Appendix contains excess pore pressure plots as determined from the results of the pore pressure measurements taken during the consolidation tests. Only two consolidometers (Test #1 and Test #4) were equipped with pore pressure ports.

Figure A.5 showed the location of the ports. The ports are numbered starting from the *bottom*. Most of the excess pore pressure plots have less than 5 ports plotted. This is because the mix had consolidated to a degree such that the surface of the slurry was below the port(s).

The self weight stress, as discussed in Chapter 4, is the average self weight stress in the sample. Therefore, for the self weight stage, the initial excess pore pressures at the bottom of the consolidometer are expected to be (and are) greater than this average value.

Many of the plots do not reflect the total change in effective stress. The cause of this is still unknown, although it may possibly be linked to gas in or near the ports. As discussed in Chapter 4, the pore pressure readings fluctuated synchronously with the slight temperature change in the laboratory. However, the pore pressure reading was constant when connected to the daily calibration unit (Figure A.6).

Negative excess pore pressures are seen on many of the plots. Because of the daily check of the transducer

calibration, it was ensured that the negative excess pore pressure measurements were not a result of the equipment.

Possible improvements on the pore pressure measuring system include a) each consolidometer should be equipped with at least 2 pore pressure transducers, to permit continual monitoring of some of the ports, and b) some type of bleed system at the ports because of the gas generated by the sludge.

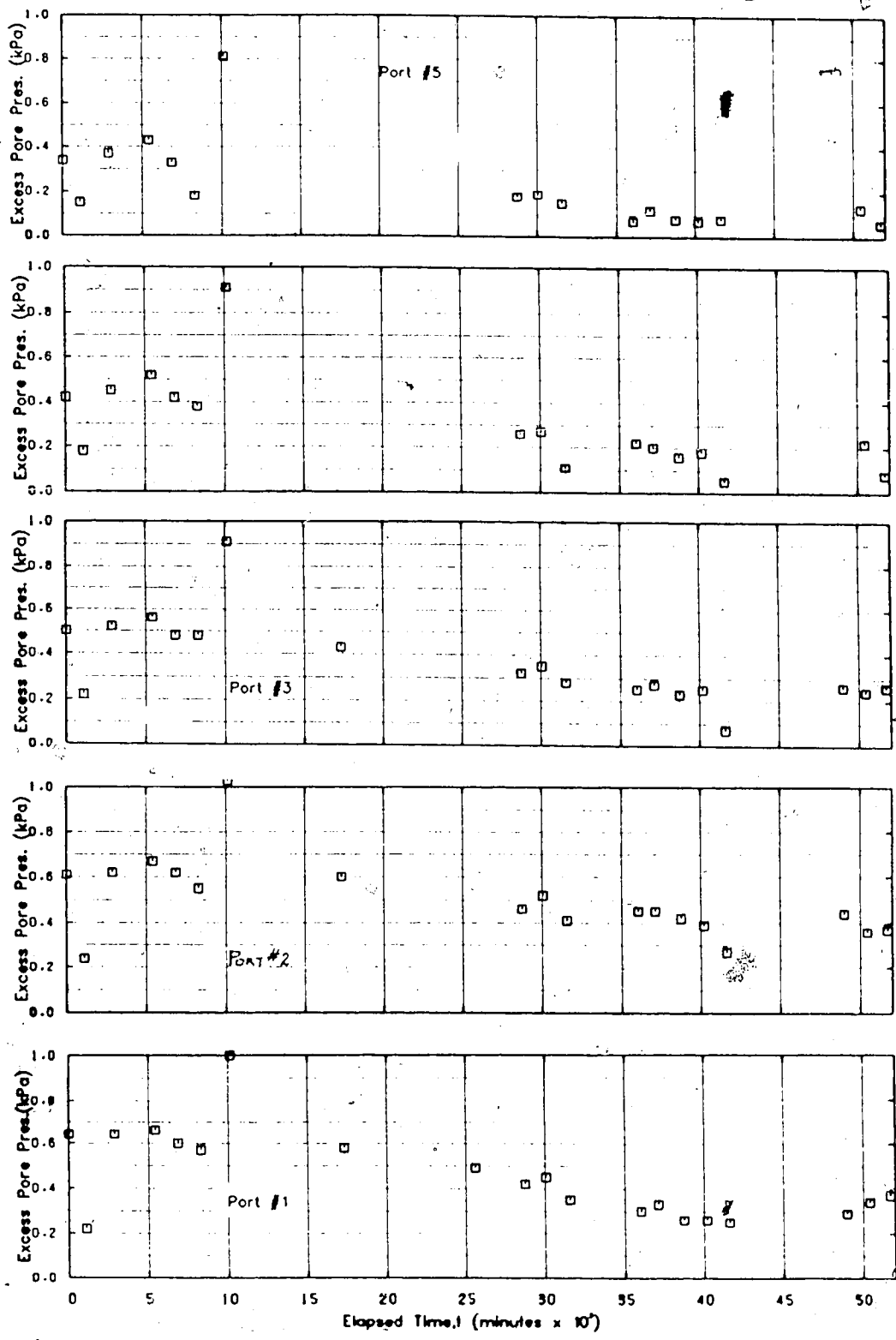


Figure C.1 Excess Pore Pressure, Test #1, $\sigma'_{ave}=0.22$ kPa (self weight)

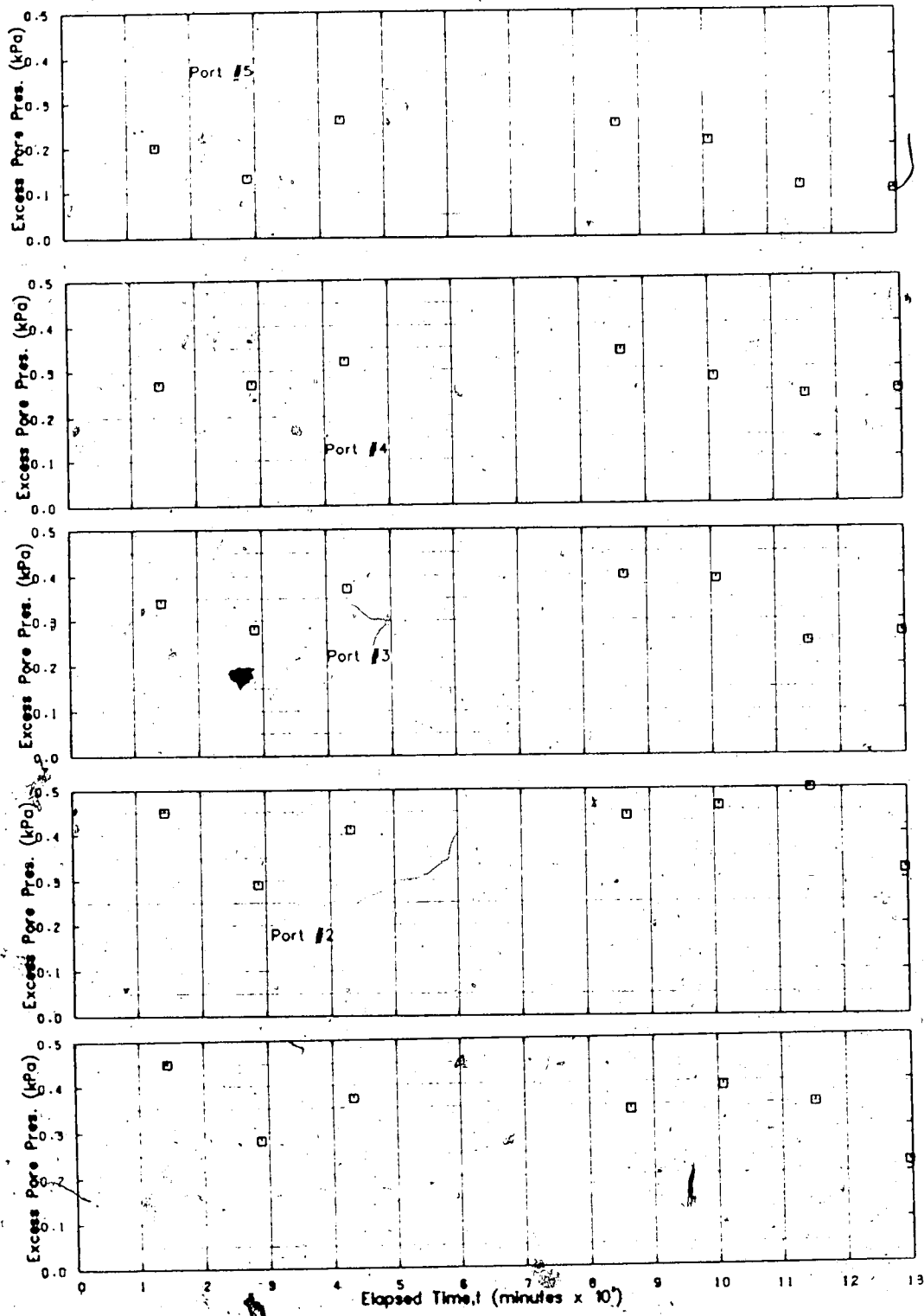


Figure C.2 Excess Pore Pressure, Test #1, $\Delta\sigma' = .23\text{kPa}$, $\sigma' = .45\text{kPa}$

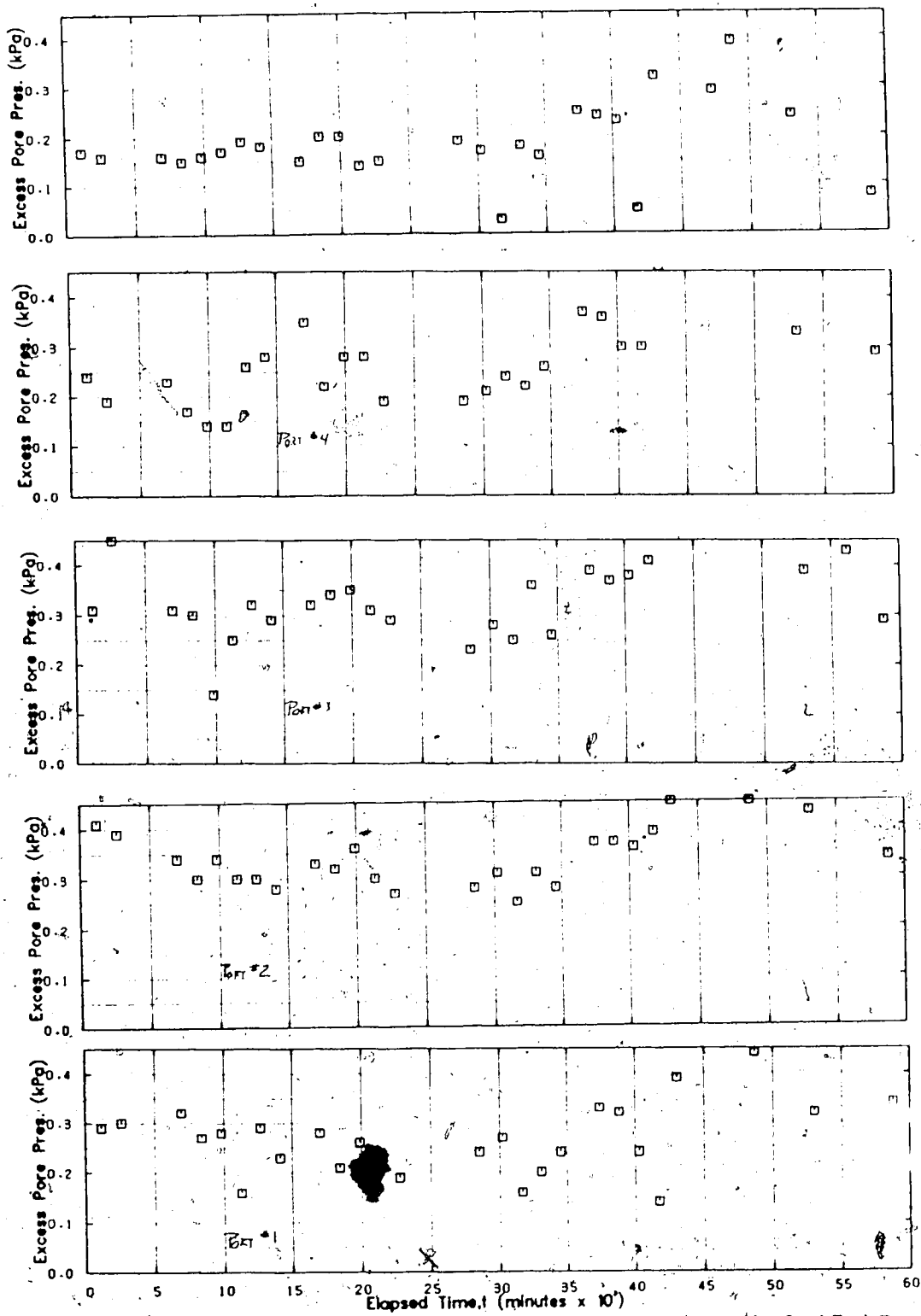


Figure C.3 Excess Pore Pressure, Test #1, $-\Delta\sigma' = 0.45$ kPa,
 $\sigma' = 0.9$ kPa

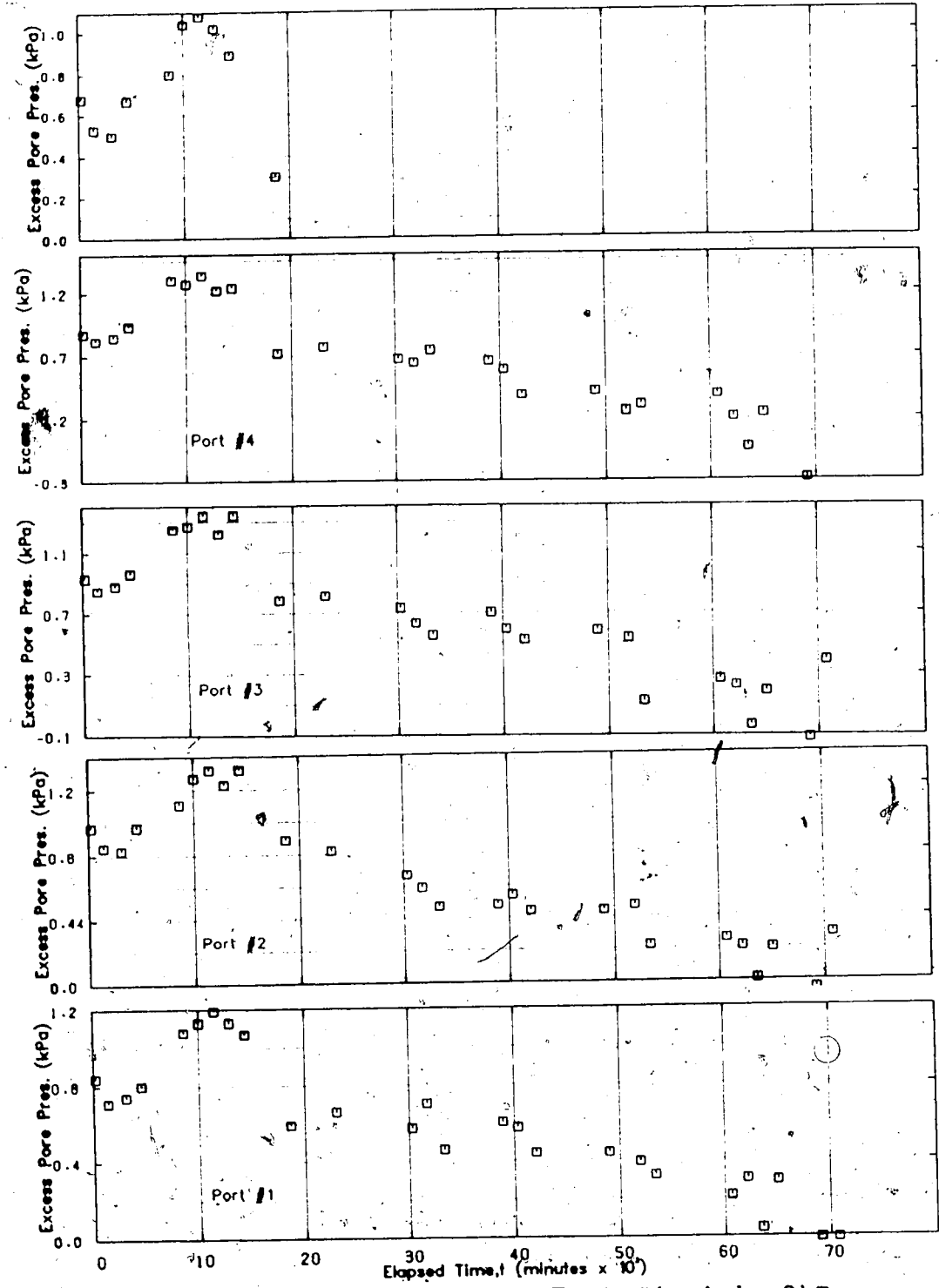


Figure C.4 Excess Pore Pressure, Test #1, $\Delta\sigma' = .8\text{kPa}$,
 $\sigma' = 1.7\text{kPa}$

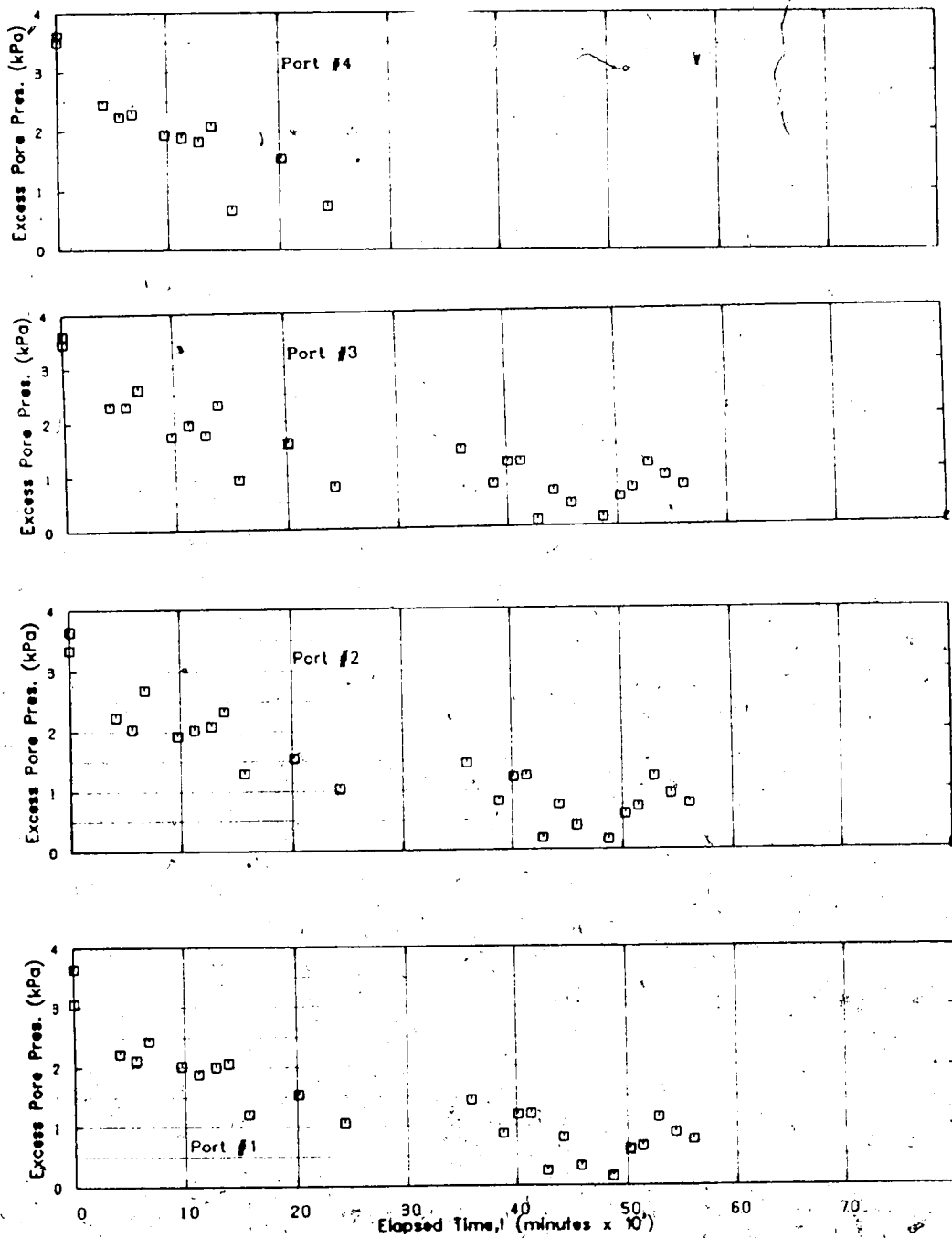


Figure C.5 Excess Pore Pressure, Test #1, $\Delta\sigma' = 3.3$ kPa, $\sigma' = 5$ kPa

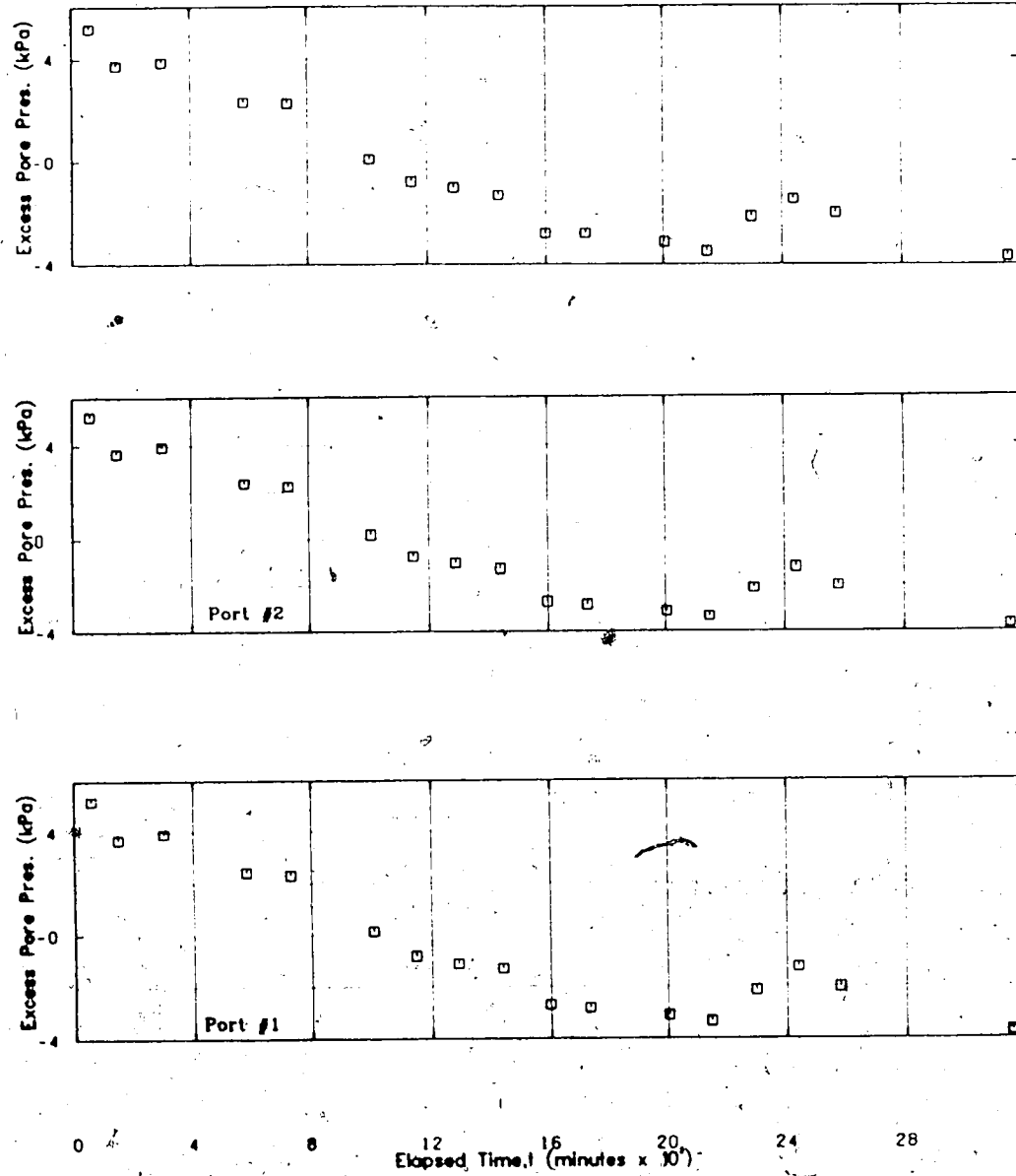


Figure C.6 Excess Pore Pressure, Test #1, $\Delta\sigma' = 6$ kPa, $\sigma' = 11$ kPa

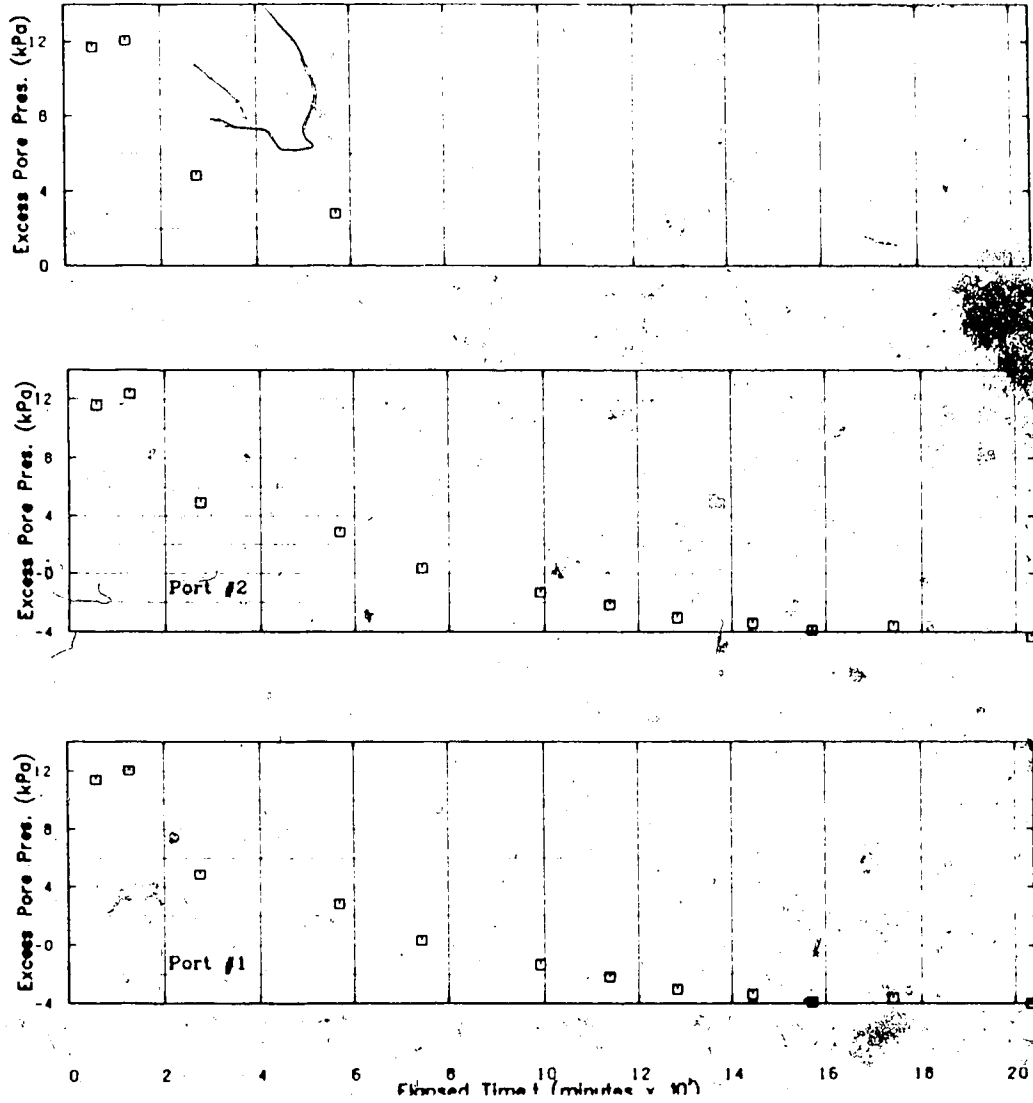


Figure 6.7 Excess Pore Pressure, Test #1, $\Delta\sigma' = 14$ kPa, $\sigma' = 25$ kPa

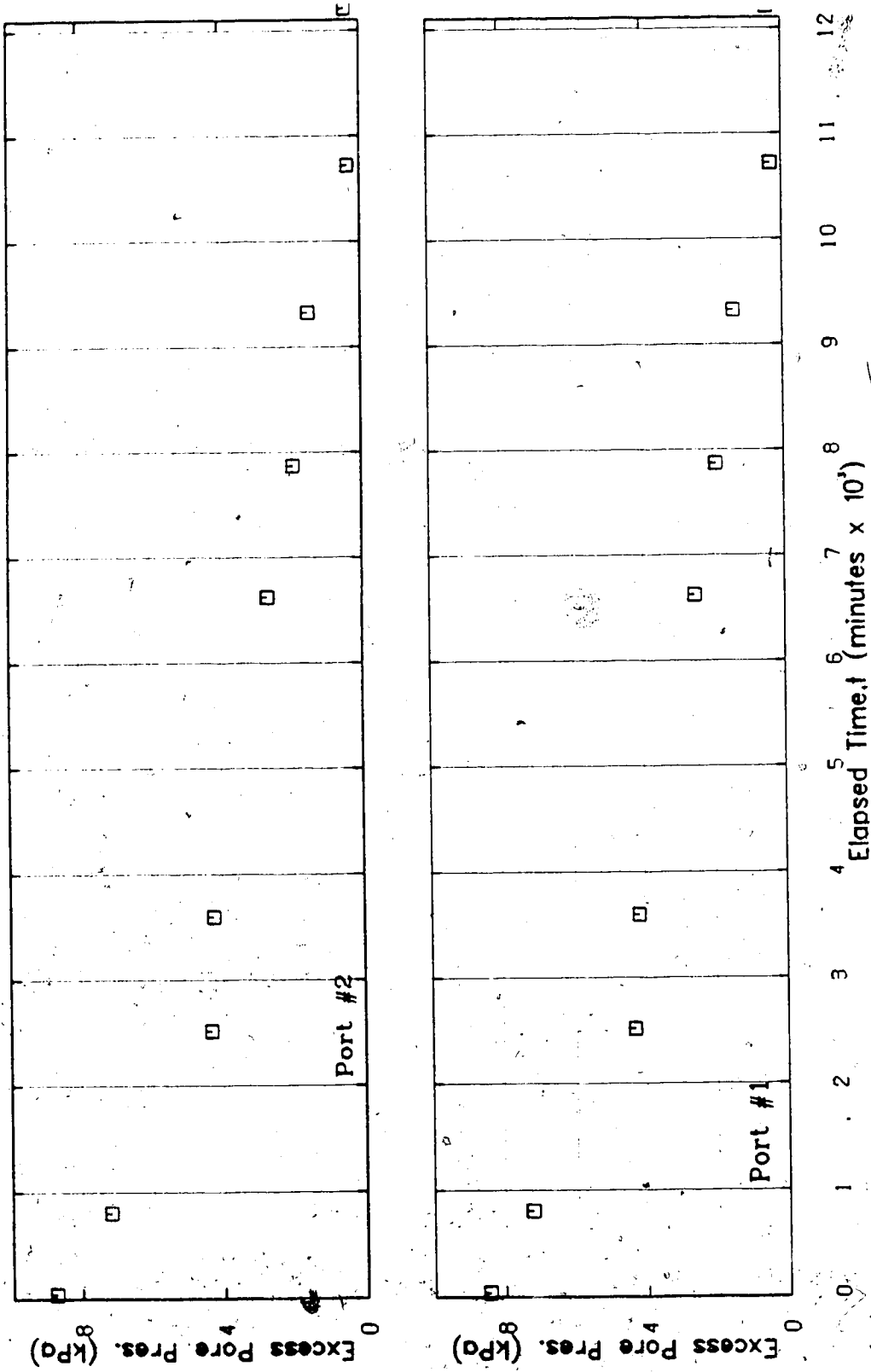


Figure C.8 Excess Pore Pressure, Test #1, $\Delta\sigma' = 20$ kPa, $\sigma' = 45$ kPa

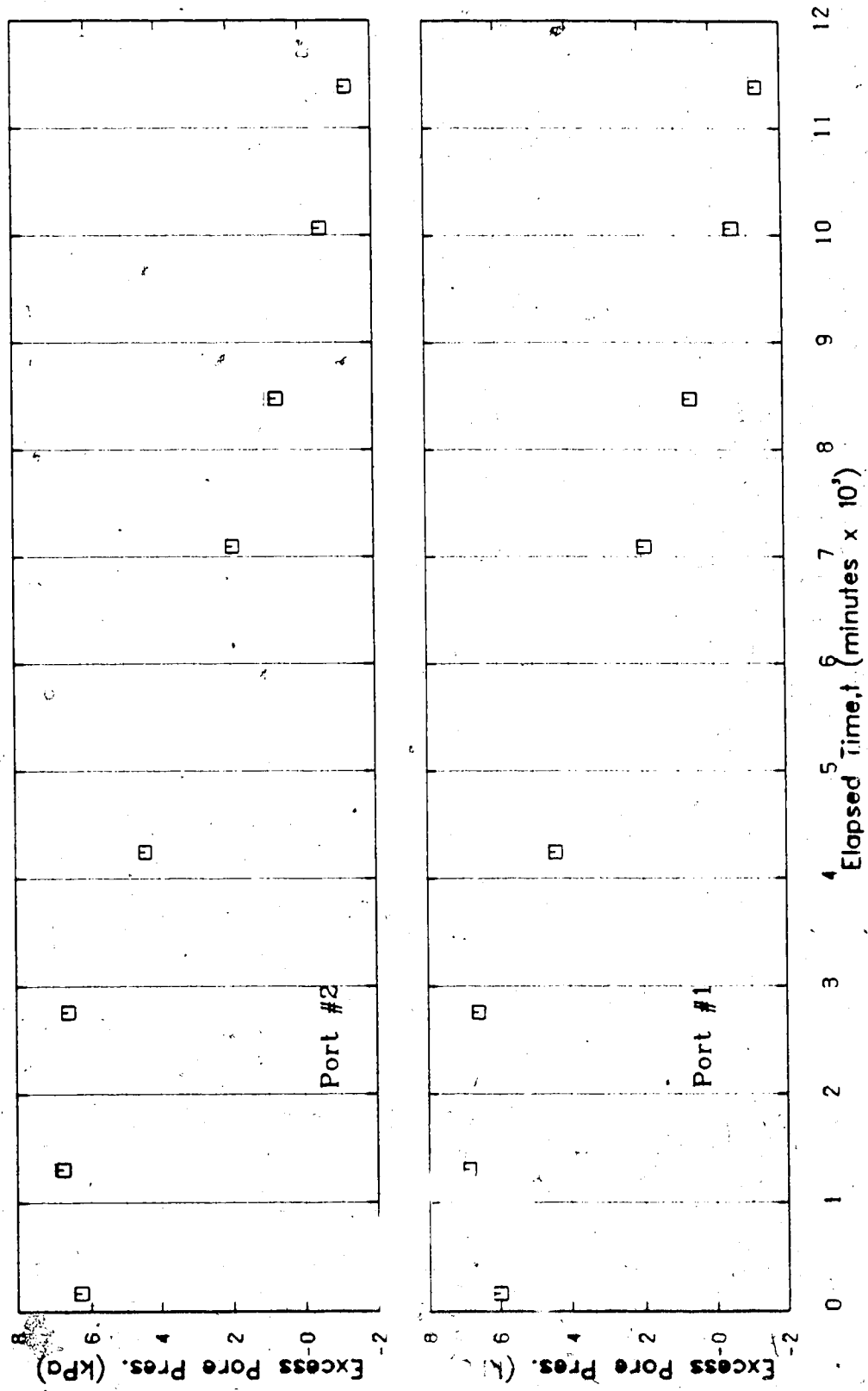


Figure C.9 Excess Pore Pressure, Test #1, $\Delta\sigma' = 55$ kPa, $\sigma' = 100$ kPa

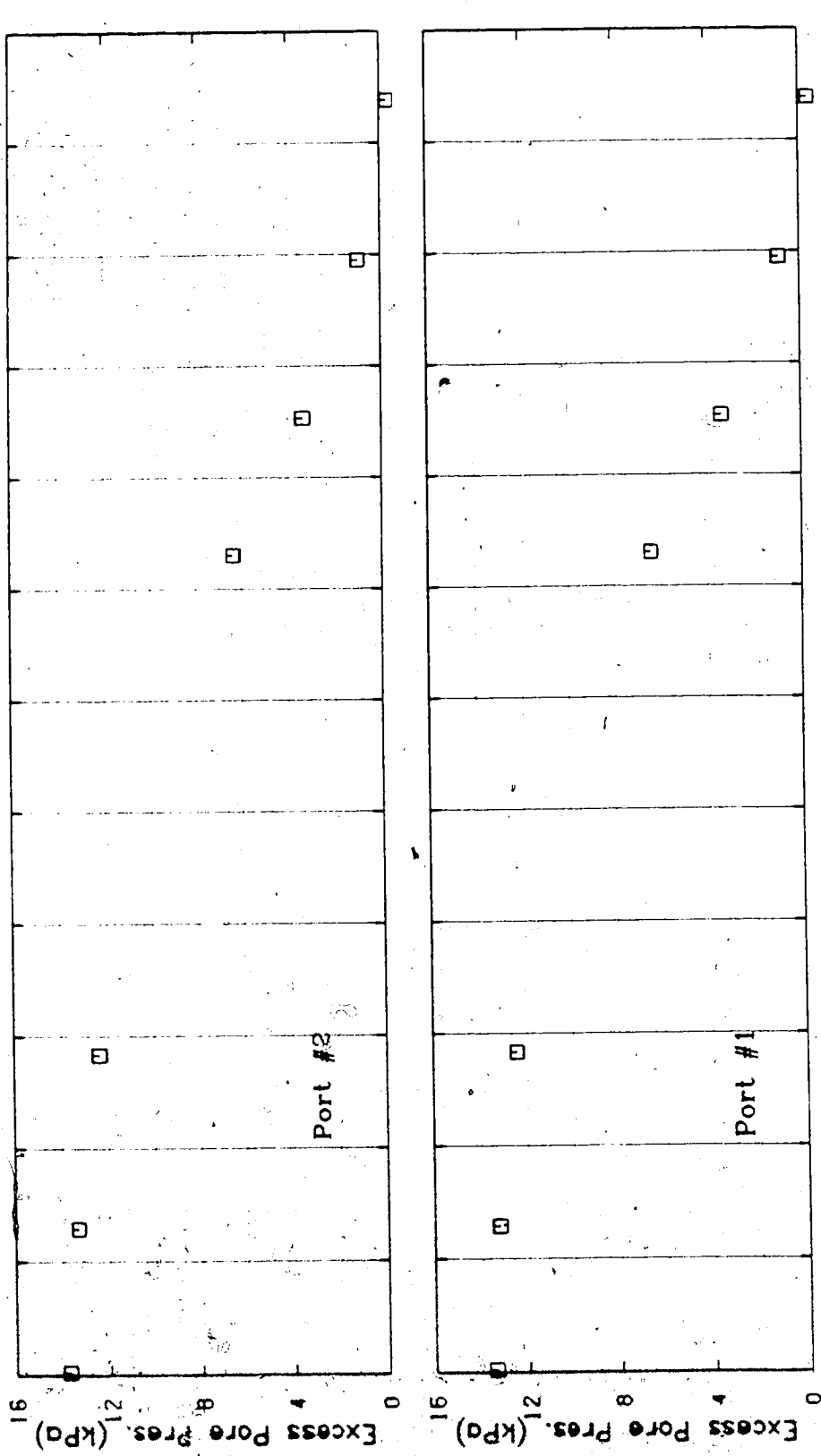


Figure C.10 Excess Pore Pressure, Test #1, $\Delta\sigma' = 100$ kPa, $\sigma' = 200$ kPa

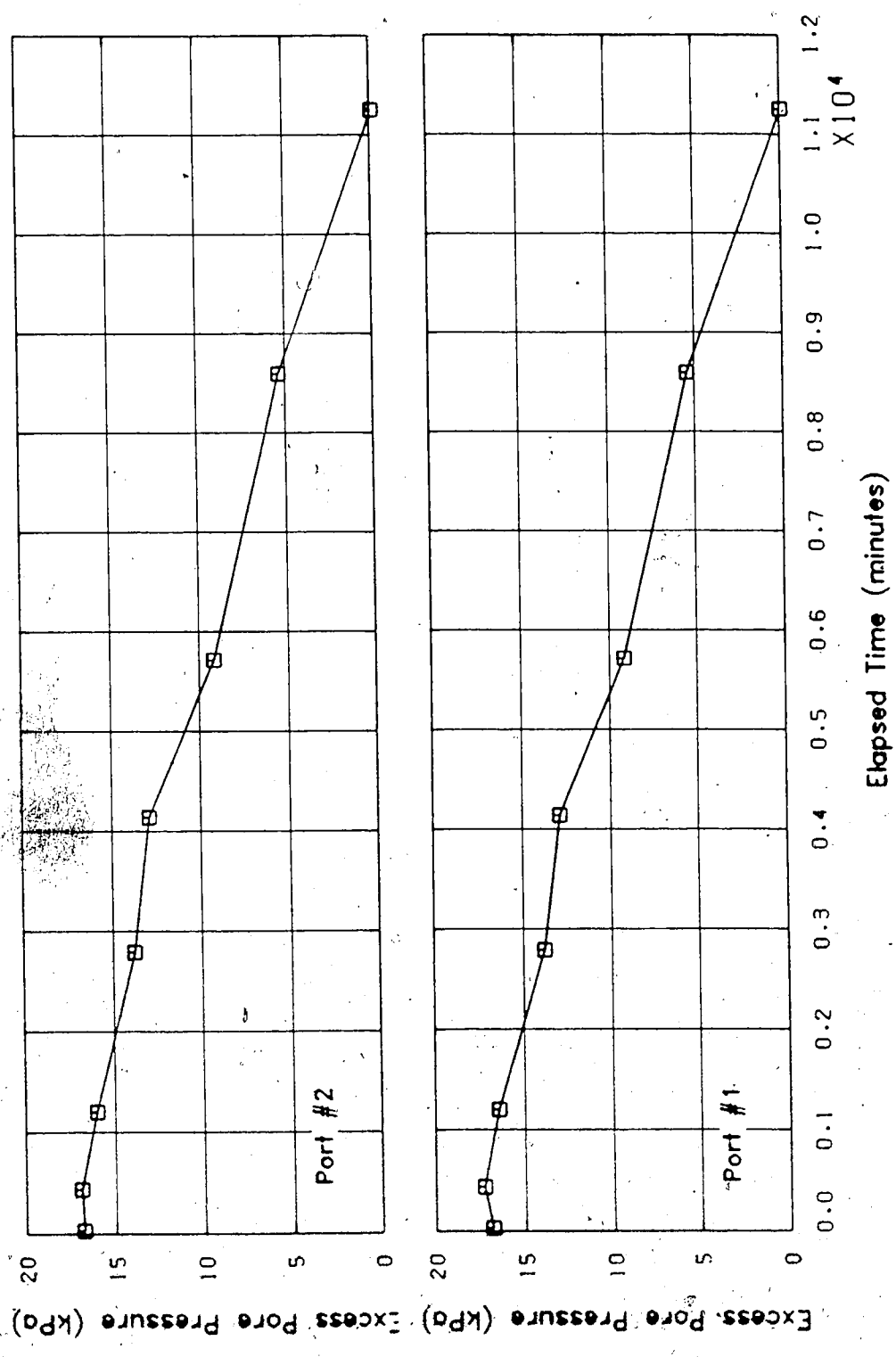


Figure C.11 Excess Pore Pressure, Test #1, $\Delta\sigma' = 200$ kPa, $\sigma' = 400$ kPa

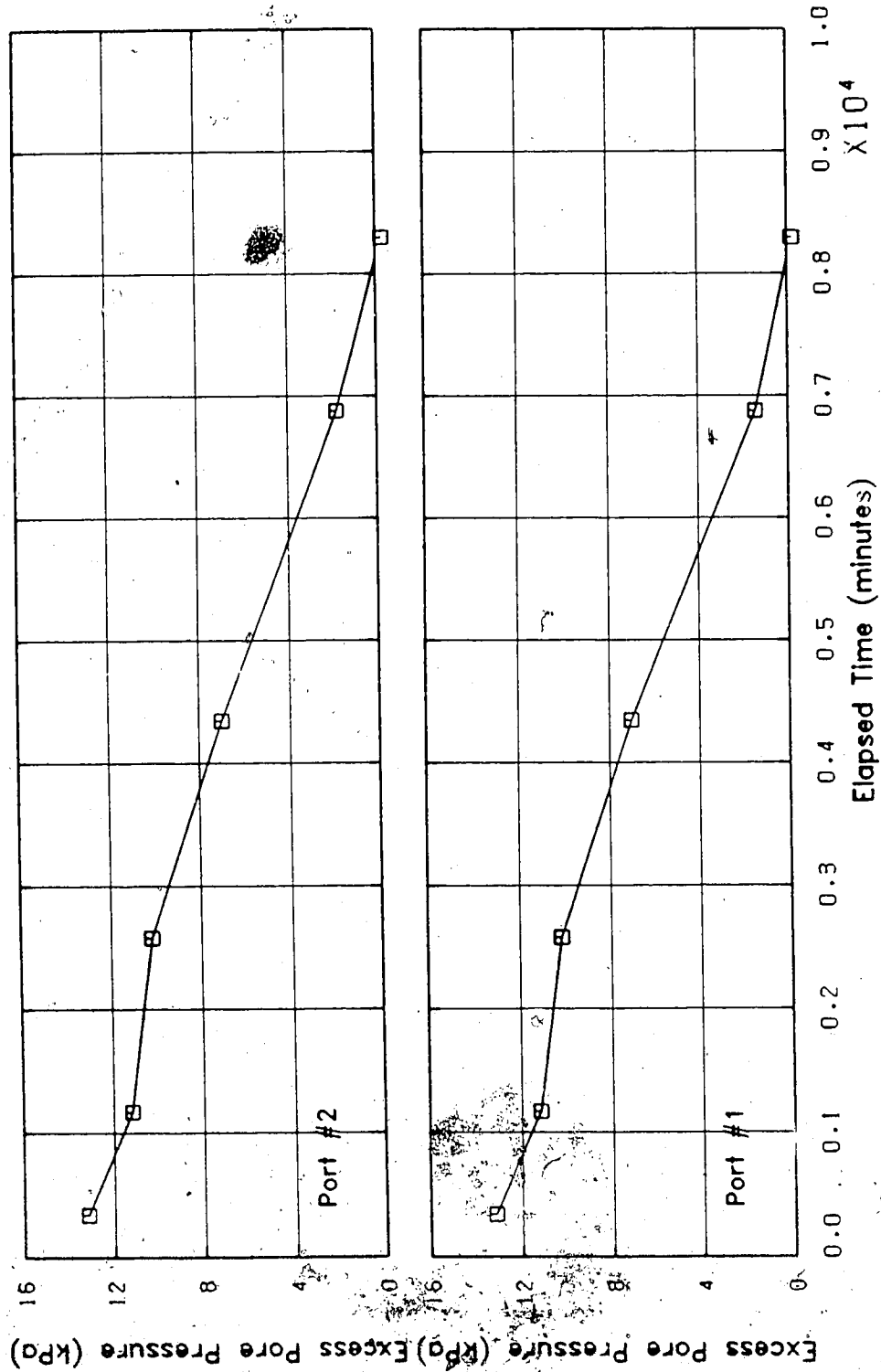


Figure 5.12 Excess Pore Pressure, Test #1, $\Delta\sigma' = 250$ kPa, $\sigma' = 650$ kPa

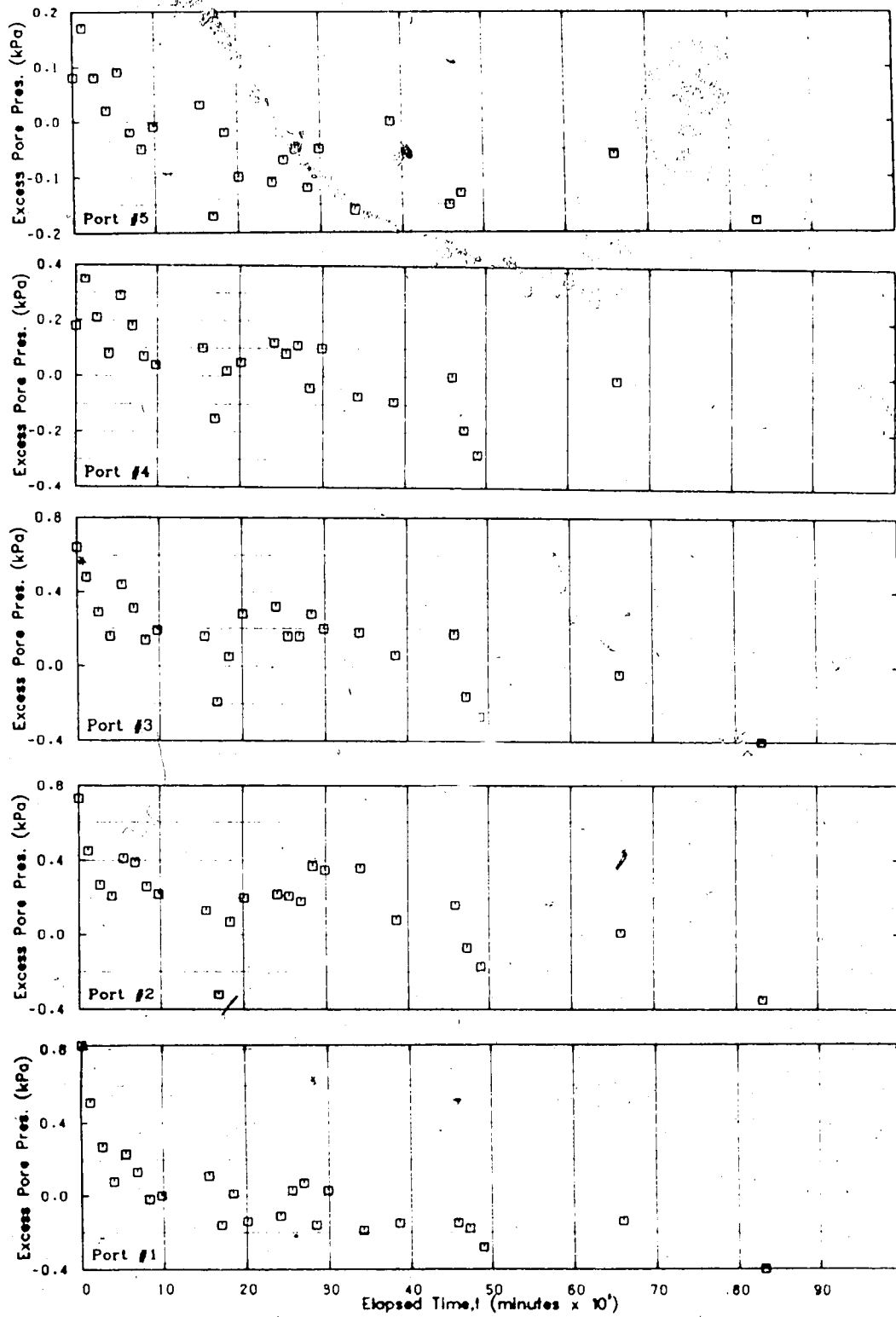


Figure C.13 Excess Pore Pressure, Test #2, $\sigma'_{ave}=0.53$ kPa (self weight)

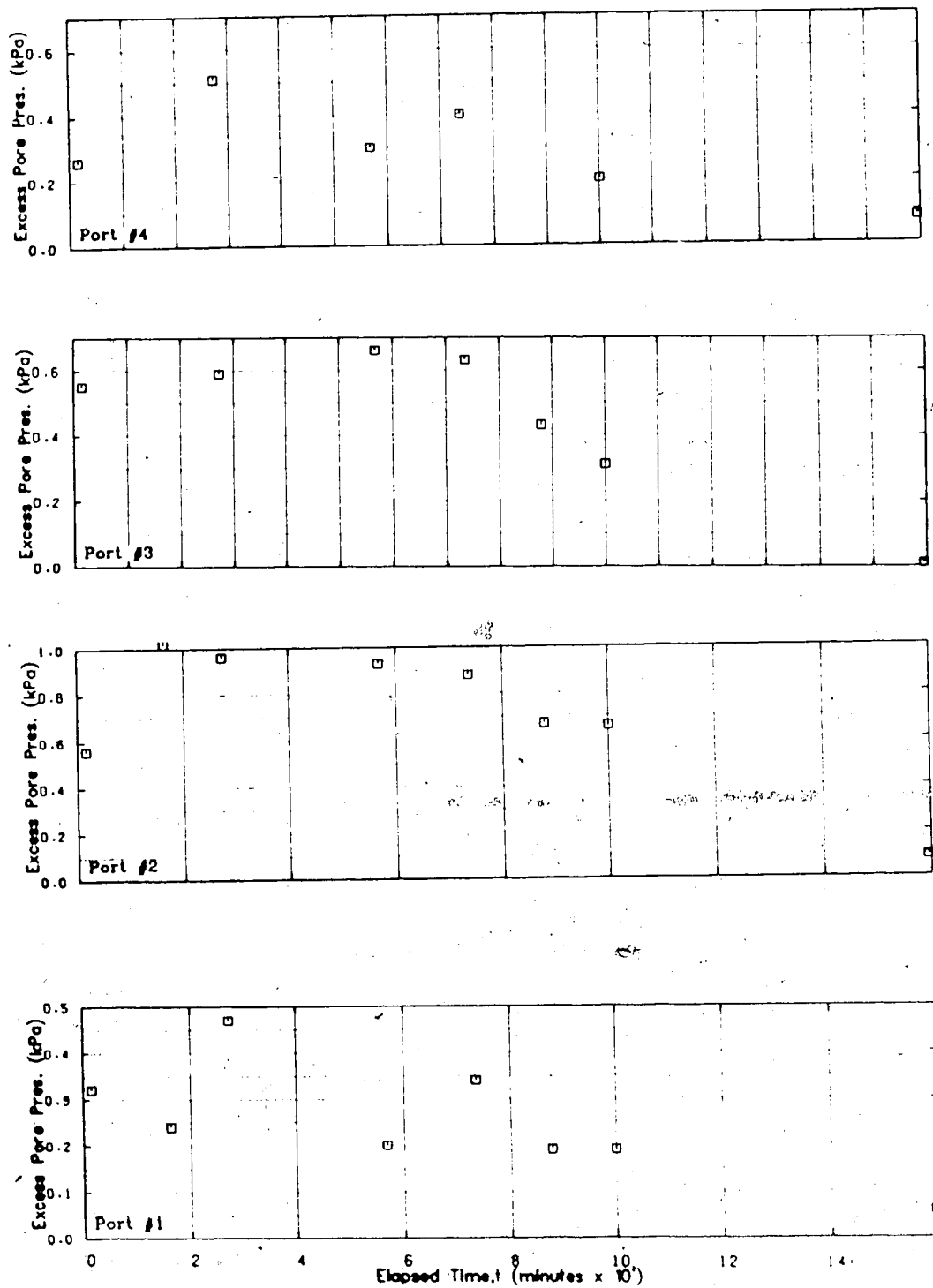


Figure C.14 Excess Pore Pressure, Test #2, $\Delta\sigma' = .47$ kPa, $\sigma' = 1.$ kPa

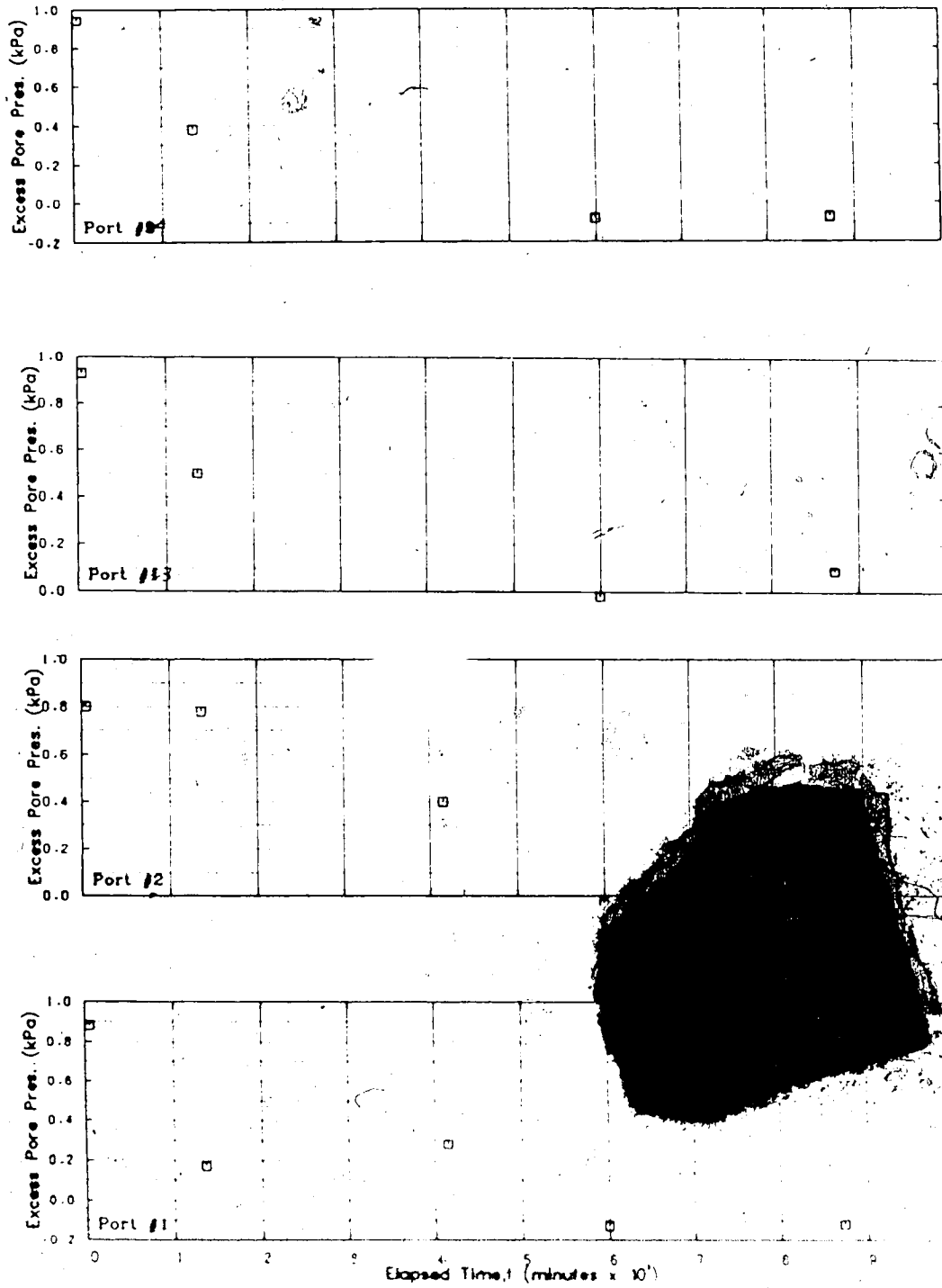


Figure C.15 Excess Pore Pressure, Test #2, $\Delta\sigma' = 1.5$ kPa, $\sigma' = 2.5$ kPa

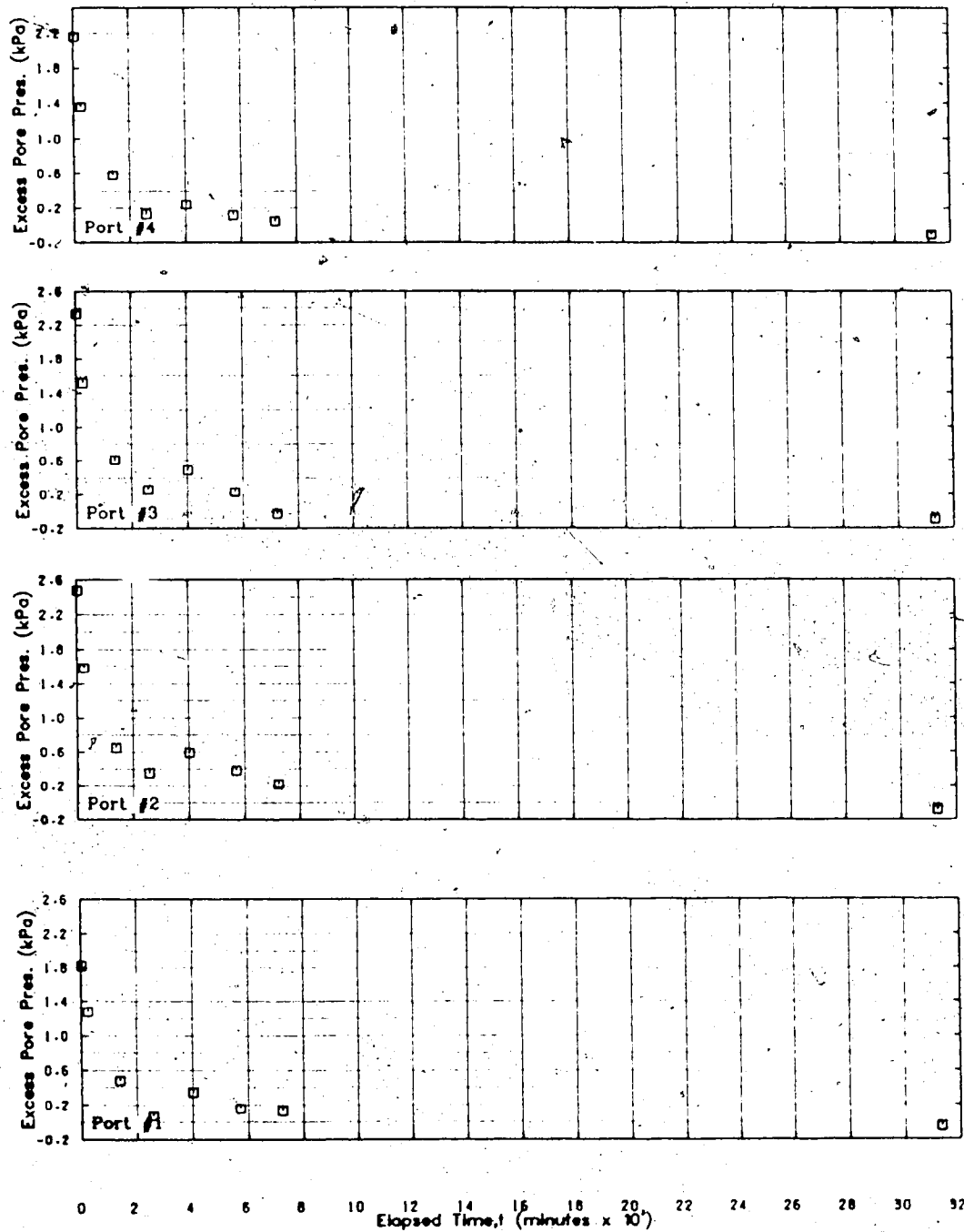


Figure C.16 Excess Pore Pressure, Test #2, $\Delta\sigma' = 2.5$ kPa, $\sigma' = 5.0$ kPa

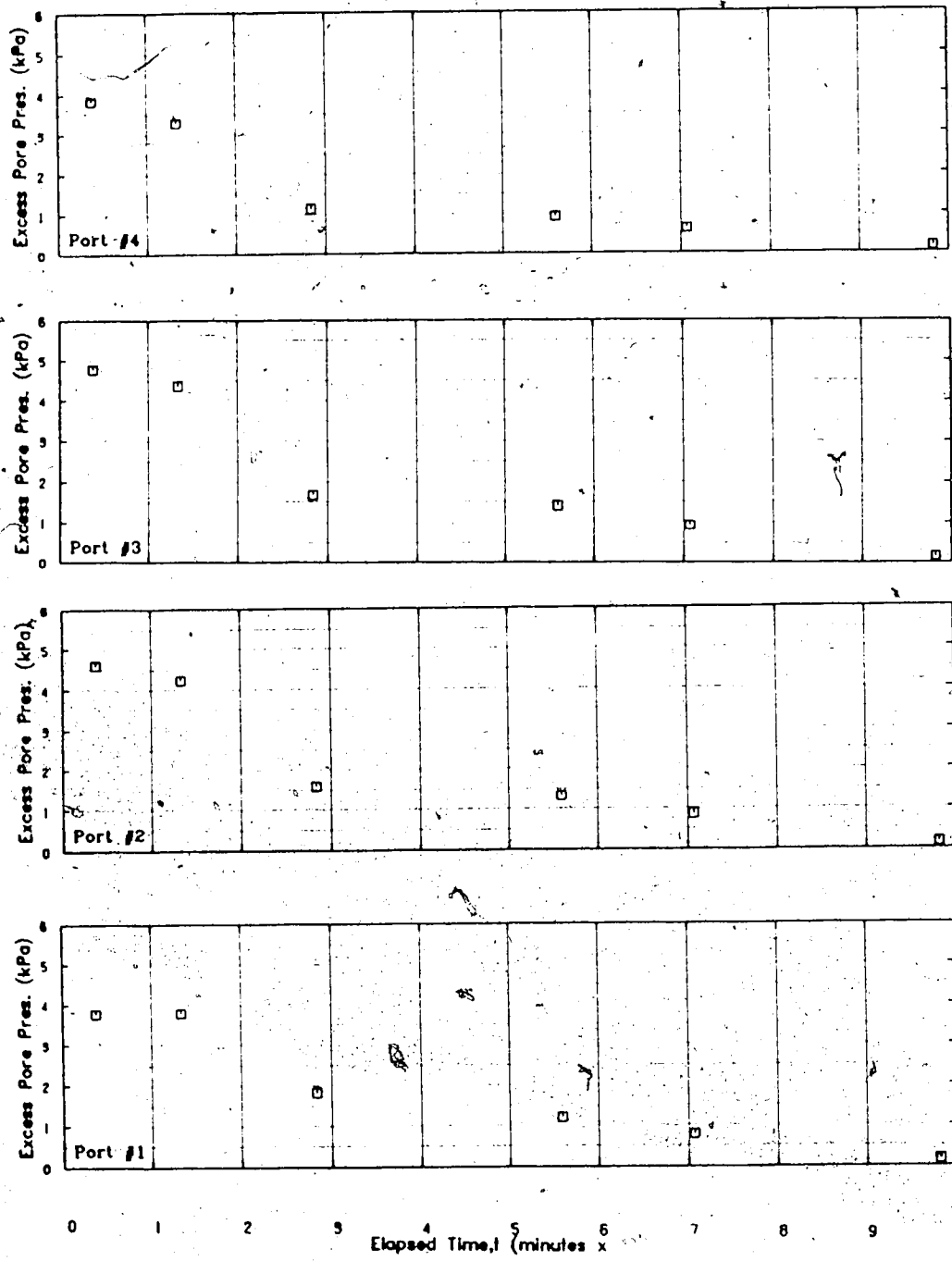


Figure C.17 Excess Pore Pressure, Test #2, $u'_0 = 6$ kPa, $\sigma'_v = 11$ kPa

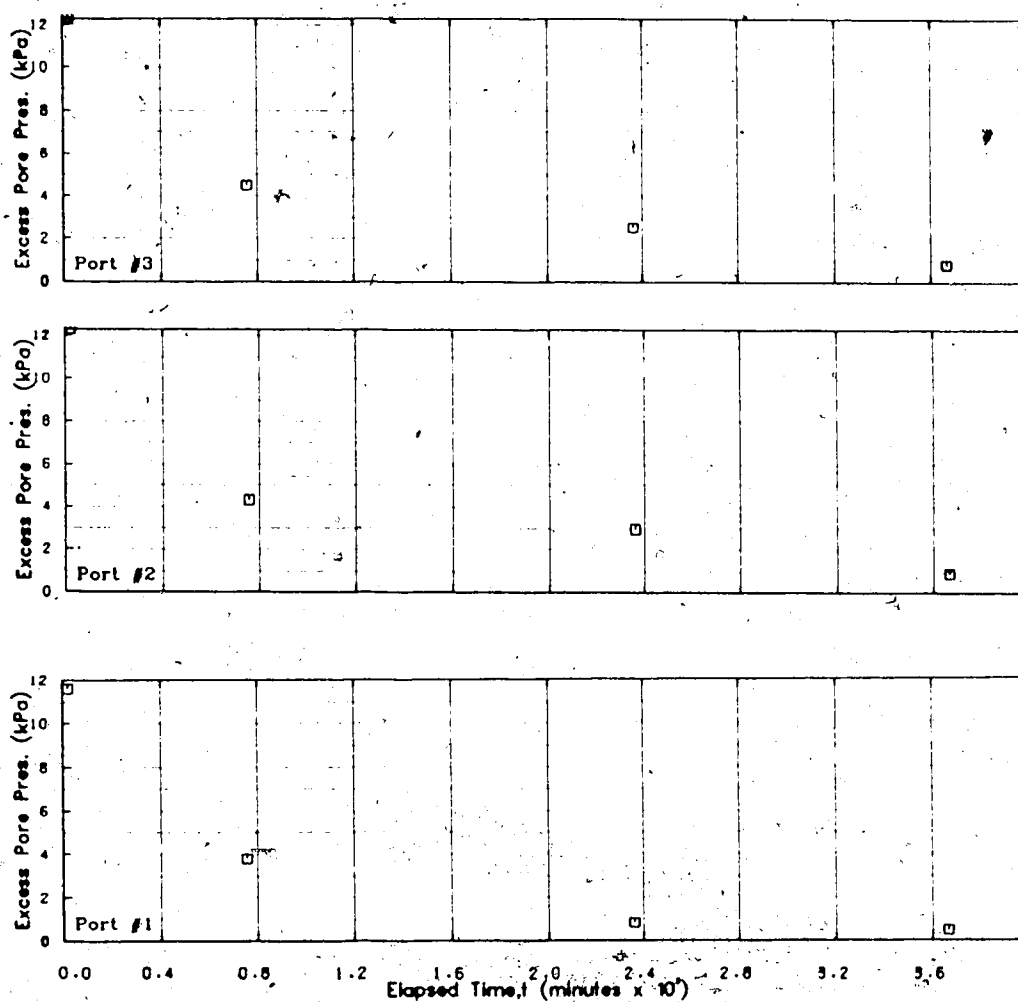


Figure C.18 Excess Pore Pressure, Test #2, $\Delta\sigma' = 12$ kPa, $\sigma' = 23$ kPa

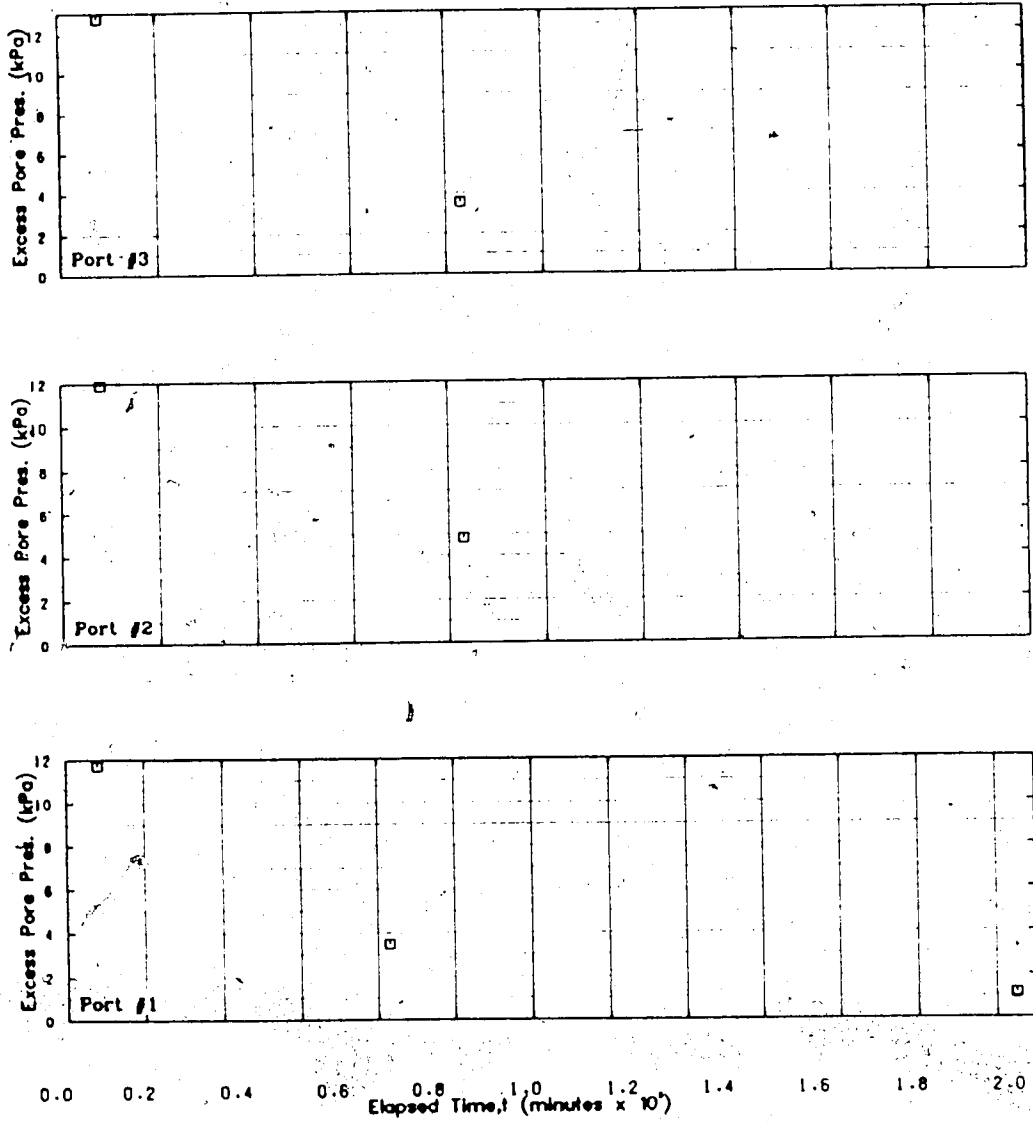


Figure C.19 Excess Pore Pressure, Test #2, $\Delta\sigma' = 18$ kPa, $\sigma' = 41$ kPa

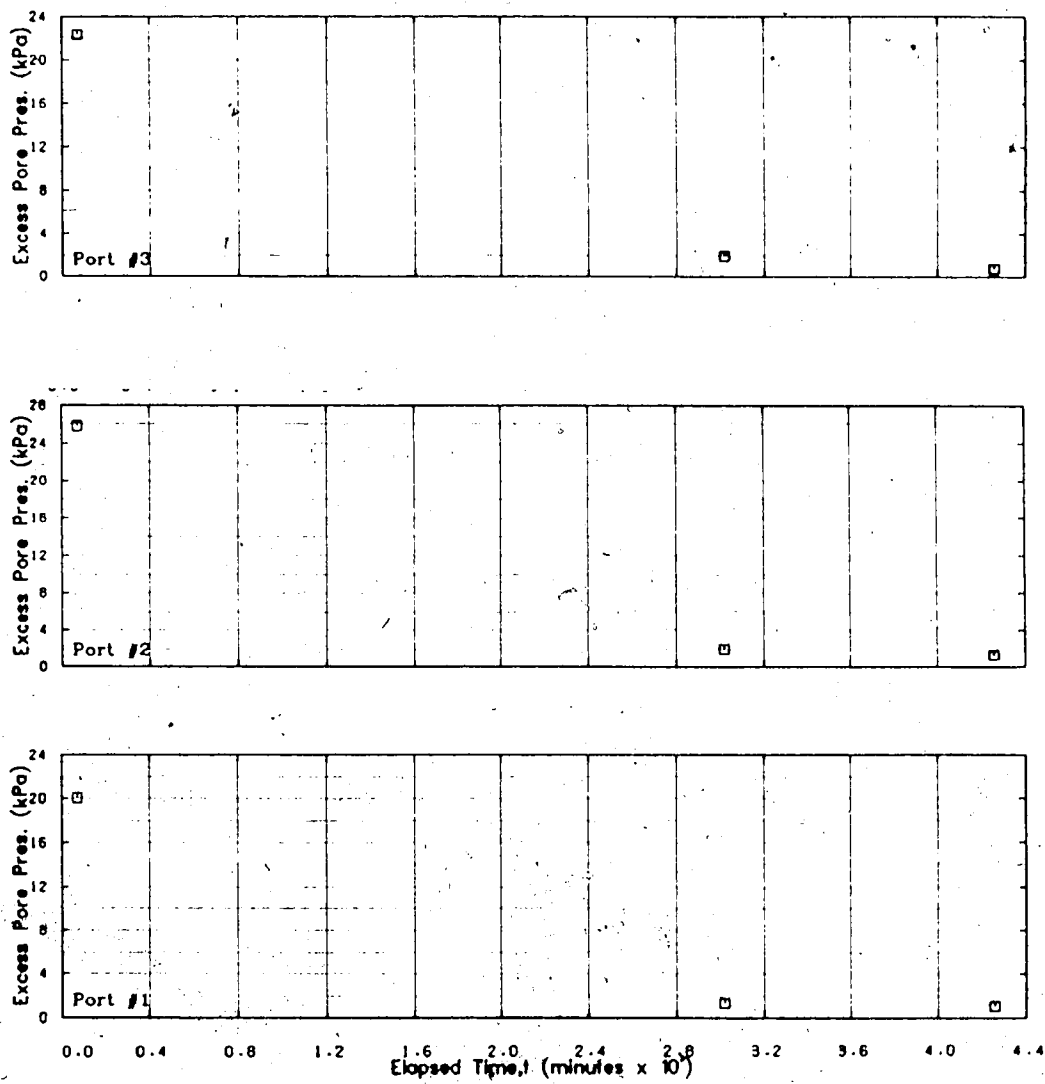


Figure C.20 Excess Pore Pressure, Test #2, $\Delta\sigma' = 45$ kPa, $\sigma' = 86$ kPa

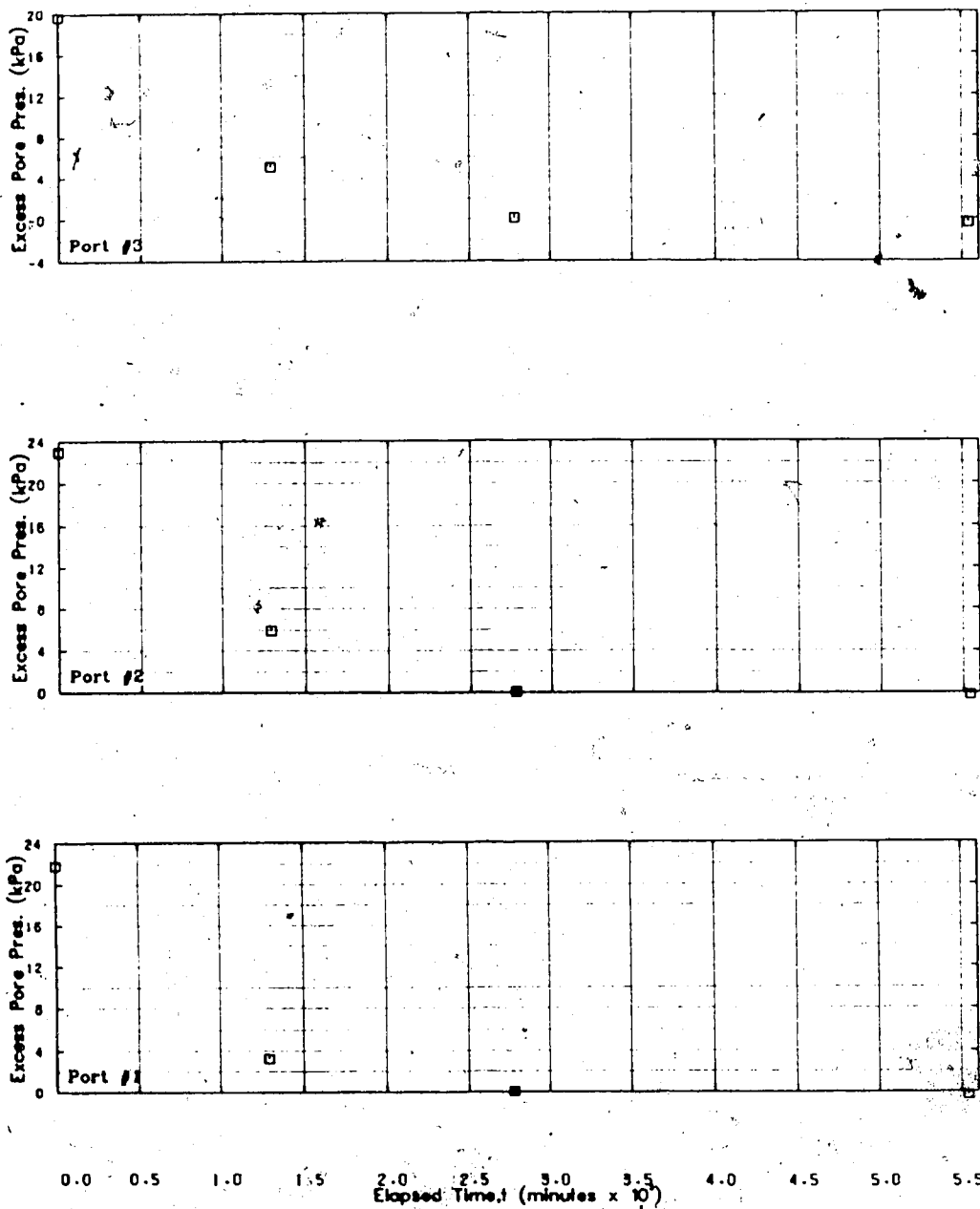


Figure C.21 Excess Pore Pressure, Test #2, $\Delta\sigma' = 84$ kPa,
 $\sigma' = 170$ kPa

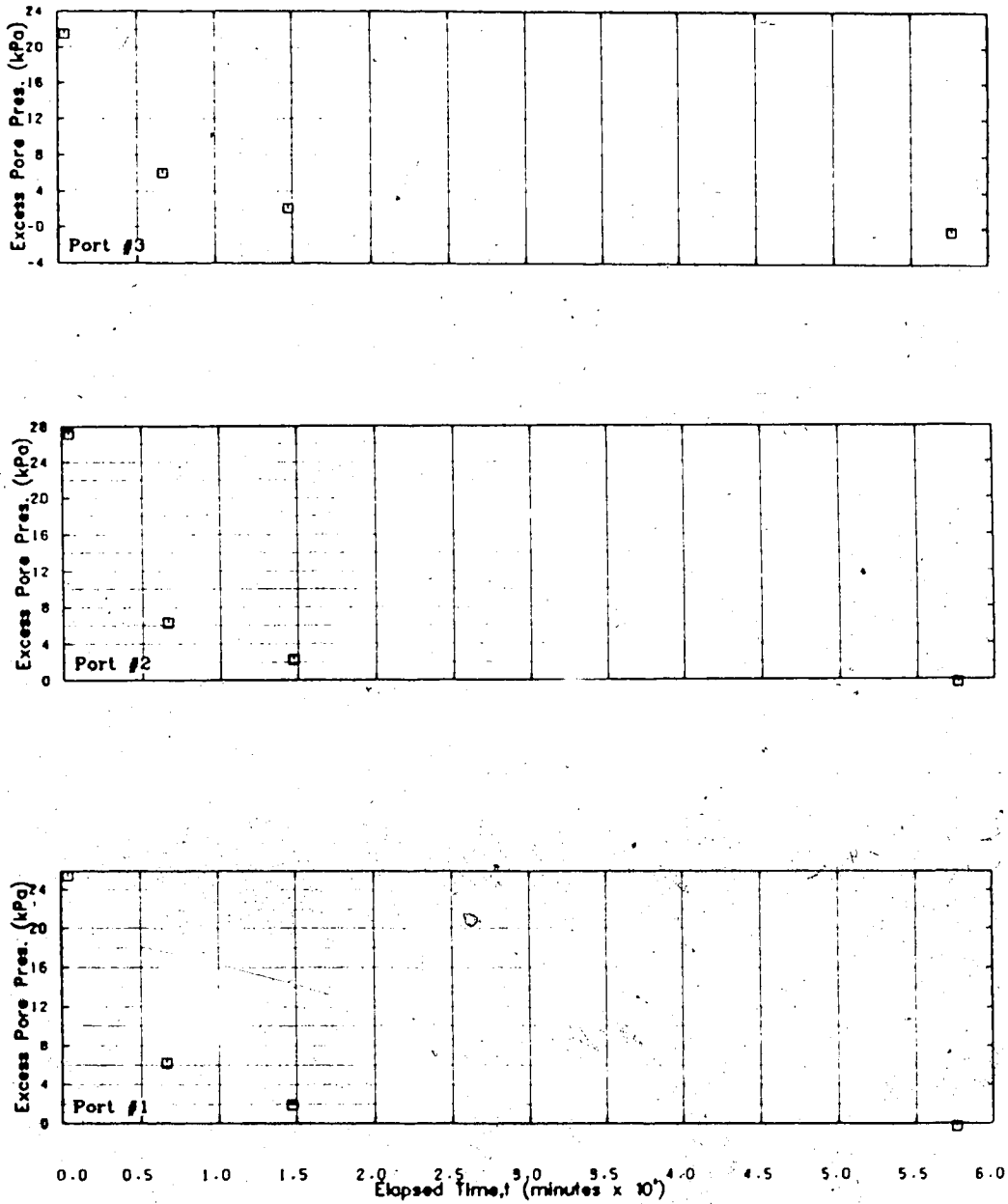


Figure C.22 Excess Pore pressure, Test #2, $\Delta\sigma' = 183$ kPa, $\sigma' = 353$ kPa

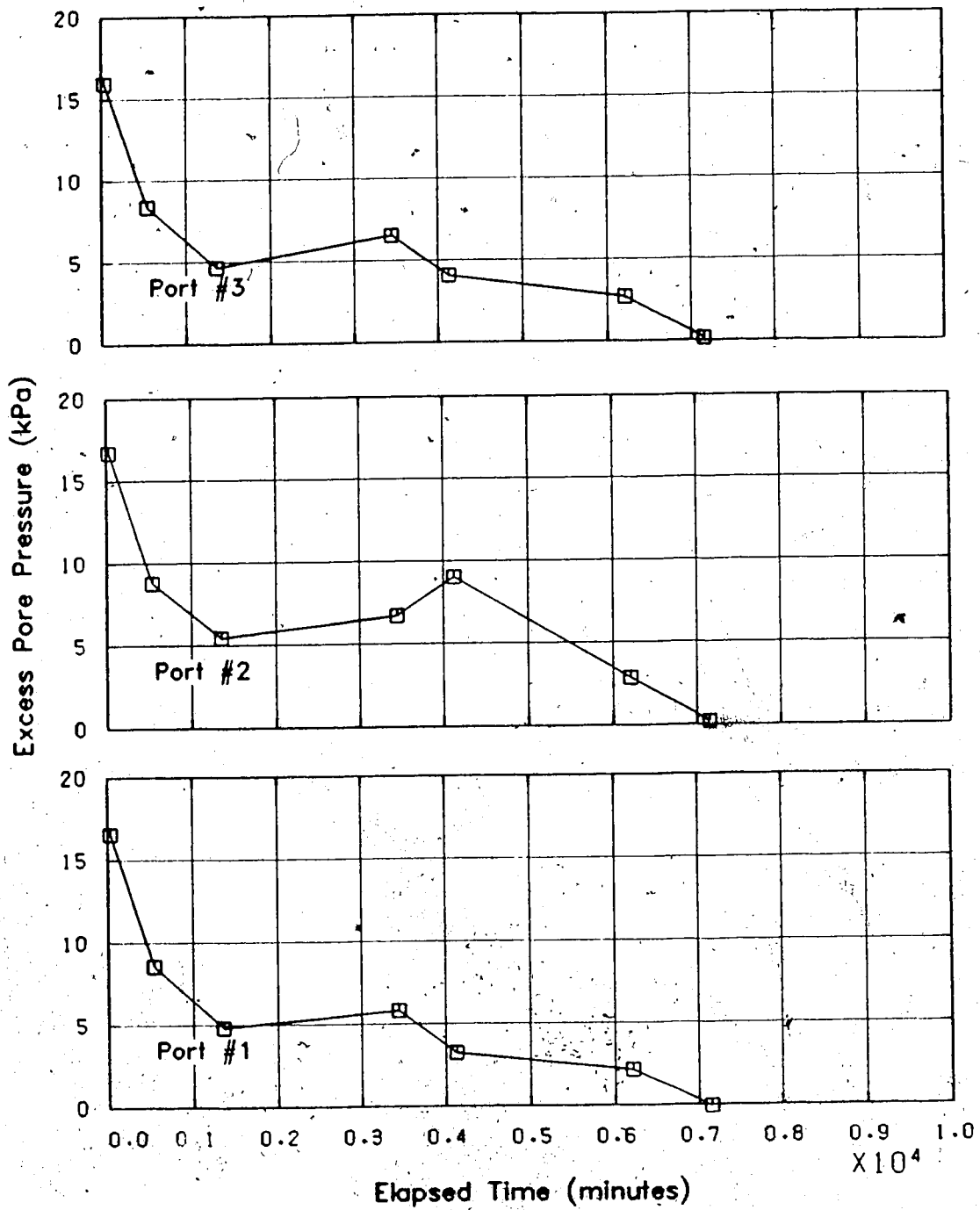


Figure C.23 Excess Pore Pressure, Test #2, $\Delta\sigma' = 110$ kPa,
 $\sigma' = 463$ kPa